Retinal Differentiation of Human Induced Pluripotent Stem Cells in a Continuously Perfused Microfluidic Culture Device

Thesis submitted for the degree of Doctor of Philosophy (Ph.D.) in Biochemical Engineering by

Nima Abdolvand

The Advanced Centre for Biochemical Engineering

Department of Biochemical Engineering

University College London

Declaration

I, Nima Abdolvand confirm that the work presented in this thesis is my own. Where information has been derived from other sources, I confirm that this has been indicated in the thesis.

Nima Abdolvand
January 2017

Abstract

In this thesis, effects of stable concentration of key growth factors on retinal differentiation of human induced pluripotent stem cells (hiPSCs) were investigated in a microfluidic culture device (MFCD). *In vitro* culture dishes such as flasks and well-plates lack microenvironmental controls required for maintaining stable culture conditions. Unlike cell culture dishes, microfluidic devices provide greater microenvironmental controls resulted from shorter characteristic length and use of laminar flow. It is hypothesised that using the MFCD, a flow rate can be found which keeps key growth factors in retinal differentiation culture in steady-state. Subsequently, steady-state concentration of growth factors would result in upregulation of retinal progenitor (Pax6, Lhx2, Six6 and VSX2/Chx10) and precursor markers (Crx and Nrl).

Initially, degradation and consumption of growth factors (DKK-1, Noggin, IGF-1 and bFGF) used in retinal differentiation were studied to establish an order of importance. These findings along with dimensionless ratios, Péclet and Damköhler numbers, were utilised to establish a perfusion rate of 130 µL/h. At this flow rate growth factors DKK1 and Noggin were delivered to the cells in steady-state conditions. A second perfusion culture with the same media exchange rate as the static culture at flow rate of 5.2 µL/h was added to act as a second control. Perfusion cultures were performed for 5, 10, and 21 days (n=3). The MFCD with higher flow rate showed significantly higher expression of markers Crx ($p<0.05$) and Rhodopsin (compared to lower MFCD, $p<0.05$)

on day 21. The MFCD with lower flow rate, showed significantly higher expression of Pax6 ($p<0.05$), Vsx2/Chx10 ($p<0.01$) and Crx ($p<0.05$) on day 5, Nrl ($p<0.01$) on day 10 and Six6 ($p<0.05$) on day 21. This was the first continuously perfused long-term (21 days) retinal differentiation of hiPSCs in a microfluidic device, and results illustrated the importance of steady-state conditions in stem cell bioprocessing.

To my parents, Rahim and Mahvash

Acknowledgements

First, I would like to thank my father for his support financially as well as spiritually not just during my Ph.D. but also throughout my academic years. I also would like to thank my mother and my sisters for their loving support and encouragements throughout these years.

I would like to thank my supervisors Professor. Nicolas Szita and Dr. Farlan Veraitch for their invaluable support, guidance, encouragement and patience throughout this project. I also would like to express my gratitude to Dr. Brian O'Sullivan and Mrs. Ludmila Ruban for their technical support, feedback and advice, in microfluidics and stem cell cultures. I would like to thank members of the microfluidic and the Regenerative Medicine groups, particularly Dr. Rui Tostoes, Zuming Tang, Vishal Sharma, Rhys Macown and Alexandre Super, for sharing their experience, advice, stimulating conversations and jokes.

I would like to thank my partner, Maria for her love, unwavering support and daily encouragements in completing this work - your patience, kindness and optimism enabled me to overcome many obstacles, especially in the past few years. Last, I would like to thank my friends Harold, Paul, Rebazar, Roman, Steve, Helena, Raoof, Sam, Masoud and Yashar for their company, unforgettable memories and their presence in my life.

Nima
January 2017

Table of Contents

List of Figures

List of Tables

Nomenclature

AMD	Age-related Macular Degeneration
BM	Basal Membrane
BMP	Bone Morphogenic Proteins
CNC	Computer Numerical Controlled
CNS	Central Nervous System
CNTF	Ciliary Neurotrophic Factor
DAPI	4',6-diamidino-2-phenylindole
DKK-1	Dickkopf-1
DMEM	Dulbecco's Modified Eagle Medium
DO	Dissolved Oxygen (concentration)
ECM	Extra Cellular Matrix
ECs	Endothelial Cells
EDTA	Ethylenediaminetetraacetic acid
EFTFs	Eye-Field Transcription Factors
ELISA	Enzyme-Linked Immunosorbent Assay
ELM	External Limiting Membrane
ESCs	Embryonic Stem Cells
FACS	Fluorescence Activated Cell Sorting
FBS	Foetal Bovine Serum
FGF	Fibroblast Growth Factor
GCL	Ganglion Cell Layer
GMP	Good Manufacturing Practice
hESCs	Human Embryonic Stem Cells
hiPSCs	Human Induced Pluripotent Stem Cells
HLA	Human Leukocyte Antigen
hMSCs	Human Mesenchymal Stem Cells
HSPGs	Heparan Sulphate Proteoglycans
HUVECs	Human Umbilical Vein Endothelial Cells
IGF-1	Insulin-like Growth Factor-1
INL	Inner Nuclear Layer

IPL	Inner Plexiform Layer
IS/OS	Inner and Outer Segments
ITSFn	Insulin-Transferrin-Selenium-Fibronectin
LIF	Leukaemia Inhibitor Factor
MEFs	Mouse Embryonic Fibroblasts
MFCD	Microfluidic Culture Device
mESCs	Mouse Embryonic Stem Cells
NEAA	Non-essential Amino Acids
NFL	Nerve Fibre Layer
ONL	Outer Nuclear Layer
OPL	Outer Plexiform Layer
OV	Optic Vesicle
PBS	Phosphate Buffer Solution
PC	Polycarbonate
PDMS	Poly(dimethylsiloxane)
PEDF	Pigment Epithelium-Derived Factor
PFA	Paraformaldehyde
PMMA	Poly (methyl methacrylate)
PSCs	Pluripotent Stem Cells
RA	Retinoic Acid
RP	Retinitis Pigmentosa
RPCs	Retina Progenitor Cells
RPE	Retinal Pigment Epithelium
qPCR	Quantitative Polymerase Chain Reaction
Shh	Sonic Hedgehog
TC-PS	Tissue Culture Polystyrene
TGF-β	Transforming Growth Factor Beta
VEGF	Vascular Epithelial Growth Factor
Wnt	Wingless-Int

Chapter 1 Introduction

1.1 Ocular Development and Human Retina

1.1.1 Human Retina Cellular Structure

Vertebrate retina includes seven major classes and by including all the subtypes, it has overall about 55 distinct cell types. (Masland et al., 2001) In adult humans, retinal tissue has limited capabilities to regenerate. Therefore, it is crucial to harness methods in which replacement of these cells are possible in case of damage or degeneration.

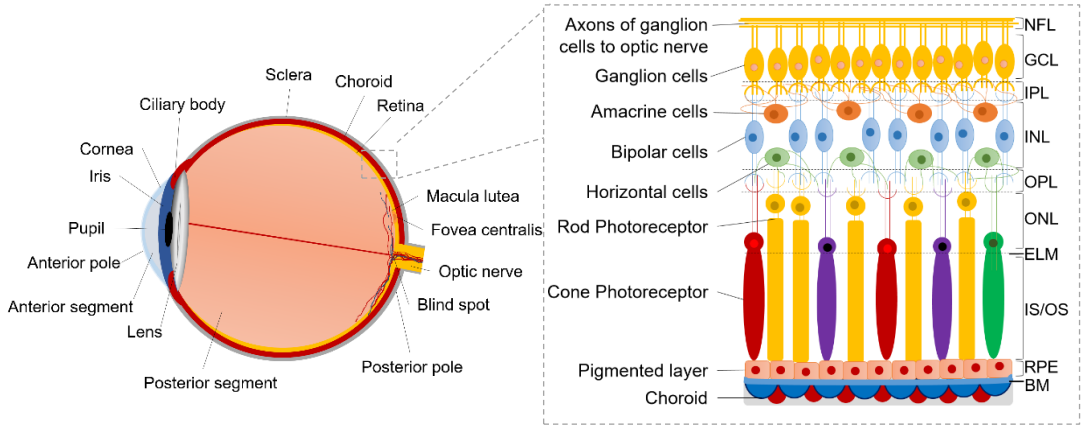

Figure 1.1 Anatomy of the Human Eye and Retinal Cellular Structure.

Retina is the tissue lining in the back of the eye, and it consists of ten distinct layers. From the inside to the back of the eye, the retinal layers are, nerve fibre layer (NFL), ganglion cell layer (GCL), inner plexiform layer (IPL), inner nuclear layer (INL), outer plexiform layer (OPL), outer nuclear layer (ONL), external limiting membrane (ELM), rod and cone inner and outer segments (IS/OS), retinal pigment epithelium (RPE) and basal membrane (BM).

In humans, the retina is a tissue lining on the inner surface of the eye, about 0.56 mm thick in the middle and 0.11 mm at the periphery. It is approximately 30-40 mm in diameter and consist of 10 layers. Going from inside to outside are nerve fibre layer (NFL), ganglion cell layer (GCL), inner plexiform layer (IPL), inner nuclear layer (INL), outer plexiform layer (OPL), outer nuclear layer

(ONL), external limiting membrane (ELM), rod and cone inner and outer segments (IS/OS), retinal pigment epithelium (RPE) and basal membrane (BM). (Kolb et al.,1991) Retina is centred on the fovea, which anatomically is a small pit in the retina tissue. Fovea is believed to have the most acute vision due to concentration of the retinal cones in this region. Central retinal is approximately an area of 6 mm in diameter. Around this point and the surrounding area to this central point is called peripheral retina. (Kolb et al.,1991)

Most vertebrate retinas are made of two synapses layers and three nerve cell layers that include rod and cone photoreceptors, bipolar, amacrine, horizontal and ganglion cells. The synaptic layers are called inner and outer plexiform layer (IPL/OPL) (Fig. 1.1) Photoreceptor cells are neuronal cells and develop as part of the central nervous system (CNS) during embryogenesis. (Heavner et al., 2012) There are three classes of these cells, which are rod, cone and the ganglion cells. Ganglion cells spread much closer to the inner side of the retina and do not contribute to the sight directly but they are found to be involved in the pupillary light reflex (PLR). PLR is involved in adapting the amount of incoming light into the eye by controlling the pupil’s diameter. (Masland et al., 2001)

Rod and cone photoreceptors are closer to the outer layer with pigmented epithelium and choroid. Rod cells are stimulated by minuscule amounts of photons and associated more with sight in the darkness. For example, the reason that colours cannot be seen in the low light conditions is due to activation of the rod photoreceptor cells only. On the other hand, cone cells

are stimulated with much higher number of photons and exist in three different types, short, medium and long according to the wavelength at which they respond to, resulting in the colour vision. (Masland et al., 2001) In the process of vision, photons are first translated into a biochemical signal before turning into an electrical one and travel through the neurons to the brain. In humans, there are approximately about 75-150 million rod cells, 7 million cones and 1.3 million ganglion cells in the retina. (Shepherd et al., 2005)

1.1.2 Retinogenesis in Vertebrates

Retinogenesis or development of the retina starts as part of the central nervous system (CNS) through an interrelated network of molecules in neuroectoderm, surface ectoderm, mesoderm and cells from the neural crest. (Lamba et al., 2008a) After gastrulation stage, a number of patterning events result in the formation of a single group of neuroepithelium in the anterior neural plate. This event is the onset of forebrain development and cells are specified to assume the ocular identity, which is named the ‘eye field’. Following this event, the eye field separates laterally to form the ‘optic vesicle’ (OV) through turning outward on itself. The either sides of the OV extend to form the lens placode, cornea, and conjunctival epithelium by overlaying on surface ectoderm. At this stage, the OV turns inward to form two optic cups, where the inner layer forms the neural retina and non-pigmented ciliary body and the outer layer forms the retinal pigmented epithelium (RPE) and the pigmented ciliary body. The peripheral progenitor cells in the optic cup form the ciliary body itself and the iris. (Fuhrmann et al., 2010) (Fig. 1.2A)

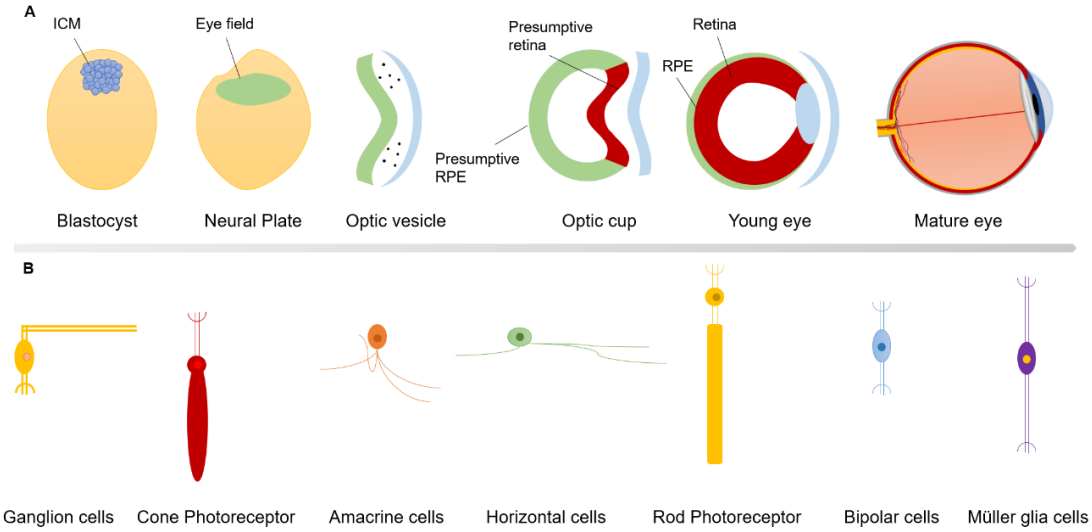

Figure 1.2 Development of the Vertebrate Retina and its Cellular Layers.

(A) Eye field forms after the gastrulation stage and separates laterally and invaginates to form the optic vesicle. Optic vesicle then invaginates to form the optic cup and the presumptive retina. The either sides of the optic vesicle extend to form the lens placode, cornea, and conjunctival epithelium. (B) The cellular development of retina starts with ganglion cells, next are cones and amacrine cells followed by horizontal cells and then rod photoreceptors and finally bipolar cells and Müller glia.

The retinal cells formation starts with ganglion cells, which are the first cells to develop in vertebrate's retina. Next are cones and amacrine cells followed by horizontal cells and then rod photoreceptors and finally bipolar cells and Müller glia. (Fig. 1.2B) (Heavner et al., 2012) However, it must be noted that the onset of the development of one cell type does not mean it follows through to the maturation. In fact, various cellular developmental stages are overlapped and active simultaneously during retinogenesis. Cells that are positioned closer to the central retina are among the first to be born and those lay on the outside are the last. (Meyer et al., 2009)

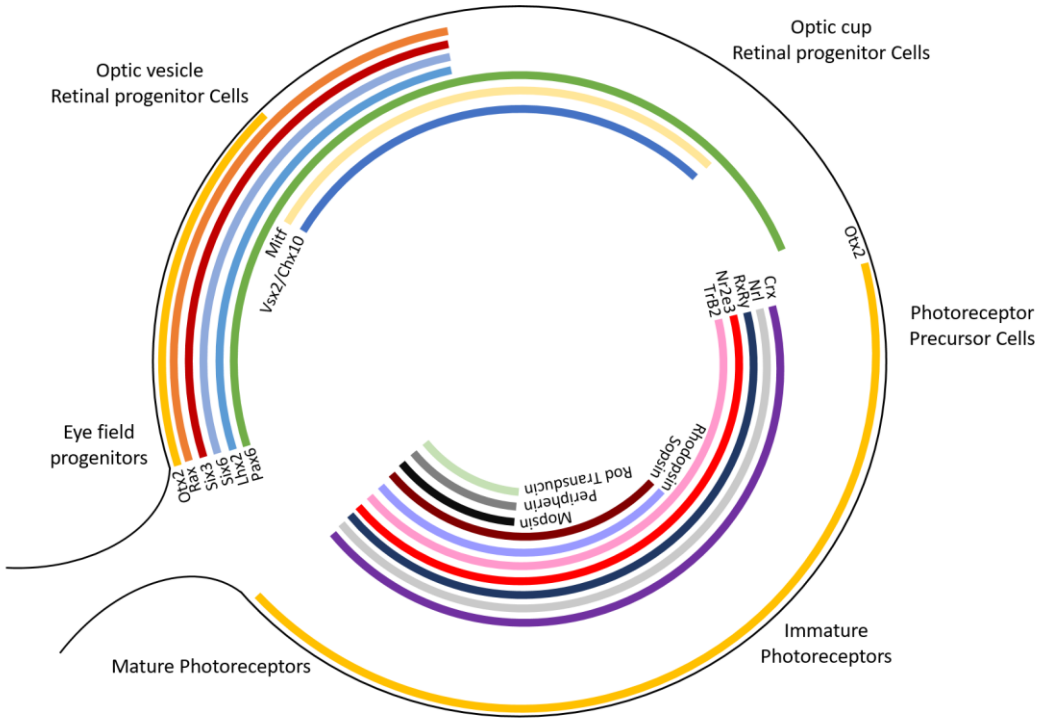

Figure 1.3 Expression of Genes During Various Stages of Retinal Development.

Schematic representation of the transcriptions factors expressed in respect to photoreceptor development. (Starting with eye-field progenitors in clockwise direction.)

1.1.2.1 Role of the Cell Signalling Pathways in Retinogenesis

The molecular mechanisms taking place behind the retinogenesis plays a crucial role in steering the process to a particular cellular lineage. Neural commitment of the cells in the ectoderm is the earliest stage of retinal development. This commitment is regulated by intrinsic production of fibroblast growth factor (FGF) and inhibited by transforming growth factor beta (TGF-β) and Wingless (Wnt) signals. At the start of gastrulation, FGF is secreted to prepare the ectodermal cells for bone morphogenic (BMP) signals while there are low Wnt signals. (Kazanskaya et al., 2000; Hashimoto et al., 2000; Streit et al., 2000; Mukhopadhyay et al., 2001; Linker et al., 2004) BMP is then repressed through secretion of its antagonists, Chordin, Noggin, Follistatin and

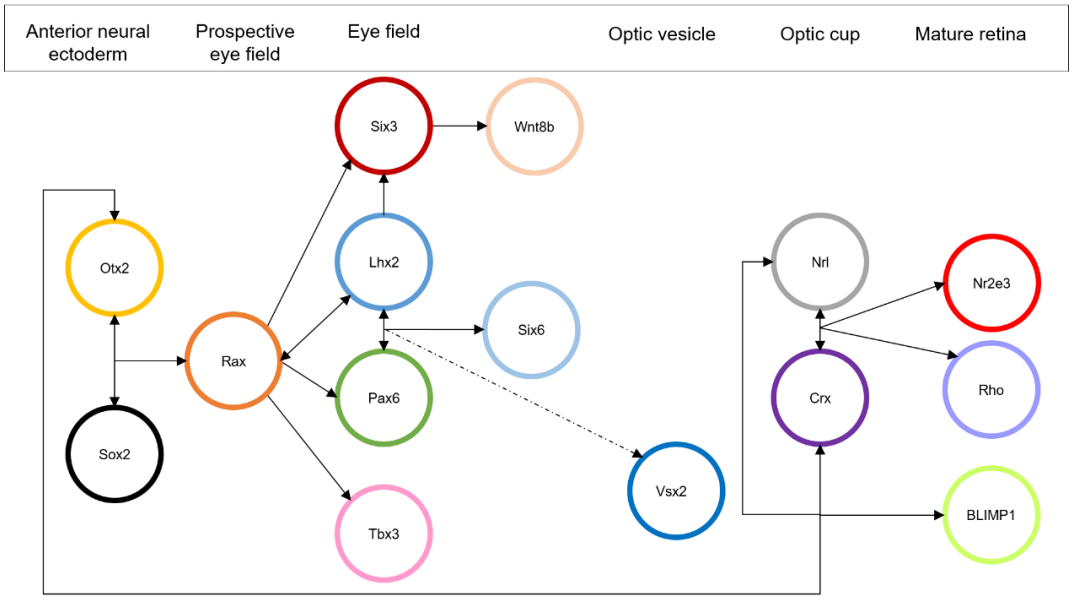

Figure 1.4 Interdependent Network of Transcription Factors During Retinal Development. Co-expression of Otx2 and Sox2, activates the expression of Rax. Rax's expression induces the expression of eye-field transcription factors (EFTFs). Co-expression of Lhx2 and Rax, activates the expression of Six3. Co-expression of Pax6 and Lhx2, upregulates the expression of Six6 and influences expression of Vsx2 and maintenance of the retinal progenitor cells. Expression of Otx2 and Crx induces the expression of BLIMP1 and Nrl. Co-expression of Crx and Nrl activates the expression of Rhodopsin and Nr2e3 in the development of mature photoreceptors.

Cerberus, to preserve the neural fate. (Hemmati-Brivanlou et al., 1994; Bouwmeester et al., 1996) Inhibition of the Wnt signalling pathway through its antagonist Dickkopf-1 (DKK-1) will result in activation of the more dorsal genes in the neural tube. In the absence of the FGF and antagonist signals, ectoderm moves toward posterior neural fate, while the presence of FGF and Insulin-like growth factor-1 (IGF-1) promotes the anterior neural development. (Rogers et al., 2009)

Neural plate is developed through the expression of Sox1 and Gbx2 in the ectoderm. Subsequently, the formation of the eyes from a single eye field is believed to be initiated through the expression of the mesodermal Sonic

Hedgehog (Shh) signals in addition of FGF and TGF-β. (England et al., 2006) Expression of Sox1, Sox2, Nestin, Musashi-1 and N-CAM signals the formation of the neural progenitors in the neural tube. The retinal identity is then formed through co-expression of Otx2 and Sox2 whereby activates the expression of Rax and eye-field transcription factors (EFTFs). (Zuber et al., 2003) EFTFs are a network of interdependent genes that include Rax, Pax6, Lhx2, Six3, Optx2/Six6 and ET/Tbx3. Rax is found to be the regulator of the EFTFs and its expression downregulates the expression of Otx2. (Andreazzoli et al., 2009)

Progression from the eye field to optic vesicle is marked by expression of FGF that represses the expression of the basic helix-loop-helix transcription factor, Mitf. Expression of Mitf leads to the formation of the RPE cells, hence its downregulation allows for expression of the marker Vsx2/Chx10. (Zuber et al., 2003) Vsx2/Chx10 is the earliest retinal specific marker that shows the presence of retinal progenitor cells. Vsx2/Chx10 is essential for proliferation and development of retinal progenitor cells and subsequently the bipolar and Müllar glia cells. However, there is great degree of plasticity in the cells present in the OV, and they still have the ability to become RPE cells if needed. (Rowan et al., 2004; Horsford et al., 2004)

Notch signalling pathway must be repressed by inhibition for development of cone photoreceptors at early stages and at later stages for development of rods. (Yaron et al., 2006) Moreover, Shh can also affect the progenitor

commitment at later stages of Notch pathway. However, the underlying molecular mechanism of Notch inhibition is still unclear. (Wall et al., 2009)

The expression of genes Otx2 and Crx induces the specification of precursor cells towards photoreceptors. Otx2 expression upregulates the other Otx family genes, which in return activates Crx expression for photoreceptor lineage. (Nishida et al., 2003) Crx is initially expressed in early post-mitotic rod and cone photoreceptor precursors and it is required for the differentiation, and development of photoreceptors. (Heavner et al., 2012) Other transcription factors involved in maturation of the photoreceptors are, the PR-domain zinc finger protein 1, BLIMP1 and basic motif leucine zipper transcription factor, Nrl. (Akimoto et al., 2006) Nrl is expressed in rod photoreceptor precursor cells and its expression along with Crx activates expression of Rhodopsin as well as Nr2e3, which induces rod photoreceptor production. (Oh et al., 2007) Nrl's highest expression coincides with differentiation of rod photoreceptors and it will be downregulated through the maturation period. (Peng et al., 2005) Other growth factors such as FGF2, taurine, activin and retinoic acid (RA), are also assist in the maturation of rod photoreceptors and promotion of Rhodopsin. (Rowan et al., 2004; Tucker et al., 2011). (Fig. 1.4)

1.1.3 Retinal Degeneration

Progressive photoreceptor degeneration often leads to blindness and is the underlying cause of many retinal degenerating diseases. It has been reported that 50% of ocular conditions resulted in blindness are due to photoreceptor degeneration. (Bunce et al., 2010) Degeneration of the retina is caused either directly — conditions that affect the photoreceptors — or indirectly —

conditions that affect other parts of the eye but result in loss of function in photoreceptors. Conditions that affect the retina directly could be due to genetic defects or age related. Among such are conditions like, retinitis pigmentosa (RP), choroideremia, Leber Congenital Amaurosis, Stargardt disease and Ushers disease. Other conditions such as age-related macular degeneration (AMD), glaucoma, diabetic retinopathy and retinopathy of prematurity, are affecting the retina indirectly resulting in compromising function of cells in the retina. (Taylor et al., 2005; Hartong et al., 2006; Minassian et al., 2011; Owen et al., 2012)

Retinitis pigmentosa (RP) is a hereditary condition caused by various genetic mutations in the retinal cells. So far most of the defected genes involved are of rod photoreceptors, however, other cells such as cone photoreceptors and retinal pigment epithelium are also affected by this condition. (Jayakody et al., 2015) During the course of the RP, the rod cells in the outer periphery of the retina start to degenerate and causes nyctalopia or night blindness. Degeneration of these cells also causes the tunnel vision, as patients will lose their peripheral vision. Ultimately, this can lead to blindness and it has been observed even from early ages in childhood. Pathologically, this appears as black pigments in the peripheral retina and also blood vessels at the optic nerve head are reduced in thickness. (Hartong et al., 2006)

Age-related macular degeneration (AMD) is the leading cause of blindness in the developed countries. As the name suggests, it is most observed in an aging eye, however, both genetic and environmental factors are involved in this condition. (Jayakody et al., 2015) AMD is diagnosed by the accumulation

of the extracellular materials in white or yellowish spots called *drusen* around the macular region in the back of the eye. Drusen is a result of the degeneration of the pigmented epithelium, which will cause the macular area in the fovea to degenerate and result in loss of the central vision. (De Jong et al., 2006) Macula is mostly populated with cone-photoreceptors and these cells are affected the most in AMD. However, the effects of the degeneration spread to the rod cells as well. AMD appears in two forms of dry and wet AMD. In the former, slow death of the photoreceptors is observed in the macular regions. However, the latter is associated with a much faster loss of vision often due to the formation of the new vessels into the Bruch's membrane and the RPE layer. (Jager et al., 2008)

Glaucoma is also an age-related condition where eye pressure is raised due to the failure of the normal in/outflow of fluid in the anterior chamber of the eye. This condition causes the blood vessels at the optic nerve to be compromised and lead to the death of the ganglion cells. (Nivison et al., 2017)

Diabetic retinopathy results as part of the diabetes and leads to uncontrollable proliferation of the blood vessels in the eye. This condition leads to leakage of the blood into the retina, hence causing damage to the photoreceptors as well as the RPE layer. In extreme cases, this can cause retinal detachment and growing vessels in the anterior chamber of the eye, which can lead to neovascular glaucoma. (da Cruz et al., 2007)

1.1.4 Current and Potential Treatments for Photoreceptor Dystrophies

The mature retina in humans has very limited ability to regenerate all retinal cells after the embryonic stage, which raises serious concerns in case of damage or conditions that affect this tissue lining. Current therapeutic solutions for treating the retinal disease include neuroprotectants, administration of antiapoptotic and anti-inflammatory agents. However, these treatments only slow down the disease progression and do not provide a cure for such conditions. (Jayakody et al., 2015)

In recent years, antiangiogenic agents such as anti-vascular epithelial growth factor (VEGF) has been used for the treatment of wet AMD. Other solutions include the use of anti-apoptotic agents such as neurotrophic agents. (Schlichtenbrede et al., 2003) Agents such as pigment epithelium-derived factor (PEDF) and ciliary neurotrophic factor (CNTF) have shown promising results in maintenance of the photoreceptors. However, due to short half-life, they require repeated administration. (Rhee et al., 2013) In case of the disease with underlying genetic disorders, gene therapy treatments have shown to be effective in animal models, however, before they can be used in humans larger and extended clinical trials are required. (Smith et al., 2011)

In patients with RP and atrophic AMD, it was found that more than 80% of bipolar and ganglion cells as well as the neuronal structure, remains untouched. (Santos et al., 1997; Mazzoni et al., 2008) This finding provided the grounds for alternative therapies such as cellular transplantation that could replace the lost photoreceptors or provide restructuring of the neuronal network for signal transduction.

One of the downsides of the cell replacement therapies is the rejection of the transplanted cells by the host, which may lead to long-term usage of the immune-suppressants and other undesired complications. In order to overcome this, patient's own cells are usually used, however, autologous cell sources are often very limited and will result in donor site morbidity. Alternative solution is to use other donors with (human leukocyte antigen) HLA-matched or very closely related to the individual. It must be noted that these methods are not feasible and not readily available for all patients. (Pearson et al., 2014)

Advances made in the field of stem cells research by Yamanaka (2006) in reprogramming fibroblasts to induced pluripotent stem cells (iPSCs), provided an unending source of pluripotent stem cells that could be used for cell therapy treatments. (Takahashi et al., 2006) Induced pluripotent stem cells (iPSCs) obtained from adult dsRed-mouse dermal fibroblasts have shown the capability of differentiating into retinal photoreceptor precursors once they are transplanted in the sub-retinal space. (Lamba et al., 2008b, 2010) Maclaren and colleagues demonstrated that postnatal post-mitotic photoreceptor precursors that express both markers Crx and Nrl can successfully integrate into the mice retina and form functional photoreceptors. (Maclaren et al., 2006) Results from various transplantation studies have shown that developmental stage of donor cells is crucial to their integrational capabilities into the host retina. Moreover, number and purity of the transplantable cell population are also crucial in increasing efficiency of their integration into the host retina. (Banin et al., 2005; Lamba et al., 2010; Tucker et al., 2011; Zhou et al., 2011; West et al., 2012; Gonzalez-Cordero et al., 2013) Therefore, optimisation of

differentiation protocols for hiPSCs in a more robust, consistent and efficient manner will be critical in providing a transplantable cell population.

1.1.4.1 Routes to Clinic: Current Clinical Trials Using Cell Therapy for Retinal Degenerating Conditions

Advances made in generation of stage-specific retinal cells from PSCs and *in vivo* proof of concept studies in demonstrating restoration of visual function using these cells, paved the way for progression to clinical studies in human subjects. (Banin et al., 2005; Lamba et al., 2008b, 2010; Tucker et al., 2011; Zhou et al., 2011; West et al., 2012; Gonzalez-Cordero et al., 2013) However, there are numerous challenges that must be overcome before we can see cell therapies used in clinics. Despite extensive research and existing knowledge about the role of intrinsic and extrinsic factors involved in photoreceptor differentiation and maturation of these cells, there are still large gaps in understanding of how these factors function and affect cells at each stage of development. (Barber et al., 2013) Upon transplantation of the newly donated cells into the host retinal, the remaining retinal cell network undergo changes to accommodate the transplanted cells. How these changes affect the visual function post-transplantation is still unclear. (Lakowski et al., 2011)

Use of ESCs as the cell source for production of retinal cells raises few challenges in terms availability, ethical concerns and most importantly, the chance of immune response and rejection by the host cells. Use of human leukocyte antigen (HLA)-haplotype matched cells for donated ESCs and iPSCs, is necessary to ensure successful transplantation of these cells. (Pearson et al., 2014) Optimisation of the current retinal differentiation

protocols is necessary before they can be used in clinical applications. As such are use of xeno-free components in generation, purifying and storage of the precursor cells under GMP compliant conditions. (Sridhar et al., 2013; Tucker et al., 2013)

Translating lab scale differentiation protocols to large scale productions for clinical studies poses many challenges in maintaining quality control during development and cryopreservation of the cells at the desired stage of development. (Nakano et al., 2012; Zhong et al., 2014) Development of accurate purification strategies for selection of the homogenous cell population is another challenge in large scale production. Currently cell surface antigens, CD markers, in rodent models have been identified for some of the photoreceptors such as rod photoreceptors. However, if the same markers can be used for human cells is still under investigation. (Eberle et al., 2011; Lakowski et al., 2011) Dosage, type and mode of administration of these cells are also dependant on the patient's condition and must be evaluated by the surgeons prior to transplantation. (Trounson et al., 2015)

In reported clinical trials for retinal dystrophies, RPE cells were among the first trials performed using both hESCs and hiPSCs. Replacement of the cells in the RPE layer appeared to be less complex than photoreceptors in inner layers of the retina. Initial studies reported by Schwartz et al., for safety of injection of hESC-derived RPE cells shown promising results. Patients with Stargardt disease and wet-AMD were treated in these trials where they received doses of 50,000, 100,000, 150,000 and 200,000 cells. No adverse condition was reported relating to the transplanted cells, however consequent studies are

still in progress and the final results are yet to be reported. (Schwartz et al., 2012, 2015).

Since then, there has been several other clinical trials for treatment of retinal conditions, addressing both wet and dry AMD, Stargardt disease, Retinitis pigmentosa and Retinal vascular occlusion (Table 1-1). Currently, clinical trials for progenitor photoreceptors are in preclinical stage, and therefore the final clinical dose size, efficacy, safety and mode of adminstration is still unknown. As summarised in table 1-1, various cell types are currently being used to treat retinal degenerating conditions, which includes pluripotent stem cell-derived retinal RPE (from both hESCs and hiPSCs), neural and retinal progenitor cells and also other cell sources such as Umbilical tissue-derived stem cells, mesenchymal and hematopoietic cells. Most of the trials performed, using subretinal transplantation as mode of delivery, specially for replacement of RPE cells. However, in trials addressing retinitis pigmentosa, intravitreal injection is used mostly to avoid focal detachment of the retina and therefore minimise damage to host photoreceptors. (Klassen et al., 2015)

Table 1-1. Clinical Trials Registered with the FDA or Japanese Ministry of Health on Using Cell Therapy for Treatment of Retinal Degenerating Conditions.

The following table includes those studies initiated or completed as of August 2017. AMD: Age-related macular degeneration; BMDSC: Bone marrow-derived stem cell; RPC: Retinal progenitor; RVO: Retinal vascular occlusion; SD: Stargardt's disease; UTSC: Umbilical tissue-derived stem cell.

No.	Sponsor/Collaborators	Cell Source	Conditions	Phase	Location	Identifier
1	Astellas Institute for Regenerative Medicine	ESCs	SD	I/IIa	Subretinal	NCT01345006
2	Astellas Institute for Regenerative Medicine	ESCs	AMD (dry)	I/IIa	Subretinal	NCT01344993
3	Astellas Institute for Regenerative Medicine	ESCs	SD	I/IIa	Subretinal	NCT02445612
4	Cell Cure Neuroscience	ESCs	AMD (dry)	I/IIa	Subretinal	NCT02286089
5	RIKEN	iPSCs	AMD (wet)	I	Subretinal	UMIN000011929
6	Stem Cells, Inc.	NSCs	AMD (dry)	I/IIa	Subretinal	NCT01632527
7	Stem Cells, Inc.	NSCs	AMD (dry)	IIb	Subretinal	NCT02467634
8	jCyte	RPCs	RP	I/IIa	Intravitreal	NCT02320812
9	jCyte	RPCs	RP	II	Intravitreal	NCT03073733
10	Centocor/Janssen	UTSCs	RP	I	Subretinal	NCT00458575
11	Centocor/Janssen	UTSCs	AMD (dry)	I/IIa	Subretinal	NCT01226628
12	University of Sao Paulo	BMDSC	RP	I	Intravitreal	NCT01068561
13	University of Sao Paulo	BMDSC	RP	II	Intravitreal	NCT01560715
14	University of Sao Paulo	BMDSC	AMD, SD		Intravitreal	NCT01518127
15	University of California, Davis	HSC	RP, SD, AMD, RVO	I	Intravitreal	NCT01736059
16	Red de Terapia Celular	BMDSC	RP	I	Intravitreal	NCT02280135
17	Mahidol University	MSC	RP	I	Intravitreal	NCT01531348
18	Chaitanya Hospital	BMDSC	RP	I/II	unknown	NCT01914913
19	Al-Azhar University	BMDSC	AMD (dry)	I/II	Intravitreal	NCT02016508
20	CHABiotech	ESCs	AMD (dry)	I/IIa	Subretinal	NCT01674829
21	Federal University of São Paulo	ESCs	AMD, SD	I/II	Subretinal	NCT02903576
22	Chinese Academy of Sciences	ESCs	AMD (dry)	I	unknown	NCT03046407
23	Southwest Hospital, China	ESCs	AMD, SD	I	Subretinal	NCT02749734
24	Regenerative Patch Technologies, LLC	ESCs	AMD (dry)	I/II	Subretinal	NCT02590692
25	Pfizer/University College London	ESCs	AMD (wet)	I	Subretinal	NCT01691261
26	ReNeuron Ltd.	RPCs	RP	I/II	Intravitreal	NCT02464436

1.2 Human Pluripotent Stem Cells

Human embryonic stem cells (hESCs) are derived from the inner cell mass of the human embryos at the blastocyst stage of the embryonic development. These cells have the potential to differentiate to all cell types in the germ layers. They also have the capacity to replicate indefinitely and maintain their pluripotency for a prolonged period. (Hiyama et al., 2007) *In vivo,* the inner cell mass will lose its pluripotent abilities upon implantation in the uterus, however, this process can be avoided by removing these cells *in vitro* and maintaining them under desired conditions. (Cai et al., 2003)

The first attempt to derive hESCs were made during the 1980s, however it wasn't until 1998 that these cell lines were established. (Thomson et al., 1998) The embryonic stem cells are usually cultured on a layer of the mouse fibroblasts that are inactivated and form adherent colonies on top of these cells. Each colony typically holds about three to four thousand cells. Other methods have also been developed to culture these cells in suspension, feeder-free and xeno-free media to prevent the risk of introducing potential pathogens into the human cells. (Hoffman and Carpenter, 2005) There are also various methods in development to use human feeder cells instead of the mouse cells, which can reduce the risk of introducing mouse pathogen into these cells. However, with human originated feeder cells the risks of pathogens still remain. (Reubinoff et al., 2000)

Due to properties of the embryonic stem cells, they can provide an unprecedented potential in treating degenerative disease. They can also be used for drug safety tests, efficacy research and to understand physiology of

different body tissues. This opportunity provides us with more effective and safer treatments across the medical field. (Chen et al., 2014) However, before stem cells can be used in cell-based therapies, there are a number of challenges that need to be addressed first. For example, at the moment the efficiency of growth of a single hESCs into a full colony is less than 1% in comparison to the mouse cells. (Puri et al. 2012) Another challenge is concerned with karyotypic changes of hESCs once they have been cultured for extended time or high passage numbers, which is dependent on the culture conditions and methods. (Chen et al., 2014) There are also concerns regarding the stability of the epigenetically modified genes in different culture conditions and other challenges in the purification of the differentiated hESCs before transplantation to avoid the formation of teratomas. (Hoffman and Carpenter, 2005)

1.2.1 Human Induced Pluripotent Stem Cells (hiPSCs)

In 2006 Shinya Yamanaka and his colleagues from the Kyoto University reported that they have successfully reprogrammed mouse fibroblast cells by use of retroviruses of Oct4, SOX2, c-Myc, and Klf4 genes. After 3-4 weeks, these cells showed similar morphology to pluripotent embryonic stem cells. (Takahashi & Yamanaka et al., 2006) These cells were selected using Fbx15+ cells against antibiotic, which showed not to be the best method for selecting the pluripotent cells. These cells were unable to produce egg and sperm cells once they were seeded into a blastocyst, had DNA methylation errors and were unable to make viable chimeras. Moreover, this method included use of c-Myc, which raises concern regarding its oncogenicity. (Liu et al., 2008)

In June 2007, Yamanaka's group along with Rudolph Jaenisch from MIT and another group from University of California showed improvements in a selection method of iPS cells by replacing Fbx15+ to Nanog. The latter also proved the importance of Nanog in pluripotency of ESCs. In this method, the DNA methylation was corrected and viable chimeras, as well as proliferation of sperms and eggs, were achieved. However, c-Myc was still used in their protocol. (Takahashi et al., 2007)

Finally, in November 2007, two groups, Yamanaka and Thomson released results of showing successful production of iPSCs from human fibroblasts. Yamanaka used the previous method tried on mouse models, but Thomson used lentiviral for the following genes of OCT4, SOX2, NANOG, and LIN28. (Yu et al., 2007)

In terms of morphology, hiPSCs are very similar to hESCs, they are round and have a large nucleus and small cytoplasm, and they form colonies similar to that of hESCs. Their growth rate and mitotic division are compatible with hESCs and express all the specific surface markers of TRA-2-49/6E, TRA-1-60/81, SSEA-3/4. In terms of the nuclear expression markers they express Oct-3/4, Sox2, Nanog, GDF3, REX1, FGF4, ESG1, DPPA2, DPPA4, and hTERT. (Puri et al., 2012) hiPSCs also shown similar differentiation patterns to hESCs in various differentiation routes such as neuronal and cardiac. Formation of the embryoid bodies and teratomas are also identical in both cell types as well as demethylation of the promoters, DNA, and histones, which results in expression of similar markers in the cell. (Bilic et al., 2012)

Differences between hiPSCs and hESCs come down to genetic stability and copy number variations of the hiPSCs in prolonged cultures. Nonetheless, hiPSCs has shown the capacity for replacing the need for the histocompatibility matching as they can be originated from the patient itself. Therefore, providing unending source of stem cells specific to each patient. (Bilic et al., 2012) It has been reported that specific hiPSC lines maintained their 'epigenetic memory' from their somatic state, which can be used as a differentiation bias in using tissue-specific hiPSCs for cell therapy treatments. (Kim et al., 2010)

1.2.1.1 Requirements for Using hiPSCs in Clinical Applications

In order to realise full potential of hiPSCs in clinical applications according to good manufacturing practice guidelines, animal components must be removed from all steps of their derivation, culture and differentiation. Early methods developed in culture of hESCs were adapted from mouse ESC cultures where leukaemia inhibitory factor (LIF) was used to maintain pluripotency of the cells. (Evans et al., 1981) However, it wasn't long before it became clear that hESCs cannot maintain their pluripotency in presence of LIF alike mouse cells and addition of feeder cells such as mouse embryonic fibroblasts (MEFs) will be necessary. (Williams et al., 1988) MEFs assist hESCs by providing them with essential molecules for their self-renewal. Among such are growth factors and cytokines, as well as extracellular matrice (ECM) components such as transforming growth factor β, activin A, laminin-511, and vitronectin. (Hongisto et al., 2012) However, secretion of large number of factors by these cells into the culture, makes it difficult to understand mechanisms in which these

molecules contribute to the maintenance of pluripotency of hESCs. (Eiselleova et al., 2008) Moreover, use of deactivation methods such as γ-irradiation or mitomycin-c will produce apoptotic factors that could produce unknown effects on hESCs culture and pluripotency. (Villa-Diaz et al., 2012) Other xenogeneic components such as animal serum replacements increase the risk of introducing pathogens into recipients upon transplantation as well as increased chance of immune response and rejection. (Mallon et al., 2006) There are also other methods in development to use human feeder cells instead of the mouse cells, which can reduce the risk of introducing mouse pathogen into these cells. However, with human originated feeder cells the risks of pathogens still remains. (Reubinoff et al., 2000; Stacey et al., 2006)

Initial attempts to produce feeder-free hPSCs used extra cellular matrices (ECM) such as Matrigel™ along with MEF-conditioned medium. (Xu et al., 2010) However, Matrigel™ also contains unknown animal components as well as having a well-known batch-to-batch variability. (Villa-Diaz et al., 2012) The fact that integrins are the main cell surface receptors mediating cell-ECM interactions lead to use of vitronectin, which has shown to support self-renewal of the hESCs via integrin αVβ5. (Braam et al., 2008) Laminin-511 is also another component of Matrigel™ which contributes to maintenance of pluripotency in hESCs. E-cadherins also separately shown an important role for maintenance of pluripotency in hESCs. (Derda et al., 2007) Therefore, use of the recombinant human (rh) laminin-511, rh vitronectin, and rh E-cadherin as an ECM in the culture of hESCs could provide the first alternatives to feeder cells and the start of defined and xenogeneic-free culture conditions.

Large-scale expansion of hPSCs for clinical applications require chemically defined components that are GMP compliant. Development of feeder-free hPSCs cultures using biological molecules as ECM as mentioned previously, can still introduce higher degree of variabilities into the culture and create more challenges during large-scale manufacturing processes. (Brafman et al., 2010) Among such are, degradation of these molecules during long-term cultures, which can create lot-to-lot variability, scalability limitations and as a result, higher manufacturing costs. Use of synthetic alternatives that could produce similar results and be more durable to manufacturing processes could provide a solution to such problems. (Irwin et al., 2011)

1.2.2 Stem Cell's Niche

The stem cell niche refers to a network of intrinsic and extrinsic factors that influence stem cells' fate. (Moore et al., 2006) Intrinsic factors include transcription factors, growth factors and molecular mechanisms. The extrinsic factors are environmental stresses, extra-cellular matrix (ECM) components (such as collagen, elastin, hyaluronic acid as well as topographical patterns), soluble factors (growth factors, peptides, hormones, proteases, morphogens and cytokines) and cell-cell interactions (juxtacrine, paracrine and endocrine signalling). Furthermore, environmental stresses include oxygen tension, pH variations, and mechanical forces. The latter can be further separated into various types such as stretch, strain, compression, and shear stress. In this section, we look at the effects of two most related environmental cues to this work, which are soluble factors and fluid flow.

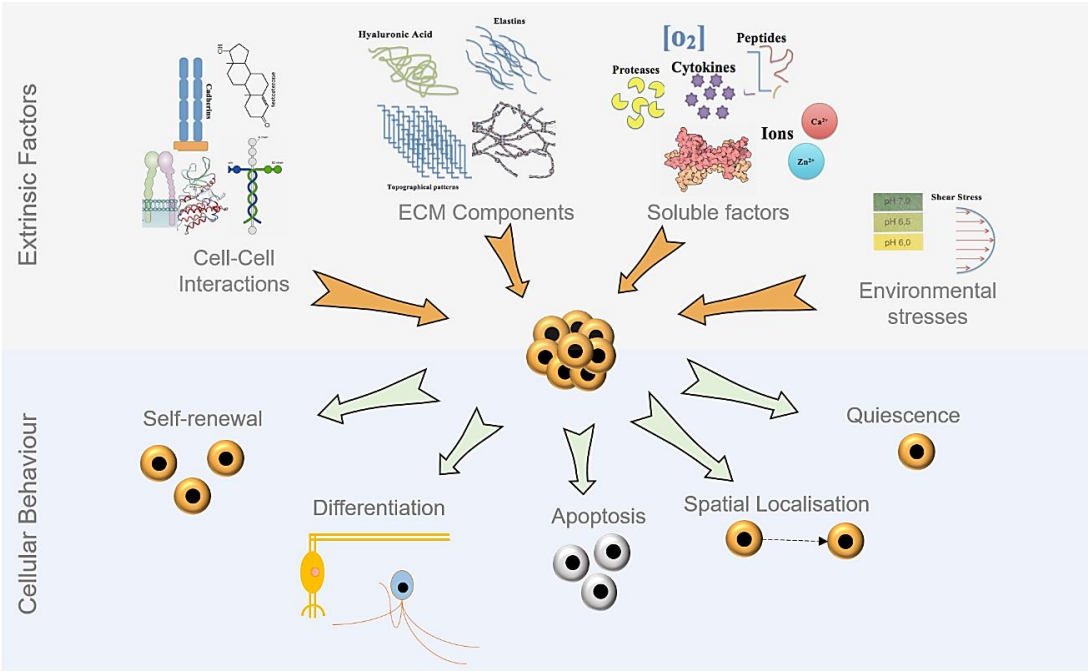

Figure 1.5 Extrinsic Factors That Influence hiPSCs Behaviour.

The environmental cues influencing the stem cells behaviours. The main cellular responses could be, quiescence, self-renewal, differentiation, spatial localisation and apoptosis.

1.2.2.1 Effects of Soluble Factors on Stem Cells' Fate

Soluble factors include nutrients such as glucose, glutamine and amino acids required for cellular survival as well as extrinsic factors secreted by the cells as part of the cell-to-cell interaction. Soluble factors have shown to influence behaviour of the stem cells toward self-renewal (e.g. the use of leukaemia inhibitor factor (LIF) in mouse embryonic stem cells or FGF2 for hESCs) or differentiation. (Hazeltine et al., 2013) The concentration gradients present in the cellular environment shown to have optimal effects on stem cells behaviour. (Titmarsh et al., 2012) Other influences of concentration gradients include pluripotent sub-states differences and reduction of heterogeneity in PSCs by using small molecule inhibitors. (Blauwkamp et al., 2012; Marks et al., 2012; Hazeltine et al., 2013) One of the major contributors to the high

production costs are soluble factors. Factors such as seeding densities and co-culture with other cell lines have also shown to be critical in process development optimisation. (Serra et al., 2012; Cigognini et al., 2013)

1.2.2.2 Fluid Flow

Other key forces inherent to the bioprocessing of stem cells are the effects of fluid flow and the shear stress. The introduction of the fluid flow affects the culture conditions such as pH, oxygen, and nutrient delivery. Depending on the flow rate, it also can influence signalling pathways and gene expression. High flow rates result in washout of nutrients and cells in continuously perfused cultures. (Korin et al., 2008, 2009) At high flow rates, effects of shear stress on the cells can also influence stem cell differentiation. (Yamamoto et al., 2004; Stolberg et al., 2009; Toh et al., 2011; Nsiah et al., 2014) Therefore, it is essential to further understand how these forces affect the culture and differentiation pathways.

With the cardiovascular system being the earliest working system in the embryos, fluid flow becomes a major player in later stages of embryogenesis. Formation of the angioblast from differentiation of embryonic stem cells to endothelial cells is governed genetically at the initial stages of development. At this stage embryogenesis, there is no blood flow as such, although there are other fluids such as interstitial fluids. It has been reported that venous and arterial gene expressions are detected before any vessels formed in the embryo. (Wang et al., 1998; Jones et al., 2006) Vascular precursors are created in the embryo and the extra-embryonic yolk sac of the mouse at around days 7.5–8 of embryogenesis. Study of the laminar blood flow at this

stage shown that shear stress of approximately 0-5.5 dynes/cm^2 is present around days 8.5–10.5 of the embryogenesis. (Ema et al., 2003; Jones et al., 2004)

The earliest sign of fluid flow presence during the embryogenesis is in gastrulation in the formation of the spatial orientation of the embryo. It was discovered that in mice, rotation of the primary cilia in the node creates a fluid flow that determines the left and right axis orientation in the embryo. (Nonaka et al., 2002) For example, this rotatory motion results in one organ such as heart to be on the left and liver to be on the right. Although there isn't any evidence of the amount of shear stress created by this fluid flow, it is evident that embryos use this force to complete a crucial stage of their development. (McGrath et al., 2002; Cartwright et al., 2004)

Primary cilia have shown the ability to sense shear stress as well as generating fluid flow. The primary cilia are reported to be present in three human Embryonic Stem Cell (hESC) lines H1, H9, and LRB003 as well as in Human Umbilical Vein Endothelial Cells (HUVECs). (Kiprilov et al., 2008) However, in the case of HUVECs, they do not appear after passage twelve and also when exposed to more than two hours of shear stress, they will disassemble. (Iomini et al., 2004) A study of the blood flow patterns in a chick embryo yolk sac showed that specification of the venous or arterial vessels had been proven to be affected by the shear stress resulted from blood flow. However, it is still unclear if this is a result of mechanical fluid flow or biochemical imbalances like oxygen tension. (Noble et al., 2003)

Mechanotransduction is referred to the process that cells translate physical forces into biochemical signals, which it will lead to a cellular response. (Merryman et al., 2009) Several studies on mapping deformations happening inside of Endothelial Cells (ECs) resulted from fluid shear stress show that shear stress experienced at the bottom of the cell surface are much higher than the forces exerted on the luminal side. However, understanding how cytoskeletal strain is linked with shear stress and how it can be fully mapped is far more complex than it is originally expected. (Helmke et al., 2003; Huang et al., 2004)

The critical amount of the shear stress required to initiate a response for various types of biological responses measured is approximately about ~1 Pa (0.1 dyne/cm^2). This has been measured over an area of 1,000 μm^2 of the entire apex of an EC, which can generate a force of about 1 nN. (Huang et al., 2004) The ways in which fluid flow affects the membrane fluidity are not quite clear. However, measurement of changes in the lateral diffusion coefficient of membrane lipids in response to a short 10s shear stress of 1 Pa, has shown that response to changes in shear stress is dependent on the methods of increasing it. A step-wise increase of shear has shown to result in an increase in diffusion coefficient where flow meets the membrane and a decrease on the opposite side of the cell. However, if shear is increased in a ramp fashion, diffusion coefficient will decrease all throughout the cell. (Haidekker et al., 2000; Jalali et al., 2001; Butler et al., 2001, 2002)

Fluid flow has been studied extensively in ECs as an important part of their function and endothelial differentiation of stem cells. Studies have shown that

ECs have the ability to detect fluid flow in their microenvironment and respond to various types of shear stresses accordingly. (Barakat et al., 2003; Resnick et al., 2003) ECs have shown that they are more adaptable to laminar flow over time and respond rapidly at the beginning of exposure to fluid flow. When initial adaptations to fluid flow have completely taken place after 24 hours, a new behavioral profile starts to emerge that can be categorized to long-term or short-term exposures to fluid flow. (Wasserman et al., 2004, 2002; Matthews et al., 2006)

Conventional culture setups lack the complexity and accuracy to imitate the endogenous cell culture environment and it has been a challenge for the research and industrial community to provide ever closer culture environment, for stem cells differentiation. (Cigognini et al., 2013) Deeper understanding of the stem cells' behaviour during differentiation is dependent on their niche and our capabilities to control it, which in turn, enables us to provide cells that could integrate into the host tissue and function more effectively. (Discher et al., 2009)

1.2.3 Retinal Differentiation Protocols for Pluripotent Stem Cells

In general, there have been two different approaches for differentiation of pluripotent stem cells. First one is the conventional 2D culture using cells in a monolayer and second one is the 3D approach in using cellular aggregates such as embryoid bodies (EBs). Initial efforts to produce retinal cells included using retinoic acid (RA) or insulin-transferrin-selenium-fibronectin (ITSFn) and bFGF to start with and finalised by co-culture with postnatal retinal cells. (Zhao et al., 2002) Next, Watanabe improved the efficiency of the telencephalic cells

by 15%, using a serum free EB system and addition of Wnt and Nodal antagonists, DKK1 and LeftyA to the differentiation medium. (Watanabe et al., 2005) In following efforts, the latter and addition of 5% serum and activin-A used to guide cells toward expression of Rax and Pax6 in the cell population (Ikeda et al., 2005) This protocol resulted in 26% of the cell population to be retinal progenitor cells (RPCs) and capable of differentiating into Crx positive cells. Lamba *et al*. in the following year used Wnt and BMP antagonists, DKK-1 and Noggin, along with IGF-1 and bFGF on Matrigel™ to produce 80% RPCs population with 12% Crx positive photoreceptor precursors in only three weeks' culture. (Lamba et al., 2006)

One of the downsides of Lamba's protocol is the use of Matrigel™ as the ECM. It is known that there are a number of growth factors in Matrigel™ that has not been identified. Moreover, there are animal components in this ECM that makes it unusable for clinical applications. (Villa-Diaz et al., 2012) Osakada in 2008 and 2009 developed a protocol using a serum free EB system along with Lefty A, along with γ-secretase inhibitor and DAPT on coatings of poly-D lysine/laminin/fibronectin. Furthermore, in later stages, FGF1, bFGF, taurine, Shh, and RA were also added to the media to improve photoreceptor maturation. This protocol resulted in 17% of the population to express Rhodopsin. (Osakada et al., 2008, 2009)

Meyer developed a rather interesting protocol by not using any growth factors but changing the culture condition from suspension to adherent and suspension again. In his work, a 2D culture was used in suspension first then plated on laminin to form neural rosettes, and then the rosettes were isolated

and transferred to suspension again to produce RPC population that were Crx positive. (Meyer et al., 2011) However, the protocol takes 80 days to develop Crx and Recoverin positive populations. Eiraku also used a mostly growth factor-free culture with growth factor reduced Matrigel™ in suspension to form optic cup structures in just one week. However, after 35 days, there were lack of neural integrity observed in the cell population. Eiraku reported that combination of intrinsic factors and the physical forces are the key regulators of the retinal differentiation in their work. (Eiraku et al., 2011) Later, the optic cup structures were separated and cultured to form morphologically identical structures to postnatal retina including all the cells types in the mature retina. The only growth factors used in this work were RA and taurine between day 10 and 14 of the culture. (Eiraku et al., 2011)

More recently, Ali and colleagues developed a protocol for generating RPCs from ESCs and iPSCs, in which EBs were cultured on Matrigel™. In this protocol neuroepithelia vesicles formed as early as day 2 of the culture and markers such as Crx and Nrl were expressed after 30 days. However, the neuroepithelia vesicles were not stable during the culture and disappeared very quickly. (Boucherie et al., 2012) Zhong et al. demonstrated formation of the photoreceptors could be independent of the RPE layer. In this work, combination of Meyer and Eiraku's protocols were used by adding growth factor reduced Matrigel™, RA and taurine. (Zhong et al., 2014) Finally, Reichman demonstrated development of RPE and neuroepithelial structures under simple neuralising conditions in only three weeks. (Reichman et al., 2014)

1.2.4 Bioprocessing Challenges for Producing Clinically Relevant Cells

One of the main processing challenges in using stem cells is the number of variations that exists in differentiation protocols. (Serra et al., 2012) Generally, in processing systems, the key input variables are identified and controlled to make sure a repeatable process can be maintained while a specific product is produced. Increased number of variations in the process, as well as degree of control that can be applied to them, is not desirable in good manufacturing practice (GMP). (Thomas et al., 2008) Key process inputs can be categorized into two groups, one being statistically controlled and the other, with high statistical variations. However, in bioprocessing of ESCs for producing target cells, variations exist in every level of production from isolation and expansion of the cells to their differentiation, purification, packaging and their delivery to clinics. (Abu-Absi et al., 2010)

Other challenge includes the time it takes for some differentiation processes to complete. For example, we saw that the shortest protocol for retinal differentiation were up to three weeks, others stretch up to 200 days. Neuronal differentiation also takes up to 10 weeks and in the case of cardiomyocytes could be even longer. The challenge here is to maintain those culture conditions and process inputs in a stable format. In a differentiation culture, the key process inputs include, ECM, soluble factors, physiochemical factors such as pH, oxygen concentration and finally physical parameters such as low shear rates and uniform fluid flow. To maintain these parameters, monitoring systems are needed to measure and report values of these parameters accurately. Moreover, control systems are needed to have in place to adjust

and maintain these parameters in the required range for each specific process. (Placzek et al., 2008)

Choice of autologous or allogeneic cell therapies can also make a big difference in terms of process development, GMP burden and system automation. Risk of cross contamination also must be accounted for in each system. (Kirouac et al., 2008) Autologous cell products have the advantage of being patient specific and pose lower chance of rejection post transplantation. However, they raise greater challenges during manufacturing processes especially when a large number of patients need the therapy. The opposite is true for the allogeneic cell products where the bioprocessing steps can be unified and be more economic. Other challenges regarding the autologous cell therapies include the source of the cells as the starting material. For example, if some cells are taken from older patients and some from younger ones, considering the genetic diversity exists in the population, in each process we could see a large number of variations in response to a differentiation protocol. Therefore, a categorizing system will be required to minimise the amount of variation resulted from the genetic diversity. On the other hand, in allogeneic cell therapies we can streamline the process with few recognised cell lines and consistently produce the same cell products in each batch. The downside with allogeneic cell therapies is in their higher risk of disease transmission, which it has been the case in master cell and tissue banks. (Rowley et al., 2010)

Perhaps one of the more pressing issues in bioprocessing of stem cells are the costs associated with producing GMP grade products. As the size of the production increases, so as the expenses associated with it. Some materials

such as reagents and growth factors do not exist in GMP grade purely due to high production costs and commercial risks. (Kirouac et al., 2008) Furthermore, other costs associated with clinical testing and running costs of a GMP facility are often substantial and require large sustained investments over a long period of time. (Preti et al., 2005)

Other challenges include product safety, quality and efficacy. It is essential to provide a process flow that minimises risks of contamination whether from a source or throughout the processing steps. (Rayment et al., 2010) It is also crucial to use purification methods to remove pluripotent cells from the population, which often were associated with the formation of teratomas. (Schriebl et al., 2009) As mentioned earlier in this section, retinal cells need to be at a specific developmental stage to be able to integrate into the host retina. Therefore, methods for detection of the key markers at this stage must be developed. Purification methods used currently such as magnetic affinity cell sorting (MACS) and fluorescence activated cell sorting (FACS), require improvements to achieve high purification standards. (Schriebl et al., 2009; Rayment et al., 2010). In regard to efficacy, tests that accurately provide *in vivo* interaction of the cells are rare. Currently, indicators such as cell density, proliferation rate and viability are used to determine the efficacy of the final cell products, which are questionable. (Lim et al., 2007; Yang et al., 2008)

1.3 Use of Microfluidic Devices in Stem Cell Studies

1.3.1 Introduction to Microfluidics

Microfluidic devices are usually comprised of channels, culture areas and other structures ranging from few micrometers to 100 µm in size. However, depending on the application, the dimensions may be adapted to serve the purpose. (Whitesides et al., 2006) Microfluidics originated from the semiconductor industry, hence using many fabrication techniques and materials such as silicone and glasses. However, in recent years use of polymers such as poly(dimethylsiloxane) (PDMS) has been a routine practice due to its ease of use and material properties. (Berthier et al., 2012) PDMS is a thermosetting polymer that is transparent (wavelengths larger than 300 nm), has high flexibility, relatively low cost, it is gas permeable and has shown to be safe in cell culture experiments. (Sia et al., 2003) However, there are also reports that PDMS absorbs smaller hydrophobic molecules and releases oligomers, which can be harmful to cell cultures. (Regehr et al., 2009)

Microfluidic devices are commonly created using lithography. In lithography, a master pattern is transferred to a solid surface, which is usually some type of an elastomeric polymer. In lithography techniques, such as soft lithography, which is a term coined by Xia and Whiteside in 1998 for several different techniques. (Xia et al. 1998) In this technique, a master mould is created by either micro-machining or photolithography and the polymer is cast out of that. In photolithography, the master pattern is usually transferred to a surface by use of mask acting as a negative and exposure to UV light or x-ray as the positive. Intensity of the light, exposure time and solubility of the material

surface will determine the depth of the pattern intended on the surface. Recently other methods such as using heat shrinkable materials and digital printers have also shown to be effective as low cost and rapid prototyping methods for manufacturing microfluidic devices. However, the accuracy of these methods is questioned and shown to be limited. (Becker and Gärtner, 2007)

The other soft lithography method is laser ablation to create structures and computer numerical controlled (CNC) micro-milling, which simply mills out the designed pattern into various substrates such as polycarbonate and aluminum. The latter can either be used directly or as a mold for casting PDMS. (Pronko et al., 1995) The limiting factors with using such method are that they are time-consuming and difficult to work with on features smaller than 5 µm. Moreover, there is also the difficulty of reaching accurate zero point on the surface of the material. On the other hand, laser ablation can create smaller sizes in a shorter time, but the surface roughness can be high due to inherent properties of the method.

Microfluidic devices are usually fabricated in parts and then attached together via methods such as using adhesives, eutectics, anodic bonding, silicon-silicon bonding, use of heat in thermal bonding, and plasma bonding. Methods used for each device are purely dependant on the application of the device, however, plasma and thermal bonding are among the most suitable methods as they do not leach materials or change dimensions of the parts due to added adhesive materials. (Becker and Gärtner, 2007)

Fluid flow at microfluidic structures are affected by viscous and inertial forces, channel length, geometry and velocity of the fluid in the channel. At low flow rates, the Reynold number dictate the characteristics of fluid flow, which is shown by a consistent movement of the fluid named laminar flow. In laminar flow, layers of the fluid can flow in parallel without creating any disturbance in each other and mixing only occurs via diffusion. (Young and Beebe, 2010) Opposite to the laminar flow is when inertial forces dictate the fluid flow characteristics, usually at higher flow rates, which results in an uneven flow called turbulent. Turbulent flow is ideal for mixing and small eddies are present throughout the flow chamber, hence assist the mixing process. However, the turbulent flow does not occur in microfluidic systems due to the smaller channel sizes. Energy-wise laminar flow is much more efficient than turbulent flow due to organized flow patterns. *In vivo*, there is only laminar flow as turbulent flow would be undesirable due to excessive workload for the circulatory system as well as being unsuitable for the cell viability. (Lawrence et al., 2008; Madihally et al., 2010)

In order to determine whether a fluid flow is laminar or turbulent, Reynold's number (N_{Re}) is typically used as an index. Reynold's number is dimensionless and is calculated using the following equation:

$$N_{Re} = \frac{\rho l_c V}{\mu}$$

Where ρ is the density of the fluid, l_c is the channel characteristic length, V is the average velocity of the fluid over the cross-section, and μ is the dynamic viscosity of the fluid. For a smooth-surfaced tube, N_{Re} less than 2,300 indicates

a laminar flow. If N_{Re} is greater than 4000 is turbulent and any values between the two limits are transitional flow. However, it must be noted that microfluidic devices generally operate in Reynold's numbers that are closer to 10, sometimes even below 1. At such low N_{Re} numbers, flow is strictly laminar. (Walker et al., 2004)

1.3.2 Benefits of Microfluidics for Stem Cell Cultures

As stated previously, materials used for differentiation studies are often costly, especially when it takes weeks and months to reach a desired developmental stage for a specific target cell. Once perfusion is introduced into the culture, it often increases the material consumption by few folds. Scaling down to microscale seems to be an obvious choice and clearly is one of the greatest advantages of using microfluidic devices for cell cultures. Furthermore, the smaller size of the microfluidic devices makes it easier to provide faster mass and heat transfer throughout a culture area. (Whitesides et al., 2006; Berthier et al., 2012)

Microfluidic devices can provide larger area to volume ratio often due to their geometric ratios. Therefore, they can provide faster reaction time between the cells, exogenous growth factors and cytokines. (Paguirigan et al., 2008) Defined geometry of the culture chamber in microfluidic devices means that there is a defined media height, thus eliminating variations that are often resulted from evaporation in conventional culture devices. Moreover, reduced evaporation results in more stable concentration of the media as well as pericellular concentrations. Visually, the meniscus effects of the medium

height are also reduced, resulting in improvements in culture monitoring. (Berthier et al., 2012)

One of the major challenges in process development for stem cells is the control of process inputs. Microfluidic devices provide much greater control over the cellular microenvironment. (Paguirigan et al., 2008) By use of laminar flow in microfluidic devices, a more uniform concentration of soluble factors can be created. (Cimetta et al., 2010) Furthermore, the fluid flow can be used to remove unwanted molecules such as waste molecules from the culture area, thus providing a more uniform pH throughout the culture. Overall, these properties of the microfluidic devices allow for more accurate mass transfer via fluid flow and hence creating a microenvironment that closely mimics *in vivo* culture conditions. (Tandon et al., 2013)

1.3.3 Differentiation of ESCs in Perfused Microfluidic Culture Devices

Microfluidic culture devices have been developed and used for various goals such as cell expansions, study of cellular functions or drug screening purposes. Scaling down to microscale provides a simpler and more controllable milieu and allows for faster response time, hence making the microfluidic devices a useful tool for understanding ESC behaviour during differentiation. (Young and Beebe, 2010)

Initial efforts on creating a fully automated high throughput microfluidic device reported by Gomez-Sjoberg *et al*. for long-term experiments such as differentiation and proliferation of the Human Mesenchymal Stem Cells (hMSCs). This device could generate 96 independent conditions as well as

their maintenance for long-term cultures. (Gómez-Sjöberg et al., 2007) Desbordes *et al*. has designed a high throughput microfluidic device to screen effects of 2800 compounds on stem cells differentiation and self-renewal of ESC. (Desbordes et al., 2008) In another study, Zhong *et al.* also designed a high throughput microfluidic platform in order to monitor the gene expression profile of a single ESC. (Zhong et al., 2008) Di Carlo *et al.* used a particular array of cell-traps in a microfluidic device to trap cells through the laminar fluid flow, hence shielding them from the shear forces while providing an opportunity to analyze them on an individual basis. (Di Carlo et al., 2006) However, there have not been reports on progress or updates on many of these devices and most importantly they only focus on one aspect of stem cell culture without considering bioprocessing perspective.

Initial studies on ECM effects on mESCs differentiation showed that hepatic differentiation is greatly affected by dosage and combination of the ECM parts. (Flaim et al., 2005) In addition, by using a microarray technique they found the ECM components that play a key role in differentiation and self-renewal of primary human neural precursors. (Soen et al., 2006) Lanfer *et al.* used a microfluidic set up to study the hMSCs growth and differentiation in regards to the ECM components and found that differentiation of the hMSCs can be guided through directional ECM patterning. (Lanfer et al., 2009) Lii *et al.* has successfully designed a microfluidic chip that allowed study of mESCs and MEFs on naturally derived ECM. (Lii et al., 2008) Peterson *et al* has used micro-patterning on PDMS to direct MSCs differentiation into musculoskeletal lineage. (Peterson et al., 2006) In another study, on effects of stress on

differentiation of the hMSCs, by culturing them in different shapes, they have found that osteogenesis and adipogenesis was achieved at high and low stress regions respectively. (Ruiz et al., 2008)

Other devices have been used to study effects of ECM and perfusion rates mostly on expansion of the hiPSCs, showing higher growth rate of hiPSCs in microfluidic device compared to static well-plates over a 1-week culture. (Yoshimitsu et al., 2014) In other studies with logarithmic increase of flow rate, the growth of mESCs were higher in terms of colony size. (Kim et al., 2006) Titmarsh *et al*. demonstrated successful 1-week continuous perfusion of hESCs in a microfluidic culture device at flow rate of 20.8 µL/h (Péclet number=1). (Titmarsh et al. 2012) Cimetta and colleagues designed a multiplexed microfluidic bioreactor that enabled a precise control over cellular microenvironment of hESCs. Using the same device, they demonstrated an ability to contain up to 120 EB samples and controlled mesodermal differentiation of hESCs. (Cimetta et al., 2014)

Some of the qualities of the culture surface that are found to have visible effects on the cellular behavior are elasticity, geometry and topography. Topography changes have proved to be one of the most effective of these qualities. In microfluidics, micropatterning techniques by using methods such as photolithography and solvent casting has been used to achieve this. For example, Recknor *et al*. used micropatterned polystyrene to study guided differentiation of neuronal progenitor cells. (Recknor et al., 2005) The same technique but on PDMS, was also used by Yim *et al.* on trans-differentiation of hMSCs into the neuronal lineage. (Yim et al., 2007) Another group used

PDMS stamps, to demonstrate the independence of the hMSCs shape to biochemical contents in differentiation. (Kilian et al., 2010) Dalby *et al*. has extensively studied osteogenic differentiation of hMSCs, in various topographical patterns such as nano-pit and islands against presence or lack of dexamethasone, which induces osteogenesis, and found that effectiveness of the right topography on differentiation of the hMSCs. (Dalby et al., 2008) Others also created microwells coated with nanofibers that are used for culture of the mESCs showing effectiveness of this method in guiding stem cell differentiation. (Gallego-Perez et al., 2010)

Among other studies performed on PSCs were a microfluidic device designed for stimulating angiogenesis in hMSCs in a 5-day perfused culture. (Jeon et al., 2014) Other studies on angiogenesis looked into effects of Flk1on ESCs, exposed to VEGF and TGF-β under shear stress of 1.5–10 dynes/cm^2 when cultured on a collagen IV-coated plates. Results showed successful vascular EC differentiation of the ESCs. (Huang et al., 2010)

A large group of studies in the field taking advantage of the inherent qualities of fluid flow at microscale and focused on the effects of shear stress on a cell population in a microfluidic culture device. Toh *et al.* created a device that can produce shear rates from 0.0016 to 16 dyne/cm^2. This study showed that fluid flow controls the expression Fgf5, the epiblast marker, by engaging the heparan sulfate proteoglycans (HSPGs). This process assists cells in sensing the shear stress present in the culture area. (Toh et al., 2011) Figallo *et al.* has also designed a microfluidic cell culture device that was used in experiments on hESCs as well as mouse myoblast. Results showed that

hESCs had higher proliferation and EC differentiation upon exposure to shear stress and myoblasts showed myotube formations aligned in the fluid direction. (Figallo et al., 2007) Endothelial differentiation of the mESCs was observed once they were exposed to shear stress of 15 dyne/cm^2. (Ahsan et al., 2010). Another study on cardiomyocyte differentiation of the ESCs, a microfluidic device made of poly (methyl methacrylate) (PMMA) was created with arrays of 900 recesses of 300x300x300 μm^3 volume was used with different flow rates. The results showed beating cardiomyocytes, proving the importance of fluid flow in the differentiation process. (Gottwald et al., 2007)

Studies on neural differentiation of neural stem cells showed that continuous perfusion of the culture enriched with FGF2 and epidermal growth factor resulted in formation of astrocytes. (Chung et al., 2005) Other studies showed importance of growth factor gradients in neural patterning by using Nestin positive ESCs. (Park et al., 2009) Similar studies showed effects of counter-gradient of LIF and RA on pluripotency of ESCs and maintenance of their phenotype. (Kawada et al., 2012) Cimetta showed effects of concentration gradients on mesodermal differentiation of hESCs and hiPSCs when tested on concentration of Wnt3a, Activin A, BMP4 and their inhibitors simultaneously over a 4-day culture period. (Cimetta et al., 2012) Finally, Titmarsh *et al.* studied early mesodermal differentiation in light of exogenous and paracrine factors in hESCs, demonstrating usefulness of microfluidic devices for understanding heirarachy of molecular regulators of mesodermal differentiation and compatibility of such devices with conventional culture systems. (Titmarsh et al., 2012)

1.4 Summary

In summary, compared to other therapeutic solutions hiPSCs can provide a readily available cell source without the need for histocompatibility matching for a diverse range of regenerative therapies. Transplantation studies show that developmental stage of the donor cells is crucial to their integrational capabilities into the host retina i.e. post-natal post-mitotic precursor cells that express Crx and Nrl. In addition, number and purity of the transplantable cell population are also crucial in increasing efficiency of their integration into the host retina. Current retinal differentiation protocols take a long time, have low efficiency and reproducibility. Moreover, considering the requirement of high number of cells for each patient, optimisation of differentiation protocols for PSCs in a more robust, consistent and efficient manner will be critical in providing a transplantable cell population.

One of the major challenges of the process development for stem cells is the control of process inputs i.e. keeping culture conditions in a stable format. In differentiation cultures, key process inputs include, ECM, soluble factors, physicochemical factors such as pH and oxygen concentration. To maintain these parameters, monitoring systems are needed to measure and report the live values of these parameters accurately so they can be adjusted according to cultural changes. Conventional culture setups such as T-flasks and well-plates lack the complexity and accuracy to imitate the endogenous cell culture environment. It has been a challenge for the research and industrial community to provide ever closer culture environment for expansion and differentiation of stem cells. Deeper understanding of the stem cells' behaviour

during differentiation is dependent on the stem cells niche and our capabilities to control it.

Microfluidic devices provide much greater control over the cellular microenvironment, often resulted from shorter characteristic length and use of laminar flow in these devices. Furthermore, the fluid flow is used to remove unwanted waste molecules from the culture area, thus providing a more uniform pH throughout the culture. Fluid flow can be used to provide more accurate mass transfer hence creating a microenvironment closest to the *in vivo* conditions. However, applying perfusion to cell culture environment requires careful considerations. Korin *et al.* has found that shear stress of $2x10^{-2}$ Pa is the minimum amount of force necessary to remove human foreskin fibroblasts from the culture surface. (Korin et al., 2007) Furthermore, Toh *et al.* discovered that the presence of shear stress on mESCs was detected at shear rates of 1.6×10^{-3} Pa. (Toh et al., 2011)

Unique qualities of the microfluidic devices have been exploited in various works to investigate different aspects of the stem cell culture and differentiation. However, there have not been any reports on progress or updates on many of these devices and most importantly they only focus on one aspect of stem cell culture without the bioprocessing perspective. Furthermore, most differentiation studies in microfluidic devices have been focused on effects of shear stress or mesodermal differentiation of pluripotent stem cells without considering steady-state concentration of soluble factors. There is some work on short-term (up to 10 days) neural differentiation of ESCs, but no work on long-term differentiation of hESCs or hiPSCs along the

ectodermal lineage, and none on the photoreceptor differentiation. Considering the advancements made in both fields of microfluidics and development of the retinal differentiation protocols for PSCs, there is an open opportunity to explore ectodermal differentiation of hiPSCs using a microfluidic device designed for bioprocess development of stem cells. Using fluid flow in creating steady-state concentration of soluble factors in a continuously perfused culture, allows for better understanding of the retinal differentiation of hiPSCs, effective optimisation of the protocols used and efficient production of clinically relevant photoreceptors.

1.5 Research Objectives

In this work, I hypothesised that, (i) a flow rate can be found which keeps key growth factors in retinal differentiation culture of hiPSCs in steady-state, and that (ii) steady-state conditions obtained at such flow rate would result in the upregulation of retinal progenitor (Pax6, Lhx2, Six6 and VSX2/Chx10) and subsequently the precursor markers (Crx and Nrl).

The objectives of this project are, (i) to study dynamics of the retinal differentiation culture, investigate degradation and consumption of key growth factors used in this culture and establish an order of importance. (ii) Next, devise a critical perfusion rate to deliver the most important growth factors by perfusion, hence creating a steady-state condition for these molecules. (iii) Assess the suitability of the microfluidic culture device for long-term differentiation culture. (iv) Finally, perform time-point perfusion studies to analyse the expression of retinal progenitor and precursor markers. Comparing the results in perfused cultures with conventional static cultures would illustrate the role of perfusion and steady-state concentration of key soluble factors on retinal differentiation of hiPSCs.

The microfluidic culture device (MFCD) used for this project was developed by Marcel Reichen and further optimised by Rhys J. Macown. So far successful perfusion culture of hESCs has been performed for up to 6 days in different versions of the device. (Reichen et al., 2012; Macown et al., 2014; Super et al., 2016).

Chapter 2 Materials and Methods

This chapter describes the methodology used for culturing cells during the experiments throughout the thesis. This includes mouse embryonic fibroblasts (MEFs) and human induced pluripotent stem cells (hiPSCs). In the second part techniques used to analyse the cells are explained. The analytical techniques include cell count, viability assays, immunocytochemical staining, qPCR, media analysis and enzyme-linked immunosorbent assay. In the third part, microfluidic culture device fabrication and assembly is explained. All other tests performed to prepare the microfluidic device for long-term perfusion culture are also explained in this part. The final part includes the statistical analysis methods used throughout the thesis.

All cell cultures apart from hiPSCs passaging were carried out in a Walker Class II Safety Cabinet (Manchester, UK). To avoid contamination latex gloves and a clean lab coat were worn at all times. All equipment used in the process were wiped clean with 70% ethanol and all relevant solutions were sterilised or filtered (with 0.22 µm filters) beforehand.

All solutions used for cell culture were pre-warmed to 37 °C in water bath. Cells were cultured in sterile conditions at 37 °C in 5% CO2 in air in a Heraeus® HERAcell® incubator. (Thermo Fischer Scientific Inc., Waltham, MA, USA), and cultured in either Nunclon™ tissue culture flasks, with filter caps or multi-well plates (Thermo Fischer Scientific).

2.1 Cell Culture

2.1.1 Mouse Embryonic Fibroblasts Culture and Preparation of Feeders

2.1.1.1 Mouse Embryonic Fibroblasts Culture

Mouse embryonic fibroblast (MEF) media was prepared using Dulbecco's Modified Eagle Medium (DMEM; Invitrogen, Paisley, UK), supplemented with 10% v/v fetal bovine serum (FBS; SeraLab, Haywards Heath, UK), 1% v/v Glutamax (Invitrogen, Paisley, UK), 1% v/v non-essential amino acids (NEAA; Invitrogen, Paisley, UK). A vial of MEFs was taken from the liquid Nitrogen and thawed rapidly at 37˚C. Once thawed, the contents of the vial was transferred to a 15mL centrifuge tube. 5 mL medium was added to the tube and centrifuged at 300 x g for 5 minutes. The supernatant was removed, and the cell pellet was re-suspended in 10 mL growth medium. The centrifuge tube was homogenized with a vortex, and 5 mL of the content was transferred to a T-25 flask. Flasks were observed under the microscope and incubated at 37˚C, 5% CO_2.

Once flasks became confluent a fresh T-25 flask was coated with 0.5 mL of 0.1% v/v gelatin (Sigma-Aldrich, Gillingham, UK) for 30 minutes prior to passaging. Spent medium in the T-25 flasks with MEFs was removed first and then washed the flasks with 6 mL of 0.1% v/v phosphate buffer saline (PBS; Sigma-Aldrich, Gillingham, UK) once. Following this, 2 mL of 0.25% bovine trypsin-EDTA was added to the flasks. Cells were incubated with the trypsin at 37°C for three minutes. The trypsin was then quenched by adding 3 mL of culture medium into the flasks. The quenched suspension was aspirated and

dispensed 3-4 times in order to create a single cell suspension and eliminate aggregates. The quenched cell suspension was then transferred into a 25 mL centrifuge tube and centrifuged at 300 x g for 3 minutes. In the meanwhile, the gelatin that was added to the fresh flasks previously, was taken out. After centrifugation, the supernatant containing the trypsin and quench medium was carefully removed from above the cell pellet. The cells were then re-suspended in the culture medium dependent on the passage split ratio (3 mL for 1:3 or 4 mL for 1:4). Cells were split at a ratio between 1:3 and 1:4 for up to 5 passages. 5 mL of standard culture medium was dispensed into the flasks. 0.5 mL cell suspension was then carefully added to each culture flask.

2.1.1.1 Preparation of Feeder cells

Mitomycin-C medium was prepared using 10 µg/mL mitomycin-C in culture medium (described above). Spent media in the T-25 flasks was removed, and flasks were washed with phosphate buffer solution (PBS) once. Mitomycin-C medium was added to flasks to cover the surface and incubated the flasks for 2-3 hours at 37˚C, 5% CO_2. Fresh T-25 flasks for feeders were prepared in the same way for the passaging described above. Following incubation, mitomycin-C was removed, and flasks were washed with PBS 3-4 times to ensure all mitomycin-C has been removed from the flasks. Feeders were removed from the flasks using trypsin-EDTA as described above and resuspended in 10 mL of MEF culture medium. Cells were counted, and 2.3 x 10^5 cells were transferred to each T-25 flasks coated with 0.1 v/v gelatine. Feeders were incubated at 37˚C, 5% CO_2 overnight and used the following day for hiPSCs passaging.

2.1.1 Human Induced Pluripotent Stem Cells (hiPSCs) Culture

The hiPSC media was prepared using Knockout DMEM (Invitrogen, Paisley, UK) supplemented with 20% (v/v) Knockout serum replacement, 1mM L-glutamine, 1% (v/v) nonessential amino acids, 100mM β-mercaptoethanol, and 4 ng/mL basic fibroblast growth factor (all Invitrogen).

One hour prior to thawing hiPSCs, MEF media was removed from feeder flasks and replaced with fresh hiPSCs media and incubated at 37˚C, 5% CO_2. A cryovial of undifferentiated hiPSCs (MSUH001 cell line) passage 65 were taken out of liquid nitrogen and thawed rapidly at 37˚C and transferred to flask prepared with feeder cells. Allowed cells to adhere to the surface (24 to 48 hours) and adjust to culture conditions after freezing. Daily observations were carried out to determine when to subculture the cells. Once successfully expanded Media was exchanged once every 48 hours and passaged once every 3-4 days. The differentiated colonies were removed from the hiPSCs flasks prior to each passage and then undifferentiated colonies of hiPSCs were transferred by scarping into a new T-25 flask. Cells were split 1:1 or 1:2 depending on the confluency.

2.1.2 Embryoid Body Formation Using AggreWell™ 400 Plate

2.1.2.1 Preparation of AggreWell™ Plate

Human EB formation medium was prepared using GIBCO® DMEM/F-12 Media (1:1) (Invitrogen, Paisley, UK), 10% (v/v) Knockout Serum Replacement (KOSR; Invitrogen), 1 ng/mL Dkk-1 (R&D Systems, Minneapolis, USA), 1 ng/mL Noggin (R&D Systems, Minneapolis, USA), 5 ng/mL IGF-1 (R&D Systems, Minneapolis, USA), 1% (v/v) N-2 Supplement (PAA Laboratories

Ltd., Yeovil, UK). 6 mLs of EB formation media per well of AggreWell™ plate was taken and pre-warmed with Y-27632 ROCK Inhibitor (ROCKi; Stemcell Technologies, Canada) to a final concentration of 10 µM.

An AggreWell™ 400 plate was removed from the packaging in a sterile tissue culture hood. The wells were pre-treated with Rinsing Solution 5% w/v Pluronic acid (5g per 100mL H_2O) to help ensure all bubbles will be displaced from the micro-wells. 2 mL of AggreWell™ Rinsing Solution was added to each well, which was to be used. Then, the AggreWell™ plate were centrifuged at 2000 x g for 5 minutes in a swinging bucket rotor that is fitted with a plate holder, to remove any air bubbles from the microwells. The plate was observed under a microscope, to check bubbles have been removed. AggreWell™ rinsing solution was removed from wells, and each well were rinsed with 2 mL EB Medium without ROCKi. 2mLs of EB formation medium (containing ROCKi) was added to each well of the AggreWell™ plate, and then the plate was put aside in tissue culture hood while preparing single cell suspension of hiPSCs.

2.1.2.2 Preparation of a Single Cell Suspension of Undifferentiated hiPSCs

EB formation medium with and without ROCKi and Tryple Express (TrypLE) were warmed to room temperature (25°C). EB formation medium with ROCKi was supplemented to a final concentration of 10 µM. Maintenance medium from the hiPSC culture plate were removed, and the cells were rinsed once with 3 mL of PBS. 2mL of TrypLE was added to each flask and incubated at 37°C and 5% CO_2 until cells detach easily from the plate with gentle shaking. The cell suspension was pipetted 2-3 times with a serological pipette to ensure

any remaining clumps are fully dissociated from the surface of the dish. Cells were then transferred to a 50 mL conical tube through a 40 µm cell strainer (Stemcell Technologies; Catalog #27305) to remove clumps. Flasks were rinsed with 5 mL of EB Medium (without ROCKi) per milliliter of TrypLE used. Cells were centrifuged at 300 x g for 5 minutes at room temperature (25°C). The supernatant was removed, and the pellet was suspended in a small volume (1-2 mL) of EB formation medium (with ROCKi), such that the cell concentration were approximately 1.2 x 10^6 cells/mL. Viable cells were counted using trypan blue exclusion assay. Samples of the re-suspended cells were diluted to 1:10 in trypan blue and mixed gently i.e. 10 µL cells + 80 µL EB medium (with or without ROCKi) and 10 µL Trypan Blue. Viable cells were counted using a hemocytometer.

2.1.2.3 Formation of EBs

Without removing the EB formation medium added previously, the appropriate volume of undifferentiated cells were added to each well. (Number of cells required per well = desired number of cells per EB x number of microwells per well) Volume in the well was adjusted to the specified final volume using EB formation medium (with ROCKi). (3 mL per well). Further pipetting was performed to ensure an even distribution of the cells. The plate was then centrifuged at 100 x g for 3 minutes to capture the cells in the microwells. The AggreWell™ plate was observed under a microscope to verify that cells are evenly distributed among the microwells then incubated the cells at 37°C with 5% CO2 and 95% humidity for 24 hours.

2.1.2.4 Harvesting Human EBs from AggreWell™ Plates

EBs were harvested 24 hours after adding the hiPSCs to the AggreWell™ plate. EB suspension culture medium was pre-warmed to 37°C. EBs were collected from microwells by firmly pipetting medium in the well up and down 2-3 times with a micropipette (p-1000). Placed EBs into a sterile 15 mL centrifuge tube. The plate was swirled to centrifuge EBs into the middle and washed several times with media. The AggreWell™ plate was observed under the microscope to ensure that all aggregates have been removed from the wells. EBs were left to settle in a 15 mL blue top centrifuge tube for 5 minutes then the supernatant was removed leaving EBs behind. EBs were re-suspended in 10 mL of media per well. The EBs were plated into a large low adherent culture dishes (Sterilin, Caerphilly, UK) with a volume of 10 mL and incubated at 37°C with 5% CO_2. The dish was shaken 1-2 times per day to distribute the EBs in the well and avoid EBs sticking together. Media was exchanged every two days.

2.1.3 Retinal Differentiation Protocol

Retinal differentiation media was prepared using media culture DMEM/F12 (Invitrogen, Paisley, UK) supplemented with 10 ng/mL human recombinant DKK-1, 10 ng/mL human recombinant IGF-1, 10 ng/mL human recombinant Noggin, 5 ng/mL basic fibroblast growth factor (bFGF) (all R&D Systems, MN, USA), 1% (v/v) N-2 Supplement, and 2% (v/v)B27 Supplement (PAA Laboratories Ltd, UK).

On day 3 of the EB suspension culture, 7 EBs were selected under a dissecting microscope and plated in each well of a 48-well plate coated with

Matrigel™ (BD Bioscience) for 1 hour prior to seeding. In growth factor degradation and consumption experiments, 30 EBs per 12-well plate was used. 250 µL of the medium exchanged per well of the 48-well plate once every 48 hours and 1 mL in 12-well plates. Cells were treated for immunostaining and were collected for qPCR on 5, 10 and 21 days. Cell numbers were measured using a VI-CELL Cell Viability Analyser (Beckman Coulter, Brea, CA).

2.1.3.1 Growth Factor's Degradation and Consumption Study

To study degradation and interaction of the key growth factors with hiPSCs, retinal differentiation media was prepared as explained in section 2.1.3. Three culture conditions were designed; one with media only, no cells or media exchange, second with cells but no media exchange and last one with cells and media exchange once every 48 hours. In the wells with cells, approximately 30 EBs were selected for each well of a 12-well plate. EBs were transferred into wells of the 12-well plate that were pre-coated with Matrigel™ (BD Bioscience, San Diego, CA, USA) prior to seeding EBs. 1 ml of differentiation media was added to each well, and plates were incubated at 37°C, 5% CO_2. (Sanyo, MCO-18AIC). Samples were collected at 0, 4, 8, 24, 36, 48, 52, 56, 72, 84 and 96 hours from start of the culture in 4 different cryovials for each growth factor (Noggin, DKK-1, IGF-1 and bFGF). The experiment was repeated 3 times (n=3) and the vials were kept at -80°C before they were analysed using ELISA as per section 2.2.3. The number of cells after each media collection was obtained using VI-CELL cell viability analyser.

2.2 Analytical Methods

2.2.1 Cell Number and Viability

2.2.1.1 Haemocytometer

Haemocytometer's chamber and cover slip were cleaned using 70% ethanol prior to use then dried and fixed the coverslip in position. 1 mL of cell suspension removed and added 10 µL of the cells to the haemocytometer chamber and it was placed under the inverted microscope and observed with a 10x objective. Cells were counted in the large, gridded squares (1 mm^2) and averaged accordingly. Number of cells counted was multiplied by 10^4 to estimate the number of cells per millilitre. In order to find the number of cells per cm^2, the concentration was multiplied by the total cell suspension volume and then divided by the culture area.

2.2.1.2 Trypan Blue Exclusion Assay

0.1 mL of 0.4% solution of trypan blue in buffered isotonic salt solution (pH 7.2 to 7.3) was added to 1 mL of cells and mixed thoroughly. Then 10 µL of the mixture was added to the haemocytometer and cells were counted. Viability was calculated using the following formulas:

$$\text{Number of viable cells} \times 10^4 \times 1.1 = \text{cells/mL culture}$$

$$\% \text{ Viable cells} = [1 - (\text{Number of blue cells} \div \text{Number of total cells})] \times 100$$

2.2.1.3 Vi-CELL Cell Viability Analyser

Cell number and viability counts were assessed in triplicate for samples collected from 48-well plates and MFCD using the VI-CELL Cell Viability Analyser (Beckman Coulter, High Wycombe, UK), according to manufacturer's

instructions. In this method, an automated approach to trypan blue exclusion method is provided by automating the process. This way the variability inherent in manual method and counting is reduced, and additional data such as cell size and real time cellular images can be obtained if required.

2.2.2 Immunocytochemistry and Microscopy

2.2.2.1 Immunocytochemistry

Spent media was removed from cell samples and cells washed with DPBS once. Cells were washed with DPBS for 5 minutes, followed by fixation with 4% paraformaldehyde (PFA) (Sigma-Aldrich, MO, USA) for 20 minutes at room temperature (25°C). Following this step cells were permeabilized with 0.3% (v/v) Triton X-100 in DPBS for 10 minutes at room temperature (all from Sigma-Aldrich). Washed samples with 2 mL DPBS and incubated in blocking solution of 5 % (v/v) FBS plus 95 % PBS for 30 minutes. A solution of primary antibody (1:200) was prepared and incubated samples with 600 mL of primary antibodies overnight at 4°C. The primary antibodies used were as follows: monoclonal mouse anti-Oct4 IgG (Invitrogen), polyclonal rabbit anti-Nestin IgG, monoclonal mouse anti-Pax6 IgG, monoclonal rabbit anti-Otx2, polyclonal goat anti-Nrl, polyclonal sheep anti-Chx10, monoclonal mouse anti-SSEA4 IgG, monoclonal mouse anti-TRA-1-60 IgM (all from Millipore), polyclonal rabbit anti-Crx (Sigma-Aldrich), monoclonal mouse anti-TRA-1-81(Abcam) and monoclonal mouse anti-SSEA1 IgM (Invitrogen). Washed each sample with 2 mL DPBS twice and incubated with 600 µl of secondary antibody solution at room temperature for 1 hour. Secondary antibodies used were as follow: Alexa Flour 488 goat anti-mouse IgG, Alexa Flour 488 chick

anti-goat IgG, Alexa Flour 532 goat anti-rabbit IgG, Alexa Flour 532 goat anti-mouse IgG, Alexa Flour 555 goat anti-rabbit IgG, Alexa Flour 568 monkey anti-sheep IgG, Alexa Flour 594 goat anti-rabbit IgG, Alexa Flour 594 goat anti-mouse IgG (all Invitrogen; 1:400) Cells were washed twice with PBS and solution of 4, 6-diamidino-2-phenylindole (DAPI; Invitrogen, 1: 1,000) with PBS and incubated for 5 min at room temperature and washed one last time with PBS.

2.2.2.2 Microscopy and Image Processing Software

Phase contrast images were obtained by using EVOS® XL Cell Imaging System microscope (Life Technologies). Fluorescence images were acquired by using fluorescence microscope (Nikon, Eclipse TE2000-U) and EVOS® FL fluorescence microscope (Life Technologies). Images for whole culture area on MFCD were stitched together using Adobe Photoshop CC software by using *photomerge* function. Areas for expanding EBs were obtained by using ImageJ 1.46 image analyser software.

2.2.3 The Enzyme-Linked Immunosorbent Assay (ELISA)

All collected media samples for degradation and consumption of the growth factor's study were centrifuged to remove dead cells and debris. The supernatants were then frozen at -80 °C until analysis could be performed. Samples were analysed using sandwich ELISA kits for bFGF, IGF-1, DKK-1 (Abcam ELISA kits, Cambridge, UK) and Noggin ELISA kit (MyBioSource plc, San Diego, California, USA). After media collection, cells were collected and counted using Vi-CELL cell viability analyser. For each ELISA, all standards were prepared according to the manufacturing protocol. 100 µL of samples

and standards were added to each well in a 96 well-plates and incubated overnight. Samples were then removed, and the plate was washed three times with 1 time wash solution. 100 µL of 1x biotinylated antibody was added to each well and incubated the plate for 1 hour at room temperature. Repeated the wash three more times and added 100 µL of prepared Streptavidin solution to each well and incubated the plate for 45 minutes at room temperature with gentle shaking. Repeated the wash again and then added 100 µL of TMB one-stop substrate reagent to each well and incubated for 30 minutes with gentle shaking. Finally, 50 µL of stop solution was added to each well and the plate was read at 450 nm using FLUOstar OPTIMA (BMG LABTECH GmbH) microplate reader.

2.2.4 Media Analysis

The spent media was recovered from cell cultures for degradation and consumption experiment. Samples were centrifuged to remove dead cells and debris. The supernatants were then frozen at -80 °C until analysis could be performed. Glucose, ammonia and lactate concentrations were measured using a multi-parameter Nova BioProfile Analyser (Nova Biomedical, MA, USA). The BioProfile Analyser has glucose, ammonia and lactate biosensors, which are amperometric electrodes with immobilised enzymes in their membranes. In the presence of oxygen and the substrate being measured, these enzyme membranes produce hydrogen peroxide (H_2O_2), which is then oxidized at a platinum anode held at constant potential. The resulting flow of electrons and current change is proportional to the sample concentration.

2.2.5 Gene Expression Analysis

Relative expression of genes for pluripotency and retinal differentiation was analysed using quantitative (real-time) polymerase chain reaction (qPCR). Cells were detached by incubation with the trypLE for 12 minutes at 37 °C and harvested by use of P1000 pipette. Cell pellets were washed with DPBS and all the remaining DPBS was removed prior to storage at -80°C for future use.

2.2.5.1 RNA extraction

RNAs were extracted using the Qiagen RNeasy kit (Qiagen, Crawley, UK). 600 µL of Buffer RLT was added to the pelleted cells according to the protocol. The lysate was well mixed and pipetted into Qiashreddes column and centrifuge at full speed for 2 minutes. A similar volume of 70% Ethanol was added to the homogenized lysate and well mixed by pipetting. Following this 700 µL of the mix was transferred to an RNeasy spin column. The column lid was closed and centrifuged for 15 s at 10,000 rpm. The flow-through in collection tube was discarded, and 350 µL Buffer RW1 was added to the RNeasy spin column. The lid was closed and centrifuged for 15 s at 10,000rpm and discarded the flow-through. 10 µL DNAse 1 was added to 70 µL Buffer RDD. Mixed by inverting the tube and centrifuged briefly. Then 80 µL DNAse mix was added to RNeasy spin column (directly to the membrane) and placed on the benchtop for 15 minutes. 350 µL Buffer RW1 was added to the RNeasy spin column. The lid was closed gently and centrifuged for 15 s at 10,000 rpm. The flow-through was discarded afterwards. 500 µL buffers RPE was added to the RNeasy spin column and centrifuged for 15 s at 10,000 rpm and discarded the flow-through. 500 µL buffers RPE was added to the RNeasy

spin column and centrifuged for 2 minutes at 10,000 rpm. The column was placed in a new 2 mL collection tube and centrifuged for 1 minutes at full speed. The RNeasy spin column placed in a new 1.5 mL collection tube; 40 µL RNase-free water was added to the membrane and centrifuged for 1 minute at 10,000 rpm. The RNA concentration was determined by measuring absorbance at 260 nm, by spectrophotometer (NanoDrop ND-1000, Thermo Scientific, Epson, UK).

2.2.5.2 cDNA Synthesis

RNA sample concentrations were normalized to that of the hiPSC control sample and cDNA was synthesized using QuantiTect Whole Transcriptome Kit (Qiagen, Crawley, UK). Added RNA in 1–5 µL nuclease-free water to a microcentrifuge tube and adjusted the volume to 5 µL using nuclease-free water. Prepared the RT mix and added 5 µL RT mix to the RNA sample, mixed by vortexing and centrifuged briefly. Incubated the RNA samples at 37°C for 30 minutes then stopped the reaction by incubating at 95°C for 5 minutes and then cooled to 22°C. Added 10 µL of ligation mix to the RT reaction, mixed by vortexing, and centrifuged briefly then incubated at 22°C for 2 hours. Added 30 µL of amplification mix to the ligation reaction, mixed by vortexing, and centrifuged briefly. Incubated the mix at 30°C for 2 hours and stopped the reaction by incubating at 95°C for 5 minutes. Amplified cDNAs were stored at -20°C before use in the next step.

2.2.5.3 qPCR

The master mix was prepared for each target gene as follow: 12.5 µL of SYBR® Green assay (Eurogentec, Hampshire, UK), 1 µL of primer pairs for

the housekeeping and target genes, β-actin, UBC, Oct4, Sox2, Nanog, Nesting, Sox17, Brachyury, Otx2, Pax6, Lhx2, Six6, Chx10, Crx, Nrl and Rhodopsin (all from Qiagen, Crawley, UK). 2 µL of cDNA (diluted 1/50 from the previous step) and 9.5 µL of RNA-free water was used to make a total reaction volume of 25 µL per well. All measurements were taken in triplicates technical and biological. All samples are normalized to levels of β-actin and UBC expression in hiPSCs. Only one sample of hiPSCs used to act as a calibrator between the time points. The plates used were hard-shell low-profile skirted 96-well plates and read using CFX Connect™ Real-Time PCR detection system (all by Bio-rad, UK).

Controls were set up in single wells including No template controls (NTC) for each primer master-mix were used containing all the components of the PCR reaction except for the template, which enables detection of PCR reagent contamination. No reverse transcription (NRT) controls were also prepared by using all components except reverse transcriptase enzyme. NRT controls enables detection of any gDNA contamination in the samples. Plates were sealed with a Microseal 'B' adhesive seal (BioRad) and centrifuged briefly before qPCR analysis was carried out. The PCR mix was initially activated for 5 minutes at 95°C and cycling conditions were as follows: denaturing at 95°C for 15 seconds, followed by annealing and extension at 60°C for 60 seconds, for 50 cycles. This was followed by melting curve analysis within the CFX Connect software that checked for non-specific amplification or the presence of primer-dimers.

2.3 Microfluidic Culture Device (MFCD)

2.3.1 Fabrication of the MFCD Parts

The microfluidic culture device consists of disposable (microfluidic chip, part of the lid and gasket) and reusable parts (top and bottom frames, interconnects and lid). Microfluidic chip and gasket are made of PDMS. Top frame, interconnects and lid are polycarbonate and bottom frame and brackets are Aluminium.

2.3.1.1 Fabrication of Polycarbonate Parts Using Micro-milling

All fabricated components and moulds were designed in the 3D CAD software package SolidWorks (SolidWorks 2011/12, Dassault Systems, France). The models were then imported into the CAM programme Mastercam (Mastercam X4 MR2, Mastercam, USA) which was used to produce CNC code. The components were milled using a Folken micro milling machine (M3400E, Folken Industries, USA) with Kyocera end mills (Kyocera Micro Tools, USA). Materials used were: 5 mm polycarbonate (PC) sheet for connectors, top frame and the lid were from 3 mm PC sheet for top plate (3 mm, 681-637, RS, UK, and 5 mm, 681-659, RS, UK). Bottom frame and clamps were fabricated using 3 mm Aluminium. (Protolab, UK)

2.3.1.2 Microfluidic Chip and Other PDMS Parts Fabrication

Microfluidic chip, gasket and gas permeable lid were cast from PDMS (Sylgard 184, Dow Corning, UK), which was mixed 10:1. The mixed PDMS was degassed in a vacuum desiccator, poured into the mould and degassed a second time. A smooth 5 mm sheet of polycarbonate was pressed over the top of the mould and the two pieces clamped between 10 mm aluminium plates. The plates were screwed together by four screws to a torque of 2 Ncm.

The assembly was set in an oven for at least 2 hours at 85°C before cooling and removing the chip from the mould. A scalpel was used to cut carefully around the parts' outlines.

A 0.12 mm thick layer of PDMS (Sylgard 184, Dow Corning, UK) was produced by spin coating. 5 mL of degassed PDMS mixture was placed in the centre of a silanised 4" silicon wafer (Prolog Semicor, Ukraine) and spun at 500 RPM for 50s in a spin coater (P6708D, Specialty Coating Systems, USA). The silicon wafers were silanised by placing them in a vacuum desiccator for one hour with ~120 µL of trichloro (1H,1H,2H,2H perfluorooctyl) silane (448931, Sigma-Aldrich, UK). The coated wafer was cured in an oven for one hour.

Moulded microfluidic chips and coated wafers were both placed in a plasma chamber (PDC-002, Harrick Plasma, USA) for 2 minutes at 30 W and 500 mTorr. The moulded chips were then carefully pressed onto the coated wafers, and the assemblies cured in the oven for one hour at 85°C. This process attaches the two PDMS layers through Si-O-Si bonds. Finally, the bonded chips are cut from the coated wafers with a scalpel. The 0.12 mm layer lifts the media inlets and outlets above the culture surface.

2.3.2 Sterilisation of The Device Using Autoclave

Tubing and the fluidic adaptors were wrapped in aluminium foil and grouped together. Parts that are made of the same material were packed in the same autoclave bags and sealed with autoclave tape. The whole petri dish was wrapped in the aluminium foil and taped. Two PC blocks that can fit in the petri dish for placing the MFCD on them were also wrapped and sealed. A small bottle of purified water (50 mL), a pair of scissors and tweezers were also

sealed in the autoclaved bags and placed in the autoclave machine to be sterilised.

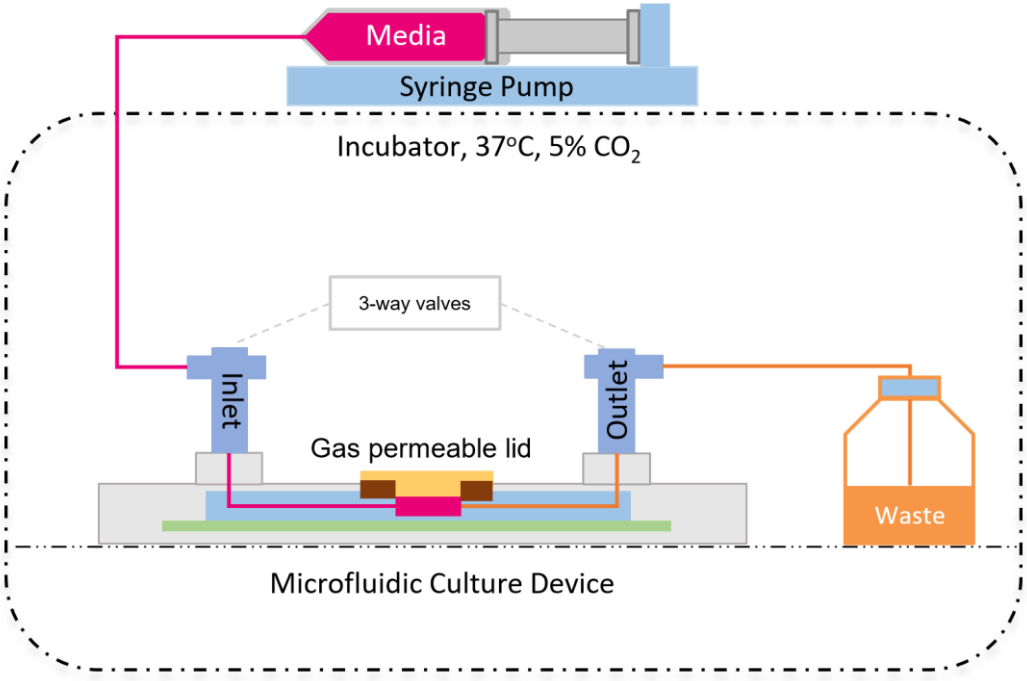

Figure 2.1 Schematic of Microfluidic Perfusion Set-up and Fluidics Assembly.

2.3.3 Device Assembly and Perfusion System

In order to study the retinal differentiation, a simple microfluidic perfusion set-up was used. The schematic of the set-up was shown in the figure 2.1 All connectors used were from Upchurch Scientific, IDEX Health & Science. Fluidic tubing used for both systems was PTFE Bola tubing with the following ID, OD and wall thickness of 0.8mmx1.6mmx0.4mm. Syringe pumps used were Aladdin programmable syringe pump and Kd Scientific 200 with 20 mL BD Plastic syringe for 130 µL/h perfusion runs and Kd Scientific, Legato 212 with 2.5 mL HSW Norm-Ject syringes for 5.2 µL/h perfusion runs. Characterisation of the syringe pumps were carried out in section 2.3.6.

2.3.3.1 Assembly of the MFCD

All parts were sprayed with 70% ethanol and placed in the biosafety cabinet prior to assembly. Packaging on glass petri dish and MFCD frames were opened first and all the parts were place in the glass petri dishes. One TC-PS slide was taken out carefully with tweezers and inserted it in the recess in the bottom frame. Connectors were screwed on the top frame, followed by placing gasket in the top frame chamber window. Microfluidic chip was inserted in the recess in the top frame with its corrected side up so that channels openings were against the inlet and outlet on the top frame.

The top frame assembly was carefully placed onto the bottom frame. Clamps were placed on top of the connectors and plastic screws were placed in their place around the device apart from the screws for the lid part. Screws were tightened with screwdriver fixed to apply 2 N.cm torque as follow: started with one of the screws in the middle and tightened it for few rounds (not all the way) then moved to the one on the opposite side diagonally. Following this moved to the screws on the outer level and repeated the same action the same until all the screws were tightened to their place.

2.3.3.2 Assembly of the Fluidic Parts and Priming the Device

Package with fluidic parts including tubing, connectors and 3-way valves (Harvard Apparatus, USA) were opened in the hood and assembled onto the MFCD. Two NanoPort gaskets (ANACHEM Ltd, UK) were placed at the inlet and outlet and 3-way valves were screwed in the connector blocks on the MFCD with use of two “1/4-28 Male to Luer Male” adaptors. A 10 cm tubing of the same OD size was used to connect the 3-way valves together to act as a

bypass to the culture chamber. Inlet and outlet tubing were then connected to the 3-way valves completing the tubing connections. The outlet was placed in waste bottle raised slightly above the MFCD culture chamber to create back pressure and immersed in DMEM/F12 culture media to avoid travelling of air bubbles towards the culture chamber.

In order to prime the channels, culture area of the microfluidic chip and tubing a 20 mL syringe (with luer-lock) filled with DMEM/F12 media was used to carefully flush the tubing from the inlet first with 3-way valves switched to allow fluid through the bypass first to the outlet. Following this, the 3-way valve at the outlet was switched to allow the flow through the culture chamber, hence pushing any gasses out of the channels. By use of a P200 pipette bubbles were carefully removed from the culture chamber until there is no visible bubbles present. Then the 3-way valve at the inlet was switched to allow flow through the culture chamber and repeated the previous steps to remove any bubbles in the culture chamber.

While the culture chamber was full of culture media a tweezer was used to carefully place the PDMS lid on the chamber and slowly pressed it into place without trapping any bubbles inside the chamber. Any excess media around the lid was collected and then the PC part of the lid was placed on the top and screwed in sequentially until it was fully sealed.

2.3.4 Adjustments Made to MFCD for Long-term Perfusion Culture

2.3.4.1 Adjustments Made to the MFCD Parts

In order to increase durability of the MFCD for long-term perfusion culture, reduce the chances of media leakage and repeatability of the experiments, some changes have been made to the materials used for key parts of the device. The experiments has been performed by Rhys Macown in frame bending analysis experiments and kindly shared. For this, bottom frame material from 5 mm PC sheet has been replaced by 3 mm anodised aluminium. Furthermore, to prevent bending of the top frame, two aluminium brackets were designed to be inserted around the connectors. All the parts were designed in SolidWorks (Dassault Systemes, UK) and were manufactured from 6082 grade aluminium by Proto Labs Ltd (Halesfield, UK). In addition, M3 stainless steel screws were also replaced by M3 nylon screws (Farnell Elements, UK). Changes made due to chemical reaction of the aluminium bottom frame and the stainless-steel screws inside the 95% humidity of the incubator, causing in deposition of debris around the screws.

2.3.4.2 Maintenance of Asepsis During Differentiation

In order to maintain asepsis during the long-term differentiation culture, autoclaving the parts and aseptic culture practice has shown to be ineffective. Therefore, 1% solution of Antibiotic-Antimycotic (100X) (Thermofishe Scientific. #15240-062) was added to the differentiation medium.

2.3.5 Burst Pressure Measurements

Burst pressure measurements were carried out to test durability of the MFCD against leaks caused by fluid flow pressures while perfusion. Furthermore, to test durability of the MFCD in regards to the changes made in the materials used for bottom frame (from PC to aluminium), aluminium brackets around the connectors and replacement of M3 stainless steel screws with M3 nylon screws (Farnell Elements, UK).

For this purpose, a 10 mL plastic syringe (613-3931, VWR, UK) was used to connect to one interconnect bar through tubing and a 3-way stopcock (732-8103, Bio-Rad Laboratories, UK). A luer lock plug was used to block the other side of the tubing connected to the other interconnect bar. The pressure sensor (40PC100G, Honeywell, USA) glued into a fitting (P-207, Upchurch Scientific, USA) with epoxy glue was connected to the 3rd port of the stopcock. A Kd Scientific 200 syringe drive was used to pump air into the MFCD at 5 mL/min and the pressure was recorded using LabVIEW software (LabVIEW 2011, National Instruments, USA) and a data acquisition card (USB-6229BNC, National Instruments, USA). The burst pressure was taken as the highest pressure logged for 3 different assemblies of the MFCD. First device incorporated with PC bottom frames and M3 stainless steel screws and no aluminium brackets. Second device incorporated Aluminium bottom frame, brackets and stainless steel M3 screws. The third device incorporated all the parts from the previous assembly but stainless-steel screws were replaced with the nylon ones. Each MFCD was assembled and disassembled 6 times and each time the burst pressure was recorded 3 times.

2.3.6 Flow rate Measurements

There are 3 different syringe pumps used for perfusion experiments. Aladdin programmable syringe pump and Kd Scientific 200 with 20 mL BD Plastic syringes for 130 µL/h perfusion experiments and Kd Scientific, Legato 212 with 2.5 mL HSW Norm-Ject syringes for 5.2 µL/h perfusion experiments. In order to evaluate the flow rates produced by the pumps a similar setup of the perfusion system was used with insertion of a flow meter (SLG64-0075, Sensirion AG, Switzerland) downstream of the outlet. In each measurement, all channels were primed with PBS beforehand and allowed 1 h for fluid to settle and then the perfusion was started at the given flow rates. Experiments were terminated by stopping the syringe pumps and allowed an extra 1 h to stop completely. Devices were disassembled and reassembled with new parts to repeat the experiment. Each measurement was repeated 3 times and the results shown as the average of the three measurements with standard deviation.

2.3.7 Oxygen Concentration Measurement

In order to ensure that there is sufficient dissolve oxygen (DO) concentration in the MFCD culture chamber, oxygen concentration measurement was carried out at the MFCD inlet and culture chamber and it was compared to the T-25 flask as a control.

For this two 2 mm planar oxygen sensing spot (PSt3, PreSens Precision Sensing GmbH, Germany) were glued in the middle of a MFCD and the T-25 flask. In addition, a Flow-through cell optodes (FTC-PSt3, PreSens Precision Sensing GmbH, Germany) was used for inlet measurements. The Flow-

through cell optode was connected to Oxy-4 mini transmitter, (PreSens Precision Sensing GmbH, Germany) via a 2 mm optical fibre with SMA connectors (POF-L2.5, PreSens Precision Sensing GmbH, Germany). The sensors used in the MFCD culture chamber and T-25 flasks were also connected using similar optical fibre fixed underneath of the culture slide using a prefabricated holder (PreSens Precision Sensing GmbH, Germany) and connected to the Oxy-4 mini transmitter.

A calibration solution of oxygen-free water was prepared using 1 g of sodium sulphite (Na_2SO_3) and 50 µL cobalt nitrate ($Co(NO_3)_2$) dissolve in 100 mL of pure water to prepare a standard solution (mass concentration (Co) = 1000 mg/L; in nitric acid 0.5 mol/L). The water becomes oxygen-free through a chemical reaction of oxygen with sodium sulphite. Cobalt acts as a catalyst and accelerates and completes the reaction of sulphite with oxygen. The bottle lid was sealed with a screw top and shaken for approximately one minute to dissolve sodium sulphite and to ensure that the water is oxygen-free. All channels were zeroed with oxygen-free solution. A second solution was prepared to calibrate the 100% oxygen concentration. To do this 100 mL water was used in a glass bottle and sparged air into the water using an air-pump for 20 minutes. All channels were calibrated to 100% using this solution.

The MFCD was primed with DPBS and the lid was closed and placed in the incubator at 37°C, 5% CO_2, 21% oxygen. The T-25 flask was prepared with 6 mL of DPBS and placed next to the MCFD in the incubator. Started the perfusion at the MFCD at flow rate of 130 µL/h, using a 20 mL syringe (BD plastic). The oxygen concentration was logged using the OXY4v2_30FB

software (PreSens Precision Sensing GmbH, Germany) provided for the Oxy-4 mini transmitter.

2.3.8 Assessment of the MFCD for Cell Culture Experiments

MEF and hiPSCs cultures were performed on the MFCD prior to differentiation cultures. This has helped in acquiring the necessary techniques in working with MFCD before proceeding to more costly and complicated differentiation culture. Furthermore, these cell cultures shown that our MFCD is capable of maintaining cells such as hiPSCs in stable conditions at flow rate of 130 µL/h.

2.3.8.1 Culture of Mouse Embryonic Fibroblasts

One set of MFCD was autoclaved and assembled with sterile TC-PS microscope slides as stated in section 2.3.3.1 MEF cells were removed from one T-25 flask according to the protocol explained in section 2.1.1.1 and were counted with a haemocytometer and their viability assessed using trypan blue exclusion assay. A given volume of the suspension was transferred to the culture chamber with cell density of 18 x 10^3 cells/cm^2 or ~ 9,000 cells the volume was adjusted to 150 µL, representing media height of T-25 flask with 6 mL of media. The MFCD was placed on polycarbonate blocks in large, glass petri dishes with approximately 5 mL of sterile water in the bottom to reduce evaporation effects and incubated at 37˚C, 5% CO_2. The device was incubated overnight monitored under the microscope at 2, 12 and 24 hours for adherence and confluency. Cells were collected after 24 hours and assessed for viability and number using trypan blue exclusion assay. The viability of the cells were compared to that of the control culture in T-25 flask. The experiment was repeated 3 times and the result was represented as the average.

2.3.8.2 Culture of hiPSCs

One set of MFCD was prepared in the same way as the previous experiments. Feeders were prepared according to the protocol in the section 2.1.1.2 and 9,200 cells were transferred to the MFCD culture chamber. The feeder cells were allowed to settle overnight. The following day hiPSC colonies were transferred to MFCD under a dissecting microscope in similar fashion that was explained in section 2.1.2. hiPSCs were allowed to settle overnight in static culture and on the following day the perfusion was started at flow rate of 130 µL/h.

Phase contrast images taken at 24 and 48 hours before cells were stained for pluripotency markers Oct4 and SSEA4. The images acquired by using an inverted fluorescence microscope (Nikon, Eclipse TE2000-U, Nikon Instruments, The Netherlands).

2.3.8.3 Expansion of EBs Vs Matrigel™ Incubation Time Study

Initial observations on seeding EBs in the MFCD showed that EBs expanded in much slower rate than those seeded in the 48-well plates. Since the culture surface and material used was the same between both devices, one possible source of difference before start of perfusion could have been due to ECM thickness resulted from Matrigel™. In order to compare expansion of the EBs in the MFCD to 48-well plate in regards to the time Matrigel™ was left in the device prior to seeding, a time-point experiment was designed. According to the retinal differentiation protocol explained in section 2.1.3, 250 and 150 µL of Matrigel™ was transferred to each well of 48-well plate and MFCD respectively and allowed to incubate for 1 hour prior to seeding EBs.

Therefore, for testing this hypothesis in the MFCD, same volume of Matrigel™ was used as per retinal differentiation protocol, but incubation time was divided to four parts of 15, 30, 45 and 60 minutes. After which Matrigel™ was removed and EBs were seeded.

Taking advantage of the lid configuration of the MFCD in making the culture chamber accessible, EBs were seeded onto the culture chamber directly. Using a P1000 pipette under the dissecting microscope, 7 EBs were carefully selected and transferred to MFCD culture chamber and 48-well plate culture dish. The lid was closed and allowed EBs to attach for 24 hours. Perfusion was started after the 24 hour incubation period and continued for another 24 hours. Phase contrast images were obtained by EVOS® XL Cell Imaging System microscope (Life Technologies) at 10x magnification for 0, 24 and 48 hours. Expansion of the EBs were measured as a ratio of expansion of the total area of the EB divided by the initial core area of the EB over time. The experiment was repeated 4 times (n= 4) in MFCD and compared to the expansion of the EBs in the 48-well plates.

2.3.8.4 Growth Factor's Interaction with PDMS

In order to test interaction of PDMS with key growth factors bFGF, DKK-1, Noggin and IGF-1, MFCD parts were autoclaved and assembled as stated in section 2.3.3.1. A 2 cm tube with same OD was used for the outlet, and a cryovial was used for media collection wrapped around an ice pack. Retinal differentiation media was prepared according to the section 2.1.4 and used to prime the device. Device was placed in the incubator at 37°C, 5% CO_2 and

perfusion was initiated at flow rate of 130 µL/h. Allowed 2 hours for the flow rate to stabilise and then replaced the cryovial with a fresh one. Media was collected after 2.5 hour, four time for each growth factor and stored at -80°C for further analysis using ELISA. The experiment was repeated 3 times (n=3).

2.3.8.5 Retinal Differentiation of hiPSCs in MFCD

For each run of retinal differentiation of hiPSCs in MFCD, two devices were prepared according to sections 2.3.3 and assembled. One device used for flow rate of 130 µL/h and one for 5.2 µL/h. Each device was coated with 150 µL of Matrigel™ for 15 minutes and primed with retinal differentiation media prepared according to section 2.1.3 before it was seeded with 7 EBs of 1,000 cells per EB. The MFCD lid was closed and the devices were incubated at 37°C, 5% CO_2 overnight. The devices were placed inside a glass petri dish with 5 mL of sterilised water at the bottom of the petri dish to reduce the evaporation effect on the MFCD. Perfusion was initiated on the next day at each respective flow rates and microscopic images were obtained once every 24 hours. The media in the syringes were replaced with fresh media once every 48 hours. Cells were collected for qPCR analysis or treated for immunostaining of the retinal markers at days 5, 10 and 21 after start of the culture.

2.3.8.6 DKK-1 Concentration in MFCD at 130 µL/h for 10 Days

A MFCD was assembled according to the previous section. Two 2 cm tubes were placed at one of the ports of the 3-way valves at the inlet and outlet for media collection. Two cryovials were fixed at the end of each tube and wrapped with an ice pack. The MFCD was seeded with 7 EBs of 1,000 cells

each according to the previous section. The MFCD was perfused at 130 µL/h for 2 hours before the 3-way vale at the inlet was turned to collect media at the inlet for 1 hour. Following this the 3-way valve was switched so it allows the perfusion through the culture chamber. Media was collected at the outlet cryovial after 2.5 hours and it was stored at -80°C for further analysis using ELISA. The experiment was repeated 3 times (n=3). A control culture in 48-well plate was used each time and number of cells in the control were counted using VI-CELL cell viability analyser.

2.4 Statistical Analysis

All experiments including cell culture and growth factors concentrations were performed in triplicate (n=3). Data points show the arithmetic mean of three biological repeats, and error bars represent one standard error of the mean (SEM) above and below the mean, unless otherwise stated. In Chapter 5 in regards to the qPCR analysis of the cells, log2 and log10 transformations were used to normalise relative expression values, and the arithmetic mean and SEM of the log values represented graphically. Gene regulation is a multiplicative process, not an additive one, therefore log transformation of the data makes its distribution more symmetrical, assigning equal weight to up or down expression of genes.

Significant differences were measured between conditions and the control by using a suitable statistical test. All statistical values calculated using the Microsoft Office Excel package 2013. The significant p-value of less than 0.05 was shown by a '*', 0.01 by '**' and less than 0.001 by '***'.

2.4.1 Paired Student's T-test

A two-tailed, paired t-test was used when means of two paired groups were compared, i.e. the MFCD with control condition (48-well plate).

2.4.2 One-Way Repeated Measures ANOVA

One-Way Repeated Measures ANOVA was used when comparing the means of three or more groups. In this test, if the overall p-value is significantly low it indicates that at least one of the means is different from the other groups compared. In this case a Post-hoc test is then required to identify exactly which one of the groups were statistically different from the others.

2.4.3 Post-hoc Tests

As mentioned in the previous section if ANOVA results had shown that there was a difference between at least one of the sample conditions and the rest, post-hoc tests were carried out to find out which samples were different from each other exactly. To do this the Tukey’s multiple comparisons post-hoc test was used. The Dunnett's test was used to compare each experimental condition with just the control condition. The calculated p-value from tests applied used to whether or not reject the null hypothesis.

Chapter 3 Stem Cell Culture and Evaluation of Growth Factors in Retinal Differentiation Media

3.1 Introduction

Human embryonic stem cells, as a therapeutic agent, have the potential to provide treatment for many conditions that once were considered untreatable. However, translating lab-scale research to large-scale manufacturing pose significant bioprocessing challenges. Producing a specific cell type, demands fine control of environmental factors to reduce variability that exists in step-wise differentiation protocols. (Serra et al., 2012) Differentiation protocols available today have low yield, are not efficient and include a large number of variability, which makes their scale-up more challenging and the whole process development cost more. (Ouyang et al., 2008)

Differentiation cultures are mostly developed in well-plates, which by design lack instrumental controls and can introduce a large number of variables into such cultures. Pluripotent stem cells (PSCs) have an inherent heterogeneity within their culture. (Hoffman et al., 2005) Therefore, maintaining pluripotent cultures through development of systematic controls that minimise these effects, would be essential in producing a homogeneous cell population.

In this chapter, the methodology used for culture of the cells, mouse embryonic fibroblasts (MEFs) and human induced pluripotent stem cells (hiPSCs) are described. Expression of the pluripotency markers were checked in the hiPSCs to test working conditions for the culture of these cells. Scale-down considerations used in the retinal differentiation protocol are explained to

provide a valid control for the microfluidic perfusion cultures. Essential normalisation steps for accurate qPCR analysis of the cells are introduced. Furthermore, expression of the key retinal markers in differentiating hiPSCs are validated considering adaptations made to the original differentiation protocol. Finally, molecular dynamics of the retinal differentiation culture is evaluated in terms of cytokine degradation and consumption. This study was essential in establishing an order of importance for these cytokines as they are regulating key cell cycles during retinogeneis, hence guiding hiPSCs toward retinal progenitors. Understanding cellular demands of these molecules will assist in selecting a perfusion rate that can create the steady-state concentration of soluble factors.

3.2 Culture and Characterisation of hiPSCs

Pluripotent stem cells have the potential to differentiate into all three germ layers: mesoderm, endoderm and ectoderm. (Thomson et al., 1998) Routine cell culture, manual handling of the cells during sub-culturing and their passage number, can cause spontaneous differentiation of the cells. The heterogeneous population of the cells must be separated either manually or by other means prior to further process development. Differentiation pathways are often a one-way route naturally and spontaneous differentiation of pluripotent stem cells toward an undesired lineage is counterproductive in costly process development efforts. Therefore, it is essential to characterise cells routinely to ensure they meet the stem cell criteria in terms of morphology and expression of key pluripotency markers. (Hoffman et al., 2005)

3.2.1 Morphology and Undifferentiated State of hiPSCs

As mentioned in the section, 2.1.1 the hiPSC line used in this work was MSUH001, passages 68 to 78. The hiPSCs were co-cultured on mitotically inactivated MEFs prepared a day before in gelatine-coated T-25 flasks. The use of a feeder layer first established by Thomson (1998), since then various number of MEF densities have been reported in the literature from 9,200 cells/cm^2 up to 70,000 cells/cm^2. (Heng et al., 2004) However, the working MEF density for each cell line differs and it must be established based on the culture of cells and their morphology. To establish a suitable MEF density for culture of the hiPSCs, two densities of 10,000 and 20,000/cm^2 were chosen. The 20,000 cells/cm^2 was chosen based on literature work reported for hPSCs (Heng et al., 2004; Maherali et al., 2008) and recommendations by the WiCell Research Institute (WiCell Research Institute Inc., 2003) as the lower limits. The 10,000 cells/cm^2 density was lower than recommendations stated previously, however it was chosen based on discussions with Ms. Ludmila Ruban and the previous practice in the lab. (Fig 3.1A, B) hiPSCs were cultured on both MEF densities and passaged twice per week based on confluency and their morphology, for 2 consecutive weeks.

The hiPSCs colonies in the flasks with 20,000 MEFs/cm^2 exhibited higher degree of heterogeneity and were more likely to differentiate spontaneously after days 3-4 post-passage. However, colonies formed over MEF density of 10,000 cell/cm^2 did not exhibit visible heterogeneity or spontaneous differentiation. hiPSC colonies grown on the MEFs with higher density became enlarged with translucent cytoplasm. In some cases, even formation of neural

rosettes was observed as a clear indication of spontaneous differentiation. (Fig 3.1 B, D). On the other hand, colonies grown on the MEF density of 10,000 cells/cm^2 provided better support for formation of the hiPSC colonies and cells showed higher degree of homogeneity in those flasks. (Fig. 3.1C)

3.2.2 Pluripotent Markers Expression of hiPSCs

Colonies were routinely passaged under the microscope once they were at least 80% confluent. Expression of pluripotent markers were used to characterise the undifferentiated state of the cells. hiPSCs of passage number 70/72 were first analysed by immunocytochemistry, at 4 days' post-passage. qPCR analysis of the pluripotent markers was also carried out to quantify the expression of these markers against the differentiation marker SSEA1. Markers stained for are cell surface keratin sulphate-related antigens Tra-1-81, Tra-1-60 and the globoseries glycolipid antigen SSEA4. SSEA4 marker was particularly used to highlight any areas of heterogeneous morphology caused by either spontaneous differentiation or cellular overgrowth. Furthermore, cells were also stained for the nuclear transcription factors Oct4 and early differentiation marker SSEA1 to detect any differentiated colonies or areas around them.

Homogenous expression of the surface and nuclear markers Tra-1-81, Tra-1-60, SSEA4 and Oct4 were observed throughout hiPSC colonies in the cultures. In some colonies, minor expression of the SSEA1 was observed (Fig 3.2 A-D), which considered to be acceptable as part of standard practice in hiPSCs culture. (Tonge et al., 2011) Instances where heterogeneity of the colony resulted in downregulation of Oct4 were presented in Figure 3.2 (E-H).

Colonies with homogeneous morphology showed positive expression of the pluripotency markers Tra-1-81, Tra-1-60, SSEA4 and Oct4. (Fig. 3.3A-H).

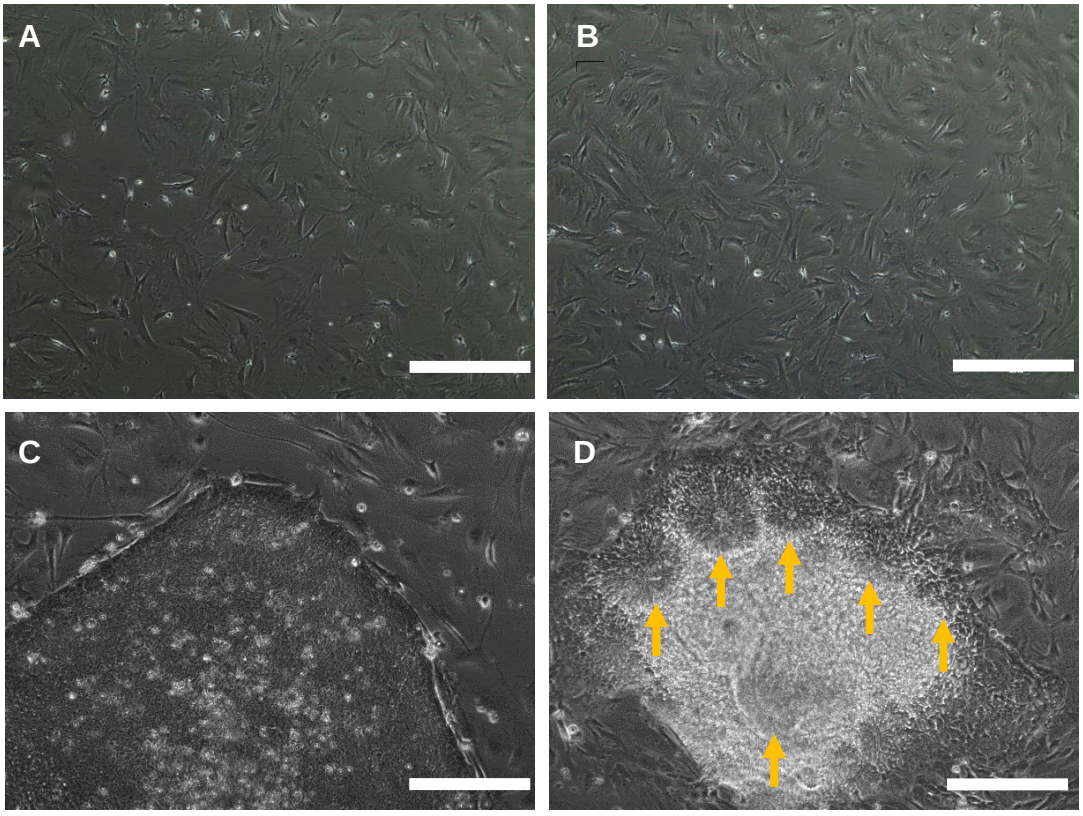

Figure 3.1 Effects of MEF Density on Morphology and Undifferentiated State of hiPSCs.

(A) MEF cultured at density of 10,000/cm^2 compared with (B) with density of 20,000/cm^2. Higher density of the MEFs restricts the formation of hiPSC colonies and could results in spontaneous differentiation of the hiPSCs (C) Densely packed colonies of the hiPSCs cultured on the MEFs with density of 10,000/cm^2. (D) hiPSCs cultured on MEFs with density of 20,000/cm^2. White arrows show areas that cells differentiated as a result of higher density of the MEFs. Larger and translucent cytoplasm of the cells are visible and formation of neural rosettes are a clear indication of spontaneous differentiation. Scale bars represent 200 µm.

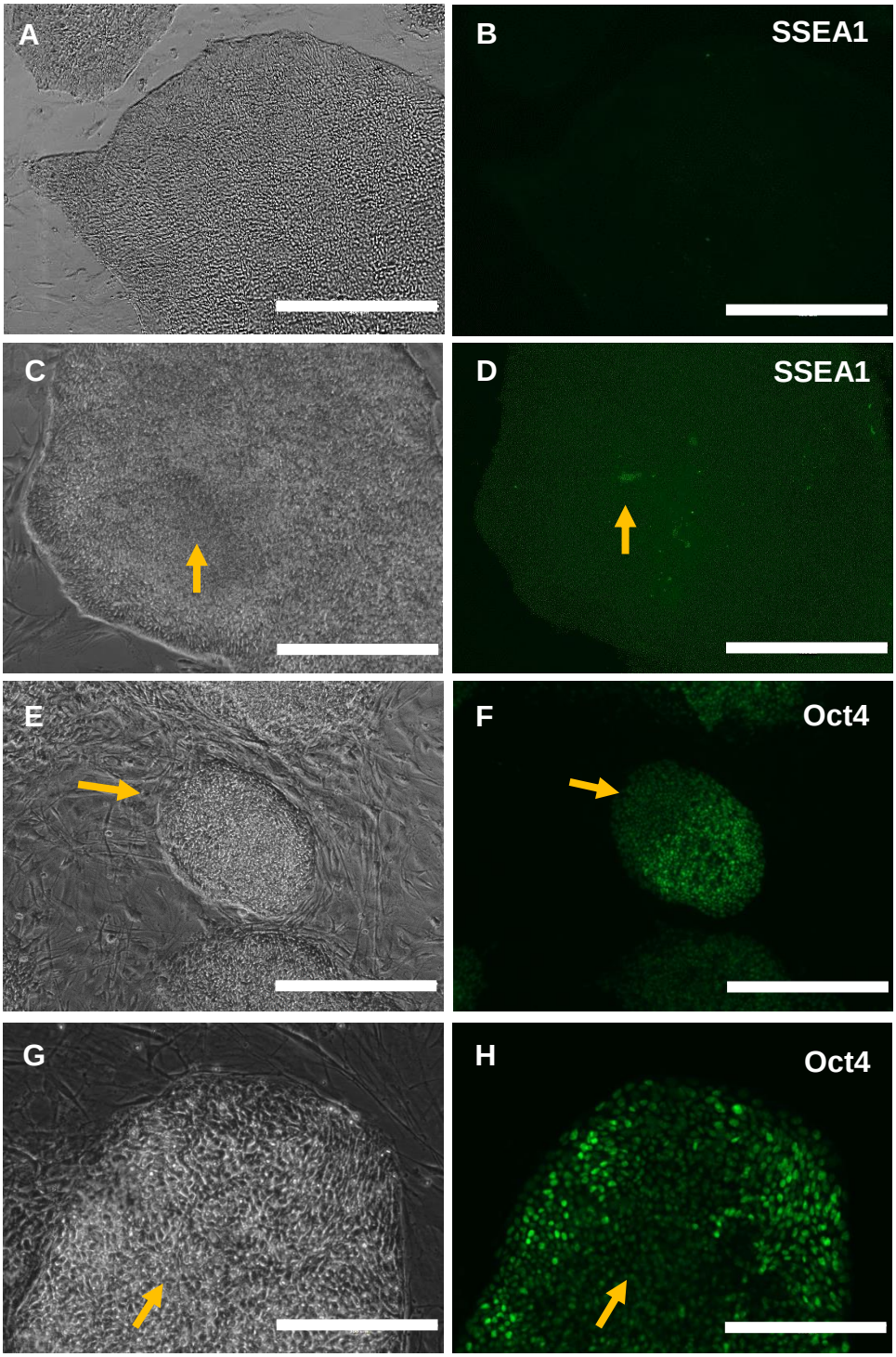

Figure 3.2 Onset of Differentiation in Heterogenous hiPSC Colonies.
(A-B) SSEA1 expression in colonies grown on MEFs with density of 10,000 cells/cm^2. Showing highly packed monolayer population of hiPSCs with round small cytoplasm. Exhibiting very small expression of the early differentiation marker SSEA1. (C) Area shown with an arrow exhibits overgrowth of the hiPSCs. (D) Onset of differentiation is shown by the expression of the SSEA1 marker. (E-H) Examples of downregulation of Oct4 in hiPSC colonies on MEFs with density of 20,000 cells/cm^2. Secondary antibody used Alexa 488. Scale bars 200 µm.

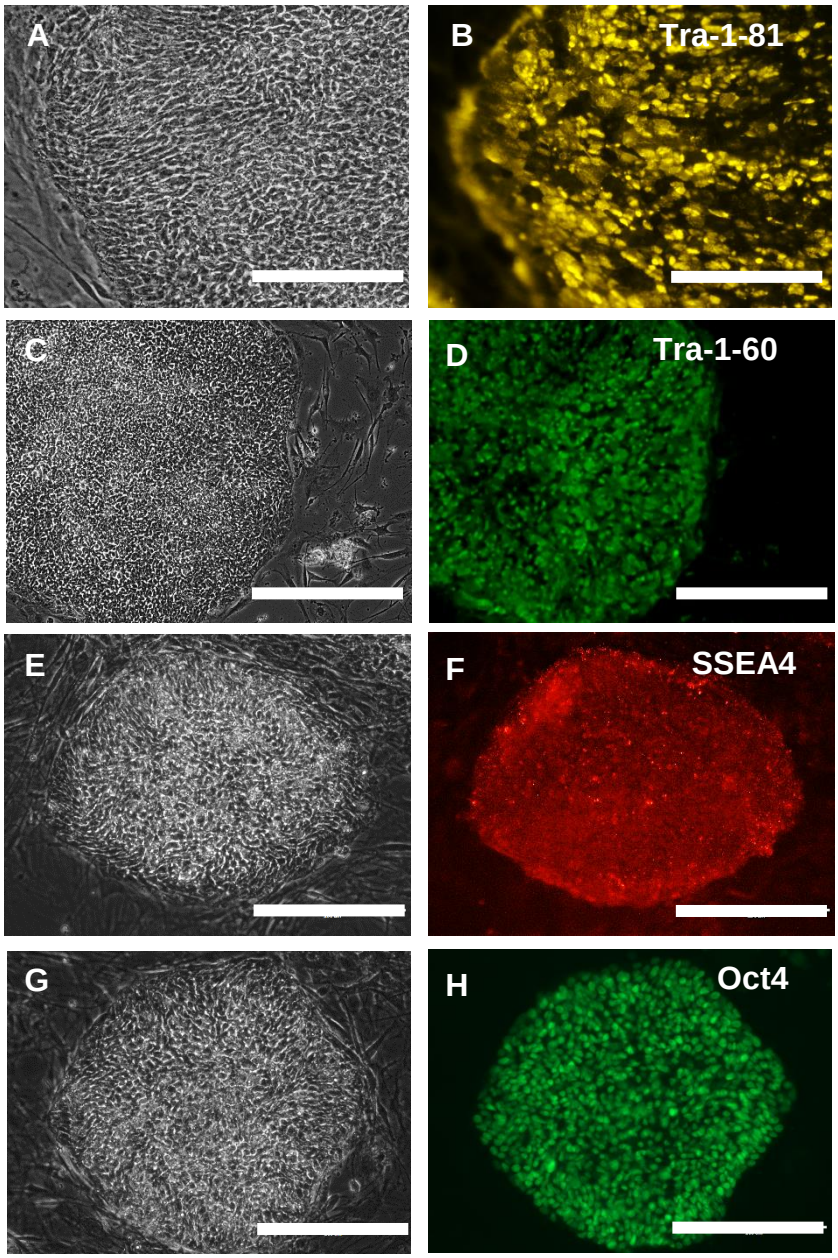

Figure 3.3. Expression of Pluripotent Markers in Homogenous hiPSC Colonies.

hiPSCs maintained and passaged twice per week. The colonies that were pluripotent, passaged to a new flask with mitotically deactivated MEF layer. The images shown in this figure represent selected phase contrast and fluorescent images of the hiPSCs at day 4 showing homogenous expression of the pluripotency markers (A-B) Tra-1-81, (C-D) Tra-1-60, (E-F) SSEA4, and (G-H) Oct4. Protein expression is visualised with secondary antibodies Alexa 532 (B), Alexa 594 (F), and Alexa 488 (D, and H). Scale bars represent 200 µm.

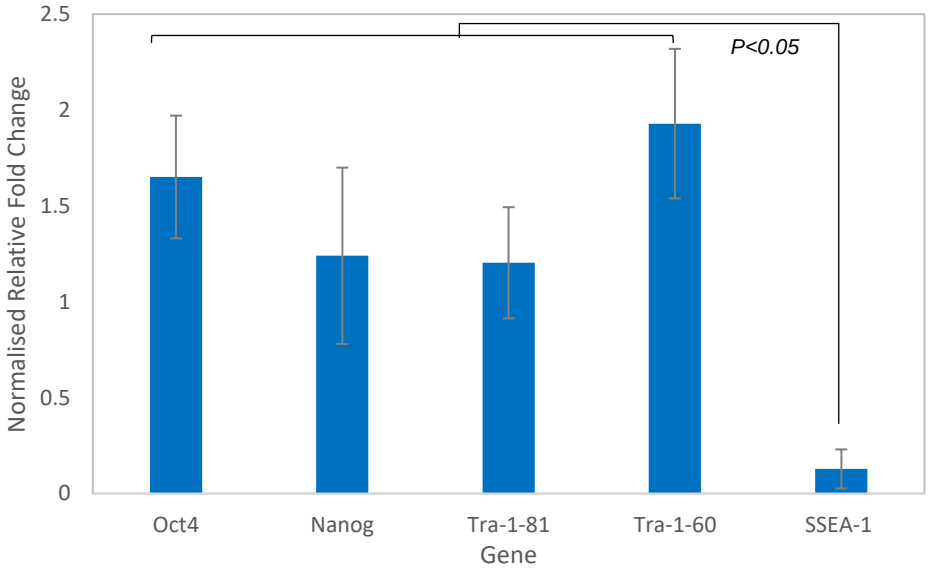

Figure 3.4 Gene Expression of Pluripotency Markers in hiPSCs Compared to Early Differentiation Marker SSEA1.

Expression of the pluripotency marker Oct4, Nanog, Tra-1-81 and Tra-1-60 relative to housekeeping genes GAPDH, β-actin in hiPSC colonies with homogeneous morphology on day 4. The nuclear (Oct4 and Nanog) and cell surface markers (Tra-1-81 and Tra-1-60) showed expression of these genes compared to SSEA1.Error bars represent one standard error of the mean about the mean of at least three independent data points (n=3).

Morphological studies of the hiPSCs cultured on higher MEF density of 20,000 cells/cm^2 revealed that hiPSC colonies showed more heterogeneity within each colony. hiPSCs in these colonies were larger and had translucent cytoplasm in the outer edges. The higher MEF density in these cultures were likely resulted in higher mechanical force exerted by the hiPSCs to create the necessary space while proliferating. Moreover, packed groups of the cells in the middle of the colony were forced to grow on top of each other, hence creating overgrowth of the cells in middle of the colonies. The immunocytochemical staining images obtained from these cells confirmed the expression of early differentiation marker SSEA1 in such areas as well as

down regulation of the pluripotency marker Oct4. The latter indicated unsuitable culture conditions using the higher MEF density, therefore it was removed from further studies and qPCR analysis. On the contrary, desired morphological observations and immunocytochemical analysis of the cultures with lower MEF density, lead to adaptation of this MEF density for future hiPSCs culture routine.

Relative expression of these markers with addition of Nanog and SSEA1 were measured using qPCR (Fig 3.4). The analysis showed 12.3 folds for Oct4, 9.2 folds for Nanog, 9 folds for Tra-1-60 and 15.1 folds higher expression of Tra-1-81 compared to the early differentiation marker SSEA1 ($p<0.05$).

Standard G banding karyotypic analyses were routinely performed on hiPSCs (MSU001 line) (TDL Genetics, Whitfield Street, London) by other lab members and the results were reported by Sharma et al. (Sharma et al., 2016). Since same cell bank was used in this work the karyotypic analyses were not performed to avoid duplication of the results. Typical G banded chromosomes were observed for the hiPSCs at passage 68 with majority of the analyses showing normal 46 XX karyotypes. However, each batch taken from liquid nitrogen was routinely subjected to morphological analysis, immunocytochemical staining and qPCR analysis for expression of the pluripotency markers as a quality control method prior to differentiation studies.

Overall, result showed suitable working density of the 10,000 cells/cm^2 for MEFs and a passaging routine of twice per week for maintaining a healthy

pluripotent hiPSCs population. homogeneity of the hiPSCs plays a key role in differentiation studies. Spontaneous differentiation of the hiPSCs takes place based on micro-environmental cues and alters the differentiation lineage of the cells, which in turn will have a direct effect on yield and efficiency of the process in achieving a target cell population. In practice, it is essential to perform gene expression and immunocytochemical staining analysis for every cell batch and make sure to use colonies that are morphologically homogeneous and show close resemblance to a healthy pluripotent population.

3.3 Retinal Differentiation Protocol and Scale-Down Considerations

Prior to investigating the effects of steady-state concentration of soluble factors on retinal differentiation of hiPSCs, it was important to characterise dynamics of retinal differentiation culture in static state. Establish expression of retinal differentiation markers at each time point and make the necessary changes to the protocol.

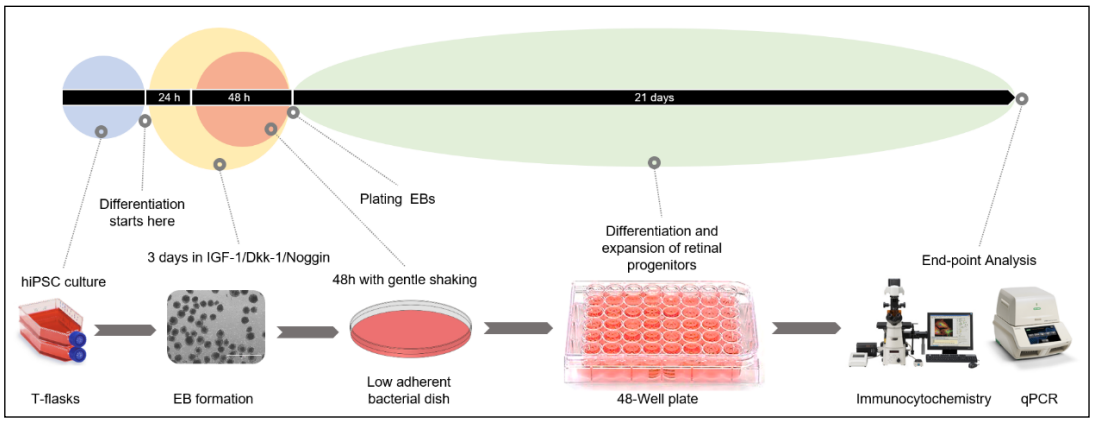

Figure 3.5 Timeline and Schematic Representation of the Retinal Differentiation of hiPSCs.

Retinal differentiation protocol used in this thesis has two major steps, formation of Embryoid Bodies (EBs) and retinal determination. In the first step, in order to make uniform sized EBs with 1000 cells per EB we used AggreWell™ plates. EBs were formed on the AggreWell™ plates on the first 24h and transferred to a low adherent bacterial dish for the next 48h. On day 3 EBs were transferred onto 48-Well plates for the retinal determination step. End-point analysis of the retinal markers expression were carried out using immunocytochemistry and qPCR.

As explained in the section 1.2.3 retinal differentiation protocols are stepwise, which makes them long and adds greater degree of complexity to the whole process. In such protocols, it is important to recognize key variables affecting the culture in each step before adapting it to a new culture condition. Figure

3.5 shows timeline and schematic representation of the retinal differentiation of hiPSCs.

The Lamba's protocol (2006) used in this work consists of two main steps. The first step is formation of cellular aggregate, or EBs, which were maintained for 3 days in suspension culture. During this time, cells were stimulated for neural differentiation by addition of Noggin, DKK-1, IGF-1, Knockout serum, and N2 supplement (As explained in section 2.1.3). Following this step, EBs transferred onto Matrigel™ coated plates for the rest of the differentiation process (3 weeks). During this period, the media is supplemented by higher concentration of the factors mentioned in the first step (according to the protocol in section 2.1.3) and addition of bFGF and B-27 to direct the cells towards retinal lineage. The knockout serum was excluded from the culture media at this step.

3.3.1 Formation of Uniform Sized Embryoid Bodies (EBs)

EB formation from ESCs is one of the most common methods for producing multi-lineage cells due to the capability of EBs to recapitulate various aspects of cell differentiation during early embryogenesis. (Kurosawa et al., 2007) Studies have shown that methods used for formation of EBs will influence their heterogeneity, aggregation kinetics, size, and differentiation pathways. (Leahy et al., 1999; Koike et al., 2007) EBs formed when ESCs are cultured in suspension without presence of anti-differentiation factors such as leukaemia inhibitory factor (LIF) or in co-culture with MEFs. (Kurosawa et al., 2007) Undifferentiated ESCs have large number of calcium-dependent adhesion glycoproteins (E-cadherins) expressed on their surface. The E-cadherins are

essential in formation of EBs through binding of the calcium molecules. In such cultures, small molecules such as Y-27632 and 2,4-disubstituted thiazole (Thiazovivin/Tzv) must be used as inhibitors of the rho-associated kinase (ROCK) pathway to reduce cell death and increase binding capacity of the ESCs. (Ungrin et al., 2008; Hwang et al., 2009; Sargent et al., 2009)

There are various methods for producing EBs, among such are, (1) static suspension culture in low adherent petri dishes, (2) hanging drop method, (3) encapsulation or entrapment of ESCs, (4) use of various bioreactors, and finally (5) use of low adherent microwells plates. (Kurosawa et al., 2007) In static suspension cultures, such as the one used in Lamba's protocol, cells usually are dissociated via manual scraping or enzymatic dissociation (collagenase IV) of ESC colonies. Though manual scraping is a relatively quick method for formation of large number of EBs, it offers no control over EB sizes and results in heterogeneity of EB shapes and their differentiation. (Bauwens et al., 2008) Other methods such as hanging drop are useful in making uniform size EBs as known density of ESCs are transferred into each drop on a petri dish lid. However, methods like this have poor media exchange and EB drops must be transferred to suspension cultures after few days. Furthermore, such methods are labour intensive, long and introduce more complexity into the differentiation process. Entrapment methods use hydrogels such as methylcellulose, hyaluronic acid, fibrin, dextran, alginate, or agarose to encapsulate known density of ESCs. Although efficient in increasing reproducibility of differentiation, they lack efficiency and are difficult in obtaining cells at the end of the process. (Rungarunlert et al., 2009)

Use of various bioreactors such spinner flasks, rotating cell culture system (RCCS), rotary orbital culture vessels and computer-controlled bioreactors, offer scalable production of EBs, efficient media exchange and are open to various process controls. On the other hand, EBs produced in such devices must be transferred to a new device to avoid formation of large aggregates; moreover, such devices do not allow microscopic observation of the EBs and often not suitable for small scale research applications. (Carpenedo et al., 2007) Alternative methods are using low adherent multi-well plates such as round/V-bottomed 96-well plates and microwell plates such as AggreWell™ (Stemcell Technologies, Canada). These devices are capable of formation of control sized EBs, provide sufficient media exchange and microscopic observation of EBs. (Choi et al., 2010) In this method EBs are formed by adding a single cell suspension of a known density to the microwell plate, plates then are centrifuged to distribute the cells evenly among the microwells and finally, captured cells are cultured for 24 hours to allow aggregation of the ESCs within each microwell. Therefore, due to advantages that such methods offer and their compatibility with retinal differentiation protocol, we used this method to produce EBs in the experiments performed in this work.

Figure 3.6A exhibits EBs formed via manual scraping in static culture dishes. As mentioned previously EBs made via this method are often irregular in shape and differentiation pathway. Furthermore, the number of cell death is much higher in such methods. (Sharma et al., 2016) Figure 3.6B, C and D shows EBs produced using AggreWell™ 400. This method consistently

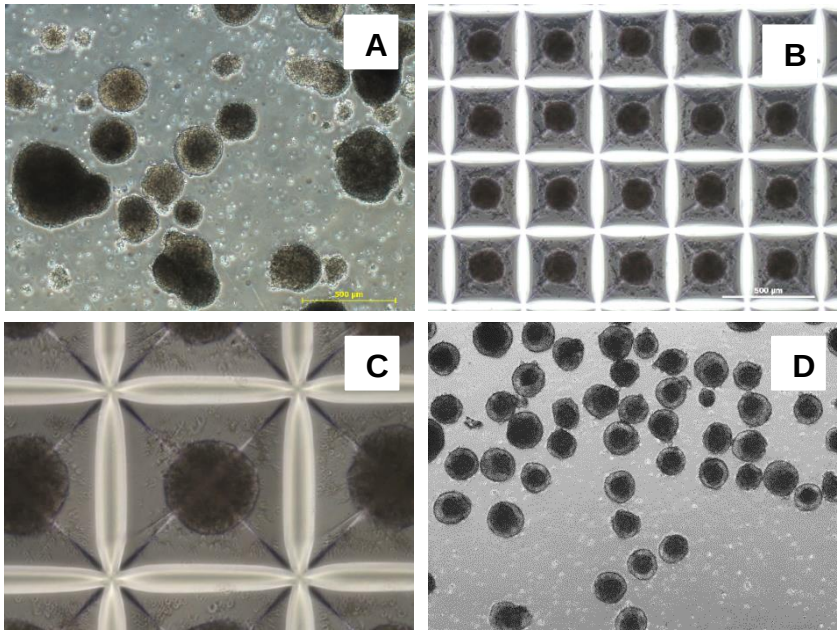

Figure 3.6 Formation of Uniform Sized EBs from hiPSCs Using AggreWell™.
(A) EBs formed via scrapping method. In this method, it is often difficult to form same size EBs and results in higher cell death. (B-D) Using micro-well plates such as AggreWel™l improves the cell viability and formation of uniform sized EBs. This method can be used to reduce variability in EB sizes and increase control over differentiation culture.

produces uniform size and shape EBs in a consistent manner with lower cell death. (Bauwens et al., 2008; Mohr et al., 2009; Markway et al., 2009)

3.3.2 Selection of the EB Size

Various studies have shown a direct correlation between EB sizes and their specific differentiation lineage. For example, cardio and neurogenesis differentiations were observed more in EBs of larger size of 450 µm in diameter and EBs of smaller sizes of 200 µm shown more endothelial differentiation. (Karp et al., 2007; Hwang et al., 2009; Choi et al., 2010) On the contrary, EBs with larger sizes have mass transfer limitation at the centre of the EB in regard to oxygen, glucose and cytokine concentration. In one study, EBs with diameter of 800 µm had relatively 50% lower Oxygen concentration at their

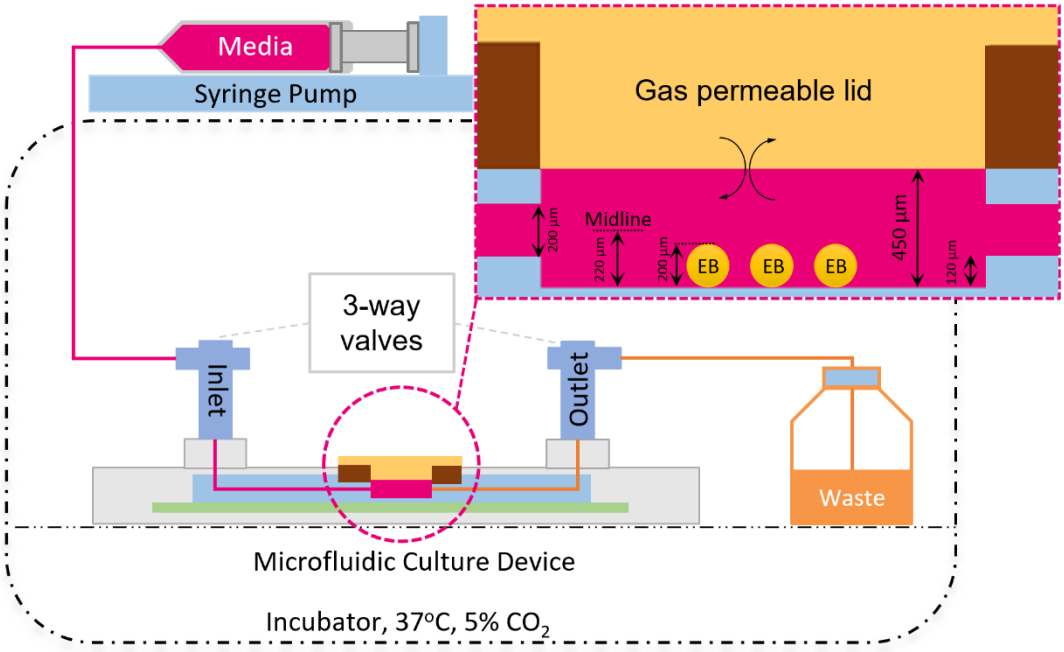

Figure 3.7 Selection of the EB Size for MFCD Culture Chamber.

The EB size and its differentiation lineage have a direct relationship. The larger EBs has shown to have more neurogenesis differentiation capabilities. However, the larger the EB, the harder it is for oxygen, nutrients and cytokines to reach the core of the EB. Studies have shown that EBs with diameter of 200-400 µm provide an ideal size for creating the right balance between soluble concentration and differentiation lineage. Provided the dimensions of the MFCD culture chamber, EBs with the diameter of 200 µm were selected for retinal differentiation protocol in MFCD.

core compared to the EBs with 400 µm in diameter. Concentration of Oxygen and general cytokines in EBs with diameter of 200-400 µm have shown no significant difference between core and surface of the EBs. (Van Winkle et al., 2012) Carpenedo (2009) demonstrated that homogeneous differentiation of EBs were dependent on uniform spatiotemporal concentration of soluble factors inside and outside EBs. Therefore, finding the right balance between the size related differentiation lineage and mass transfer limitation is essential in creating true steady-state concentration of the soluble factors in the culture. (Carpenedo et al., 2009)

V-bottomed microwell plates such as AggreWell™400 provides microwells with 400 µm diameter, which is suitable for producing EBs of 50–3000 cells per EB. The culture chamber of our MFCD has height of 450 µm, and height of the channel inlet into the culture chamber is 220 µm. Considering the inlet channel height, mass transfer limitations and lineage specific differentiation, using EBs of 1000 cells per EB with diameter of 200 µm offers the best choice for our MFCD and retinal differentiation of hiPSCs. Schematics of how EBs fit into the culture chamber is shown in Figure 3.7.

3.3.3 Considerations for Gene Expression Analysis

To measure expression of mRNA at various stages of differentiation process, real-time quantitative polymerase chain reaction (RT-qPCR) was used. RT-qPCR has the sensitivity and required accuracy to measure small changes in gene expression and considered as a “gold standard” nowadays. However, accuracy of RT-qPCR is dependent on various factors such as assay design, protocol, RNA integrity, template quantity, proper normalisation and selection of the right reference genes. (Arya et al., 2005; Nolan et al., 2007) Existence of variability in these factors and inconsistency in processing and analysing data can result in inaccurate and wrong interpretation of the experimental results. The inherent challenges associated in preparing RNA samples used in RT-qPCR requires one to use normalisation at various steps to reduce variability. Figure 3.8. explains various steps involved in RT-qPCR and indicates the required normalisations at each step during the process. (Guénin et al., 2009; Liu et al., 2015)

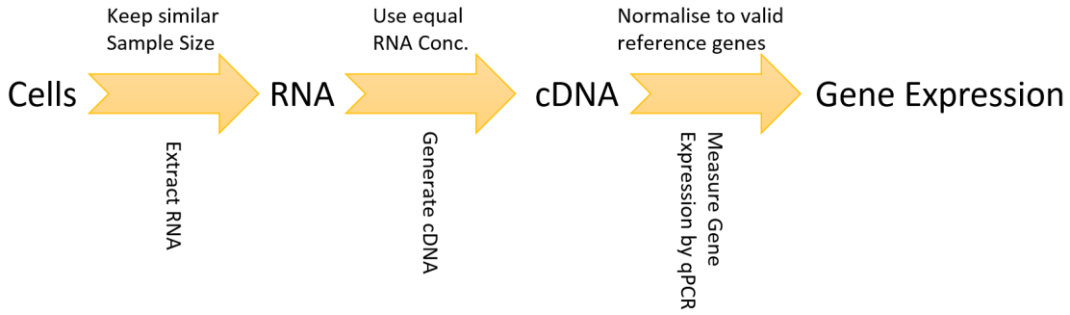

Figure 3.8 Essential Normalization Steps During the qPCR Protocol.

Accuracy of the qPCR is dependent on proper normalization at key steps during the protocol. Having similar sample sizes is essential in obtaining similar RNA after the extraction process. The next normalization step requires to use equal RNA concentration before creating the cDNA library. The final step in normalization involves the selection of the right reference genes.

3.3.3.1 Sample Size

Size of each sample have direct effect on the quantity of the RNA obtained. When designing experiments involved with cells in an adherent culture, it could be difficult to obtain the same number of cells in each well of the culture plate. Cells can replicate differently under different conditions, grow on top of each other and create complex 3D shapes, which makes it extremely challenging to control. Therefore, using the same sample volume/weight is the initial step to take to control variability at this stage. (Huggett et al., 2005) The microfluidic culture device (MFCD) used throughout this thesis has a culture chamber with the area of 0.52 cm^2. In order to match this area with a well-plate that is conventionally used for differentiation studies, we chose 48-well plate, which has the area of 0.95 cm^2. Though this is a larger area than MFCD's, it was the smallest size before 96-well plate that we could use. Moreover, 48-well plate

had fewer difficulties in terms of seeding EBs, media height similar to our MFCD and well bottom shape compared to the 96-well plate. In order to keep sample sizes equal both cultures were seeded with the same number of cells and unified EB sizes.

3.3.3.2 RNA Quality and Quantity

The RNA quality can be analysed via various methods, gel OD measurement, OD measurement using NanoDrop, denaturating agarose gel-electrophoresis or using more modern lab-on-chip technologies such as Bioanalyzer 2100 (Agilent Technologies, USA) and Experion (Bio-Rad Laboratories, USA). (Fleige et al., 2006) The UV measurements at 260 nm is specified for nucleic acids, 280 nm for proteins and 230 nm for contamination. The ratio of optical density of 260/280 used for quality assessment of the extracted RNA and OD of 260/230 used for measuring the purity of the sample. For A260/280 a value of 1.8 to 2.1 is considered acceptable. (Fleige et al., 2006) A higher value of these indicators is often due to genomic DNA, salt concentrations, carbohydrates, peptides, phenol and guanidine thiocyanate that is present at the lysis buffer at the extraction stage. (Becker et al., 2010) We used NanoDrop (ND-1100, NanoDrop Technologies, USA) for measurement of OD throughout this thesis. A value of just above 2 is considered acceptable for A260/230 measurements.

The other factor to consider here is the RNA concentration after extraction from each sample. Before proceeding to the cDNA synthesis step it is essential to have similar concentration of the RNA. Moreover, when dealing with large samples, the amount of RNA obtained is often sufficient to include enough

copy numbers of the transcripts of interest and hence, proceed with the cDNA synthesis step. However, when experiments performed at smaller scales this could become an issue. When the copy number of the transcripts of interest is 10 or less in a sample, stochastic problems will occur, which means there are unequal amount of a low number of transcripts in a diluted solution. (Fleige et al., 2006) Therefore, before proceeding to the cDNA step a whole transcriptome amplification may be required to make sure all transcripts are represented equally.

3.3.3.3 Normalising to the Right Reference Genes in hiPSCs

RT-qPCR allows quantification of relative expression of target genes compared with one or a group of internal genes commonly expressed in a cell line, which are referred to as reference genes. One of the most important feature of these internal genes is that their expression level does not change as a result of treatments applied to the cellular population. Some of the most commonly used reference genes are β-actin, glyceraldehyde-3-phosphate dehydrogenase (GAPDH), hypoxanthine-guanine phosphoribosyl transferase (HPRT) and 18S ribosomal RNA. (Huggett et al., 2005) These internal genes have been used extensively in various publications and believed to have stable expression levels. However, different studies have shown that they are not as stable as they once thought to be. In fact, the activity level of each gene is dependent on type of sample, time of collection and the treatment applied. (Suzuki et al., 2000; Warrington et al., 2000; Vandesompele et al., 2002) Therefore, a validation process must be carried out before selection of these

genes to minimise the errors associated with selecting irrelevant reference genes.

M-value is used to validate stability of expression of reference genes. The genes with lowest M-value considered to be the most stable. For homogenous cultures, a value of <0.5 is considered acceptable for the M-value and for intra-run coefficient variation (CV) a value of <0.25. It is reported that the optimal number of the reference genes used is dependent on the samples and combination of the genes used. (Ling et al., 2011) Based on various publications for hiPSCs retinal differentiation, four reference genes GAPDH, β-actin (ACTB), Ubiquitin C (UBC) and TBP, were selected and a study was designed to evaluate their stability. (Lamba et al., 2006; Osakada et al., 2009; Mellough et al., 2012)

Figure 3.9 shows stability study performed on the mentioned genes and their mean CV. In order to make sure that results are valid for different conditionings, both untreated hiPSCs and samples from 5,10 and 21 days' retinal differentiation cultures were used to perform the study. For this purpose, the GeNorm algorithm incorporated into the CFX Connect software was used to perform all the calculations. (Vandesompele et al., 2002)

Results shown that only two combinations of the reference genes used (GAPDH/TBP and ACTB/UBC) have a M-value below 0.5 and mean CV of below 0.25 for hiPSCs going through retinal differentiation. Combination of the β-actin and UBC showed the lowest M-value of 0.1021 and CV of 0.0354. Therefore, it was considered to be the most stable combination of the

reference genes for the hiPSCs line used in the process of retinal differentiation.

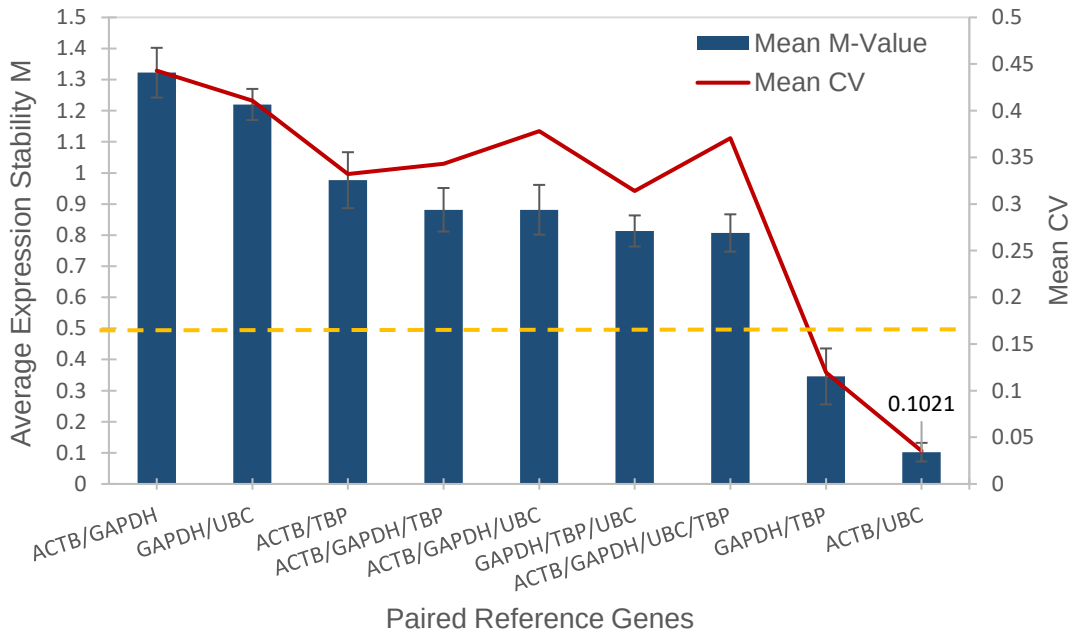

Figure 3.9 Reference Gene Validation Using Average Expression Stability (M Value).

M-value was used to study expression stability of paired reference genes in hiPSCs. The reference genes used were β-Actin (ACTB), GAPDH, UBC and TBP. For homogeneous cultures, an M-value of <0.5 and coefficient variation of <0.25 is considered acceptable. However, as a rule, the lower the M value, the higher the stability of the paired reference genes. ACTB/UBC has showed the lowest value in this study with M-value of 0.1021 and a CV of 0.0354. Error bars represent one standard error of the mean about the mean of at least three independent data points (n=3)

3.4 Time-point Expression of Retinal Markers

In order to test the protocol in light of adjustments made so far, we performed a 5, 10 and 21 days' retinal differentiation of the hiPSCs and compared the expression profile of the relevant genes in each stage with that of the pluripotent hiPSCs. This analysis also helped us to expect which genes will express once we introduce perfusion into the culture. For this purpose, we performed two types of end-point analysis, immunocytochemical staining and RT-qPCR.

3.4.1 Expression of Oct4, Nanog, Nestin and Otx2 on Day 5

Immunocytochemical staining was performed for Nestin and Otx2 at 5 days. (Fig 3.10) Nestin is a neuronal progenitor cells marker that regulates intermediate filaments formation during central nervous system (CNS) development. Nestin is downregulated during later stages of development. (Michalczyk et al., 2005) Otx2 expression is essential for development of anterior structures of the CNS, however like Nestin it is downregulated at the later stages of retinal differentiation to allow for eye field specification. (Jayakody et al., 2015)

Figure 3.11 shows qPCR analysis for gene expression at 5 days. Relative expression of pluripotent markers Oct4 and Nanog compared to hiPSCs showed Oct4 with only 30% and Nanog 20% expression of these genes relative to hiPSCs. A clear downregulation of these genes as cells progressed through this differentiation step. Nestin and Otx2 showed 68% and 42% respectively higher expression of these markers relative to hiPSCs.

Upregulation of these genes compared to the pluripotent markers indicates CNS development.

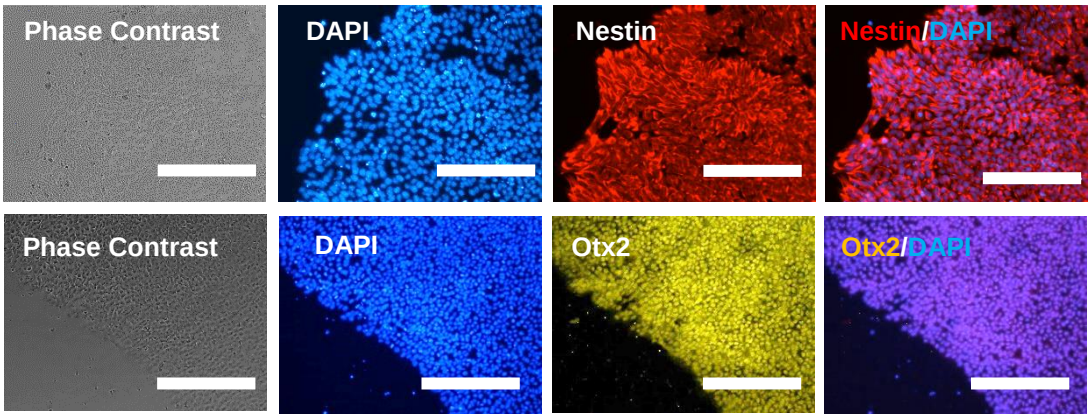

Figure 3.10 Expression of Nestin and Otx2 on Day 5 of Retinal Differentiation of hiPSCs.

Immunocytochemical staining after day 5 of retinal determination step. Both Nestin and Otx2 showed uniform expression. The overlay shows the expression of these markers with DAPI. Indication of cytoplasmic and nuclear expression of Nestin and Otx2 respectively. Secondary antibodies used Alexa 594 (Nestin) and Alexa 532 (Otx2). The scale bar represents 200 µm.

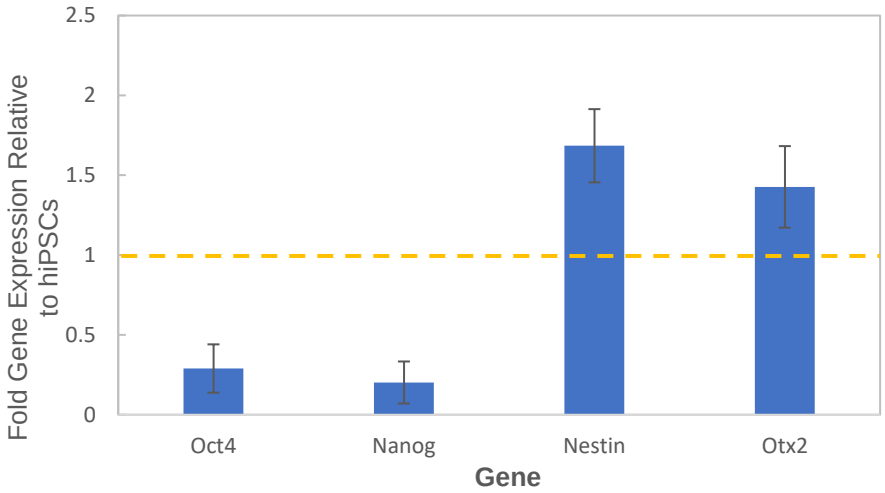

Figure 3.11 qPCR Analysis of Pluripotency Markers on Day 5 of Retinal Differentiation of hiPSCs.

Relative expression of the pluripotency genes Oct4 and Nanog on day 5 compared to that of the hiPSCs. Value of one indicates similar level of expression as in hiPSCs. The expression of Oct4 and Nanog were downregulated in 5 days' retinal determination culture. On the other hand, the expression of the Nestin and Otx2 were upregulated by 68 and 42% respectively. Error bars represent one SEM about the mean of 3 independent data points (n=3).

3.4.2 Expression of Pax6, Lhx2, Six6 and Vsx2/Chax10 on Day 10

Expression of the eye field transcription factor (ETEF) Pax6 and optic vesicle (OV) marker Vsx2/Chx10 was observed across all cultures. (Fig. 3.12) Figure 3.13 shows expression of these genes on day 10 using RT-qPCR analysis. Pax6 shows a clear upregulation on day 10 with an expression of 92 folds higher than that of the hiPSCs. Lhx2 is upregulated by 256 folds compared to the hiPSCs and Six6 was 3632 folds. Vsx2/Chx10 was expressed 59,517 folds higher than its levels in the hiPSCs.

Pax6 plays a key role in the optic cup development and retinal neuron's specification. It is expressed in the multipotent retinal progenitor cells as well as post-mitotic horizontal and amacrine cells. (Heavner et al., 2012) The network of the EFTEs are interrelated and dependant on each other. Expression of Otx2 and Sox2 induces the expression of Rax and Rax's expression activates expression of Lhx2, Six3 and Pax6. (Zuber et al., 2003) Six6 is a key marker in formation of optic cup and it is activated through cooperation of Pax6 and Lhx2. (Tétreault et al., 2008) Vsx2/Chx10 is expressed in presumptive neuronal retina, which along with other EFTFs are believed to have reciprocal relationship in compartmentalisation and development of the optic cup. (Jayakody et al., 2015) Vsx2/Chx10 is the first of the specific retinal markers and its expression indicates the onset of neural retinal development. (Horsford et al., 2004)

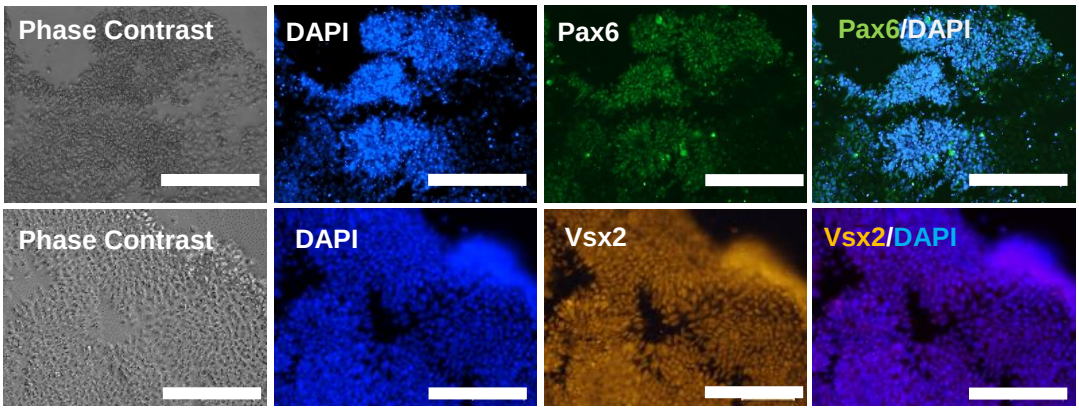

Figure 3.13 Expression of Pax6 and Vsx2/Chx10 on Day 10 of Retinal Differentiation of hiPSCs.

Immunocytochemical staining after day 10 of retinal determination step. Both Pax6 and Vsx2/Chx10 show uniform expression throughout the culture. The overlay shows the expression of these markers with DAPI. Indication of nuclear expression of these markers. Secondary antibodies used Alexa 488 (Pax6) and Alexa 568 (Vsx2). The scale bar represents 200 µm.

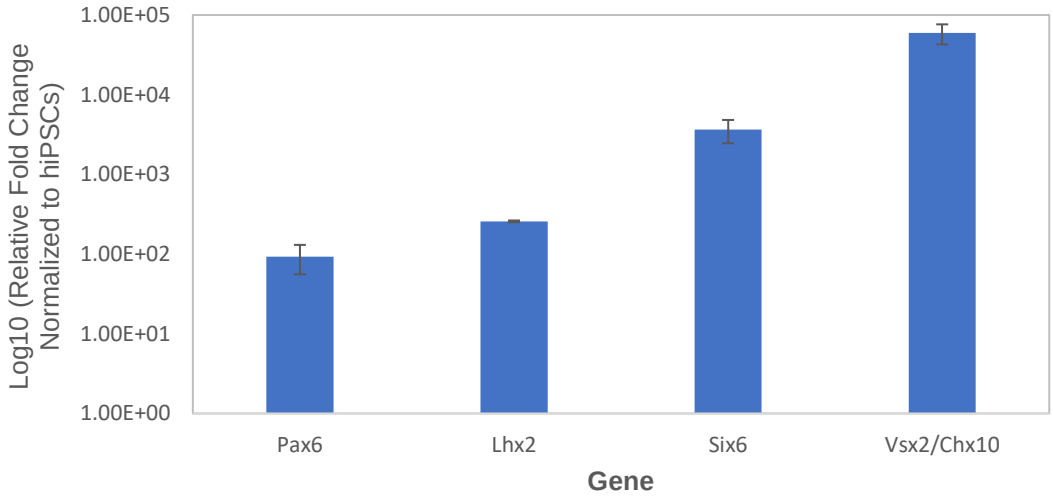

Figure 3.12 qPCR Analysis of Pax6, Lhx2, Six6 and Vsx2/Chx10 on Day 10 of Retinal Differentiation of hiPSCs.

Pax6 shows 92 folds higher expression than that of the hiPSCs. Lhx2 is upregulated by 256 folds compared to the hiPSCs and Six6 was 3632 folds. Vsx2/Chx10 was expressed 59,517 folds higher than its levels in the hiPSCs, indicating the presence of neuroretinal progenitors as part of the optic vesicle formation. Error bars represent one SEM about the mean of 3 independent data points (n=3).

3.4.3 Expression of Crx and Nrl on Day 21

Photoreceptor precursors markers, Crx and Nrl were expressed on day 21 of the differentiation culture. (Fig 3.14) Figure 3.15 shows RT-qPCR analysis of Crx and Nrl expression on day 21 of the differentiation culture. Crx was expressed 10 folds higher than that of the hiPSCs and Nrl was 30 folds higher.

Crx is expressed in retinal progenitors committed to become photoreceptors; they are also expressed in mature photoreceptors. Crx expression indicates the presence of photoreceptor progenitors in the cell population. (Furukawa et al., 2000) Nrl expression promotes development of rod photoreceptors. (Mears et al., 2001) Maclaren and colleagues observed that post-mitotic precursors that express both Nrl and Crx have better rate of integration into the host retina post-transplantation. (Maclaren et al., 2006; Lamba et al., 2010)

Otx2 is activated again at maturation stages of photoreceptor and is found to trans-activates the Crx expression. (Nishida et al., 2003) Nrl expression was found to act as a molecular switch in development of rod photoreceptor by directly influencing rod-specific genes. Furthermore, Nrl inhibits the S-cone pathway via activation of Nr2e3 gene. Therefore, showing that Nrl is required for rod photoreceptors formation. (Mears et al., 2001)

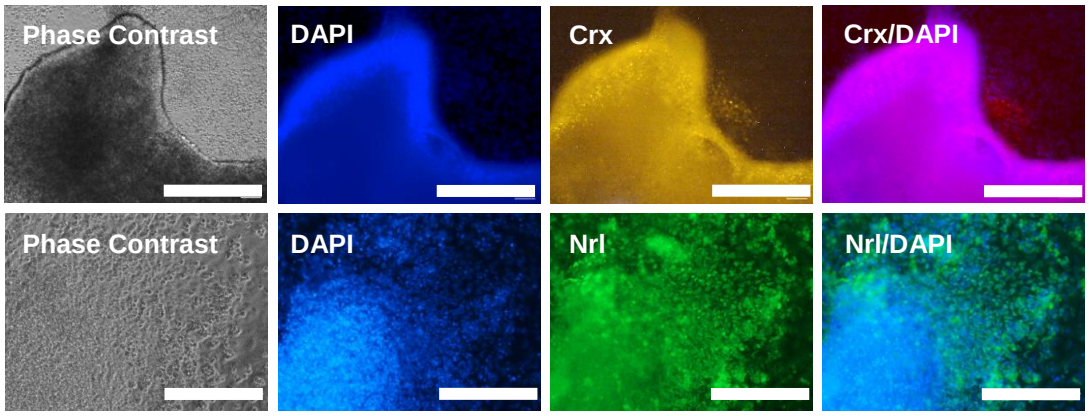

Figure 3.14 Expression of Crx and Nrl on Day 21 of the Retinal Differentiation of hiPSCs.

Immunocytochemical staining after day 21 of retinal determination step. Both Crx and Nrl were expressed uniformly throughout the culture. The overlay shows the expression of these markers with DAPI. Indication of nuclear expression of these markers. Secondary antibodies used Alexa 532 (Crx) and Alexa 488 (Nrl). The scale bar represents 200 µm.

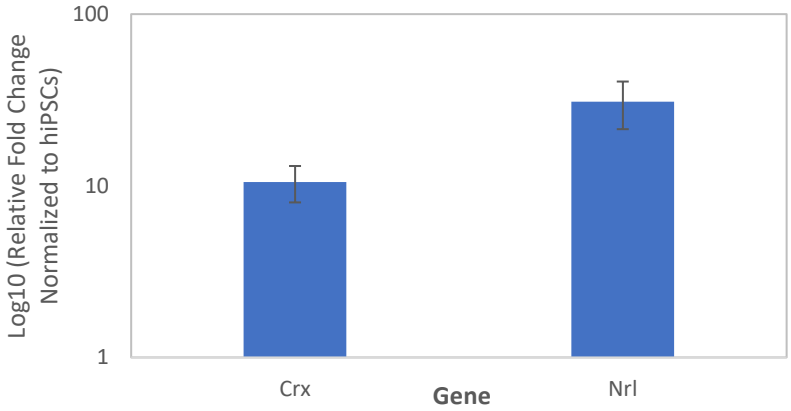

Figure 3.15 qPCR Analysis of Crx and Nrl on Day 21 of the Retinal Differentiation of hiPSCs.

Relative expression of the retinal progenitor markers on day 21 of the retinal determination culture compared to that of the hiPSCs. Crx was upregulated 10 folds and Nrl 30 folds higher than hiPSCs. Crx is a marker specific to retinal progenitors committed to become photoreceptors. Crx is expressed in both rod and cone photoreceptors. Nrl is expressed in rod photoreceptors. Error bars represent one SEM about the mean of 3 independent data points (n=3).

3.5 Degradation and Consumption of Growth Factors in Retinal Differentiation of hiPSCs

There are series of induction steps in development of vertebrate retina based on molecular models that have been studied in humans and animal models. (Zuber et al., 2003; Heavner et al., 2012) The first stage is the neural induction that is regulated by fibroblast growth factors (FGFs), bone morphogenetic proteins (BMP) and Wingless-Int proteins (Wnts). Antagonising these signalling pathways by using Noggin (for BMP) and DKK-1 (for Wnt signalling pathways) has shown to be an effective method in directing hESCs towards forebrain development. (Watanabe et al., 2005; Itsykson et al., 2005) Inhibition of these signalling pathways lead to production of various anterior neuronal cell populations, which must be guided towards retinal progenitor lineage. Therefore, addition of growth factors such as insulin-like growth factor-1 (IGF-1) has shown to be essential at this stage for production retinal progenitor cells. (Lamba, et al. 2008a).

In order to establish an order of importance we investigated degradation and cellular requirements of these four growth factors DKK-1, Noggin, IGF-1 and bFGF in the well-plate cultures. This study will assist us to better understand the cellular dynamics and adapt our perfusion flow rate to address those cellular needs and hence create a steady-state concentration of soluble factors in demand.

3.5.1 Study Design

To study the degradation and consumption of the four key growth factors in retinal differentiation at 37°C, three conditions were considered to undertake

this study. In the first condition differentiation medium was used alone without presence of any cells to study degradation of the growth factors. In the second condition hiPSCs were added to each well; however, no medium exchange did take place to observe consumption of the growth factors compared to their degradation and their possible production. In the third condition, medium and cells were used and medium was exchanged once every 48 hours as per retinal differentiation protocol. The latter was used to observe cellular demands where the initial input concentration was used within the first 48 hours. The study was performed for the first 96 hours of the differentiation culture after EBs were prepared and seeded onto the Matrigel™ in well-plate cultures. In all conditions 1 mL of medium was used with consideration of using 100 µL of collected media for each growth factor and 500 µL for metabolic analysis and the final 100 µL as a buffer for errors.

3.5.2 Degradation of bFGF, Noggin, DKK-1 and IGF-1

Figure 3.16 (A-D) shows the analysis of DKK-1, bFGF, Noggin and IGF-1 concentrations during the first 96 hours of retinal differentiation of hiPSCs. DKK-1 had the fastest initial rate of degradation. (Fig 3.16A) In the first 8 hours only 48% of the initial stock remained. bFGF and Noggin (Figs 3.16B-C) degradation showed 69% and 46% drops in their initial concentrations within the first 24 hours. IGF-1 showed no degradation at 37°C. (Fig 3.16D)

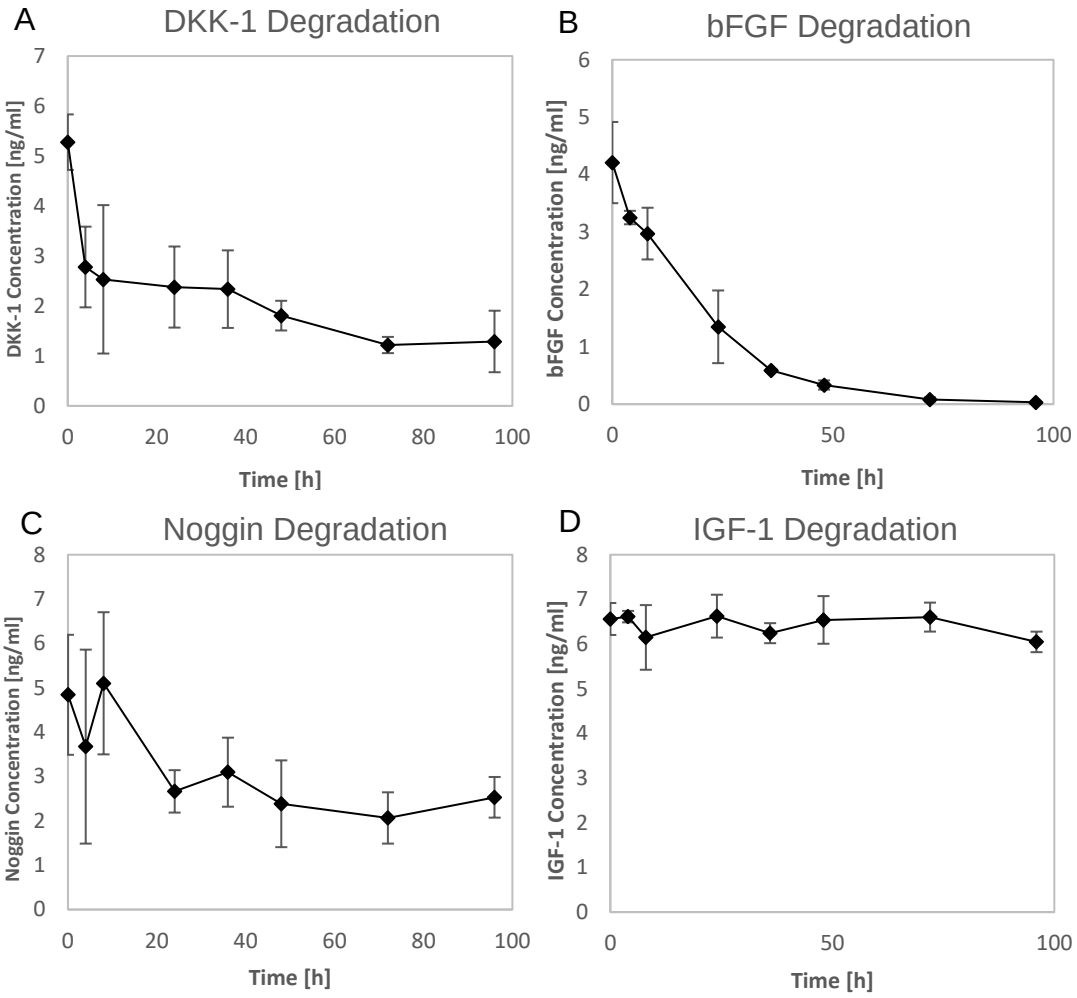

Figure 3.16 Degradation Profile of bFGF, Noggin, DKK-1 and IGF-1 at 37°C over 96 h at 37°C.

(A) Degradation of the DKK-1 shows that this cytokine degrades by 48% of its initial concentration within the first 8 hours. After 72 h only 23% of DKK-1 remains. (B) bFGF degrades gradually with 69% of its initial concentration remains after the first 24 h. After 72 h, 99% of this growth factor was degraded. (C) In the first 24 h, 46% of the Noggin degrades. The remaining concentration was stable for the rest of the study. (D) IGF-1 did not show any visible degradation over the course of 96 h. Error bars represent one SEM about the mean of 3 independent data points (n=3).

3.5.3 Consumption of bFGF, Noggin, DKK-1 and IGF-1

As explained earlier measurements for consumption of the growth factors were taken in the presence and absence of a full medium change at 48 hours to detect possible production of these growth factors by the cells. After obtaining the consumption of the growth factors and their respective cell numbers at each collection point, then cellular consumption rate of each growth factor was calculated. The consumption rates were calculated by subtracting the degradation from the consumption value and then divided by the number of cells collected at each time-point. The cellular consumption rates per hour were calculated by dividing the value of consumption in those hours by the number of hours.

Figure 3.17A shows the consumption of DKK-1, where it falls by 66% of its initial concentration in the first 8 hours. The cellular consumption rate of DKK-1 in the first 8 hours was 0.3 $x10^{-5}$ $ng.ml^{-1}.Cell^{-1}.h^{-1}$. (Fig 3.17B) DKK-1 consumption rate decreased by 12% more between 8 and 24 hours where it remained stable before the media exchange at 48 hours. After the media exchange, the consumption rate was similar to the first 8 hours. There was an increase in DKK-1 concentration after 84 hours indicating that perhaps cells had started to secrete the growth factor. These results showed that more than 50% of the DKK-1 is lost 8 hours after inoculation or the medium exchange. Figure 3.17C-D shows that concentration of bFGF remained high in presence of cells in cultures with and without media exchange. This is interesting as it shows that bFGF concentration was maintained by the cells and its production

could be linked to the increasing number of the cells in the culture. bFGF production was fastest in the first 8 hours at 0.54 $x10^{-5}$ $ng.ml^{-1}.Cell^{-1}.h^{-1}$.

Noggin had the highest demand compared with all other growth factors with a consumption rate of 0.18 $x10^{-4}$ $ng.ml^{-1}.Cell^{-1}.h^{-1}$ in the first 8 hours. (Fig 3.17E) Noggin's consumption rate was 6 times more than DKK-1 in the first 8 hours. After the 8 hours, Noggin's concentration remained until the media exchange at 48 hours. After the media exchange, 92% of the Noggin was consumed within the first 4 hours at the rate of 0.17 x 10^{-4} $ng.ml^{-1}.Cell^{-1}.h^{-1}$ (Fig 3.17F)

Figure 3.17G shows concentration of IGF-1 with consumption rate of 0.58$x10^{-5}$ $ng.ml^{-1}.Cell^{-1}.h^{-1}$ in the first 8 hours. Consumption rate of this growth factor decreased to 0.13 $x10^{-5}$ $ng.ml^{-1}.Cell^{-1}.h^{-1}$ between 8 and 24 hours and it remains unchanged until the media exchange at 48 hours. Following the media exchange IGF-1 was consumed at much lower rate of 0.02 $x10^{-5}$ $ng.ml^{-1}.Cell^{-1}.h^{-1}$ for the rest of the experiment. (Fig 3.17H)

To summarise, the study of the growth factors' interaction with hiPSCs and their degradation at 37°C showed that; of all 4 growth factors, DKK-1 has the fastest degradation rate followed by bFGF, Noggin and IGF-1 respectively. In regard to consumption rate, Noggin had the highest consumption rate followed by IGF-1 and DKK-1. During this study, bFGF was produced, showing highest rate of production by the cells during the first 96 hours. In conclusion, to create a steady state soluble factor concentration, a flow rate must be selected that provides a steady concentration of DKK-1 and Noggin in the culture medium.

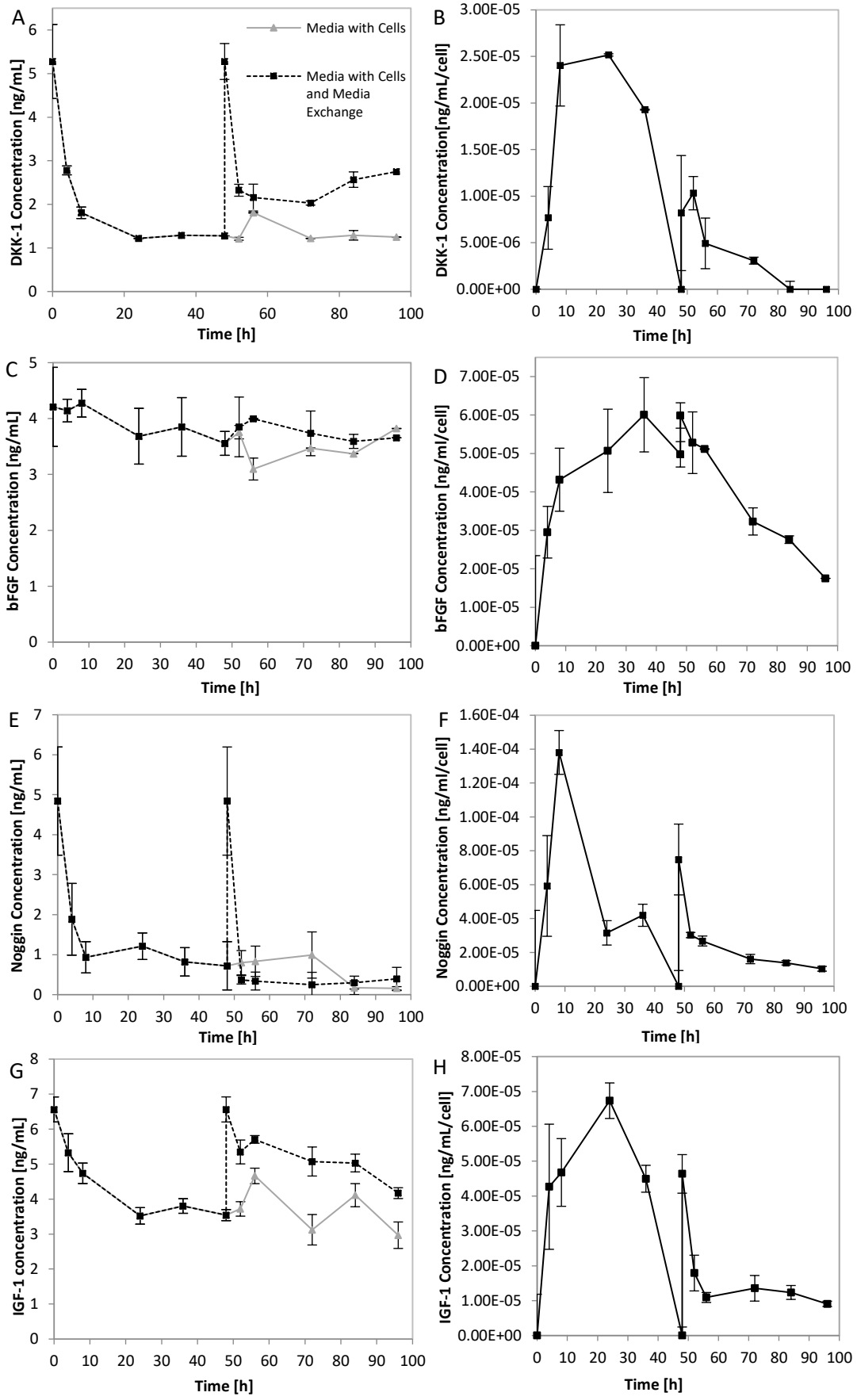
A
Media with Cells
Media with Cells and Media Exchange
DKK-1 Concentration [ng/mL]
Time [h]
B
DKK-1 Concentration[ng/mL/cell]
Time [h]
C
bFGF Concentration [ng/mL]
Time [h]
D
bFGF Concentration [ng/ml/cell]
Time [h]
E
Noggin Concentration [ng/mL]
Time [h]
F
Noggin Concentration [ng/ml/cell]
Time [h]
G
IGF-1 concentration [ng/mL]
Time [h]
H
IGF-1 Concentration [ng/mL/cell]
Time [h]

Figure 3.17 Consumption of bFGF, Noggin, DKK-1 and IGF-1 in the First 96 h of Retinal Differentiation of hiPSCs.

(A) DKK-1 concentration shows 66% fall in its initial concentration in the first 8 h. (B) The cellular consumption rate of DKK-1 in the first 8 hours was 0.3 x10^{-5} ng.ml^{-1}.Cell^{-1}.h^{-1}. The highest amount of consumption for DKK-1 takes place in the first 24 h. After the media exchange at 48 h, the consumption rate of this cytokine drops to only 40% of its cellular consumption in the first 48 h. (C) bFGF concentration remained constant during the experiment, indicating the possible production of this factor by the cell. (D) Shows production of the bFGF during the first 96 h. bFGF was the only cytokine that was produced during the retinal determination step. (E) More than 80% of the Noggin was consumed in the first 8 h. (F) Noggin's consumption rate was the fastest among the growth factors with the rate of 0.18 x10^{-4} ng.ml^{-1}.Cell^{-1}.h^{-1}, which was 6 times more than that of DKK-1. (G) In the first 24 h, 47% of the initial concentration of the IGF-1 was consumed. After the media exchange the consumption rate of the IGF-1 dropped by 31%. (H) IGF-1 consumption rate was highest after Noggin. Error bars represent one SEM about the mean of 3 independent data points (n=3).

3.5.3.1 Analysis of Metabolic Factors During Consumption Study

Medium analysis of the metabolic factors, glucose and lactate was also performed for all culture conditions during the consumption study. Results showed that glucose levels in the wells without any cells showed no changes in concentration during the 96 hours. In wells with cells but no media exchange, dropped by 35% and wells with media exchange, by 28.3%. Lactate concentration levels only raised by 0.74 g/L and 0.37 g/L in wells without and with media exchange respectively. No sudden drop in glucose or rise in lactate levels were detected, showing no detrimental effects on cells during the course of experiment. (Fig. 3.18)

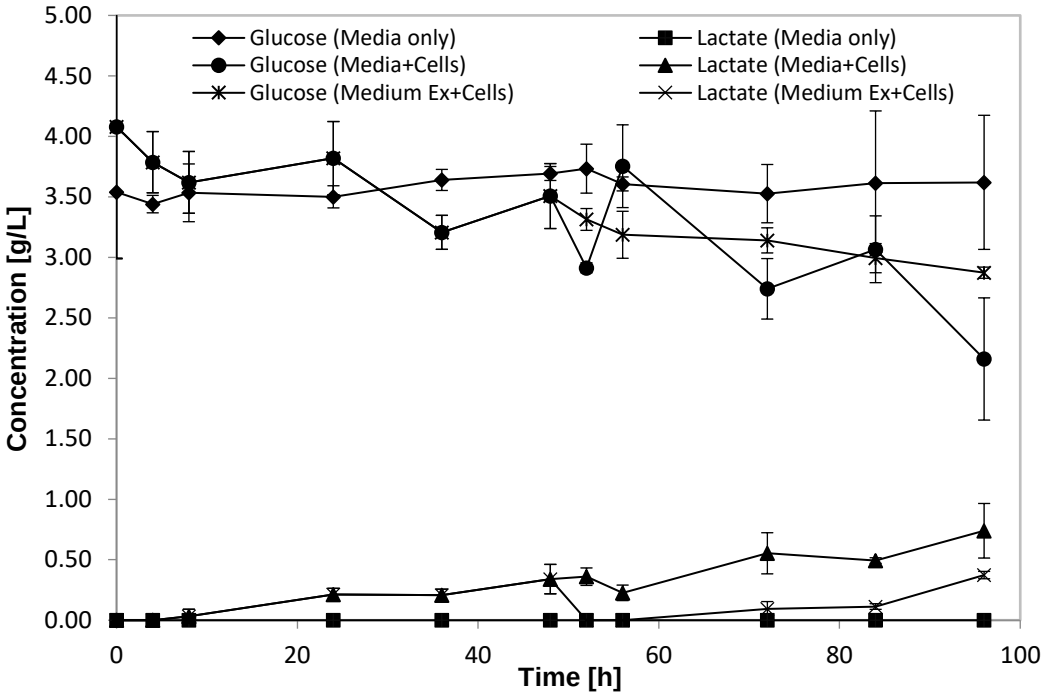

Figure 3.18 Spent Media Analysis of Retinal Differentiation of hiPSCs During the Consumption Study.

Glucose concentration showed no significant changes in wells with media during the 96 hours. In wells with cells but no media exchange, dropped by 35% and wells with media exchange, by 28.3%. lactate concentration levels only raised by 0.74 g/L and 0.37 g/L in wells without and with media exchange respectively.

Results of the degradation studies showed that DKK-1 had the fastest degradation rate in the first 8 hours and bFGF had the highest degradation in the first 24 hours of retinal differentiation. As explained in section 1.1.2.1 the neural commitment of the cells in ectoderm is regulated by production of the bFGF at the start of gastrulation stage and inhibited by TGF-β and Wnt signals. (Streit et al., 2000) Inhibition of the Wnt signalling pathway via its antagonist DKK-1, allows for induction of the dorsal genes in the neural tube and formation of the forebrain. bFGF prepares the cells for BMP signals while Wnt pathway is inhibited. (Kazanskaya et al., 2000; Hashimoto et al., 2000)

Further studies into consumption and production of these molecules, revealed that bFGF concentration is maintained by the cells and since it is not stable over extended periods of time at 37°C, therefore it has been produced by the cells intrinsically. It was reported that addition of heparin to the culture medium can increase bFGF's half-life significantly. (Damon et al., 1989) However, since results showed production of this growth factor by the cells, therefore it will not be necessary to use heparin in this protocol. Moreover, since effects of heparin on the cells and its interaction with other cytokines is unclear it is best avoided at this stage.

Noggin is the antagonist to BMP signalling pathway and its role is to preserve the neural fate. (Hemmati-Brivanlou et al., 1994; Bouwmeester et al., 1996) The increased demand for Noggin after the media exchange shows that it must be provided to the cells during the early stages of differentiation. IGF-1 also plays a crucial role in the anterior neural formation and it is essential in later stages of retinal differentiation. In this study, IGF-1 shown to be resistant to degradation during the course of 96 hours and its consumption by the cells is decreased after the media exchange. Therefore, it may not be essential to actively provide this growth factor to the cells. It also must be noted that IGF-1 is the smallest molecule of the group and therefore it will require higher flow rate to reach steady-state condition in the culture medium.

Finally, DKK-1 had the higher degradation rate compared to other growth factors, which can limit its consumption given during the short availability period. The interesting observation here was decreased demand for this growth factor after the media exchange at 48 hours. Nonetheless, the relatively

high demand for this molecule and its essential role in inhibition of Wnt signalling pathway at the earlier stage of retinal differentiation indicates that it must be provided to the cells at a steady-state.

Other supplements included in the retinal differentiation medium are B27 and N2. Presence of these supplements has also shown to enhance EFTFs expression with N2 resulting in higher efficiency of photoreceptor maturation. (Mellough et al., 2012) B27 contains 21 and N2 includes 6 different molecular ingredients. Some of their key molecules include, bovine serum albumin (BSA), transferrin, and insulin. In this study, due to importance and costs associated with growth factors we only studied consumption of these molecules. However, in order to create steady-state condition via use of perfusion molecular contents of these supplements also have to be accounted for as they play a key role in retinal differentiation of hiPSCs.

The spent media analysis study was performed to detect any detrimental changes in concentration of glucose and lactate during the experiment. Aerobic and anaerobic metabolism are the most common means of providing energy for the cells. The cells' metabolic state has a significant effect on the differentiation and both protein activation and protein conformation of the stem cells. (Gatlik-Landwojtowicz et al., 2004; Vishwasrao et al., 2005) As a result, cells metabolic state will have a direct effect on growth factors and their function during the differentiation.

Glucose concentration across all three culture conditions did not show any sudden drops or sign of depletion to critical levels during the experiment. The

glucose concentration in cultures without media exchange was lower than those with media exchange, however no significant difference was observed between the two conditions. Lactate is a by-product of glycolysis and is an indicator of anaerobic metabolism in cell culture. The increased levels of lactate indicate hypoxic conditions or rapid increase of metabolic activity. (Vishwasrao et al., 2005) Concentration of this molecule also did not show any sudden increase among all culture conditions. The higher concentration of the lactate in cultures without the media exchange was expected, however there was no significant difference observed between the two conditions.

3.6 Summary

The pluripotency of the stem cells can be characterised using various indicators such as morphology, expression of pluripotency markers qualitatively as well as quantitatively. The culture of induced pluripotent stem cells exhibited their tendency to spontaneously differentiated as a result of genetic and epigenetic factors. (Hough et al., 2009; Narsinh et al., 2011; Tonge et al., 2011; Singh et al., 2013) Culture and characterisation of the cell line used in this thesis (MSUH001-hiPSCs) also confirmed that it is prone to spontaneous differentiation as the other cells lines co-cultured with MEFs. (Draper et al., 2004) The effects of MEF's density on heterogeneous expansion of these cells showed the need for a strict working routine with condition that minimises the influence of these environmental cues. Nevertheless, the issue of heterogeneity exists within such cultures and its effects on the process yield and purity is uncertain.

Prior to using these cells for differentiation cultures as a valid control, several factors had to be considered and adjusted in different steps of differentiation protocol. One of the main varying factors was the size of EBs and method of production. As discussed in section 3.3.1 methods used for creating the EBs will have a direct effect on their heterogeneity, size, aggregation kinetics and differentiation pathway. Methods such as static suspension cultures have low control over EB size, number of cells per EBs and the cell death. Other methods such as hanging drop methods and encapsulations will create more varying factors to the process, are difficult to scale-up and labour intensive. With aim of scaling down to adjust the process for the microfluidic culture, we

required a method that can allow for control in the number of cells per EB resulting in the same EB size, to be simple with fewer steps and highly reproducible so that we can create EBs of the same size and number every time to reduce variability between cultures. Among various methods used to form EBs, use of low adherent micro-well plates were the most appropriate.

In choosing the right EB size, two opposing factors were in consideration. First was the relationship between the EB size and its differentiation lineage and second the relationship between mass transfer limitations and the EB size. Various studies shown EBs with larger sizes of 450 µm and above show more neurogenic differentiation capability and EBs with smaller sizes of below 200 µm show more endothelial differentiation capability. On the other hand, EBs of larger size face mass transfer limitations in terms oxygen transfer, glucose and cytokine penetration. Concentration of cytokines in EBs with sizes of 200-400 µm were not significantly different, hence indicating a range of ideal size in regard to mass transfer and differentiation lineage. The other factor needed consideration here was the dimensions of the culture area of the MFCD. Having the height of 450 µm inside the culture chamber with the media inlet at the height of 220 µm, EBs with size of 200 µm in diameter seemed to be the ideal choice. This size allowed each EB to have approximately 1000 cells per EB.

Using unified sized EBs also allows for greater control over the sample size in both well-plates and the MFCD. However, in respect to total RNA extracted from each sample it may be different due to culture conditions. Therefore, total amount of RNA for each culture condition must be quantified and then

normalised to the same concentration levels before it is used for the cDNA synthesis. Extracted RNA could be contaminated with genomic DNA, salt, carbohydrates, peptides, phenol and guanidine thiocyanate present at the lysis buffer at the extraction stage. Therefore, measurement of the quality and purity of the extracted RNA is also essential and will affect the accuracy of the gene expression analysis downstream. The final key point in performing accurate qPCR analysis is selection of the right reference genes. Dependence of optimal number of reference genes on sample type and combination of the genes used, was confirmed by results of the gene expression stability analysis. This finding also confirmed that using multiple reference genes does not necessarily increase the accuracy of the gene expression analysis.

On proceeding to retinal differentiation of hiPSCs, on day 5, down regulation of the pluripotency markers Oct4 and Nanog coincided with upregulation of Nestin a neuronal progenitor marker Nestin and Otx2. This was further confirmed by immunocytochemical staining of the retinal markers, indicating that hiPSCs are progressing towards anterior CNS lineage. On day 10, expression of series of eye field transcription factors (EFTFs) Pax6, Lhx2, Six6 and Vsx2/Chax10 were expected on the route to retinal progenitor lineage. This expectation was confirmed through upregulation of these markers in qPCR analysis relative to hiPSCs. The EFTFs include a network of genes that are interdependent in their expression. Otx2 and Sox2 expression triggers the expression of Rax, which subsequently activates expression of Lhx2, Six3 and Pax6. (Zuber et al., 2003) Six6 is expressed in formation of optic cup through cooperation of Pax6 and Lhx2. (Tétreault et al., 2008) Vsx2/Chx10 is the first

of the specific retinal marker that is expressed in the optic vesicle (OV) and its expression indicates the presence of retinal progenitors, and hence onset of neural retinal development. (Horsford et al., 2004)

Since it was discovered that post-mitotic precursors cells that express both Nrl and Crx have the highest chance of integration into the host retina post-transplantation, expression of these two markers were of interest at the end of the differentiation protocol. (Maclaren et al., 2006; Lamba et al., 2010) On day 21, qPCR analysis showed expression of these markers, which was further confirmed with immunocytochemical staining. Nrl, a rod photoreceptor specific marker showed 2 folds' higher expression than Crx, a cone and rod photoreceptor marker. In other studies, Nrl has shown to inhibit S-cone pathway via activation of Nr2e3 gene, hence allowing for rod photoreceptors formation. (Mears et al., 2001)

Degradation study of the growth factors revealed that DKK-1 and bFGF had the fastest degradation rate at 37°C. Noggin's degradation rate was 3 times slower than DKK-1 and 1.5 times than bFGF. IGF-1 did not show any degradation during the 96h study. Studying the consumption of these growth factors by the hiPSCs, showed that bFGF was produced by the cells and Noggin, IGF-1 and DKK-1 had the highest demand respectively in the first 48 hours of the culture. According to different studies BMP and Wnt signalling pathway inhibitors i.e. Noggin and DKK-1, along with IGF-1, are critical factors in guiding the hESCs towards retinal lineage. (Kim et al., 2011; Lamba et al., 2008a) Presence of these molecules in the differentiation medium directs the expression of EFTFs such as Pax6, Vsx2/Chx10, Lhx2 and Six3. Moreover,

other studies confirmed that DKK-1 and Noggin are two key enhancers of the retinal and photoreceptor progenitors.

In conclusion, Noggin and DKK-1 seem to be the key growth factors that had to be provided to the cells due to their high demand and degradation rate. bFGF is produced by the cells and IGF-1 has very low degradation rate at 37°C. An online and quick method for detection of these molecules in the culture medium does not exist, therefore creating a perfusion regime that could provide a balanced concentration of these cytokines is essential in creating a steady-state concentration of soluble factors based on molecular demands and dynamics of the differentiation culture.

Chapter 4 Assessment of Microfluidic Culture Device for Retinal Differentiation of hiPSCs

4.1 Introduction

Retinal differentiation medium is a highly-defined media with specific growth factors that guide cells through various stages of differentiation. These growth factors often contribute to the high cost of process development. In the previous chapter, the cellular demands of such factors, their stability and possible production rate were determined. Now a suitable perfusion rate based on the cellular demands and degradation of these factors can be established. Microfluidic devices designed specifically for culture of cells can provide high degree of control over cellular microenvironment, soluble factors and physical properties of the culture. These qualities can be utilised to better understand complex biological phenomena taking place during culture and differentiation processes.

In this chapter, first we look at the use of shear stress as a mean for establishment of an operational window for performing perfusion cultures in the MFCD. Next, we utilise dimensionless ratios such as Péclet (Pe) and Damköhler (Da) numbers to find a critical perfusion rate and starting cell densities for creating a steady-state concentration of soluble factors.

In the second section, we assess the mechanical and fluidic suitability of the MFCD for long-term perfusion cultures. Operational parameters such as pH, temperature, asepsis and oxygen concentration as well as burst pressure and fluid flow at desired flow rates are evaluated. In the final section, cell culture

capabilities of the MFCD are assessed by culture of MEFs and hiPSCs before proceeding to culture of EBs on chip. Adjustments made to the differentiation protocol for expansion of EBs in MFCD are explained and possible absorption of growth factors to PDMS is evaluated. Morphological evaluations and immunocytochemical staining were used as an end-point analysis of the cultures. Last, DKK-1 concentration in MFCD was measured over a course of 10 days culture to study differences in consumption of this key molecule in MFCD and static well plate culture.

4.1.1 Operational Parameters During Cell Culture Experiments in MFCD

Successful culture of stem cells requires certain operational parameters to be controlled and maintained in a defined range. These parameters include, shear stress, temperature, pH, osmotic pressure, dissolved oxygen concentration, nutrients, ECM, and removal of the waste products. Following are parameters that were kept in a defined range during the culture conditions. Other parameters explained in section 4.2 and 4.3 were tested in MFCD to make sure they are within the defined range for creating steady-state concentration of soluble factors.

4.1.1.1 Temperature

For human stem cells and the human induced pluripotent stem cells the optimum culture temperature is usually 37°C. In order to maintain this temperature throughout the culture, the MFCD was maintained in temperature-controlled incubators.

4.1.1.2 Osmotic Pressure

The osmotic pressure has a direct effect on the cellular viability and its function and it is created through the medium composition. Differentiation medium is often very defined and changes to its composition has direct effect not just on the cellular function but also on their differentiation pathway. (Chaudhry et al., 2009) In conventional well-plate cultures in an incubator at 37°C, medium evaporation will take place in these conventional vessels. Which consequently leads to an increase of the osmotic pressure. To overcome this effect, incubators are often humidified using evaporating water placed in water tanks designed at the bottom of the incubators. For all our cultures humidity was maintained by the incubators at 95% to avoid any possible evaporation from the culture medium.

4.1.1.3 pH

The pH plays a critical role in dynamics of the biochemical reactions inside the cells. Consequently, it effects the maintenance and differentiation pathways of stem cells toward a specific lineage. Therefore, it is essential to maintain the physiological pH i.e. between 7.0 and 7.4 to avoid any negative effects on the cells. (Wuertz et al., 2009) pH is also a function of the biochemical composition of the medium and it is affected by culture conditions such as CO_2 composition in the gaseous content of the culture area as well as chemical waste from the metabolic reactions inside the cells. Lactic acid often present in the metabolic waste decreases the pH of the medium, which its effect is balanced out by presence of bicarbonate created from the CO_2 in the gas phase (5%) of the incubator.

However, as cells grow the amount of lactic acid released into the culture increases as well and the buffering effect of using bicarbonate alone will decreases. Therefore, it becomes necessary to exchange the media regularly to maintain culture's homeostasis. In conventional cultures, the medium exchange is performed manually, however in perfused cultures such as our MFCD, this will take place according to the perfusion flow rate. For example, at the flow rate of 130 µL/h, media is replaced more than 5 times in one hour, which is approximately once every 12 minutes.

4.2 Establishment of the Critical Perfusion Rate for Steady-state Concentration of Soluble Factors

The ability to translate macro-scale *in vitro* cell culture into microscale, requires knowledge of physicochemical microenvironment of the cells, design and operational principals for microfluidic devices and cell culture techniques. (Walker et al., 2004) Stem cells' niche is composed of nutrients, soluble factors, cell signalling factors and waste molecules, which has a direct effect on their survival and behaviour of the cells. Other physicochemical properties such as pH, surface structure, temperature and oxygen tension provide a cell and process specific milieu to regulate stem cells function. Studies directed at cellular microenvironment help clarify cellular functions *in vivo* and further assists in providing an efficient working protocol in meeting therapeutic demands. (Kirouac and Zandstra, 2008; Serra et al., 2012)

The cell signalling pathways are regulated by biomolecules such as cytokines, hormones and growth factors to determine the cell fate. These soluble factors are distributed via diffusion through autocrine and paracrine processes. The effects of these signalling factors on the cells are dependent on their local concentration, degradation and their affinity to cell surface receptors. (Discher et al., 2009) The soluble concentrations exist in the vicinity of the cells often act as a signalling factor itself and in case of differentiation cultures, guide the cells to a particular lineage. (Kinney and McDevitt, 2012) In conventional cell culture environments such as well-plates, chemical gradients form naturally through diffusion. In such cultures, pH, osmolality, and soluble factors' concentration will change constantly between the media exchanges. Factors

such as pH can be controlled partially through CO_2 concentrations provided in the incubator. (Young and Beebe, 2010) However, accumulation of the waste products as a result of metabolic activities of cells, shift this balance toward a disfavoured environment. Concentration of the nutrients and soluble factors are also affected by cellular consumption, degradation and production. (Ungrin et al., 2011) In scaled-down differentiation cultures such as microfluidics, one of the main objectives is to apply more control over environmental factors to reduce variability that exist in macro-scale cultures. (Walker et al., 2004)

Continuous perfusion of the culture, assists in removal of the waste molecules and provides cells with essential nutrients. However, the key question here is, how fast the perfusion rate must be to provide a balanced physicochemical culture environment for a differentiation culture such as retinal differentiation. Diversity that exists in terms of different molecules in a highly-defined culture media such as retinal differentiation, means that different flow rates are needed for steady supplementation of different soluble factors. In the previous chapter, we studied the culture dynamics in the static form and established an order of importance in terms of consumption and degradation rates for the key growth factors used. Using the latter, physical properties of the MFCD and required media exchange rate, we can establish operational boundaries for continuous perfusion of the culture in microscale before determining the best perfusion rate.

4.2.1 Perfusion Rate Boundaries for Retinal Differentiation in MFCD

In microchannels the media height above the cells considered to be most important dimension due to length and width of the channels being much larger comparatively. Therefore, channel height becomes the limiting factor for diffusion of the soluble factors. Beebe and colleagues determined that the effective culture time in a microchannels are linearly proportional to the channel height compared to the media height in well-plates. (Yu et al., 2005; Young and Beebe et al., 2010) For example, in retinal differentiation culture in 48-well plates the medium is exchanged at 250 µL per 48 hours. The media height in the 48-well plate is 2.3 mm, which compared to our MFCD culture area height (450 µm) is 5.1 times higher. Considering the exchange rate of once per 48 hours, therefore for MFCD the media must be replenished 5.1 times faster than the well-plate, i.e. 48 divided by 5.1 results in exchange time of once per 9.4 hours. Having a culture chamber volume of 23.4 µL in MFCD, therefore, flow rate of 2.5 µL/h could be the minimum flow rate for our MFCD.

In very low flow rates, mass transport takes place via diffusion often due to having higher diffusive rate of molecules than the flow rate itself. Therefore, the usual concerns often shift towards, nutrient degradation, concentration gradients and difficulty in maintaining such low flow rates. However, in selecting the upper perfusion boundary, one needs to consider wash-out of the nutrients and soluble factors before they get the chance to be taken up by the cells, and most importantly possible effects of the hydrodynamic shear stress on the culturing cells.

4.2.1.1 Effects of Shear Stress in Selecting the Upper Perfusion Boundary

In adherent cell cultures that are perfused, fluid flow by medium applies shear stress over the cells. There is a certain threshold for each cell type to initially experience the negative effects of the fluid flow and then detach from the culture surface. These threshold boundaries are dependent on the cell and culture type, surface coating and period of time that cells are exposed to the fluid flow. Studies conducted by Toh (2011), Korin (2007) and Lu (2004) on effects of shear stress on mouse embryonic stem cells (mESCs) and human foreskin fibroblasts (HFFs), showed that ability of the cells for enduring shear stress are time and type dependant. (Lu et al., 2004; Korin et al., 2007; Toh et al., 2011) For example, in Korin and Lu's studies on HFFs, under a constant perfusion regime, fibroblasts could only endure shear stress of less than 20 mPa for constant flow and 100 mPa for only few minutes. Toh on the other hand, discovered that mESCs showed negative effects of the shear such as limited growth and expansion at shear rates of $>4.5x10^{-1}$ Pa. In HFF using a threshold of $5x10^{-2}$ Pa resulted in similar culture characteristics as well as a gene expression profile compared to the static culture. In mESCs, shear rates of $>1.6\times10^{-3}$ Pa showed similar expansion rate and morphology, however the gene expression profile for Fgf5 gene were different to the static culture, indicating the effects of shear at this level. (Toh et al., 2011)

In our microfluidic culture device, Reichen reported that finite element modelling showed a mean hydrodynamic shear stress of 1.33×10^{-4} Pa ± 0.37×10^{-4} Pa at the height of 10 µm above the culture surface at a flow rate of

300 µL/h. The analytical solution for hydrodynamic shear stress with assumption of infinite parallel plates at the culture surface was reported to be 1.48×10^{-4} Pa, supporting the finite element modelling results. (Reichen et al., 2012) Comparing these results with the previous studies, the shear stress experienced in our device is still an order of magnitude lower than the threshold experienced by mESCs showing effects of the shear stress. Therefore, even at flow rates as high as 300 µL/h used for expansion of the hESCs, wash-out of the cells are unlikely. In our MFCD, the shear stress of 1.6×10^{-3} Pa requires a flow rate of 3600 µL/h. Even though such high flow rate can potentially result in wash-out of key growth factors and nutrients and its effect on retinal differentiation culture is not clear, it could be used as the upper boundary in our perfusion rate calculations to establish a clear range of operation. Figure 4.1 shows the perfusion rate boundaries as well as respective shear stress rates associated with them in our MFCD.

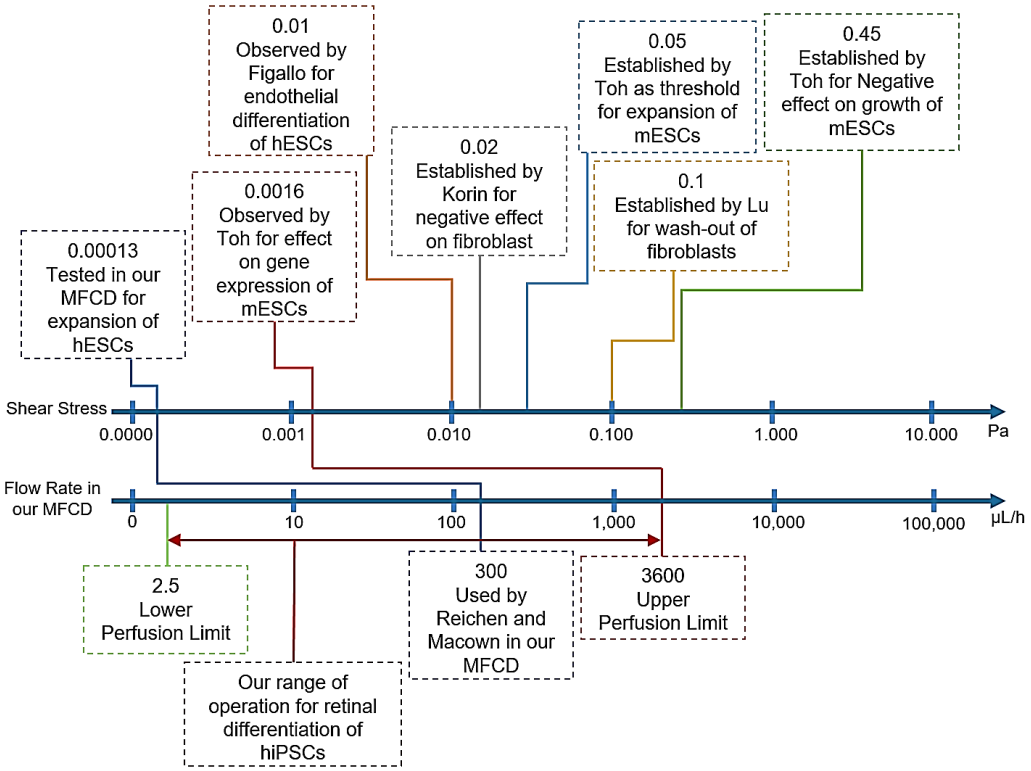

Figure 4.1 Perfusion Boundaries and the Shear Stress Associated with Various Perfusion Rates.

The potential range of operation for perfusing retinal differentiation culture is shown using previous studies to establish a minimum and maximum flow rate. The top line shows the shear stress studies performed on adherent cell cultures. The lowest shear rate that acts as a threshold for creating negative effects on the expression of Fgf5 gene in mESCs, were used to act as the upper perfusion rate boundary. The lower perfusion boundary was set as the perfusion rate equal to that of the medium exchange rate for retinal differentiation in 48-well plates.

4.2.2 Convective Delivery of Growth Factors

Now that we have established the perfusion boundaries, we need to look at the delivery of key specieis within this range in order to create a steady-state condition. To do this, the reaction diffusion equation (Equation 4.1) is often used to model spatiotemporal fluctuations in species' concentration inside a bioreactor.

(4.1)

$$\frac{\partial c_i}{\partial t} + u \,.\nabla c_i = \nabla \,.(D_{ei}\nabla c_i) + R_{i,net}$$

Where c_i is the concentration of soluble species in the media, D_{ei} is the effective diffusivity of species *i*, *u* is the velocity profile of media inside the culture device, and $R_{i,net}$ is the net volumetric degradation, secretion and uptake of the species *i*. In microfluidic devices, channel's width are often much greater than its height. Therefore, by ignoring the changes that takes place along the width of the channel, we can arrive at a 2-D representation of the culture area. In this model media flows in the x-direction (Length of channel, *L*) and diffusion of the growth factors takes place along the height (*h*) at the y-direction. (Mehta et al., 2006) In this model, adherent cells are assumed to be at the bottom of the chamber. However, for simplification purposes, if cellular thickness considered to be negligible, then R_i disappears due to coupling of the equation 4.1. at the boundry condition with cellular and volumetric uptake rate.

Therefore, considering these assumptions, for a non-dimensional scenario, the following equation is derived from equation 4.1.

(4.2)

$$\lambda \frac{\partial C_i}{\partial \tau} + U \frac{\partial C_i}{\partial X} = \frac{\alpha}{Pe} \frac{\partial^2 C_i}{\partial Y^2}$$

Where λ is the ratio of time scales (τ_r/τ_d = *L*/(τ_d<*u*>), τ_r is the residence time, τ_d is the cellular proliferation doubling time), *α* is the geometric ratio (*L*/*h*), and *Pe* is the Péclet number. Equation 4.2 was non-dimensionalised to broaden its applicability in finding determining factors in distribution of the soluble factors in the culture area. Based on Mehta's work, *Pe/α* shown to have a controlling effect on the concentration of the species delivered via medium flow rate. A value of greater than 1 for the *Pe/α* denotes the species of interest are carried out by convection i.e. via fluid flow to the cells and values of less than 1, indicates diffusive delivery of these soluble factors. Therefore, in order to create a steady-state concentration for a target species in the culture area, the following equation can be used:

(4.3)

$$\frac{\mathrm{Pe}}{\alpha} = \frac{Uh^2}{D_e L}$$

U is the flow velocity, *h* is the channel height, D_e is diffusion coefficient of the growth factor, and *L* is the channel length.

As mentioned in the previous chapter growth factors used in retinal differentiation protocol were Noggin (46 kDa), DKK-1 (25.8 kDa), IGF-1 (7.5 kDa), and bFGF (17.4 kDa). Since diffusion coefficients of these molecules have not been reported yet, to calculate the *Pe/α* for we used diffusion

coefficients of fluorescently labelled dextrans of known molecular sizes (10, 20 and 40 kDa) (Table 4-1).

Table 4-1. Variables Used for Calculations of Péclet Number.

Variable	Values	Units	Reference
D_{10kDa} @37°C in Water	4.00E-10	m^2s^{-1}	(Cimetta et al. 2010)
D_{20kDa}@37°C in Water	8.00E-11	m^2s^{-1}	(Braga et al. 2004)
D_{40kDa}@37°C in Water	6.00E-11	m^2s^{-1}	(Cimetta et al. 2010)
Length	4.00E-3	m	Measured
Width	1.30E-2	m	Measured
Height	4.50E-4	m	Measured
T	Residence time	min	Calculated

Figure 4.2 shows the calculated *Pe/α* ratio and the corresponding flow rates required to have each species of the known molecular size in convective delivery. Each line in the figure represents a fluorescently labelled dextran with sizes of 10, 20 and 40 kDa from right to left. Where the line intersects with the *Pe/α* =1, it shows the minimum flow rate required to have the species of the respective size and higher in convective delivery. Therefore, based on these calculations, for species of 10kDa and higher a flow rate of 650 µL/h is required. This means bFGF, Noggin, and DKK-1 will be in convective delivery at this flow rate. Flow rate of 130 µL/h will place all species of 20 kDa and more in convective delivery, which includes DKK-1 and Noggin. Finally, in flow rate of 100 µL/h any species of 40kDa and higher will be in convective delivery, which only includes Noggin out of all growth factors. IGF-1 has a molecular

weight of 7.5 kDa, which requires a flow rate of more than 650 µL/h to be delivered to the cells by convection.

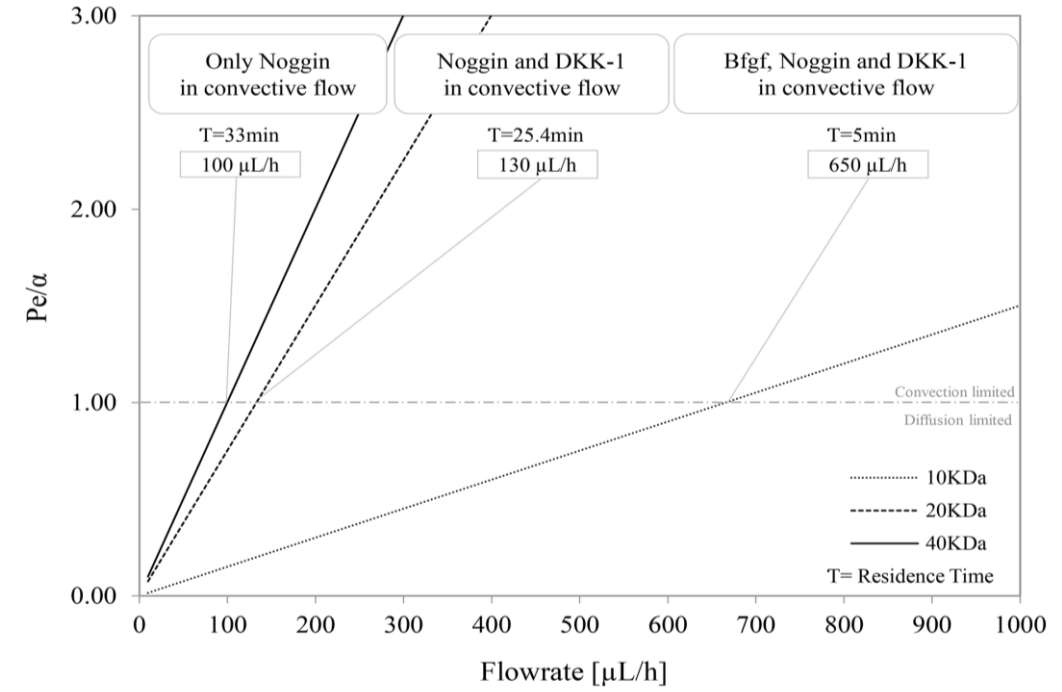

Figure 4.2 Critical Perfusion Rate for Convective Delivery of Species Using Péclet Number. Solid black line represents the molecules with molecular weight of 40kDa, dashed line, 20kDa and dotted line, 10kDa. Pe/α>1 represents the convective delivery of the species by fluid flow to the cells and Pe/α<1 denotes the diffusive delivery of the molecules. The intersection of the representative lines with the Pe/α=1 shows the minimum required flow rate for having the molecules of that size and above in convective delivery mode. The minimum perfusion rate for having molecules such as DKK-1 and larger in convective delivery to the cells is 130 µL/h. D_e of fluorescent Dextrans at 37°C in water D_{e10KDa}=4.00E-10m^2s^{-1}, D_{e20KDa}=8.00E-11m^2s^{-1}, D_{e40KDa}=6.00E-11m^2s^{-1}. T represents the residence time for media to pass through the cell culture chamber.

Other species with considerable molecular weight that can be effected by perfusion rate and included in the retinal differentiation protocol are B27 and N2 supplements. B27 along with DKK-1 were reported to enhance expression of eye field transcription factors (EFTFs). Addition of the N2 supplement into the differentiation media has shown to yield in higher efficiency of

photoreceptor maturation. (Mellough et al., 2012) B27 comprises of 21 and N2, 6 different molecules. The list includes, bovine serum albumin (BSA) (66.5 kDa), transferrin (80 kDa), and insulin (5.8 kDa) among the molecules with the highest molecular weights that will be affected by the flow rate.

Results from the growth factors' consumption study in the previous chapter and perfusion rate calculations here in this chapter, shows that there is a higher demand for DKK-1 and Noggin at the start of the differentiation culture. DKK-1 degrades very rapidly at 37°C within only 4 hours, whereas molecules such as IGF-1 is less affected by temperature. bFGF on the other hand, is produced by the cells and degrades much more slowly at 37°C. Noggin, DKK-1 and IGF-1 has shown to play an important role in the enhancement of the differentiation of hiPSCs towards retinal progenitors. (Lamba et al., 2006) This is further coupled with the key role of B27 and N2 supplements during the differentiation process. A flow rate that could deliver all these growth factors to the cells in our MFCD, could be well above 650 µL/h, which places the smaller molecules at convective delivery, however, it could also result in wash-out of the heavier and more important cytokines. Moreover, species like bFGF are produced by the cells and IGF-1 showed resistance to degradation. Therefore, having these molecules in convection may not be as necessary as the other growth factors. Therefore, perfusion rate of 130 µL/h will place any molecule of 20 kDa and larger in convection, which for retinal differentiation protocol suggests that DKK-1, Noggin, BSA and transferrin will be delivered to the cells via convection. At this flow rate, a steady-state condition can be created based on cellular demands of retinal differentiation of hiPSCs.

In order to have additional experimental control for the perfused differentiation cultures, beside the static well-plate control we decided to use a second MFCD with a different lid height that allows similar medium height in the 48-well plates. The new lid assembly provides the culture chamber with the medium height of 2.28 mm to closely match the media replacement rate to that of the static culture. Flow rate of 5.2 µL/h was used for this MFCD, which is equal to 250 µL per 48 h.

4.2.3 Using Damköhler Number to Establish Critical Cell Density

Now that we have determined the operational window and desired flow rate to have the molecules with molecular weight of 20 kDa and more delivered to the cells, we can look into the cell density as a factor that effect the spatiotemporal concentration of the cytokines. For this purpose, we can use another dimensionless ratio named Damköhler number. Damköhler number analyses the characteristic times for diffusion of a species compared to the time it takes to be taken up by the cells. This is defined using the equation 4.4:

(4.4)

$$Da = \frac{\tau_D}{\tau_r} = \frac{\frac{h^2}{D_e}}{\frac{C_0.h}{r_m.\sigma}} = \frac{r_m.h.\sigma}{D_e.C_0}$$

where C_o is the substrate concentration at the start, r_m denotes the growth factor consumption rate by the cells, D_e is the diffusion coefficient of the growth factors, σ is the cellular concentration, and h is the culture chamber height. For retinal differentiation protocol the values for the r_m, growth factor consumption rate and diffusion coefficient has not been reported. Therefore,

we used values of TGFα (5.5 kDa) in mouse fibroblasts and BSA (66.5 kDa) in hESCs as representatives of the smaller and larger cytokines respectively. (Figs 4.3 and 4.4) Furthermore, we plotted the Damköhler number against cell density for the oxygen, to analyse the limitations of these species in our MFCD and know when the balance shifts to diffusion for the cells.

Table 4-2. Variables Used for Calculations of Damköhler Number.

Variable	Values	Units	Reference
D_{O2}	3.30E-9	m^2s^{-1}	(Allen et al. 2003)
$D_{TGFα}$	1.00E-10	m^2s^{-1}	(Oehrtman et al. 1999)
$D_{Albumin}$	7.00E-11	m^2s^{-1}	(Cimetta et al. 2008)
r_{mO2}	2.50E-18	mol. $cell^{-1}$. s^{-1}	(Allen et al. 2003)
$r_{mTGFα}$	1.66E-22	mol. $cell^{-1}$. s^{-1}	(Oehrtman et al. 1999)
$r_{mAlbumin}$	3.80E-22	mol. $cell^{-1}$. s^{-1}	(Cimetta et al. 2008)
C_{0-O2}	0.21	$Mol.m^{-3}$	(Allen et al. 2003)
C_{0-GF}	0.19	$Mol.m^{-3}$	Calculated

Various heights in the culture chamber (100, 225 and 450 μm) were also included to evaluate sensitivity of the species to height in our MFCD. Da > 1 denotes a diffusive transfer of the species and Da < 1, denotes an uptake limited transfer of the species. Values used for calculations are reported in table 4.2. At low cell densities mass transfer is limited by the consumption rates, which means cells taking up growth factors when they need them. As cell population increases, the competition for growth factors increases too, therefore these species are transferred to the cells based on how fast they can diffuse through the medium. The result showed chamber height has minimal influence on the Damköhler number for larger molecules, however for smaller

molecules, height plays a more critical role at higher cell densities. Overall, cellular requirements for larger species happen at much lower cell densities compared to the smaller molecules. Therefore, the need for convective delivery of larger molecules is critical in maintaining the steady-state culture condition. Oxygen levels shown to be in uptake limited regime even at higher cell densities of 1.00×10^8 cells/cm^2.

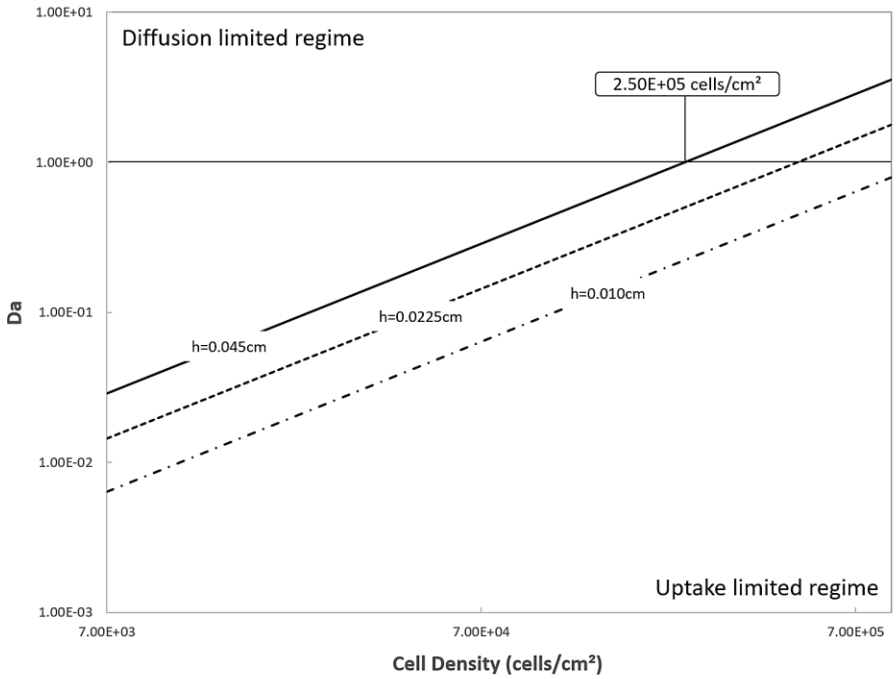

Figure 4.3 Damköhler Number as a Function of Cell Density for TGFα in Mouse Fibroblasts.

Damköhler number is the ratio of the total cellular uptake rate to the diffusive rate from the culture media. TGFα in mouse fibroblast activates a signaling pathway for cell proliferation, differentiation and development. (MW of 5.5KDa) TGFα represents the smaller molecules in the culture media and cell density of 2.5E+05 cells/cm^2 shows the border line cell population for having this molecule taken up by the cells based on the reaction rate with cell surface receptors. At higher cell populations, a diffusive limited uptake becomes dominant, indicating cellular competition for this molecule, hence the requirement for perfusion to deliver this molecule to the cells. All data used for calculation of the Da were collected from Table 4-2. Measurements are taken at chamber heights of 450 µm (MFCD chamber height), 225 µm (Medium inlet into the culture chamber) and 100 µm (middle of the EBs placed in the culture chamber) calculated for the MFCD.

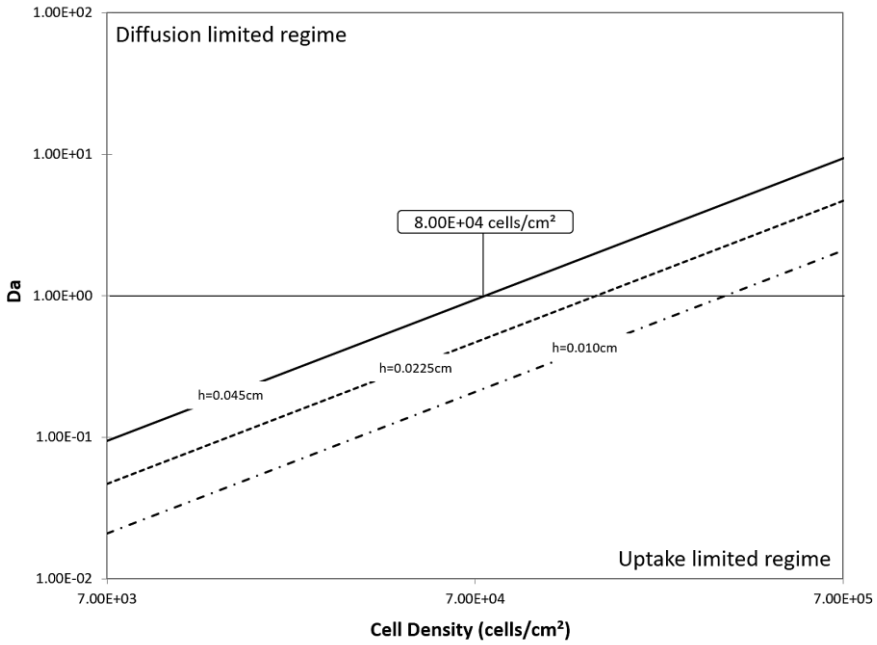

Figure 4.4 Damköhler Number as a Function of Cell Density for Albumin in hESCs.

Albumin (MW of 66.5 kDa) represents the larger cytokines in the culture media. Cellular density of 8E+04 cells/cm² represents a stage at cell growth in the culture for reactive limited uptake of this molecule.

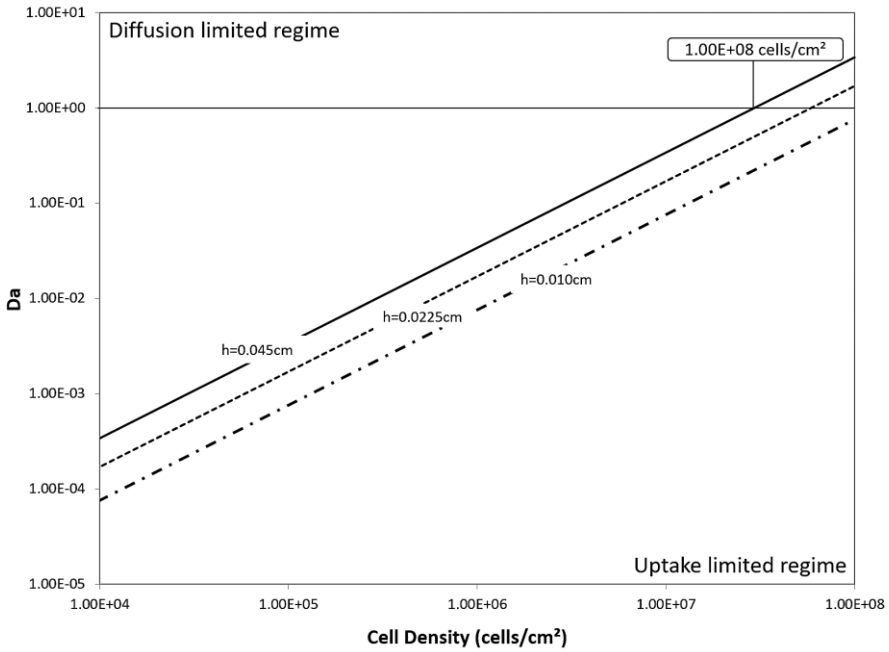

Figure 4.5 Damköhler Number as a Function of Cell Density for Oxygen in Rat Hepatocytes.

Cellular density of 1E+08 cells/cm² represents the critical stage at cell growth in the culture when addition of the oxygen to the culture media becomes necessary.

4.3 Assessment of the Microfluidic Culture Device for Retinal Differentiation of hiPSCs

Successful culture of cells in a microfluidic device demands high degree of control over physicochemical and physiological aspects of the cellular microenvironment. The accuracy of these cultural controls is dependent on the device design, fluidic and environmental controls as well as instrumentations used for monitoring these parameters.

The initial goal in this section is to evaluate suitability of the microfluidic culture device designed previously by Reichen *et al.* (2012) in our lab for long-term adherent differentiation cultures such as retinal differentiation. As explained in section 4.2.2.1 our MFCD at flow rate of 300 µL/h can provide a shear stress of up to 2 orders of magnitude lower than the threshold that can affect the mESCs negatively. Our MFCD previously demonstrated successful 3 days' expansion culture of hESCs (Reichen et al., 2012) and 84-hour expansion of mESCs. (Macown et al., 2014; Super et al., 2016)

The modular design of the MFCD is greatly suited to use in a stepwise differentiation protocol such as retinal differentiation. The lid design allows for direct seeding of the EBs into the culture chamber, thus reducing the negative effects of transferring EBs through microfluidic channels via direct seeding method. The cassette design also allows for easier and more efficient collection of cells at the end of the process, reducing the chance of losing precious cell samples. The shortest retinal differentiation protocol is 21 days, to study cells during this process means the MFCD must maintain a bubble/leakage-free operation and be resistant to infection.

In this section, changes made to the original design and tests performed to compare them are reported. Assembly and operation of the device is also reviewed, and finally the operational flow rates, oxygen concentration and growth factor concentration at target flow rate are evaluated.

4.3.1 MFCD Parts Changed Compared to the Initial Model

An investigation into the final prototype of MFCD by Macown and Super et al. (2016) showed the likely compression difference between the middle and edges of the chip resulted in failure of the device and high leakage rate. At the centre of the issue was the amount of torque applied to the screws for sealing of the device.

As a result, a torque of 2 N.cm was advised for complete sealing of the device which on the down side applies the least compression force on the PDMS chip. Therefore, still the chance of leakage was high in long-term cultures as the compression was also dependent on material and thread properties and prone to change at higher temperatures like 37°C. In order to overcome this issue, a clamping solution was advised by Macown, wherein a 3mm aluminium brackets were placed around the connectors and the 5mm polycarbonate bottom frame was also replaced with a 3mm aluminium bottom frame. (Fig. 4.6B) The changes made to the device assured a uniform compression force applied to the top frame and was impartial to small variations in the screw torques. The second issue raised while testing the device for long-term perfusion was the chemical reaction of the aluminium clamps and frame with stainless steel screws. This issue resulted from formation of a battery like environment inside the high humidity environment of the incubator and

consequently formation of metallic debris around the screws. In order to overcome this issue, the M3 stainless steel screws were replaced with M3 nylon (polyamide) screws (Premier Farnell Limited, UK). Figure 4.6 C-D shows the assembly of the MFCD using the M3 nylon screws, the microfluidic chip and its cross section.

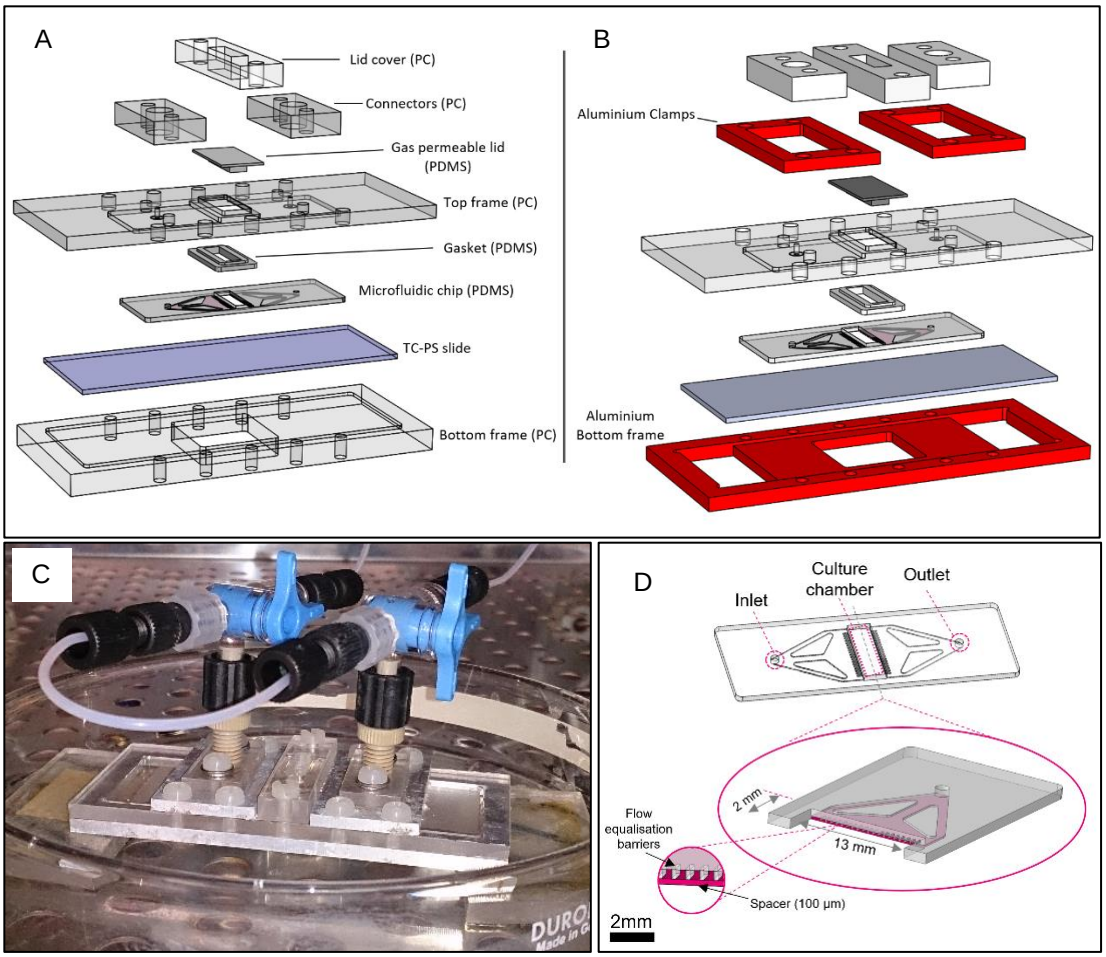

Figure 4.6 Exploded and Assembled View of the Microfluidic Culture Device and Chip.

(A) Exploded view of the previous prototype of MFCD including different parts and the material they are made of. (B) The new prototype of the MFCD and parts that are added (Aluminium clamps) and replaced (Aluminium bottom frame) in red. Courtesy of Macown and Super. (C) Assembled MFCD with fluidic connections. (D) Microfluidic chip and its cross section and dimensions.

4.3.2 Bubble-free Assembly of the MFCD

In the process of preparing the MFCD for perfusion, having a robust priming method to remove bubbles trapped in the channels and culture area is essential. Presence of bubbles not just disturbs the flow of the medium but most importantly are detrimental to cellular viability. This issue becomes even more critical in microfluidic devices as there is no space above the culture chamber as in traditional culture dishes for gases to escape to, leading to entrapment of bubbles in the culture area. The modular design of our MFCD with ability to access the culture chamber through an open lid allowed us to use this feature for removal of the bubbles while preserving the asepsis of the MFCD.

Priming method developed by Super et al. (2014) was adopted by use of a bypass created between two 3-way valves at the inlet and outlet of MFCD with a 10 cm of 1/16” OD tubing. The bypass allowed to direct the flow by using the 3-way valves in either directions of the culture chamber. Initially the culture medium was pushed through the tubing using a syringe drive bypassing the culture chamber to prime the tubing. Then, the flow was directed through the inlet of the MFCD to remove the bubbles at the upstream part of the chip. Using a pipette, air bubbles that were pushed through to the culture chamber were removed along the excess medium. Then the flow was directed to pass through the outlet into the culture chamber, removing bubbles in the downstream area of the chip. At the final step, the lid was placed on the culture chamber and slowly fitted in place to seal the MFCD. (See Appendices Fig. 7.1 A-J)

4.3.3 Burst Pressure Measurements

To evaluate the robustness of the new assembly of the MFCD compared to the previous prototype, burst pressure measurements were carried out. The modular design of the device requires different parts are fitted through multiple compression points in order to fully seal the device. In burst pressure measurements, positive air pressure is applied to a fully assembled device via a syringe drive. The maximum pressure that a sealed device can withstand before failure due to pressure release through openings in between the parts, is recorded as the burst pressure.

We compared three different assemblies of the MFCD, the first version with 5 mm polycarbonate bottom frame and M3 Stainless screws, the second version with aluminium clamps and 3 mm aluminium bottom frames and stainless steel M3 screws and finally the third version with aluminium clamps and 3 mm aluminium bottom frames and nylon screws. The burst pressure recorded for these devices were 50 kPa, 59 kPa and 55 kPa with standard deviations of 4.0, 1.4 and 2.5 kPa respectively (n=6). (Fig. 4.8) The burst pressure measurements showed that using aluminium clamps and bottom frame has increased the robustness of the device compared to the first version, and using plastic screws had minimal effects on burst pressure measurements compared to the stainless-steel screws.

In comparing the burst pressure to the flow rate, Macown *et al.* (2014) reported that the pressure at flow rate of 500 mL/h is 20 kPa across the device. Since our intended perfusion rate is 130 µL/h, which is three orders of magnitude lower than the reported flow rate. Therefore, there is low probability of leakage

at this flow rate. There was no significant difference in burst pressure measurements between different assembly versions. Therefore, use of the Nylon screws did not produce significant changes to burst pressure limits of the MFCD.

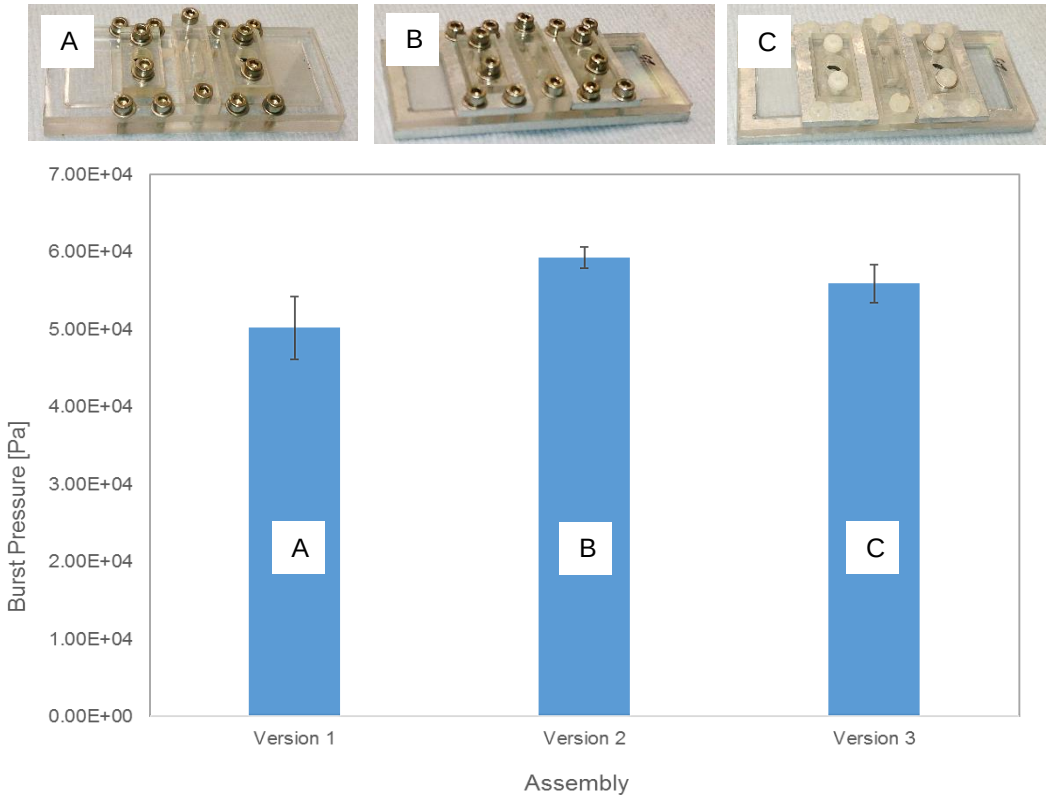

Figure 4.7 Burst Pressure Measurement Comparison Between Different Assemblies of MFCD.

(A) Version 1 of MFCD with stainless-steel screws showed burst pressure of 50±4.0 kPa. (B) Version 2 of MFCD with Aluminium clamps and bottom frame and stainless-steel screws showed burst pressure of 59±1.4 kPa (C) Version 3 of MFCD assembly with Aluminium clamps and bottom frame and Nylon screws and burst pressure of 55±2.5 kPa. There was no significant difference between different assemblies of the MFCD. (n=6)

4.3.4 Maintenance of Asepsis in the MFCD

All equipment and MFCD parts used in the experiments were autoclaved prior to start of the experiments. The only exceptions were the 3-way valves and TC-PS slide. The TC-PS slides were sterilised at the manufacturer's site and only opened in the biosafety cabinets and transferred to the device using a sterilised tweezer. The 3-way valves were made of polyethylene (PE) at their stem, therefore were not autoclavable. To sterilise them they were immersed in 70% ethanol solution overnight prior to use in the experiments. Priming and seeding of all the devices were carried out under the biosafety cabinet. However, regardless the care taken to aseptically assemble the device, the rate of contamination was high at the initial cell culture experiments on chip.

Presence of parts that could not be autoclaved and exposure of the device to the unsterile environment of the incubators was the possible reason for occurrence of the contaminations. Therefore, to overcome this issue, 1% Antibiotic-Antimycotic solution was used in all the culture media. No sign of contamination was observed after addition of the Antibiotic-Antimycotic solution in the rest of the experiments.

4.3.5 Dissolved Oxygen Concentration

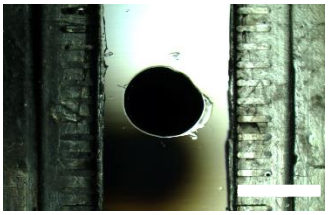

Figure 4.8 Placement of the Oxygen Sensor in Culture Area of MFCD. 2 mm sensor spot (PreSens, Germany) glued in the middle of the MFCD culture chamber. The scale bar represents 2 mm.

As explained previously the MFCD benefits from a cell culture chamber, which is covered with a removable PDMS lid allowing sufficient surface area for transfer of oxygen to the medium. In all experiments, the MFCD was kept inside the incubator with 21% oxygen in the ambient. However, to ensure that there is sufficient oxygen passes through the PDMS lid, dissolved oxygen concentration at both the inlet and culture area of the MFCD was measured and it was compared that to the T-flask measurements taken simultaneously inside the same incubator. In order to do this, we used two 2 mm sensor spots (PreSens, Germany) glued in the middle of a MFCD (Fig. 4.8) and a T-25 flask. Moreover, one flow through sensor was also used at inlet of the MFCD to measurement the incoming oxygen concentration into the device. Before start of the measurements all the channels were zeroed with zero oxygen solution using 1 g sodium sulphite (Na_2SO_3) and 50 µL cobalt nitrate (Co(NO3)2) dissolve in 100 mL water. All channels were also calibrated for 100% oxygen concentration. (see Fig. 7.2 for calibration curve). Phosphate buffer solution was used for perfusing the device at flow rate of 130 µL/h. T-25 culture flask was used as the control and all measurements taken at 37°C in the incubator.

Figure 4.9 shows the oxygen concentration at the inlet and culture area of the MFCD and a T-flask monitored over a 24 h period (n=3). The measurements

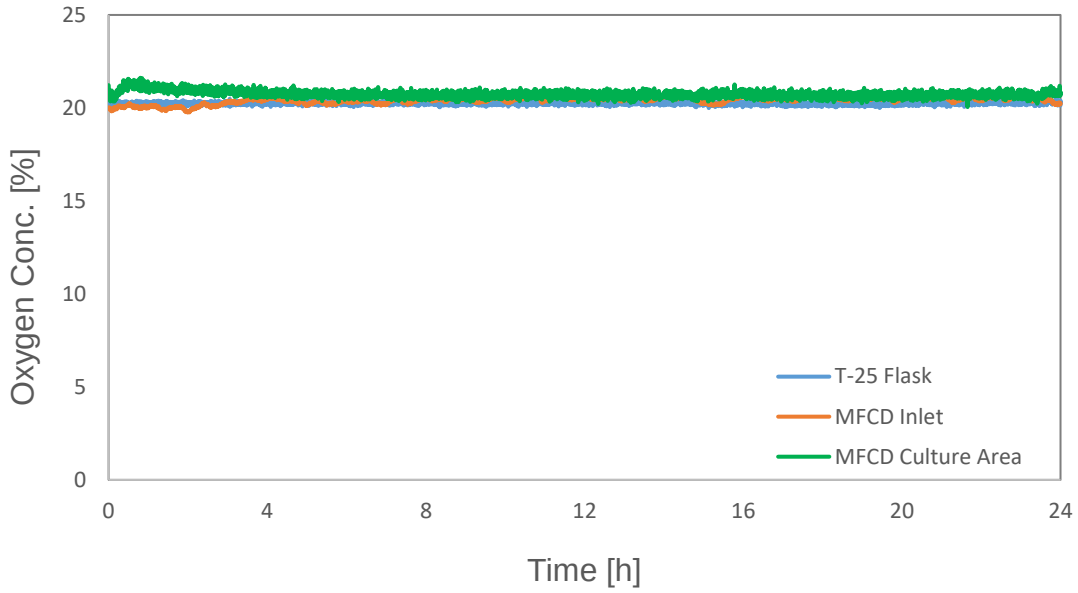

Figure 4.9 Oxygen Concentration Measurements in MFCD at 37°C in Incubator.

Oxygen concentration measurement at the inlet (orange line) and culture area (green line) of the MFCD. The average oxygen concentration at both MFCD inlet and the culture area was 21% similar to the control at T-25 flask.

showed an average of 20.76% dissolved oxygen concentration in the MFCD at the inlet and the culture area showed the average of 21.04% and the control culture showed the average of 20.92%.

In conventional culture vessels, such as well-plates and T-flasks, oxygen is provided via the headspace above the culture medium. The partial pressure in the headspace determines the amount of dissolve oxygen in the culture medium. In microfluidic culture devices, the dissolved oxygen can be controlled by use of the gas permeable materials such as poly(dimethylsiloxane) (PDMS) in device parts or silicone tubing in the fluidics. By using gas permeable materials, MFCD can be kept in oxygen controlled ambient like incubators. Results showed that sufficient oxygen is passed through the PDMS lid of the MFCD.

4.3.6 Flow Rate Measurements

In section 4.2 we concluded that flow rate of 130 µL/h is the suitable flow rate for creating a quasi-steady-state concentration of the soluble factors based on the cellular demands of the hiPSCs. Moreover, added a second perfusion rate of 5.2 µL/h as a second control for the perfusion culture that has the same medium replacement rate as that of the well-plate control. To create the desired flow rates, we used syringe drives for their operational simplicity and ease of use. Prior to starting the long-term experiments three different syringe pumps were evaluated for their accuracy and operating precision.

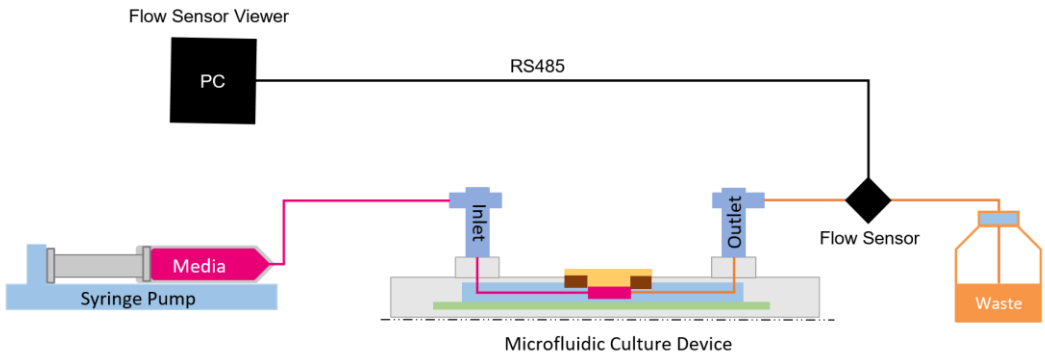

Figure 4.10 Schematics of the Setup for Flow Rate Measurements in MFCD Using Different Syringe Pumps.

The flow meter SLG64-0075 (Sensirion AG, Switzerland) was placed downstream of the outlet, connected to the "flow sensor viewer" programme via RS485 USB cable.

For flow rate of 130 µL/h we tested two syringe pumps Aladdin syringe pump and KD Scientific 200 with a 20 mL syringes (BD- Plastic) and for the lower flow rate of 5.2 µL/h we tested KD Scientific Legato 212 with 2.5 mL Norm-Ject syringes. For both flow rate measurements, we used SLG64-0075

(Sensirion AG, Switzerland) flow meter at the outlet of the MFCD at room temperature. (Fig. 4.10)

Figure 4.11 shows the result of three flow rate measurements taken on Aladdin syringe pump at 130 µL/h. The average flow rate measured on this pump was 132.18±6.24 µL/h. In the first measurement, there seems to be a massive outburst of the fluid flow at the start of the experiment, which was believed to be caused by adherence of the syringe plunger to the syringe wall. This is often caused by the rubber at the tip of the plunger. The resistance created at the site prevents the plunger to move forward and once the forward force from the syringe pump overcomes it, it causes the plunger to jump forward and create the observed effect. Clearly this effect could have a negative effect on the cells if the fluid flow outburst reaches the shear rate thresholds. The other reason for such effects are embedded in the design of the syringe pump itself. The output movement in pump often results from transfer of the motor power through series of cogs and threaded bars. The higher the precision of these parts, the smoother transfer of the motor power and fewer pulsatility in the fluid flow. Ignoring the flow outburst in the first measurements, using this syringe pump takes around two hours for the flow to stabilise at the desired flow rate with an average of 2±6.24 µL/h being above the target flow rate.

Figure 4.12 shows the flow rate measurement using the KDScientific 200 syringe pump at 130 µL/h. The average flow rate for this pump was 130.64±4.95 µL/h. Overall, it takes around an hour for the flow to stabilise and less deviation from the target flow rate. Therefore, decision was made to use this pump for the perfusion experiments at 130 µL/h.

Figure 4.13 shows the flow rate measurement using the KDScientific Legato 212 for flow rate of 5.2 µL/h. The average flow rate measured using this pump was 5.10±1.6 µL/h. The standard deviation showed a 30% change in the flow rate, which at such low flow rates is caused by the pulsatility inherent to syringe pumps. Moreover, the error rate for the Sensirion flow meter was reported by the manufacturer to be ±1.5 µL/h at such low flow rates. This error rate was similar to the standard deviation obtained from the measurements. This perfused culture was added as a second control to provide similar medium exchange rate to the static culture. Since displacement of the medium was of interest here, to ensure that pump delivered the given rate of 250 µL per 48 hours, the displacement of the plunger was marked on the syringe, which showed consistent volume displacement in all experiments performed.

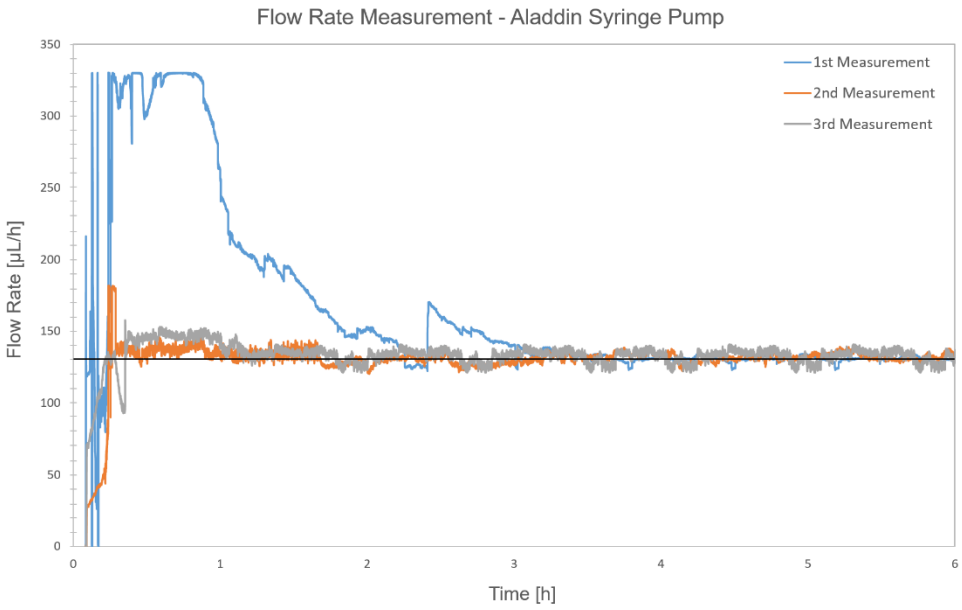

Figure 4.11 Flow Rate Measurements at 130 µL/h Using Aladdin Syringe Pump.

Flow rate measurements taken at 130 µL/h using Aladdin syringe pump. The outburst of the fluid flow at 1st measurement was due to adherence of the syringe plunger to the wall. The average flow rate measured using this pump was 132.18±6.24 µL/h. The straight black line represents the flow rate of 130 µL/h. The average time for fluid flow to stabilise using this pump was around 2 hours. PBS was used as the medium and all measurements were taken on bench-top and at room temperature. (n=3)

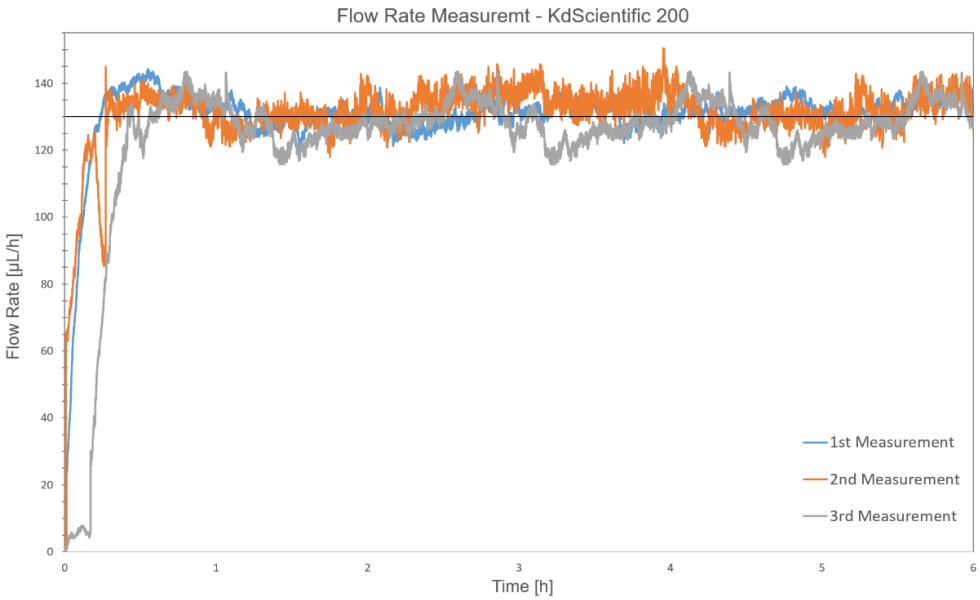

Figure 4.12 Flow Rate Measurements at 130 µL/h Using KDScientific 200 Syringe Pump.

Flow rate measurements taken at 130 µL/h using KDScientific 200 syringe pump. The average flow rate measured using this pump was 130.64±4.95 µL/h. The straight black line represents the flow rate of 130 µL/h. The average time for fluid flow to stabilise using this pump was around 1 hours. Showing better performance for creating the target flow rate. PBS was used as the medium and all measurements were taken on bench-top and at room temperature. (n=3)

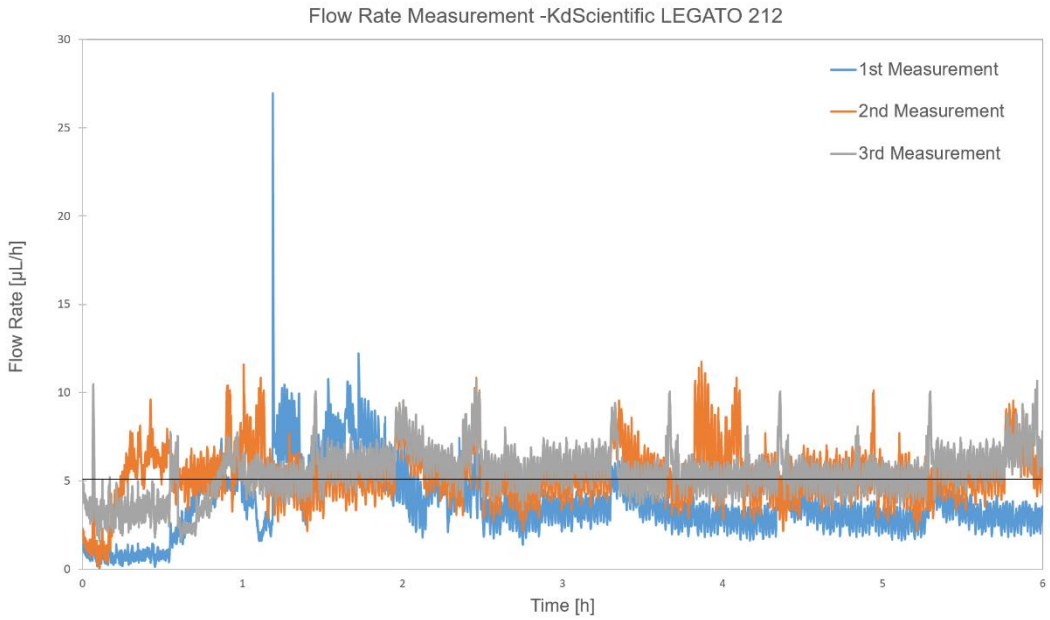

Figure 4.13 Flow Rate Measurements at 5.2 µL/h Using KDScientific Legato 212 Syringe Pump.

Flow rate measurements taken at 5.2 µL/h using KDScientific Legato 212 syringe pump. The average flow rate measured using this pump was 5.10±1.64 µL/h. The straight black line represents the flow rate of 5.2 µL/h. The average time for fluid flow to stabilise using this pump was around 2 hours. PBS was used as the medium and all measurements were taken on bench-top and at room temperature. (n=3)

4.4 Assessment of the Cell Cultures in the MFCD

Now that we have evaluated the operational parameters and tested the robustness of the MFCD in the past two sections, it is time to explore the cell culture capabilities of our MFCD considering retinal differentiation culture. The aim of this section is to adapt the retinal differentiation protocol to requirements of the culture at microscale and make the necessary changes before performing long-term differentiation culture.

4.4.1 Mouse Embryonic Fibroblast Culture in MFCD

The initial cell culture experiments were aimed at capability of the MFCD to sustain living cells while we improved our skills in microfluidic cell culture and handling cells from flasks to the MFCD. Therefore, the first experiment was designed to look at viability of the Mouse Embryonic Fibroblasts (MEFs) culture over a 24 hours' period (n=3). In this experiment, the MFCD and 48-well plates were seeded with 6.5×10^4 MEFs. The cells were counted for viability using trypan blue exclusion assay and delivered the desired cellular concentration to the MFCD. Cells were incubated in a closed MFCD without perfusion and then harvest after 24 h and counted for viability.

Figure 4.14 shows images of the MEFs cultured on chip and the 48-well plate. MEFs cultured in MFCD showed similar morphology to the control culture. Figure 4.15 shows viable cell count in both vessels. Viable MEFs concentration harvested from the MFCD were $11.3\text{x}10^4$ showing 95% viability compared with $11.8\text{x}10^4$, i.e. 97% viability in the 48-well plate. Results exhibited successful expansion of the MEFs over a 24 h period in the MFCD.

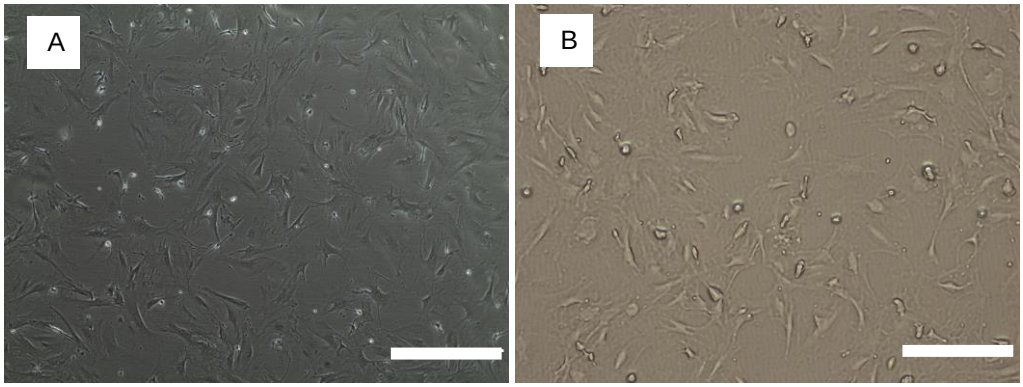

Figure 4.14 Mouse Embryonic Fibroblasts Culture in MFCD and 48-well Plate.

Culture of Mouse Embryonic Fibroblasts (MEFs) in 48-well plate (A) and MFCD (B). Both cultures show similar morphology of the cells. MFCD showed successful culture of MEFs over a period of 24 hours. (n=3) The scale bar represents 200 µm.

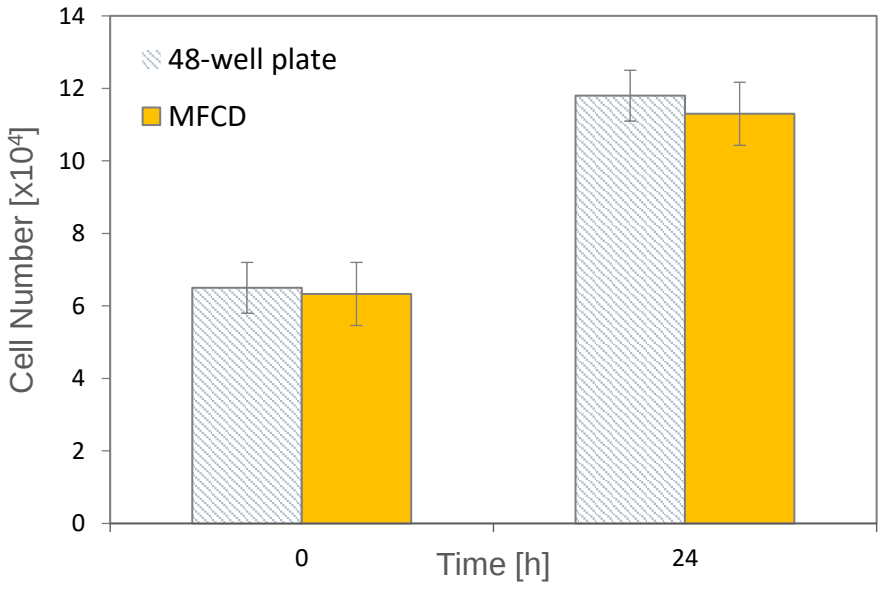

Figure 4.15 Cell Viability Assessment of MEFs in MFCD Compared to the 48-well Plate. Assessment of the viability of MEFs in MFCD showed 95% viability in 24 hours' period compared to 97% viability in 48-well plate. MFCD showed successful expansion of the MEFs over a 24 h period. (n=3).

4.4.2 hiPSCs Co-culture in MFCD

Following the successful culture of the MEFs we proceeded to test co-culture of the mitotically inactivated MEFs with hiPSCs over a period of 72 hours. After seeding MEFs in the MFCD, 24 hours static culture was allowed for the cells to adhere to the culture surface. On the second day, the media was changed to the hiPSCs culture media and then 3.0×10^4 hiPSCs were transferred to the culture area and incubated over night before starting perfusion on the third day for a 24-hour period (n=3).

Figure 4.16 (A-D) shows the comparison of the cells in the MFCD and 48-well plate. hiPSCs showed similar morphology with round and large cytoplasms in MFCD compared to the well-plate culture. Following the culture on the third day, immunocytochemical staining was performed for the pluripotency markers Oct4 and SSEA4 on hiPSCs in MFCD and the well plate. Figure 4.17 exhibits the immunostaining images for the mentioned pluripotency markers in both cultures. Both cultures showed positive and homogenous expression of these markers, hence confirming the suitability of the MFCD for longer term cultures.

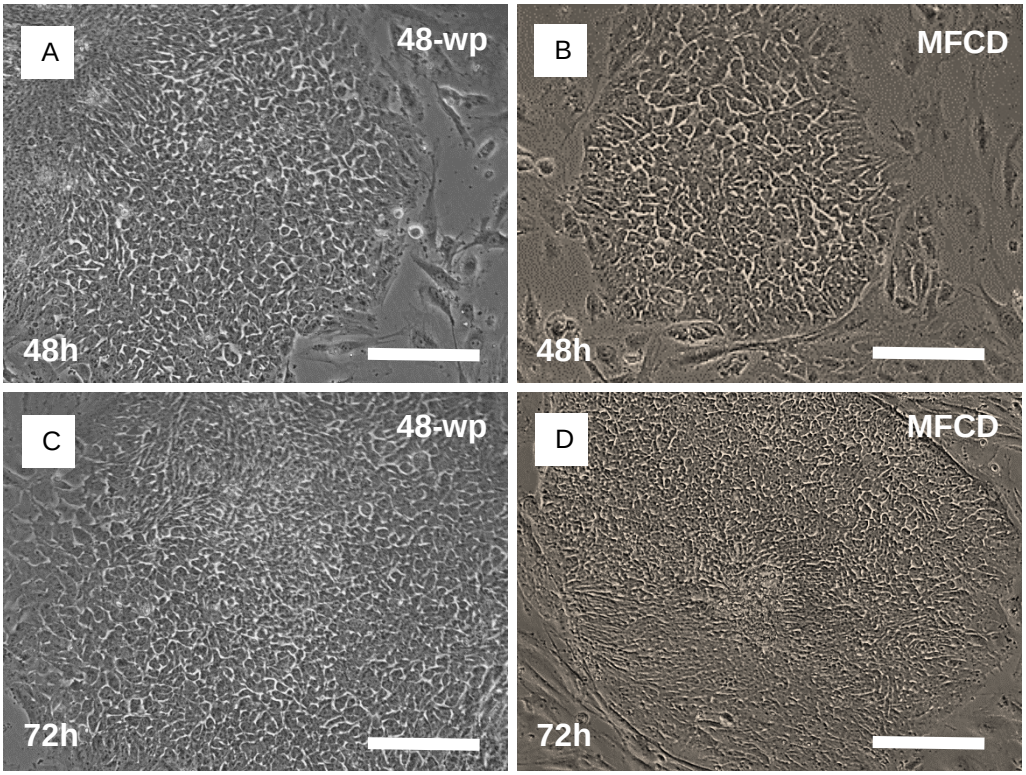

Figure 4.17 hiPSCs Culture in MFCD and 48-well Plate for 72 h.

Culture of hiPSCs in 48-well plate (A and C) and MFCD (B and D) over a period of 72 hours. Both cultures show homogenous expansion of the cells. Showing capability of the MFCD for culture of hiPSCs. The scale bar represents 200 µm.

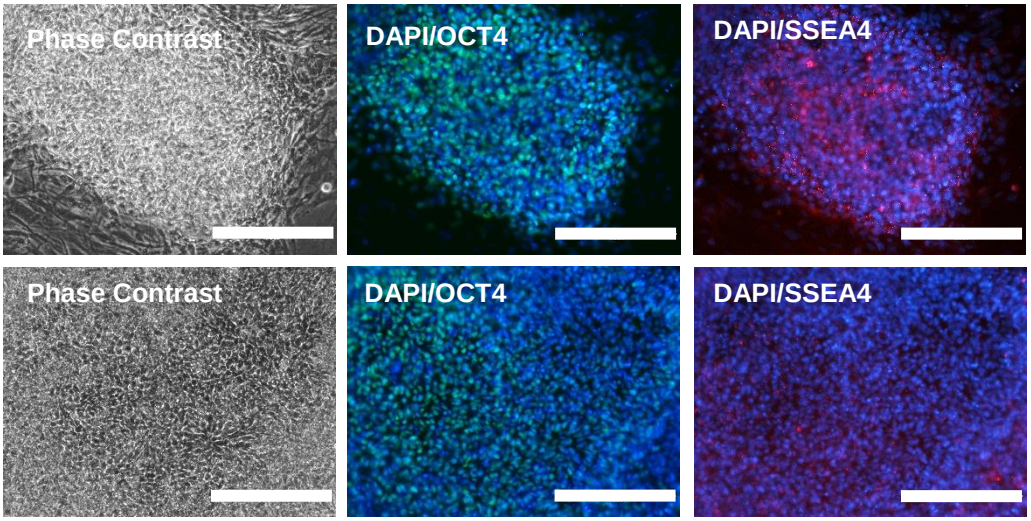

Figure 4.16 Expression of Pluripotency Markers of hiPSCs Culture in MFCD After 72 h.

Phase contrast and merged images of expression of DAPI and OCT4 and DAPI and SSEa4 for hiPSCs culture in 48-well plate (top row) and MFCD (bottom row). MFCD showed successful expansion of the hiPSCs and expression of the pluripotency markers. Secondary antibodies used Alexa 488 (Oct4) and Alexa 594 (SSEA4). The scale bar represents 200 µm.

4.4.3 Effects of Matrigel™ on Expansion of EBs in MFCD

Following the successful 72 hours culture of the hiPSCs on chip, we proceeded to retinal differentiation cultures. As explained in chapter 3 the differentiation protocol starts with formation of the EBs in a 3-day culture before transferring EBs onto the well-plates for the rest of the differentiation culture. Similar to hiPSCs culture, a 24-hour period was allowed before starting perfusion so that EBs adhere to the culture surface. To quantify the expansion rate of the EBs, ImageJ software was used to measure the area of the expanded EB (Flat area) and divided that to the area of the initial EB (Dense area). (Fig 4.18) Culture of EBs in the MFCD showed that the expansion rate of the EBs were 3.5 and 9 times less than those in the static 48-well plate after 24 and 48 hours respectively.

It was hypothesised that slower expansion rate of the EBs in the MFCD could be due to thickness of the Matrigel™ coating used. Since equal volume of Matrigel™ was transferred onto both MFCD and the well-plate, it was decided to look into the timing that it was incubated in both devices. According to the protocol the Matrigel™ solution was incubated in the MFCD for 1 hour prior to seeding of the EBs. Extra cellular matrix (ECM) components in the Matrigel™ solution will sediment during the incubation time, hence creating the bedding for the cells to adhere to the surface and grow into. However, if the culture area geometries of the MFCD were as such that too much ECM components

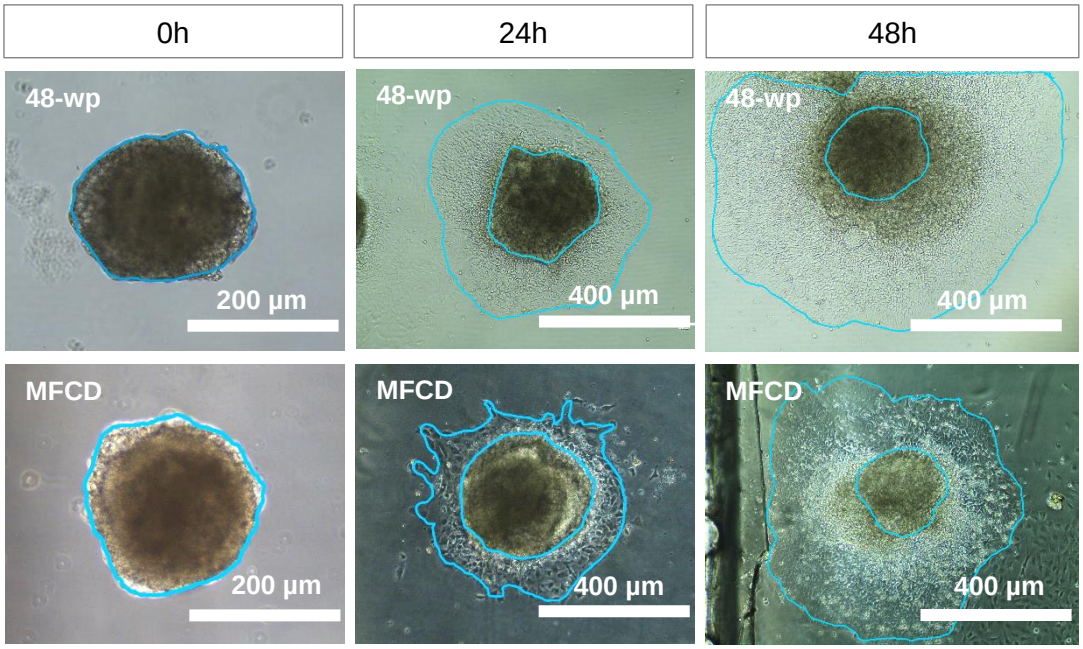

Figure 4.18 Expansion of hiPSC EBs in 48-well Plate Compared to the MFCD.

Using ImageJ software, the area of an expanded EB (Flat area) was measured and divided by the area of the initial EB (Dense area) to quantify the expansion of the in MFCD. EBs in MFCD showed 3.5 and 9 times slower expansion rate compared to the 48-well plate at 24 and 48 h culture.

were adhered to the surface in a way that prohibit the movement of the cells, therefore shortening the incubation time should result in faster expansion of the cells in the MFCD.

In order to test this hypothesis, a study was designed in which Matrigel™ was incubated in both MFCD and the well-plate for the usual 60 mins, and then for two MFCD's shorter times of 30 and 15 mins. Then EBs were cultured and the area measurements were taken as explained previously. Figure 4.19 shows the expansion rate measurements at different incubation times. The increase in expansion time of EBs in MFCD with shorter incubation time confirmed the hypothesis regarding the ECM density in MFCD culture area. Therefore, 15

minutes incubation time for Matrigel™ was adapted for both well-plate and MFCD.

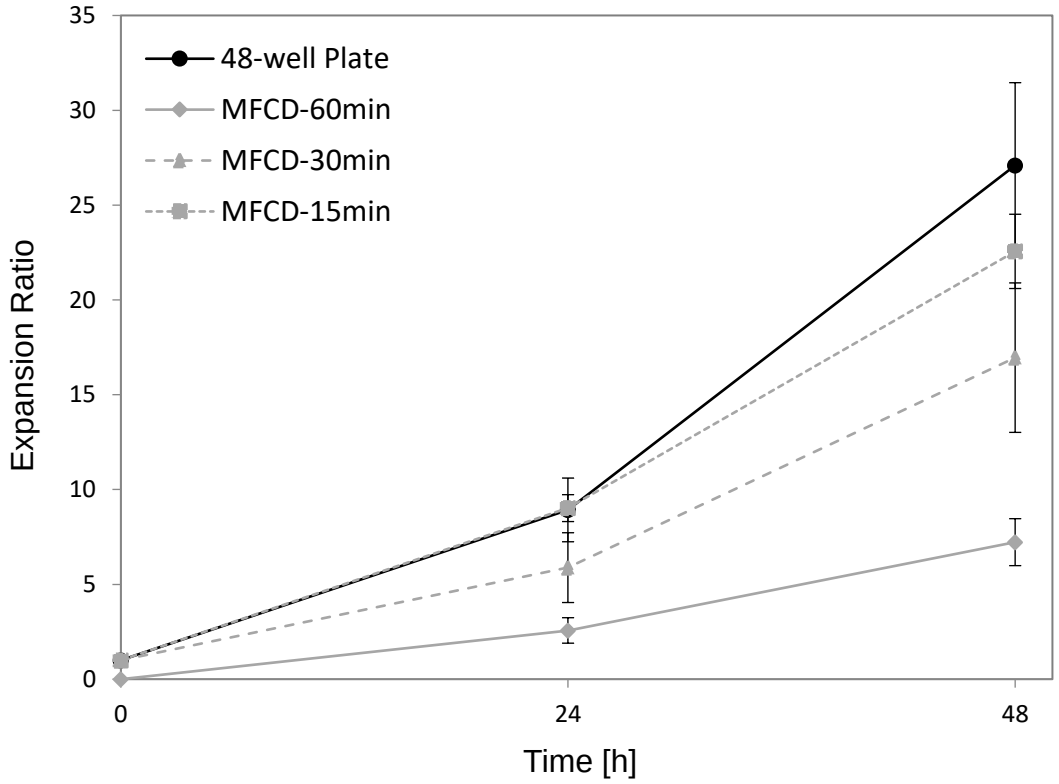

Figure 4.19 Effect of Matrigel Incubation Time on Expansion of EBs in MFCD.

The figure shows indirect relationship between Matrigel incubation time and expansion of EBs in MFCD. The expansion ratio is the area of the expanded EB (Flat area) divided by the initial area of the EB (Dense area). Shorter incubation time of 15 min resulted in faster EB expansion rate similar to the 48-well plate control culture. (n=4)

4.4.4 Absorption of Growth Factor by PDMS

In order to find out if the key growth factors used in the retinal differentiation protocol are absorbed by the PDMS in microfluidic chip we perfused the MFCD without presence of cells at the flow rate of 130 µL/h. To avoid the negative effects of the degradation at 37°C, experiments were performed on benchtop at room temperature. The Media was collected after 2 hours at the outlet of the MFCD and compared the growth factor concentration to that of the stock solution.

The concentrations of bFGF, DKK-1, Noggin and IGF-1 collected at the outlet of MFCD were 8.07±0.56, 9.13±0.45, 7.87±0.65 and 7.31±0.13 ng/ml respectively. The measured stock concentrations of these factors were 8.11±0.55, 9.22±0.42, 7.89±0.57 and 7.20±0.67 ng/ml. (Fig. 4.20) There was no significant difference between the stock and the outlet concentrations of these growth factors. Showing that PDMS had no effect on concentration of these growth factors once perfused through the MFCD.

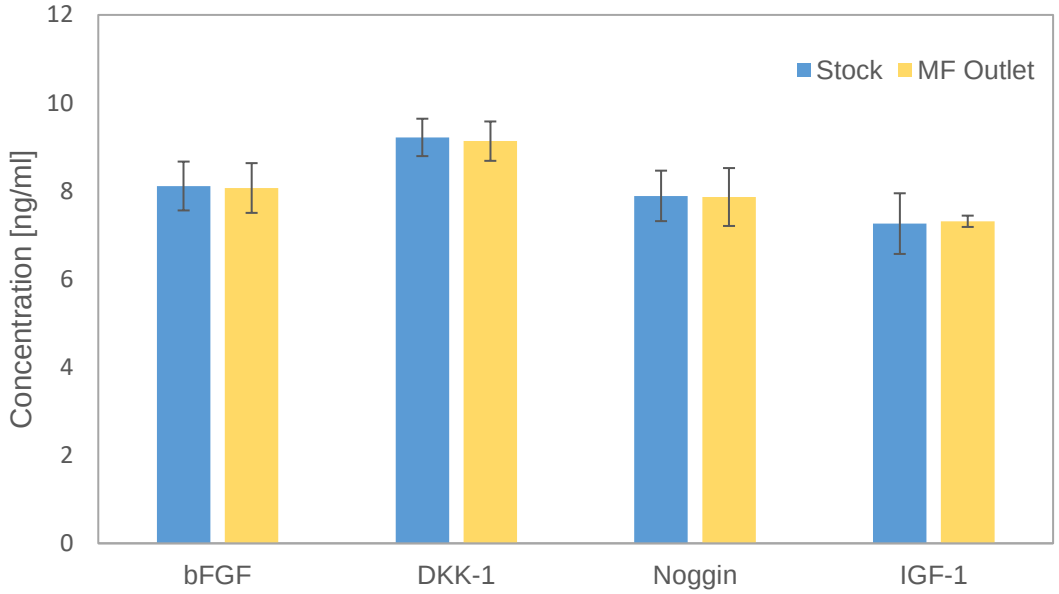

Figure 4.20 Growth Factors' Absorption by PDMS at 130 µL/h.

Shows concentration measurements of growth factors used in retinal differentiation protocol after 2 hours of perfusion in MFCD. The result was plotted next to the stock solution concentrations for each growth factor. No significant loss of the growth factors was observed in this study. Error bars represent plus and minus standard deviation. (n=3)

4.4.5 Culture of EBs in MFCD, Morphological Evaluations and Expression of Pluripotency Markers

In this study, short-term expansion of EBs in MFCD were tested over a period of 48 hours and cultures were evaluated morphologically. Furthermore, immunocytochemical staining was used for pluripotency genes OCT4, SSEA4 and Tra-1-81 to observe down regulation of the markers as cells progress through differentiation.

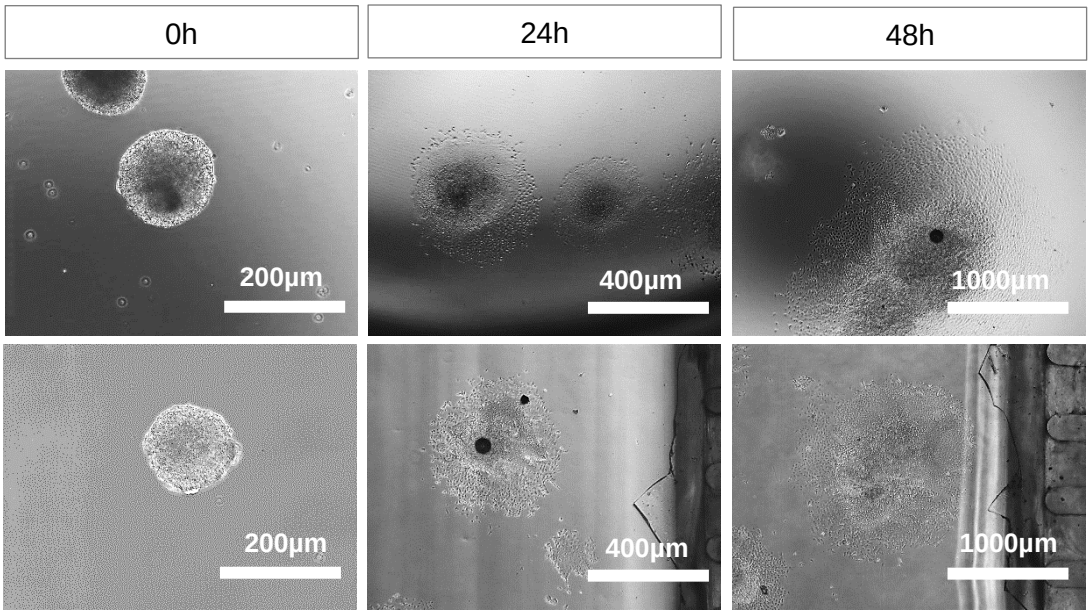

Figure 4.21 Culture and Expansion of hiPSC EBs in MFCD for 48 h.

Shows successful culture of EBs in MFCD (lower row) over a 48h period. EBs cultured in MFCD show similar expansion as the 48-well plate (top row) confirming robustness of the MFCD for longer cultures such as differentiation cultures.

Figure 4.21 shows similar expansion of the EBs in MFCD compared to the 48-well plate culture. Both cultures showed identical expansion rate and cellular morphology during the study. Figure 4.22 (A-L) shows down regulation of the pluripotency markers in differentiated areas of the expanding EBs. Both MFCD and 48-well plate shows similar expression of these markers.

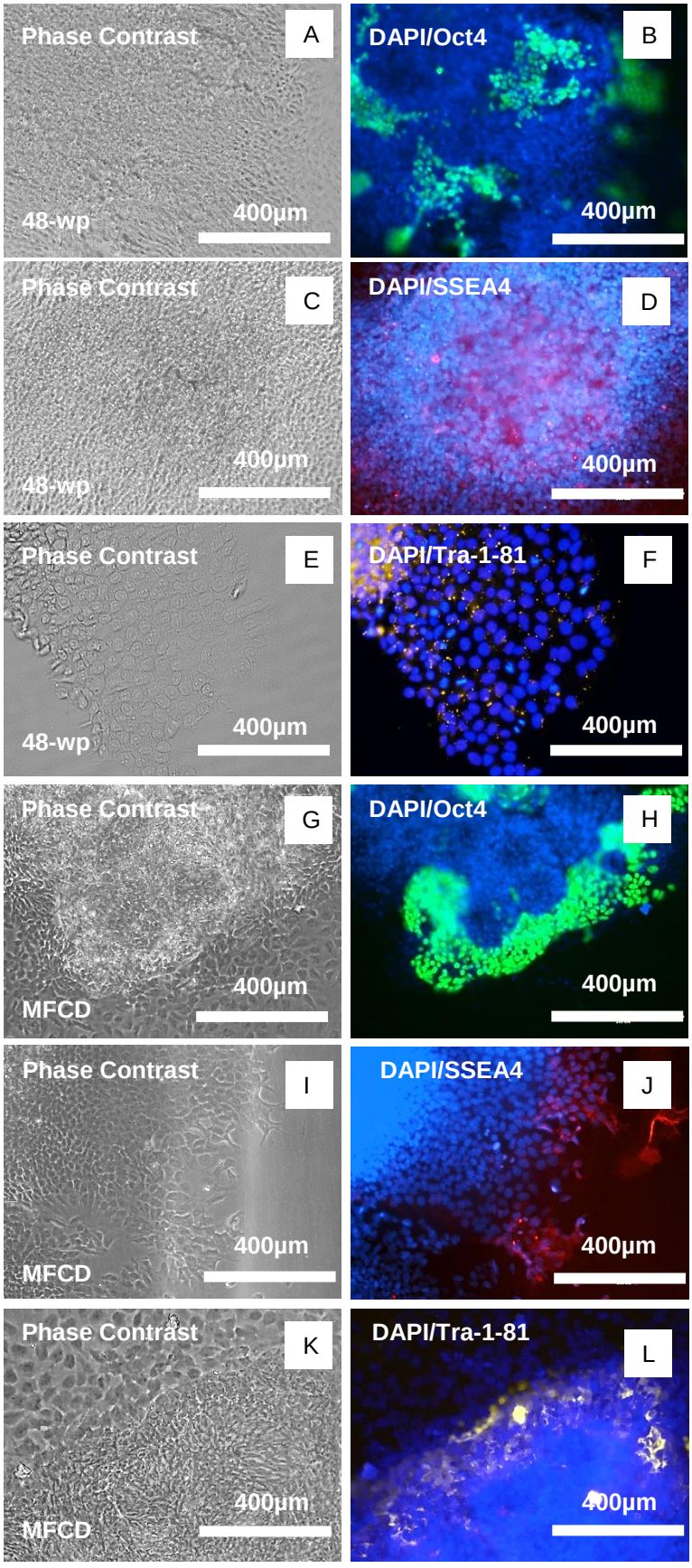

Figure 4.22 Downregulation of Pluripotency Markers Oct4, SSEA4 and Tra-1-81 in Differentiating hiPSC EBs in MFCD After 48 h.

Phase contrast and merged images of pluripotency markers with DAPI in both 48-well plate (A-F) and MFCD (G-L). In both cultures the areas that were differentiated showed no expression of these markers. Overall, downregulation of the pluripotency markers was observed in perfused and control culture. Secondary antibodies used Alexa 488 (Oct4), Alexa 594 (SSEA4) and Alexa 532 (Tra-1-81).

4.4.6 DKK-1 Concentration at 130 µL/h

Based on calculations in section 4.2.2 the perfusion rate of 130 µL/h will deliver molecules with molecular weight of 20 kDa and above to the cells convectively. The key growth factor at this perfusion rate is DKK-1 with a MW of 25.8 kDa. Therefore, to test steady-state concentration of this growth factor in the MFCD, its concentration was measured at the inlet and outlet of MFCD during a course of 10 days' retinal differentiation culture at 130 µL/h. The measurements in MFCD was compared to the DKK-1 concentration in 48-well plate, which was used as the control. (Fig. 4.23)

The 48-well plate showed a pulsed exposure to DKK-1 experienced by differentiating cells. This was due to the medium exchange once every 48 hours. As culture proceeded, drops in DKK-1 levels became less and less pronounced, which from day 6 the concentration of DKK-1 showed minimal changes to input concentration levels. In the continuously perfused MFCD, concentration of the DKK-1 at both inlet and outlet, was significantly higher ($p<0.01$) than the 48-well plate at 24 and 48 hours. The difference in concentration between inlet and the outlet implies that cells were indeed consuming DKK-1 as it passed through the chamber. DKK-1 consumption in MFCD at the outlet showed a 45% reduction in consumption of this factor within the first 48 hours compared to the static culture, at a steady manner, avoiding peaks and troughs observed in the control culture. The concentration was lowest during the early stages of the process at which point suggests that consumption of this factor was the highest. Results from this study correlates

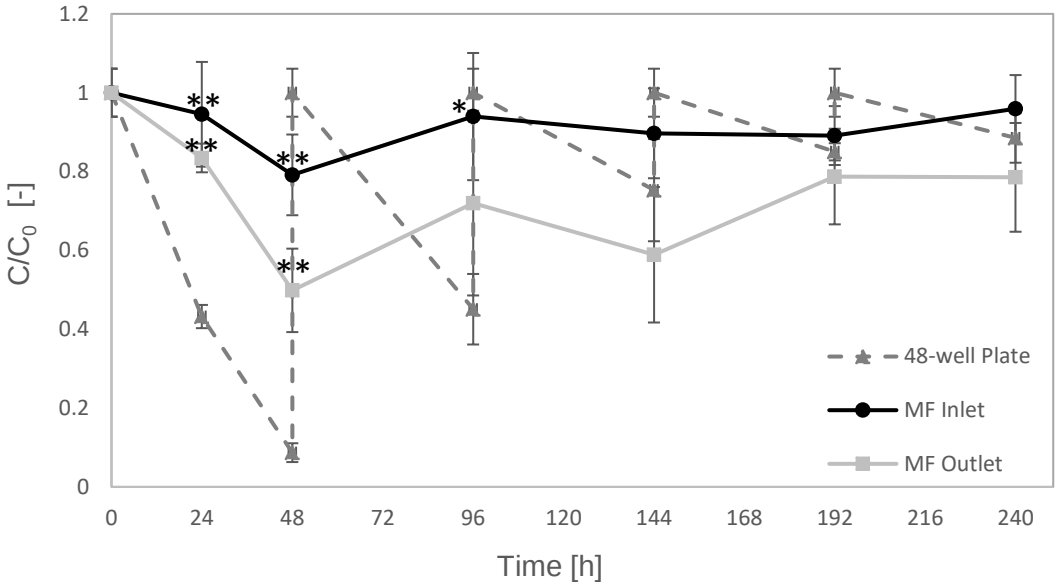

Figure 4.23 DKK-1 Concentration in MFCD over 10 Days' Retinal Differentiation of hiPSCs. Shows DKK-1 concentration measurements in 48-well plate, MFCD inlet and MFCD outlet. Both inlet and outlet of MFCD show significant difference in concentration ($p<0.01$) at 24 and 48 h compared to the 48-well plate control. The drop in DKK-1 concentration at the outlet of MFCD indicates consumption of this growth factor by the cells. Compared to the DKK-1 concentration in 48-well plate, MFCD provides more stable concentration of this growth factors to the cells at the flow rate of 130 µL/h. Error bars represent one SEM about the mean of 3 independent data points (n=3) A repeated measures ANOVA indicated a significant difference in the expression of each gene between the 3 conditions. To establish significant different between conditions, a Tukey's post-test was applied.

with the previous DKK-1 consumption study in section 3.5 where 90% of the DKK-1 was consumed within the first 48 hours.

The recovered levels of the DKK-1 on day 6 in the control culture could perhaps, be associated with a reduction in the activity and/or number of the low-density lipoprotein receptor-related protein 6 (LRP6). (Li et al., 2010) DKK-1 inhibits Wnt signalling by binding to the LRP6 receptors, it is hypothesised that as cells progress through different stages of retinal differentiation, these receptors change and does not interact the same way as they did at earlier

stages of differentiation. The alternative reason for reduced consumption of the DKK-1 could be due to production of this growth factor by the cells. Based on degradation studies, DKK-1 degrades rapidly within the first 8 hours, therefore its presence in the culture could be due to its production by the cells. Regardless of the underlying reason for this phenomenon, it could suggest that presence of this growth factor is not essential to the culture at this point and perhaps could be omitted from the protocol at this stage.

4.5 Summary

In selecting an operational window for retinal differentiation of hiPSCs under perfusion, we looked at effects of shear stress for choosing the upper perfusion limit and medium replenishment rate requirements for selecting the lower limit. Toh reported that shear stress of 1.6×10^{-3} Pa will result in no effects on morphology and minimal changes in gene expression of mESCs. Using this shear rate as the upper boundary means in our MFCD we will have a flow rate of 3600 µL/h. (Toh et al., 2011) For selecting the minimum perfusion rate we compared the height ratio of 48-well plate and our MFCD and it was established that our device has to be replenished 5.1 times more than the well-plate. Based on the culture area dimensions, flow rate of 2.5 µL/h was the minimum flow rate we could use to have the same exchange rate as in the well plate culture. At this flow rate medium in the MFCD is replenished once every 9.4 hours.

To create steady-state concentration of soluble factors, we utilised dimensionless ratios such as Péclet and Damköhler number to find the best perfusion rate. Based on non-dimensionalisation of 2D reaction diffusion equation, Péclet number over alpha was used to find the critical perfusion rate for having various molecules (based on MW) to be in convective delivery to the cells. Using the consumption and degradation studies in the previous chapter, perfusion rate of 130 µL/h was selected to have molecules of 20 kDa and larger delivered to the cells via the fluid flow. At this flow rate, molecules such as DKK-1, Noggin, BSA and transferrin are delivered to the cells, hence creating a steady-state conditions based on cellular demands.

Using Damköhler number against cell density for TGFα, Albumin (as representative of smaller and larger molecules respectively) and oxygen we established the critical cell density for having these molecules in diffusive limited regime. Performing these measurements at different heights of the medium showed low sensitivity of the parameter on the Damköhler number and confirming that delivery of the growth factors is limited by their consumption rate.

A number of quality control tests were performed to evaluate robustness of the MFCD for long-term differentiation cultures. Burst pressure measurements revealed that there was no significant difference between the improved prototype and the previous versions. Furthermore, use of the nylon screws does not result in loss of robustness in terms of burst pressure and the sustainability of the device. Dissolved oxygen concentration measurements showed there is identical oxygen concentration in MFCD inlet and the culture area at 21%. In evaluating the pumping solution, KDScientific 200 showed more accurate delivery of the 130 µL/h flow rate and KDScientific Legato 212 for flow rate of 5.2 µL/h.

Assessment of cell culture capabilities of the MFCD, revealed successful culture of MEFs and co-culture of hiPSCs in terms of viability, morphology and expression of pluripotency markers OCT4, SSEA4 and Tra-1-81. Initial culture of EBs resulted in significantly slower growth of EBs in MFCD compared to the 48-well plate. An investigation into the cause of this slow growth revealed an indirect relationship between Matrigel™ incubation time and rate of expansion in EBs. It was discovered that 15 minutes' incubation of Matrigel™ in MFCD

result in similar growth rate of EBs in 48-well plates. Possible absorption of growth factors with PDMS was tested and showed no observable loss of the growth factors in MFCD outlet measurements at flow rate of 130 µL/h. Proceeding to adjustments made to Matrigel™ incubation time, EBs cultured in MFCD showed similar expansion in MFCD compared to the 48-well plate. Furthermore, cultures were compared morphologically and showed similar down regulation of the pluripotency markers over a course of 48 hours.

Finally, assessment of the DKK-1 concentration in MFCD over a course of 10 days culture, revealed that at flow rate of 130 µL/h, MFCD can provide more stable concentration of this growth factor compared to the 48-well plate culture. Moreover, DKK-1 seemed to be either produced by the cells in the well plate culture after 96 hours or there is a reduction in reaction with LRP6 surface receptors. DKK-1 concentration on day 6 was similar to input levels in 48-well plate culture, showing no requirement of this growth factor by the cells at this stage of development.

Chapter 5 Retinal Differentiation of hiPSCs in MFCD

5.1 Introduction

In chapter 3, hiPSCs were characterised to ensure their pluripotency and establish a passaging routine for their maintenance. Normalisation steps required for accurate gene expression analysis was explained and validated the expression of the key markers during retinal differentiation of hiPSCs. Finally, studied key growth factors used in retinal differentiation culture and an order of importance was established based on cellular demands and degradation rate of these molecules.

In the previous chapter, shear stress was used to establish a window of operation for perfusing retinal differentiation culture. Next, dimensionless ratios such as Pe and Da numbers were utilised to find the critical perfusion rate for creating steady-state soluble concentration. MFCD was assessed for long-term perfusion cultures by addressing issues raised regarding the leakage, asepsis and expansion of the EBs. Initial perfusion cultures showed similar expansion and differentiation of the hiPSCs in MFCD compared to the control culture.

In this chapter, results of the two previous chapters were brought together to initiate the perfusion cultures at two flow rates of 130 µL/h for creating steady-state concentration of soluble factors and a lower flow rate of 5.2 µL/h as a second control with similar medium height and same medium replenishment rate as the static control culture. In each run, one well of the 48-well plate culture was used as the control for one MFCD at low flow rate and one at high

flow rate. All perfusion cultures at different flow rates were performed simultaneously and in 4 independent replicates at each time-point (5, 10 and 21 days). One set of the runs were used for immunostaining and the other 3 were collected and stored at -80°C for RT-qPCR analysis. Morphological analysis of perfused cultures was performed to identify similarities and differences between the perfused and the control cultures. Finally, gene expression profile of the perfused cultures for pluripotency to germ layer, eye-field and retinal progenitor markers were performed and compared to the well-plate control culture.

5.2 Considerations for Gene Expression Analysis

As explained in chapter 3, Lamba's protocol for retinal differentiation of the hESCs used in this work. The initial step in the protocol starts with formation of EBs, where neural differentiation stimulation of the cells takes place by incubating them with Noggin, DKK-1, IGF-1, Knockout serum, and B27 supplement. Once EBs were formed, 7 EBs were transferred onto the Matrigel™ coated well of the 48-well plate and 7 EBs into culture area of each MFCD. At this stage, higher concentration of the growth factors used in addition of bFGF and B-27 to initiate retinal differentiation. 24-hour static incubation was allowed in MFCDs before starting perfusion for 5, 10 and 21 days. Figure 5.1 show a schematic representation of the retinal differentiation cultures performed in MFCD and 48-well plate.

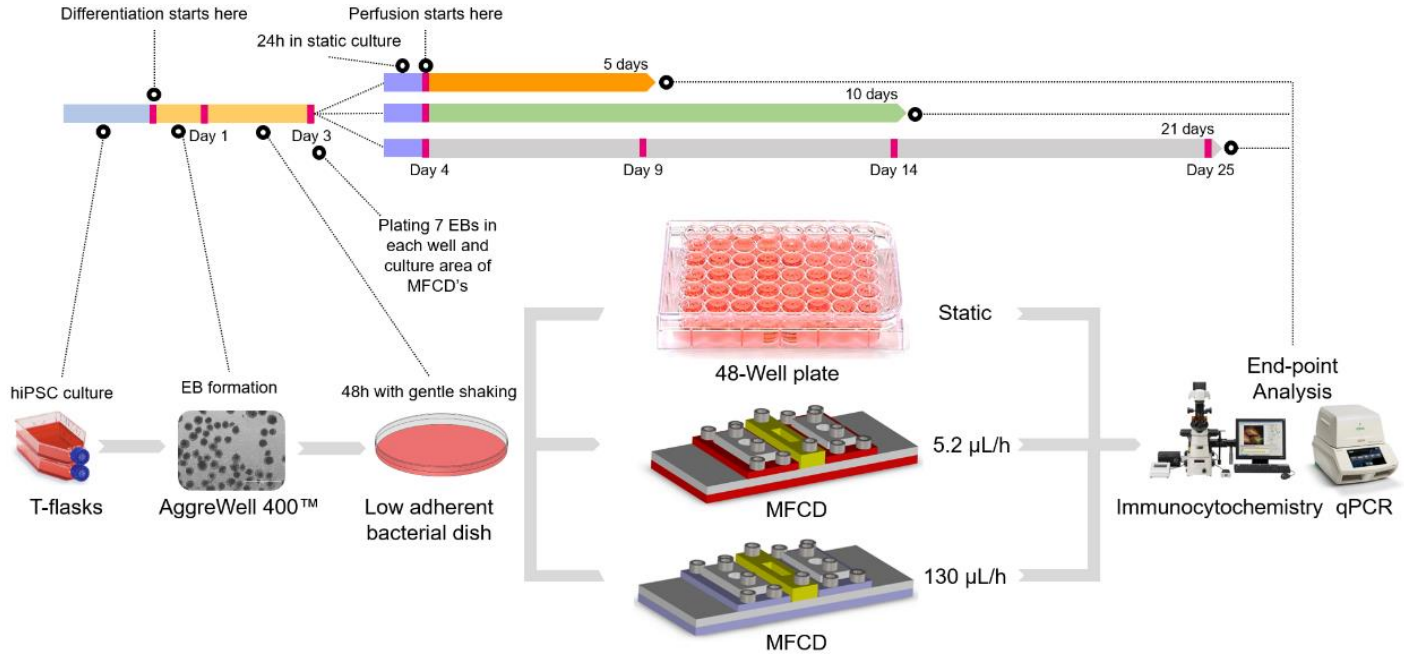

Figure 5.1 Process Flowchart of the Retinal Differentiation of hiPSCs Under Perfusion in MFCD.

The stepwise process of retinal differentiation was initiated by formation of the EBs using AggreWell™, followed by a 2 days' culture of the EBs with gentle shaking in low adherent bacterial dish. EBs were transferred onto one well of 48-well plate and MFCD coated with Matrigel for retinal determination step. Following a 24-hour static incubation for attachment of the cells to the culture surface, started perfusion at two flow rates of 130 and 5.2 µL/h. The lower flow rate of 5.2 µL/h provides similar medium height and identical medium exchange rate to the 48-well plate control, providing a second control for the MFCD with higher flow rate. Expression of the retinal markers was analysed using immunocytochemistry and qPCR. The reported time on the top of the progress lines indicates the time taken in each processing step and the one below shows the overall differentiation time.

5.2.1 Normalisations for Gene Expression Analysis

In section 3.3.3 it was explained that multiple normalisation is required at different stages of the qPCR analysis to have accurate measurement of the gene expression. At the initial step prior to RNA extraction, it was essential to use the same sample size in both control and the study group. This step has a direct effect on the total amount of RNA extracted and consequently on the amount of usable cDNA that can be used for qPCR analysis. The extracted RNA must be checked for its quality and purity before proceeding to the next step. The next essential normalisation step is the use of equal concentration of the RNA for cDNA synthesis step, which often involves using a control such as untreated hiPSCs as a calibrator.

5.2.1.1 Sample Size

The culture area of the 48-well plate (0.95 cm^2) is nearly twice as large as the MFCD area (0.52 cm^2). In order to find out if cells expand in similar numbers in MFCD and the control 48-well plates, both devices were seeded with 7 EBs and the same number of cells per EB i.e. 1000 cells per EB, making a total of 7000 cells per culture area. Cells were collected at the end of each time-point and counted using Vi-Cell cell counter (Beckman Coulter, USA). Figure 5.2 shows cell counts between 48-well plate and the MFCD for a period of 5 days. Result showed concentration of the cells in the control culture reached 4.1±8.3 $x10^4$ and in MFCD were 3.3±5.6 $x10^4$ cells/ml by the end of day 5. Cell counts showed comparable number of cells in both cultures, however, the lower concentration of the cells in MFCD requires further normalisation at later steps of qPCR.

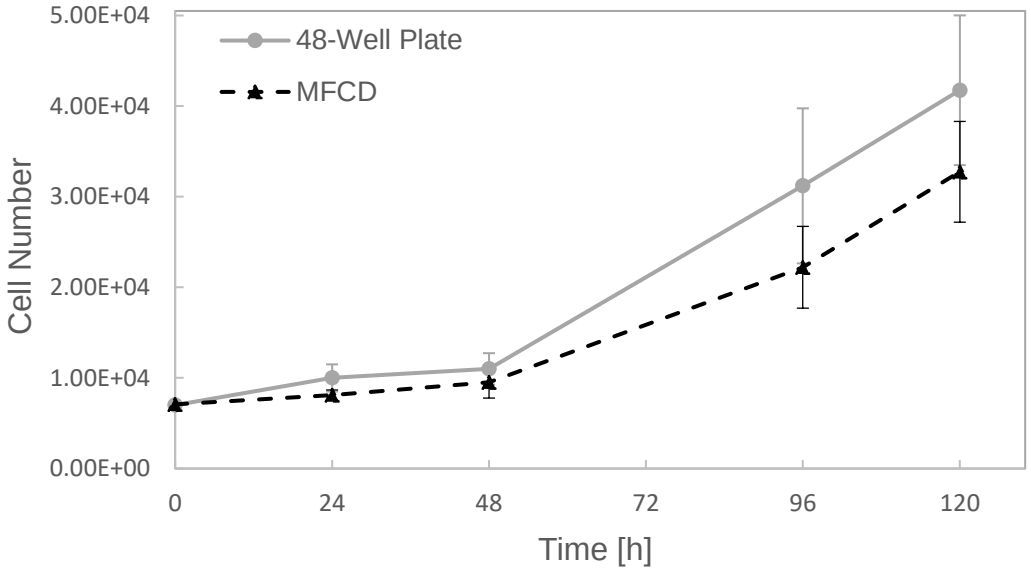

Figure 5.2 Comparison of the hiPSCs Concentration in 48-well Plates and MFCD.
Cell counts in 48-well plate and MFCD shown similar concentration of cells up to 48 h. The cells in the 48-well plates showed higher average cell numbers after the 48 h, however they weren't significantly different from the cell numbers in MFCD. Error bars represent one SEM about the mean of 3 independent data points (n=3).

5.2.1.2 Total RNA Concentration

Proceeding to perfusion cultures at different flow rates and time lines, we extracted the RNA and plotted a box-chart to demonstrate distribution of the RNA concentration from each culture. Figure 5.3 shows this distribution of the total RNA extracted from samples in 48-well plate, MFCD at flow rate of 5.2 µL/h and 130 µL/h. The amount of RNA obtained from 48-well plate and MFCD at 5.2 µL/h shown to be statistically different from those of the MFCD at 130 µL/h. Therefore, it was essential to normalise each sample to an equal concentration before proceeding to cDNA synthesis.

Since a large number of the RNA concentrations obtained from samples in both control and lower flow rate MFCD were below 100 ng/µL, it was decided

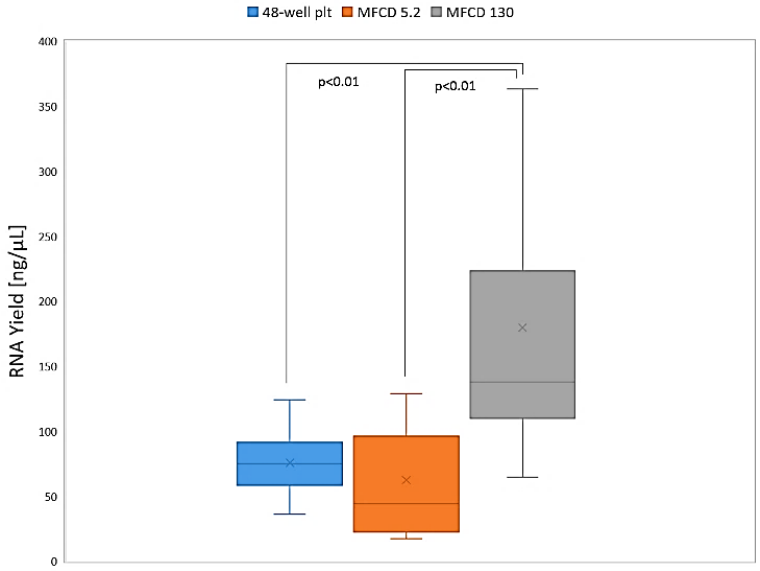

Figure 5.3 Total RNA Exctarted from Differentiated hiPSCs in Each Culture Vessel. RNA concentrations after the extraction for each culture condition. Box chart was used to show the spread of these values across different culture vessels. MFCD with faster flow rate of 130 µL/h showed significantly much higher concentration of the total RNA extracted compared to the 48-well plate and MFCD with slower flow rate. Therefore, it was essential to normalise the RNA concentrations at this step before proceeding to the cDNA synthesis step. Error bars represent one SEM about the mean of 9 independent data points (n=9). A repeated measures ANOVA indicated a significant difference in the expression of each gene between the 3 conditions. To establish significant different between conditions, a Tukey's post-test was applied.

to amplify the whole transcriptome to make sure all the target transcripts are represented at a sufficient and equal quantity. The QuantiTect® Whole Transcriptome kit (Qiagen, Germany) was used to amplify the concentration of each sample to 200 ng/µL before it was used for RT-qPCR. One sample of untreated hiPSCs was used to act as a calibrator to show relative up/down regulation of different markers at various stages of the differentiation process. Therefore, all RNA sample concentrations were first normalised to that of the hiPSC's concentration before performing cDNA synthesis.

5.2.1.3 RNA Quality and Purity

The RNA quality was assessed using NanoDrop. (ND-1100, NanoDrop Technologies, USA) As mentioned in section 3.3.3.2, the 260nm wavelength used for nucleic acids, 280nm for proteins and 230nm wavelength used for detection of contaminations. For evaluating quality of the extracted RNA, the 260/280 ratio is used and for its purity 260/230 ratio. Values of 1.8 to 2.1 is often in range of acceptable quality for OD of A260/280. (Fleige & Pfaffl, 2006)

Figure 5.4 shows the A260/280 measurements obtained from samples at 5 (sample number 1,2,3), 10 (sample number 4,5,6) and 21 days (samples 7,8,9). Ratio of 1.86 was the lowest and 2.1 the highest absorbance obtained. For contamination evaluation, A260/230 ratio of 2 is considered an acceptable number. Figure 5.5 shows the measurements obtained for the A260/230 for the samples collected at 5 (sample number 1,2,3), 10 (sample number 4,5,6) and 21 days (samples 7,8,9). Ratio of 1.36 was the lowest and 2.0 the highest absorbance obtained. Both quality and purity of the RNA samples obtained were within the acceptable range, indicating integrity of the RNA samples used for the qPCR analysis.

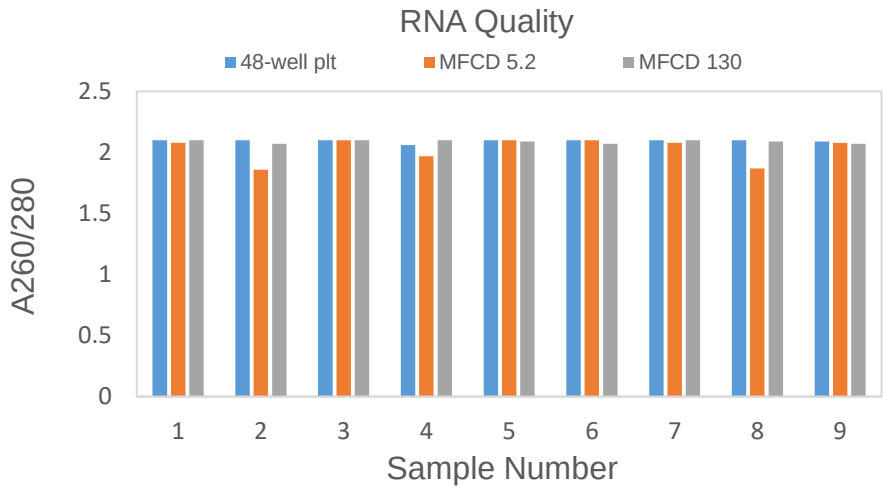

Figure 5.4 RNA Quality Measurements at A260/280 Obtained from Samples in MFCD and 48-well Plate.

The measurements obtained for the quality of RNA samples collected at 5 (sample number 1,2,3), 10 (sample number 4,5,6) and 21 days (samples 7,8,9). A ratio of 1.8 to 2 is considered to be acceptable quality for extracted RNA samples. (n=3)

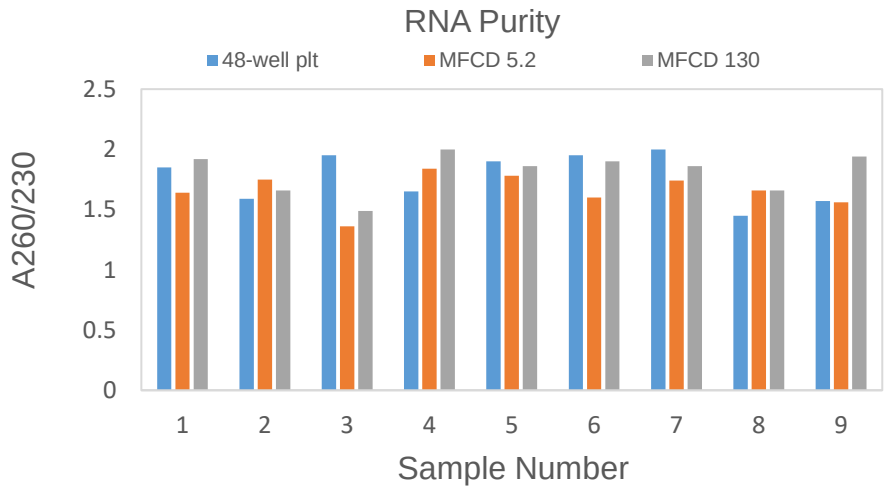

Figure 5.5 RNA Purity Measurements at A260/230 Obtained from Samples in MFCD and 48-well Plate.

The measurements obtained for the purity of RNA samples collected at 5 (sample number 1,2,3), 10 (sample number 4,5,6) and 21 days (samples 7,8,9). A ratio of up to 2 is considered to be acceptable purity for extracted RNA samples. (n=3)

5.3 Morphological Evaluation of the Cultures under Perfusion

Morphological analysis of long-term cultures such as retinal differentiation can be challenging as each culture can and will expand differently. Differences such as the location of the EBs on the culture plate and distance from each other creates different physical dynamics that could result in changes in cellular behaviour. Therefore, to better understand these changes and make them more comparable, analysis of the cultures was based on three observational parts. Starting with expansion of the EBs in each culture, then evaluated the commonly occurring features among different culture vessels and finally identified the exclusive features in each culture.

5.3.1 Expansion of the EBs

The expansion of the EBs was monitored by gradual growth of cells away from the core of EBs in the first couple of days after seeding. Overall, all three cultures showed similar expansion of the EBs. In 48-well plate cultures, EBs had a tendency to aggregate more prior to spreading in the culture area. However, in the MFCD this behaviour was less observed, especially in MFCD with slower flow rate, where EBs showed more independence in their expansion. On the other hand, the MFCD with slower flow rate of 5.2 µL/h showed less cellular growth compared to the other two cultures during the initial expansion period. However, in later stages of the culture, the cell density in the MFCD with slower flow rate became identical to that of the control 48-well plate culture. (Fig. 5.6)

Figure 5.7 shows panoramic view of the culture area in MFCD at both flow rates. Similar expansion of the EBs was observed in both flow rates up to day

10. The cellular growth in MFCD with flow rate of 130 µL/h seem to result in higher number of cells compared to the lower flow rate. The MFCD chip was designed as such that provides higher flow rate on either side closer to the frame. Growth of the cells in MFCD with higher flow rate seemed to be inhibited at these sites up to day 10, a feature that was not observed in MFCD with lower flow rate.

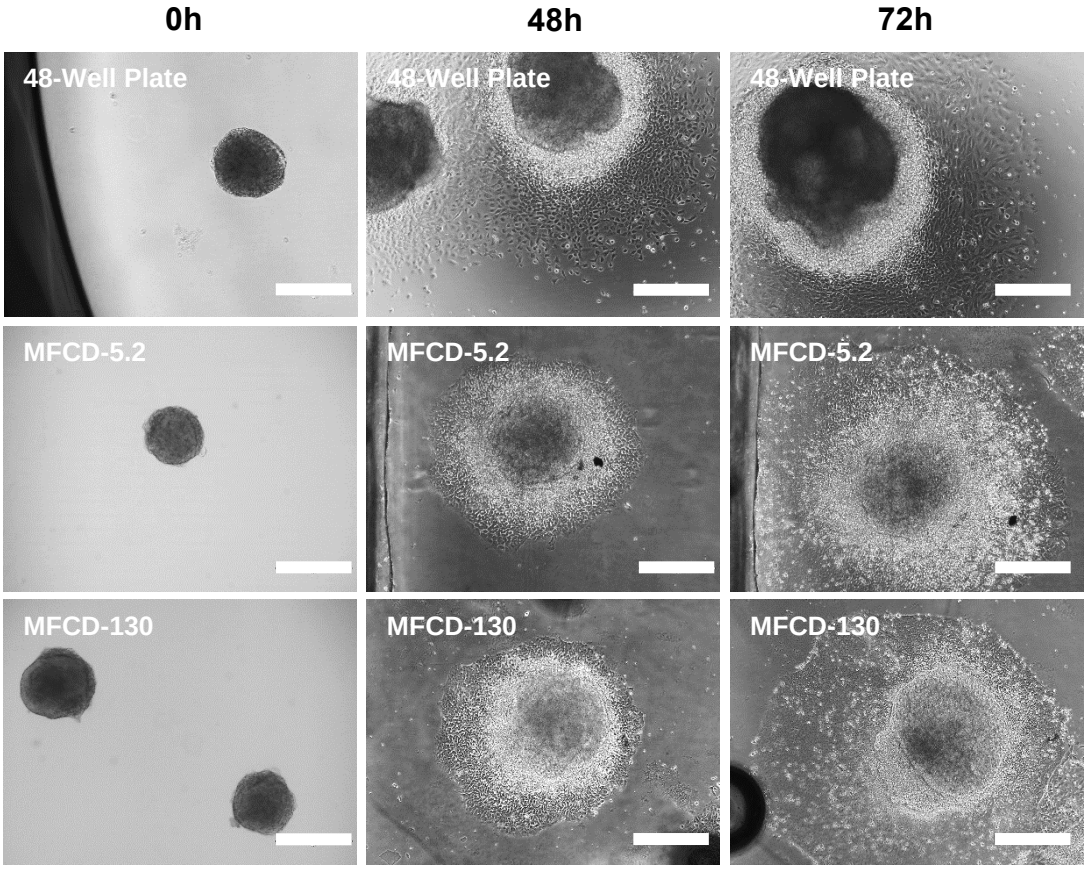

Figure 5.6 Expansion of the hiPSCs EBs Across the Culture Devices Under Perfusion.

EBs in the 48-well plates shown a tendency to aggregate more creating a much denser 3D area compared to the MFCDs. Generally, EBs expanded in the same fashion and rate comparatively across all devices. First column shows EBs at seeding, second column are EBs at 48 h, after one day of perfused culture and the last column are EBs at 72 h. Scale bar represents 200 µm.

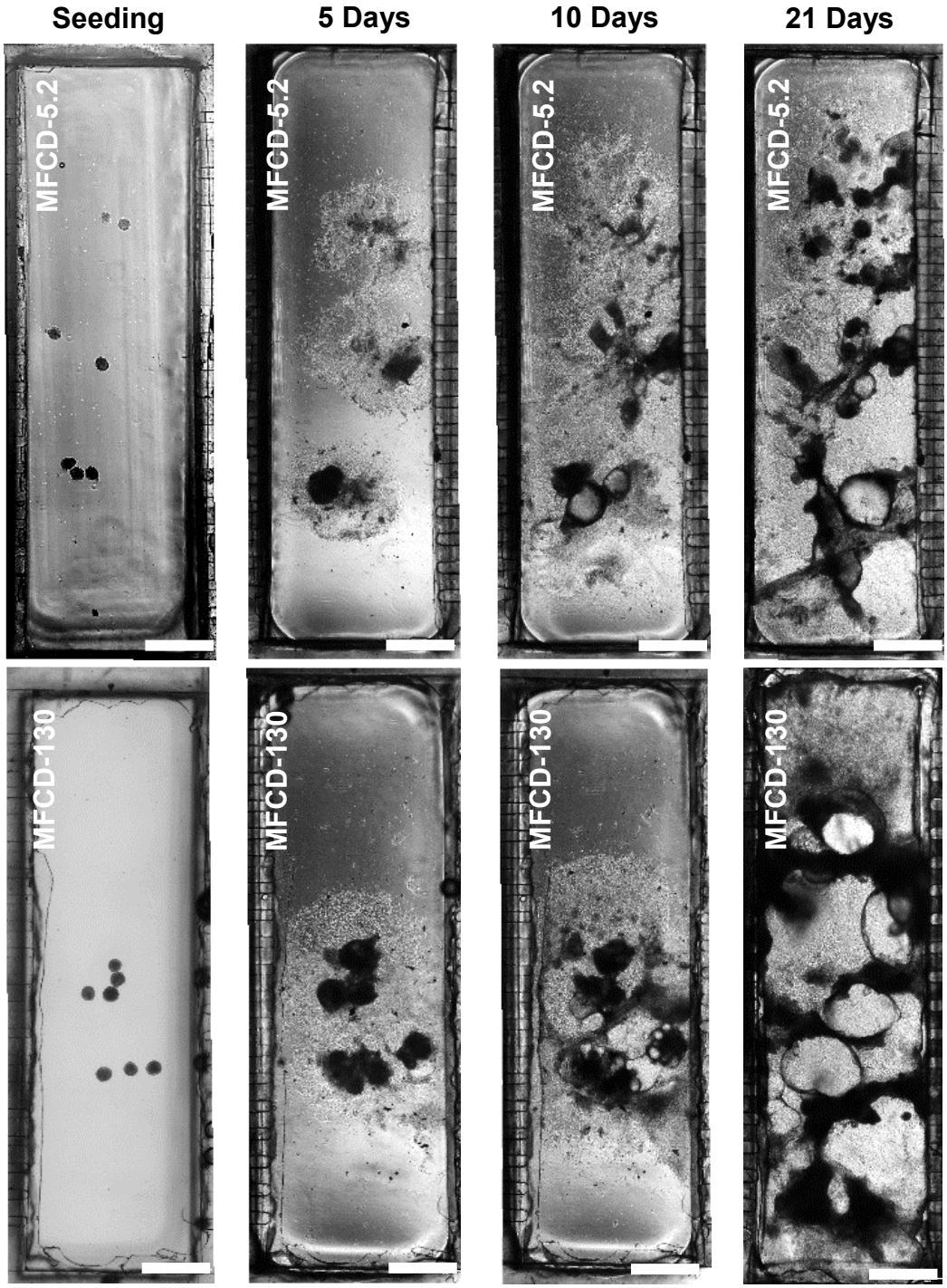

Figure 5.7 Panoramic View of 21Day Retinal Differentiation of hiPSCs in MFCD.

Day 5 image of the culture area shows a similar expansion of the EBs in both cultures with cells growing away from the core of the EBs. On day 10, cellular expansion continued in both culture with a more monolayer in the MFCD with slower flow rate and thicker multi-layer in MFCD with faster flow rate. Cells in MFCD with faster flow rate did not grow into either longitudinal extremity of the culture area where flow rate was faster. However, this pattern did not persist in later stages of the culture where cells expanded across the culture area on day 21. Scale bar represents 1000 µm.

5.3.2 Common and Exclusive Features in Each Culture

As cultures proceeded to day 5, appearance of 3D structures was observed on all three formats. One of the most prominent features appeared during the course of differentiation cultures was the neural rosettes. The neural rosettes are formation of the columnar cells in a radial fashion, which express markers that are mostly expressed in neuroepithelial cells in the neural tube. The neural rosette often act as a signature for the development of neuroprogenitors in ESCs differentiating cultures. (Wilson et al., 2006) hESCs and hiPSCs treated with IGF-1, shown to have the appearance of neural rosettes at early stages of differentiation. (Lamba et al., 2006) IGF-1 is also essential in formation of the eye and retinal progenitors. (Pera et al., 2001)

In the control 48-well plate cultures, they formed at days 5-7 and remained for few days before disappearing at days 8-9. In the MFCD with lower flow rate of 5.2 µL/h, they were formed at day 8-9 and stayed longer, before disappearing at days 12-14, showing a delayed appearance. (Fig 5.8) The neural rosettes did not appear at the MFCD with higher flow rate of 130 µL/h. The delayed appearance of the neural rosettes at low flow rates and their lack of in higher flow rates, suggests that perhaps formation of this feature is dependent on autocrine signalling factors that have been wash out or affected by the fluid flow at higher flow rates.

Some of the most common features observed in the 48-well plate cultures were aggregation of the EBs into a large core, which often resulted in formation of more complex 3D structures. In MFCD with lower flow rate, a monolayer of the cells spreading throughout the culture area was observed. Multi-layer 3D

formations in this device lacked morphology and less observed compared to the other formats. In MFCD with higher flow rate, a more uniform multi-layer of cells was observed in areas where cells were spreading. Like the MFCD with lower flow rate, the 3D structures lacked any morphology. However, there were much larger number of these formations comparatively.

Finally, in both MFCDs, the cellular debris remained on top of the culture and was not washed away by the fluid flow. This phenomenon did not seem to interfere with the growth of the cells in both perfused devices. However, it's effect on cellular function or the differentiation culture is unclear. (Fig 5.9)

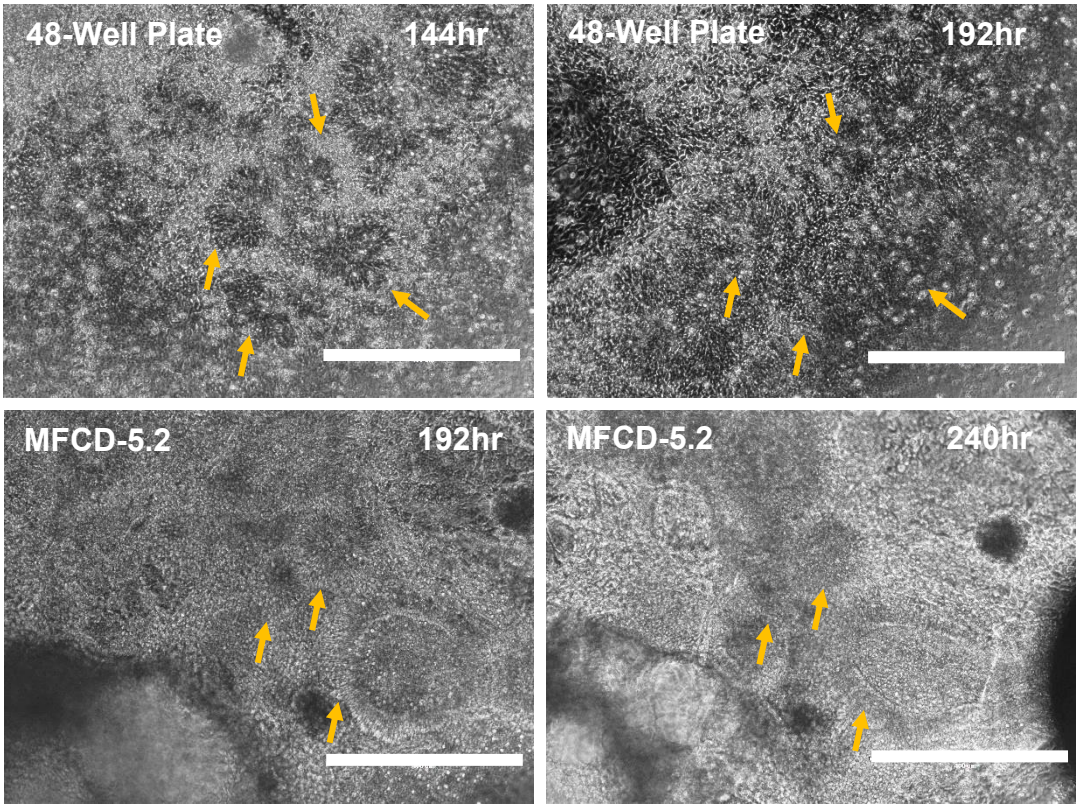

Figure 5.8 Delayed Appearance of Neural Rosettes in MFCD with Flow Rate of 5.2 µL/h During Retinal Differentiation of hiPSCs.

Neural Rosettes are radial formation of the columnar cells and a signature of the neuroprogenitors cells. They often formed around days 5-7 in the control 48-well plate before disappearing on days 8-9. In MFCD with lower flow rate of 5.2 µL/h, neural rosettes appeared on day 8-9 and stayed longer before disappeared on days 12-14. Neural rosettes did not appear in the MFCD with higher flow rate of 130 µL/h. Delayed appearance of the neural rosettes indicates that signalling factors involved are affected by the perfusion. Scale bar represents 200 µm.

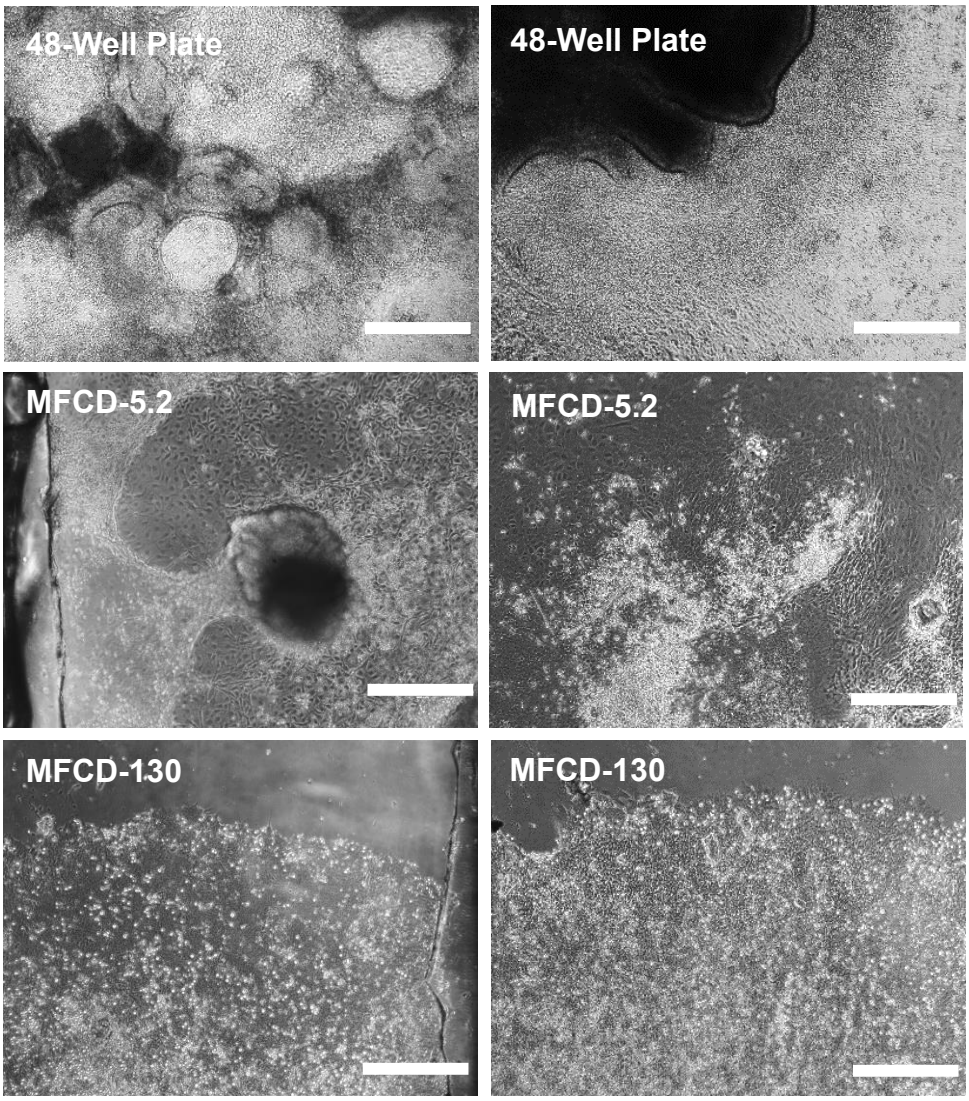

Figure 5.9 Common Features Observed in Expansion of hiPSC EBs in Each Culture Vessel.

Among the common features observed in each culture device were, aggregation of the EBs in 48-well plates and formation of complex 3D structures. In MFCD with lower flow rate often exhibited a monolayer expansion of cells and larger amount of cellular debris. MFCD with higher flow rate often showed a uniform expansion of the cells specially between day 10 and 21. Scale bar represents 400 µm.

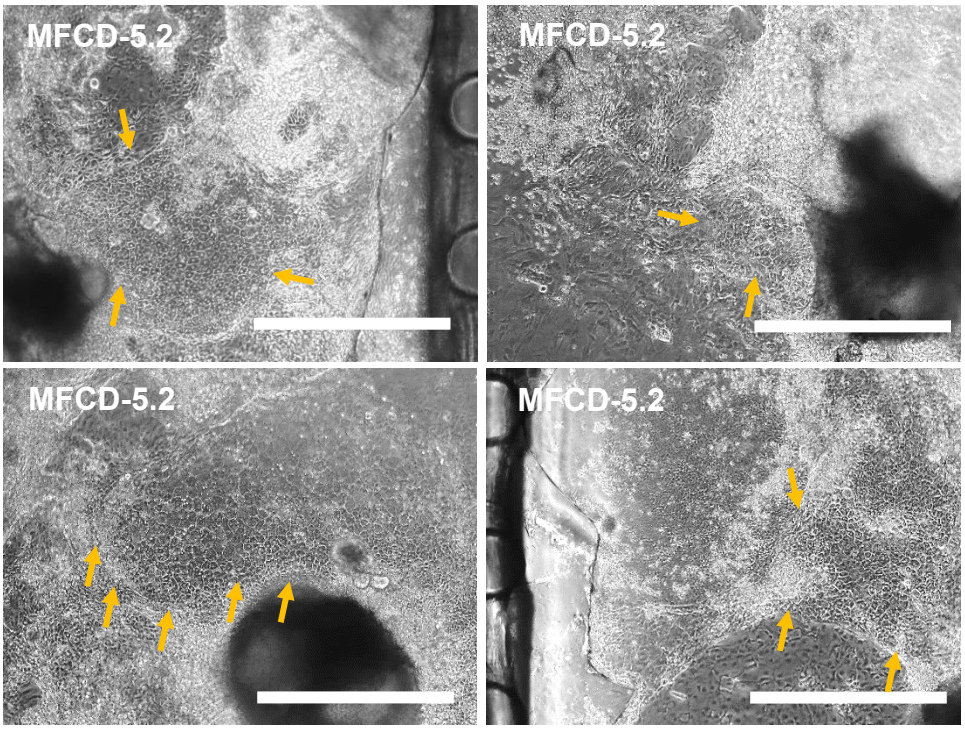

Figure 5.10 Formation of the RPE-like Cells in MFCD with Flow Rate of 5.2 µL/h.

One of the exclusive features appeared among the culture formats, were formation of the polygonal RPE like cells around days 10-12 of the culture. Lack of pigmentation in these cells could be due to higher expression of Vsx2/Chx10. Scale bar represents 200 µm.

Among other features observed during differentiation, was unique appearance of layers of polygonal cells, resembling to early RPE cells' morphology between days 10 and 12 in the MFCD with lower flow rate of 5.2 µL/h. During retinal differentiation of ESCs, after formation of the neural tube, if marker Mitf is expressed in retinal progenitor cell in the optic vesicle and the optic cup, it will guide the cells toward RPE formation. However, if markers such as Vsx2/Chx10 expressed it will give rise to expression of Crx and Nrl, and formation of the photoreceptor precursors. (Ikeda et al., 2005; Osakada et al., 2009) It is worth noting that these cells did not show the presence of the pigmentation, normally present in RPE cells. It was found that expression of

Vsx2/Chx10 in RPE population, leads to lack of pigmentation in these cells. (Rowan et al., 2004) This feature did not appear in control or the other MFCD culture. Figure 5.10 shows instances of this cellular layer appeared in MFCD with lower flow rate. Lack of the RPE like formations in the static and MFCD with higher flow rate, indicates the flow response dependency of these formations. However, the mechanisms in which lower flow rate affects the culture to form these cells is unclear and requires further investigation.

5.4 Expression of the Pluripotency, Germ Layer and Retinal Markers

Following the morphological analysis of the cultures we carried out time-point analysis of an array of pluripotency, germ layer and retinal markers on 5, 10 and 21 days' perfusion culture samples. For this purpose, we used immunocytochemical staining and qPCR to study effects of perfusion in more details.

5.4.1 Downregulation of the Pluripotency Markers

To monitor progress of the differentiation in perfused devices, expression of pluripotency markers Oct4, Nanog and Sox2 on 5, 10 and 21 days were used. (Fig. 5.11) Moreover, immunocytochemical staining was used on day 5 for expression of Oct4, SSEA4 and Tra-1-81 to visually confirm pluripotency downregulation. (Fig. 5.12) As hiPSCs began to differentiate in the first 5 days of the culture, downregulation of the pluripotency markers was observed among all culture devices as well as the control culture. Continued downregulation of pluripotency markers Oct4 and Nanog with no significant differences between the MCFD and 48-well control was observed on days 10 and 21. However, for Sox2, following an initial downregulation on day 5, it showed upregulation in all cultures apart from MFCD with slower flow rate of 5.2 µL/h.

Sox2 has a dual function as a pluripotency marker for stem cells and also as a neural ectoderm transcription factor. (Heavner et al., 2012; Adachi et al., 2013) Upregulation of Sox2 was expected as the cells progress to differentiate into neural retinal lineages, where this gene cooperates with another early

retinal marker Otx2 to activate expression of the gene Rax. Rax plays a key role in development of the eye field by affecting expression of several eye field transcription factors (EFTFs). (Andreazzoli et al., 1999; Zuber et al., 2003; Danno et al., 2008) Heavner, studied the role of Sox2 in the mouse retina and suggested that it antagonises the Wnt signalling pathway in the developing retina. Consequently, it will positively affect the maintenance of the neurogenic lineage while regulating the formation of the optic cup progenitors. (Heavner et al., 2014)

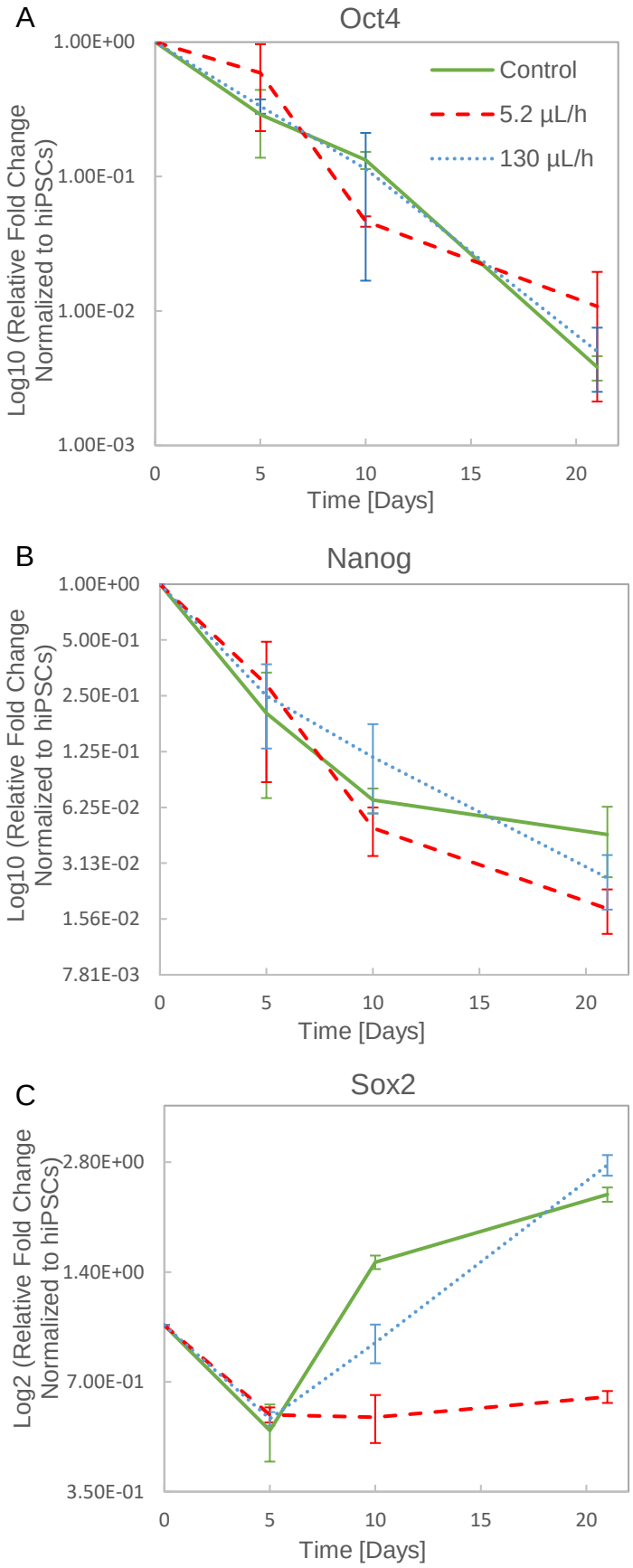

Figure 5.11 Gene Expression of Pluripotency Markers Oct4, Nanog and Sox2 in hiPSCs During Retinal Differentiation Culture.

*(A) Shows down regulation of the pluripotency markers Oct4 as differentiation proceeded to day 21. (B) Expression of Nanog during the differentiation culture, this marker also was downregulated as culture progressed. (C) Sox2 showed initial downregulation on day 5 across the different culture formats. Sox2 was upregulated again from day 10 in MFCD with faster flow rate and the control culture. Sox2 expression in the MFCD with slower flow rate plateaued at levels expressed on day 5 for the rest of the experiment. Error bars represent one SEM about the mean of 3 independent data points (n=3). A repeated measures ANOVA test was used to indicate a significant difference in the expression of each gene between the perfused cultures and the static control culture, at each time point: *p<0.05; **p<0.01. To establish exactly which conditions were significantly different from each other, a Tukey's post-test was applied.*

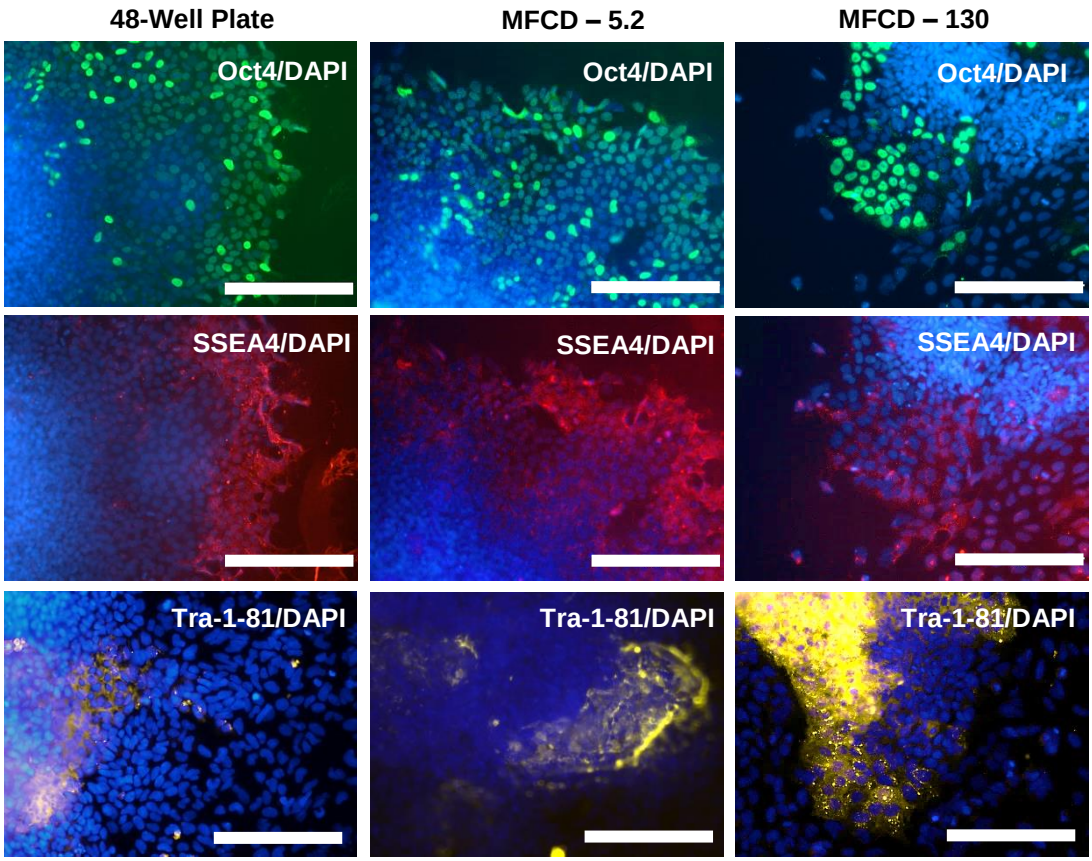

Figure 5.12 Downregulation of Pluripotency Markers Oct4, SSEA4 and Tra-1-81 in hiPSCs During Retinal Differentiation.

Immunocytochemical staining of pluripotency markers as a visual confirmation of the differentiation progress after 5 days of the perfusion culture across all culture devices. Most of the pluripotency markers were expressed at the periphery of the EBs. Secondary antibodies used Alexa 488 (Oct4), Alexa 594 (SSEA4) and Alexa 532 (Tra-1-81). Scale bar represents 200 µm.

5.4.2 Expression of Germ Layer Markers

In the next step, expression of early germ layer markers was analysed to observe effect of perfusion on differentiation lineage of the hiPSCs. To do this we analysed expression of Brachyury (a mesoderm marker), Sox17 (an early endoderm marker) and Nestin (a neuroectoderm marker). The ectoderm develops into the surface ectoderm, neural crest, and the neural tube. The neural tube of the ectoderm develops into, brain, spinal cord, posterior pituitary, motor neurons and retina. Retinal differentiation is part of ectoderm layer and develops along the rest of the central nervous system initially. (Heavner et al., 2012)

Gene expression analysis of these markers on days 5, 10 and 21 showed an initial increase in the expression of Brachyury and Sox17 up to day 5 in all three culture devices and then followed by downregulation for the rest of the culture. It was interesting to note that Brachyury's expression in MFCD with higher flow rate of 130 µL/h, was significantly higher ($p<0.05$) on day 21 compared to the other cultures. On the other hand, Sox17 showed significantly higher expression ($p<0.05$) in MFCD with lower flow rate of 5.2 µL/h at the same time-point. Significant expression of the mesodermal and endodermal markers at the late stages of retinal differentiation may have a less significant effect on the homogeneity of the culture. However, since expression of both markers are undesirable for retinal differentiation, further investigation is required to establish a flow rate/regime that could mitigate expression of such unwanted markers.

Nestin is the marker for CNS progenitor cells and plays an important role in structural organization of the cells during early development acting as the intermediate filaments. During differentiation, Nestin is downregulated and instead is replaced by the lineage specific intermediate filaments. (Michalczyk et al., 2005) The qPCR analysis of Nestin showed continuous increase in expression during the culture. Overall, it increased 2.2 folds for the MFCD with lower flow rate, 4.8 folds for MFCD with higher flow rate and 6.6 folds for the control culture on day 21. (Fig 5.13 C) There was no significant difference between the control culture and the perfused ones. Figure 5.14 shows immunocytochemical staining for positive expression of this gene on day 5 across different culture vessels.

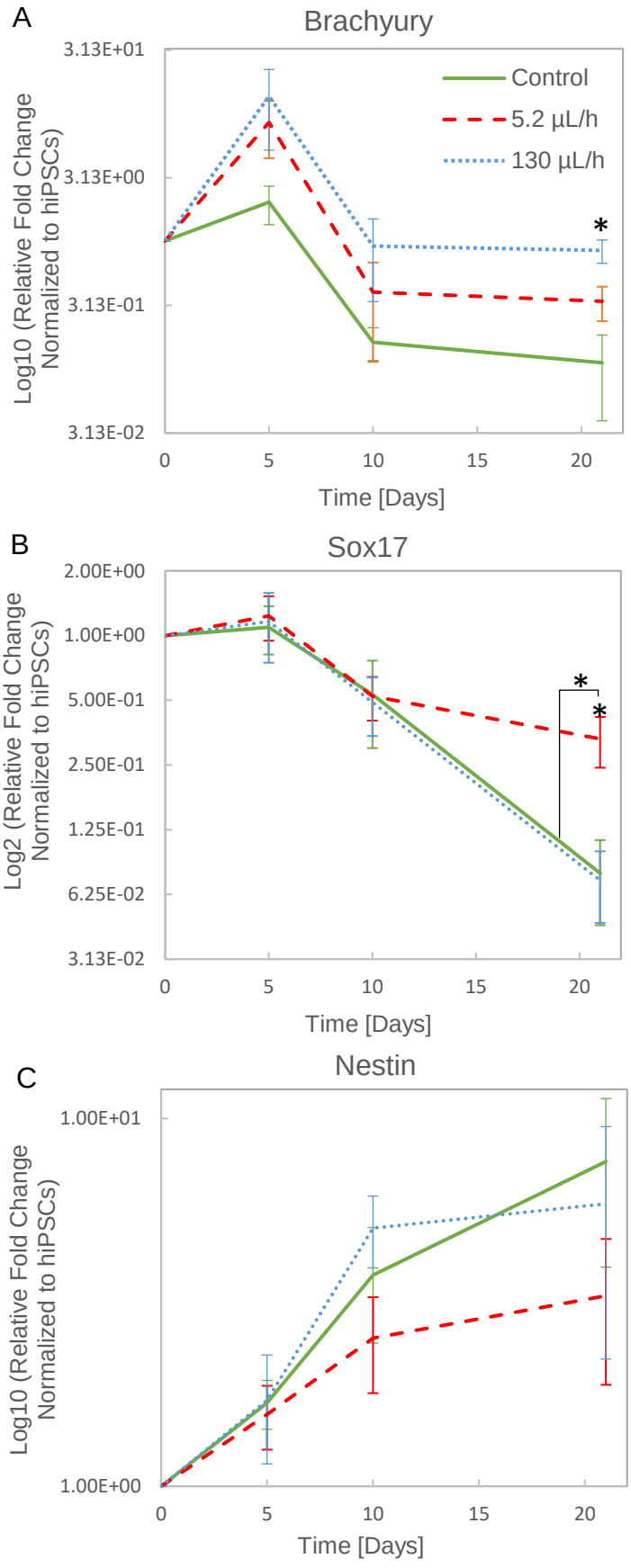

Figure 5.13 Expression of the Germ-layer Markers, Brachyury, Sox17 and Nestin During Retinal Differentiation of hiPSCs.

*(A) Expression of Brachyury (mesoderm) on days 5, 10 and 21, showing upregulation of this marker on day 5 across the different culture devices compared to the hiPSCs. On day 10, expression of this mesodermal marker was downregulated and remained the same up to day 21. Expression of this marker was significantly higher ($p<0.05$) than the control culture on day 21, indicating the negative effects of the fluid flow in this culture device. (B) Shows expression of the Sox17 (endoderm) over the course of differentiation culture. Generally, Sox17 was downregulated throughout the culture across different formats. However, on day 21, expression of this marker was significantly different than the other culture devices ($p<0.05$). (C) Shows upregulation of Nestin (ectoderm) throughout the differentiation cultures. There was no significant difference between the culture formats. Error bars represent one SEM about the mean of 3 independent data points (n=3). A repeated measures ANOVA test was used to indicate a significant difference in the expression of each gene between the perfused cultures and the static control culture, at each time point: *$p<0.05$. To establish exactly which conditions were significantly different from each other, a Tukey's post-test was applied.*

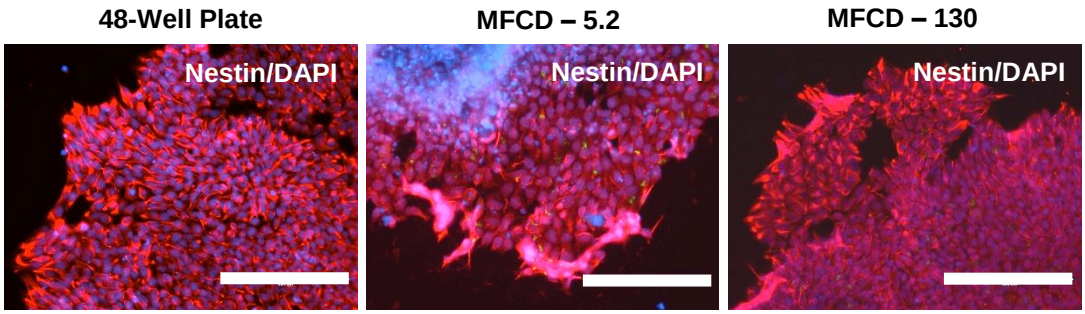

Figure 5.14 Expression Nestin on Day 5 of Retinal Differentiation of hiPSCs Across Different Culture Devices.

Shows positive expression of Nestin, an ectodermal marker on day 5 of the culture. Nestin is an intermediate filament that plays a key role in structural organisation during the early developmental stages. Secondary antibodies used Alexa 594 (Nestin). Scale bar represents 200 µm.

5.4.3 Expression of the Eye-Field Transcription Factors

As explained in chapter 1, eye-field transcription factors (EFTFs) are composed of a number of genes that form a network for regulation of the eye development in vertebrates. The EFTFs regulate the intrinsic and extrinsic cell signalling pathways that restructures the optic vesicle along its axes. (Tétreault et al., 2008) Among the network of EFTFs, we analysed the cultures for Otx2, Pax6, Lhx2 and Six6 on days 5, 10 and 21 to study effects of steady-state concentration of soluble factors on expression of these markers.

Otx2 expression on day 5 was upregulated in the control culture, whereas its expression was downregulated in both perfused devices. We observed the highest expression of the Otx2 on day 10 across all cultures, prior to its downregulation again on day 21. There was no significant difference in expression of Otx2 in any of the time points. (Fig. 5.15 A) Otx2 is one of the early retinal progenitor markers that is required in the anterior structure

development, however it will be downregulated at later stages for eye-field specification. Co-expression of Otx2 along with Sox2, induces expression of Rax in the eye-field. Rax is a key marker in upregulation of the EFTFs such as Pax6, and Lhx2 and hence coordination of the eye-field formation. (Andreazzoli et al., 1999; Zuber et al., 2003; Danno et al., 2008)

Pax6 expression was highest on day 5 in the MFCD with lower flowrate of 5.2 µL/h ($p<0.05$), 4.5 fold higher compared to the control culture and 6 folds higher compared to the other MFCD. Expression of this marker increased in all formats on day 10 with no significant difference from each other and on day 21, MFCD with flow rate of 130 µL/h showed 2.7 times lower expression of this marker than the control culture ($p<0.05$). (Fig. 5.15 B)

Almost all the multipotent retinal progenitor cells, post-mitotic amacrine and horizontal cells express Pax6. (Brzezinski et al., 2011) Pax6 expression along with Lhx2, also promotes expression of Six6, which is the marker expressed in differentiating neural retina. (Tétreault et al., 2008) In humans with mutations affecting Pax6, often show complications such as aniridia, a condition resulted from malformation of the iris, and in some occasion result in microphthalmia, corneal cataracts, and macular and foveal hypoplasia. (Heavner et al., 2012)

Lhx2 showed steady increase in expression throughout the cultures with no significant difference in expression between all three formats. Overall, MFCD with higher flow rate showed on average of higher expression of this marker by 3.7 times on day 5, 2.9 times on day 10 and 1.6 times higher than the control culture. (Fig. 5.15 C) Lhx2 expression is often linked with expression

of Pax6 and their expression are equally important in development of the eye. (Porter et al., 1997) In studies that Lhx2 was inactivated conditionally the optic vesicle development was stopped prior to optic cup formation. However, the expression of other EFTFs such as Pax6, Rax, and Six3 continued in the optic vesicle. (Hägglund et al., 2011)

Expression of Six6 showed upregulation of this marker across devices on day 5. However, while both control culture and MFCD with lower flow rate continued to increase on days 10 and 21, expression of this marker in MFCD with higher flow rate, slowed on day 10 and plateaued afterward. The average expression of this marker in MFCD with higher flow rate was significantly lower ($p<0.05$) than the other MFCD on day 21. The only culture device that showed continuous increase in expression up to day 21 was the MFCD with lower flow rate, with final expression of 3.37 times higher than the control culture and 27.6 times higher than the MFCD with higher flow rate. (Fig. 5.15 D) Six6 is a retinal and optic cup determinant factor during the eye-field development, and mutations that affect this gene often result in anophthalmia. (Heavner et al., 2012) Figure 5.16 confirms positive expression of markers Otx2 and Pax6 on day 10 across all devices.

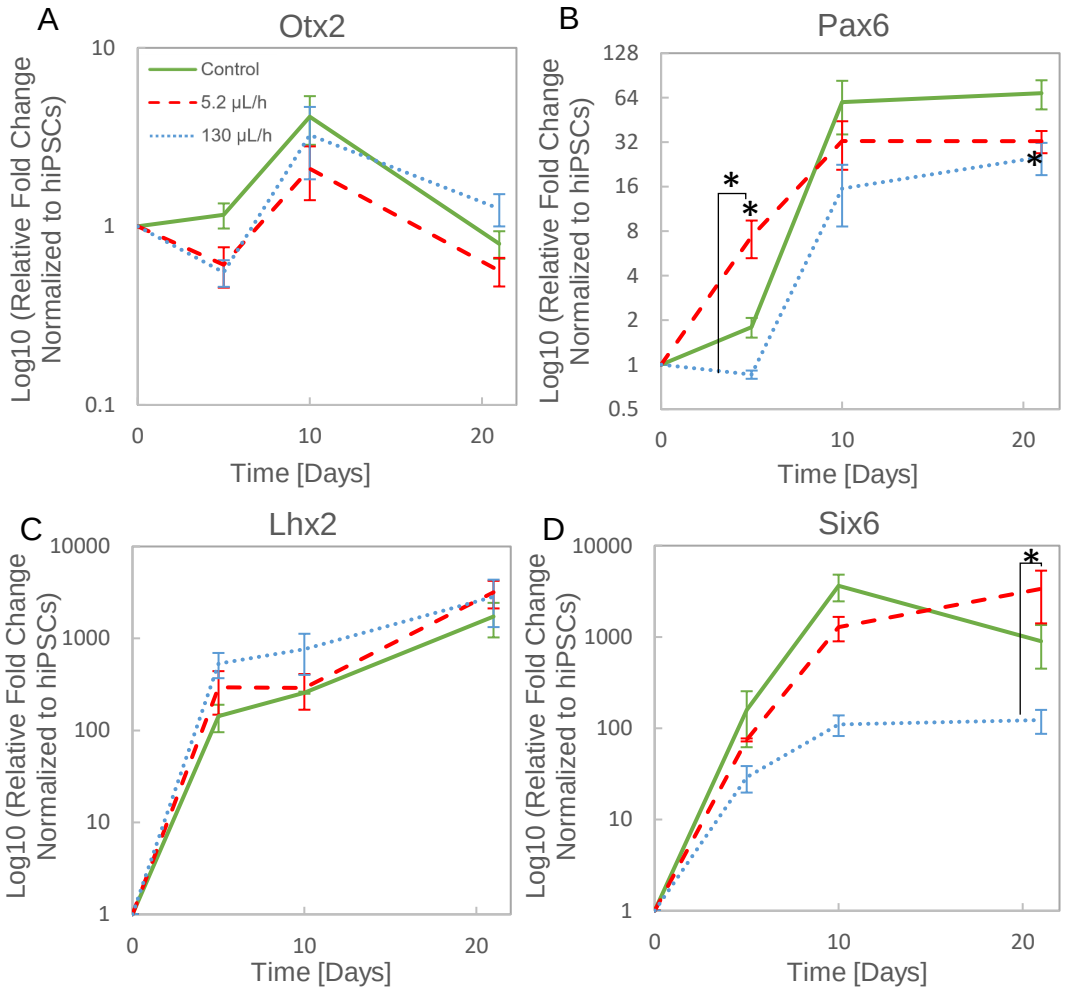

Figure 5.15 Expression of Otx2, Pax6, Lhx2 and Six6 in All Culture Formats During Retinal Differentiation of hiPSCs.

*(A) Shows expression of Otx2 during the differentiation process across the culture devices. Generally, there was upregulation of this marker on day 10 in different culture formats with no significant difference comparatively. (B) Pax6 expression was significantly higher ($p<0.05$) in MFCD with lower flow rate compared to the other MFCD and the control culture on day 5. Expression of this marker peaked on day 10 across different culture vessels and remained the same for the rest of the differentiation culture. MFCD with higher flow rate showed significantly lower ($p<0.05$) expression of this marker compared to the control culture on day 21. (C) Shows expression of Lhx2 across the culture formats during differentiation. All cultures showed steady increase in expression of this marker during the 21 days differentiation culture. However, both perfused MFCD cultures showed higher expression of this marker on average compared to the control culture. (D) qPCR analysis of the Six6 expression revealed increased expression of this marker up to day 10 across all culture formats. The MFCD with higher flow rate and the control culture showed expression of Six6 plateaued between day 10 and 21. Whereas, the MFCD with lower flow rate continued to increase in expression of this marker, where it was significantly higher ($p<0.05$) than the other MFCD on day 21. Error bars represent one SEM about the mean of 3 independent data points ($n=3$). A repeated measures ANOVA test was used to indicate a significant difference in the expression of each gene between the perfused cultures and the static control culture, at each time point: *$p<0.05$. To establish exactly which conditions were significantly different from each other, a Tukey's post-test was applied.*

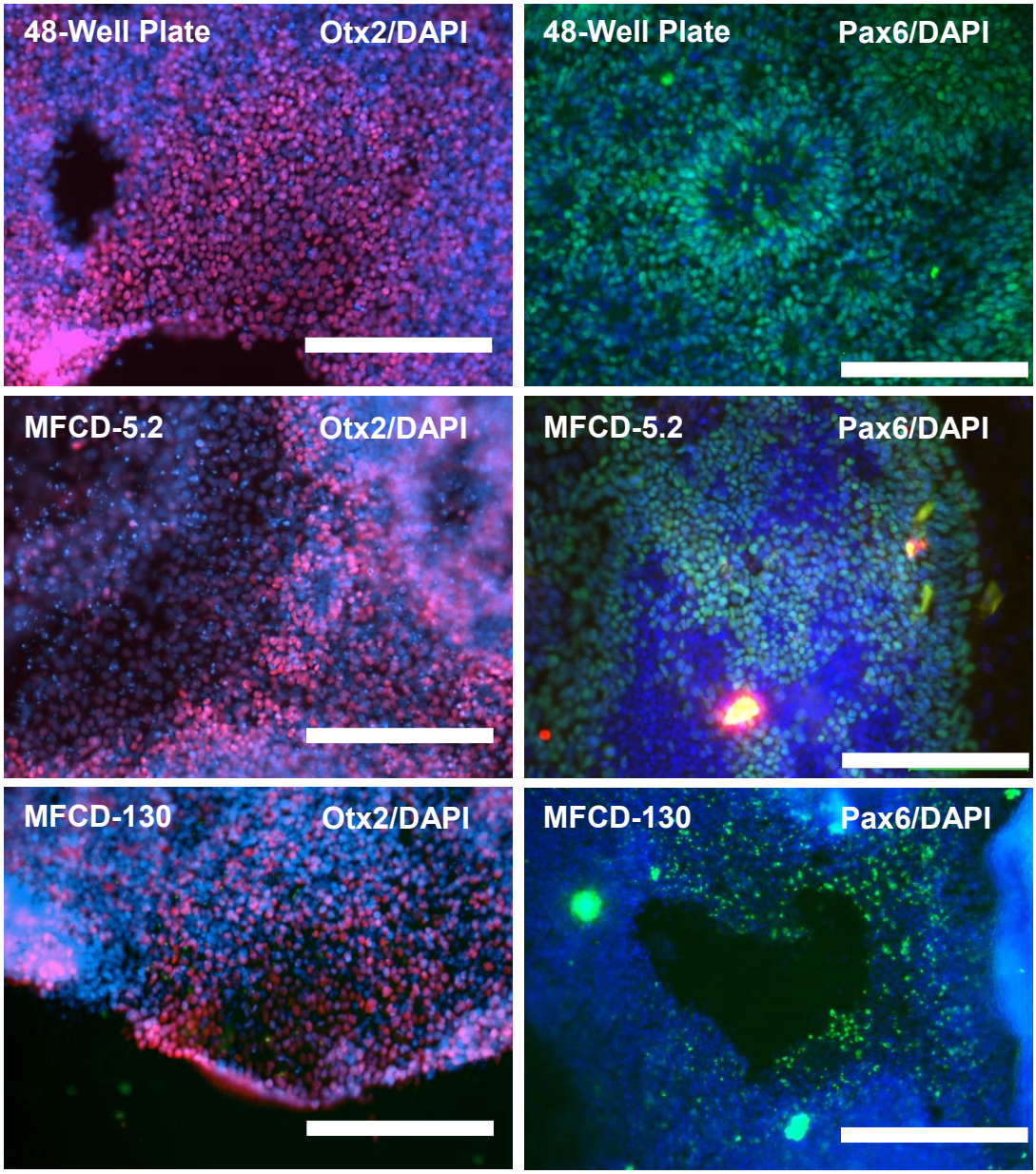

Figure 5.16 Expression of Otx2 and Pax6 in Control and Perfused Cultures on Day 10 of Retinal Differentiation of hiPSCs.

Immunocytochemical staining of Otx2 and Pax6 on day 10 of the culture, confirming expression of these markers qualitatively across different culture vessels. Otx2 expression along with Rax, induces the expression of EFTFs including Pax6, hence assisting in development and specification of the eye-field. Secondary antibodies used Alexa 488 (Pax6), and Alexa 555 (Otx2). Scale bar represents 200 µm.

5.4.4 Expression of Optic Vesicle Marker Vsx2/Chx10

Vsx2/Chx10 is a transcription factor associated with the formation of retinal stem cells capable of differentiating into retinal neurons and it is required for development of retinal precursor cells, retinal progenitor cells and bipolar cells (an interneuron in the retinal inner nuclear layer). (Katoh et al., 2010) Mutations affecting this gene, resulted in microphthalmia and abnormalities in the peripheral structures such as the ciliary body. (Rowan et al., 2004) Development of cells in the optic vesicle (OV) branches to two possible lineages, neuroretinal progenitors that express Vsx2/Chx10, or retinal pigment epithelium (RPE) progenitors, which express marker Mitf. It has been discovered that Vsx2/Chx10 expression has an indirect relationship with expression of Mitf i.e. expression of Vsx2/Chx10 downregulates the expression of Mitf. Therefore, preventing formation of the RPE cells. (Horsford et al., 2004).

Gene expression analysis of this marker in perfused cultures showed a sharp increase in its expression on day 5 of the differentiation culture in both MFCDs compared to the 48-well control. The MFCD with lower flowrate of 5.2 µL/h showed 400 times higher expression than the control culture ($p<0.01$). Expression of this marker was also significantly higher than the MFCD with higher flow rate of 130 µL/h ($p<0.01$). The highest expression of this marker on day 10 observed in the MFCD with higher flow rate with expression of 1.8 $x10^5$ folds relative to the hiPSCs. Expression of Vsx2/Chx10 downregulated in MFCD with higher flow rate on day 21, but continued to increase for both MFCD with lower flow rate and the control culture reaching values of $1.87x10^5$

and 1.5x10^5 respectively. There was no significant difference between the cultures in expression of Vsx2/Chx10 on 10 and 21 days. In morphological studies, we observed formation of polygonal cells in MFCD with lower flow rate. As explained earlier high expression of the Vsx2/Chx10 in RPE population will result in lack of pigmentation in these cells. (Fig. 5.17) Figure 5.18 shows positive expression of this marker across the culture devices on day 10.

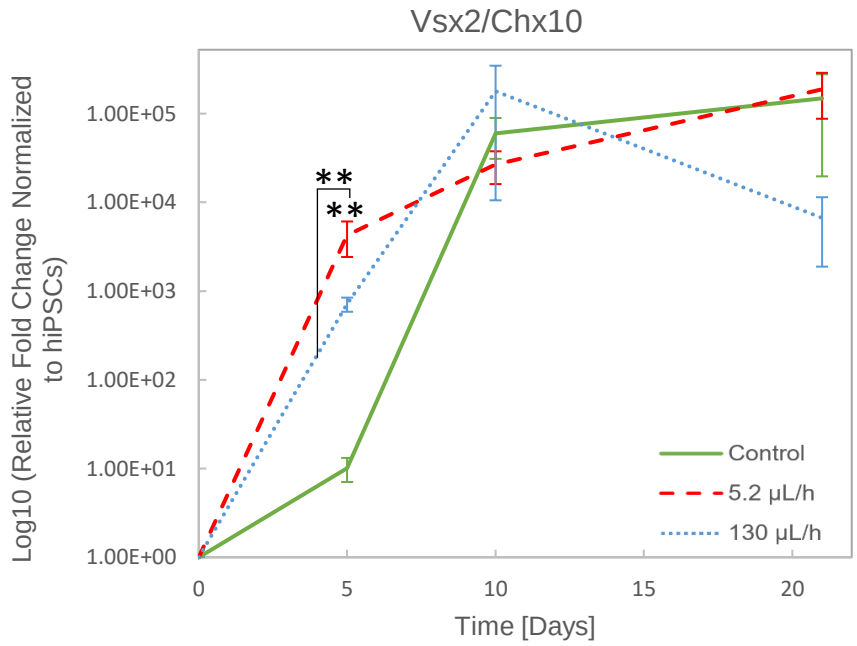

Figure 5.17 Gene Expression Analysis of Vsx2/Chx10 in Control and Perfused Cultures During Retinal Differentiation of hiPSCs.

*Vsx2/Chx10 is a key marker in retinal progenitor cells and promotes the expression of Crx and Nrl, hence development of retinal neurons. Both perfused cultures showed significantly higher ($p<0.01$) expression of this marker on day 5 compared to the control culture. Moreover, expression of VSx2/Chx10 in MFCD with lower flow rate was also significantly higher ($p<0.01$) than the other MFCD. Expression of this marker reached its peak for the MFCD with higher flow rate on day 10. However, control culture and MFCD with lower flow rate showed continued increase in expression of this marker up to day 21. Error bars represent one SEM about the mean of 3 independent data points (n=3). A repeated measures ANOVA test was used to indicate a significant difference in the expression of each gene between the perfused cultures and the static control culture, at each time point: *$p<0.05$; **$p<0.01$. To establish exactly which conditions were significantly different from each other, a Tukey's post-test was applied.*

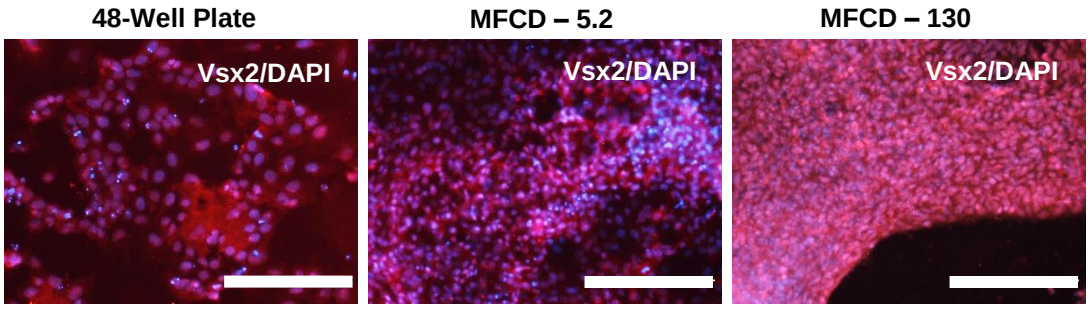

Figure 5.18 Expression of the Vsx2 in Control and Perfused Cultures on Day 10 of Retinal Differentiation of hiPSCs.

Showing positive expression of the marker Vsx2 across all culture devices on day 10 of the culture. Vxs2/Chx10 expression plays a determining factor in differentiation of optic vesicle cells toward retinal progenitor cells by supressing the expression of the RPE cells Mitf. Secondary antibodies used Alexa 568 (Vsx2). Scale bar represents 200 µm.

5.4.5 Expression of Photoreceptor Precursor Markers

The qPCR analysis of the cultures showed that expression of Crx was significantly higher (26.5 times) in the MFCD with lower flow rate when compared with 48-well controls ($p<0.05$) on day 5. Similar to expression of Vsx2/Chx10, expression of this marker continued to rise on day 10 with no significant difference in expression levels among the culture devices. On day 21, there was significantly more expression of Crx at the MFCD with higher flowrate of 130 µL/h ($p<0.05$) compared to the MFCD with lower flow rate and the control culture. The expression of Crx at this time-point was 7.4 times higher than the MFCD with lower flow rate and 40 time higher than the control culture. Overall, both MFCDs outperformed the standard 48-well static cultures at this time point. (Fig. 5.19 A)

The qPCR analysis of Nrl revealed that this marker was expressed the most in MFCD with lower flow rate on day 10. Compared to other devices, expression of this marker was significantly ($p<0.01$) higher than the other

MFCD (16.2 times) and the control culture (11.5 times). Extended culture in the MFCD at both flowrates was associated with the downregulation of Nrl where there were comparable levels of this key transcription factor in all three culture systems. (Fig. 5.19 B)

Crx and Nrl have previously shown to be key markers for photoreceptor precursors that are capable of translocating into the retina and differentiating into full functional photoreceptors upon transplantation. (Maclaren et al., 2006) Crx has a regulatory function in development of rod and cone photoreceptors. Mutations affecting this gene has shown to lead to inactive rod and cone photoreceptors. (Furukawa et al., 2000)

It was reported that Otx2 expression will trans-activates the expression of Crx and Crx expression regulates the expression of Rhodopsin. (Nishida et al., 2003) Nrl plays a key role in rod photoreceptor development by acting as a 'molecular switch' in directing rod-specific genes. Moreover, Nrl was found to inhibit the formation of S-cones pathway by activating Nr2e3 expression and also assists in regulation of Rhodopsin (Rehemtulla et al. 1996; Mears et al., 2001)

Finally, the expression of Rhodopsin, a receptor protein found on the surface of rod cells was assayed. (Reeves et al., 2002) Rhodopsin is the latest marker of differentiation used to characterise the MFCD. At the end of the culture period, expression of Rhodopsin was 2 times higher than the control culture and 11.3 times higher than MFCD with lower flow rate. Cells differentiated under the higher flowrates expressed significantly ($p<0.05$) higher levels of

expression than the slower flow rate MFCD, indicating that there may be a minimum flowrate needed to effectively differentiate hiPSCs into mature photoreceptor cells. (Fig. 5.19 C)

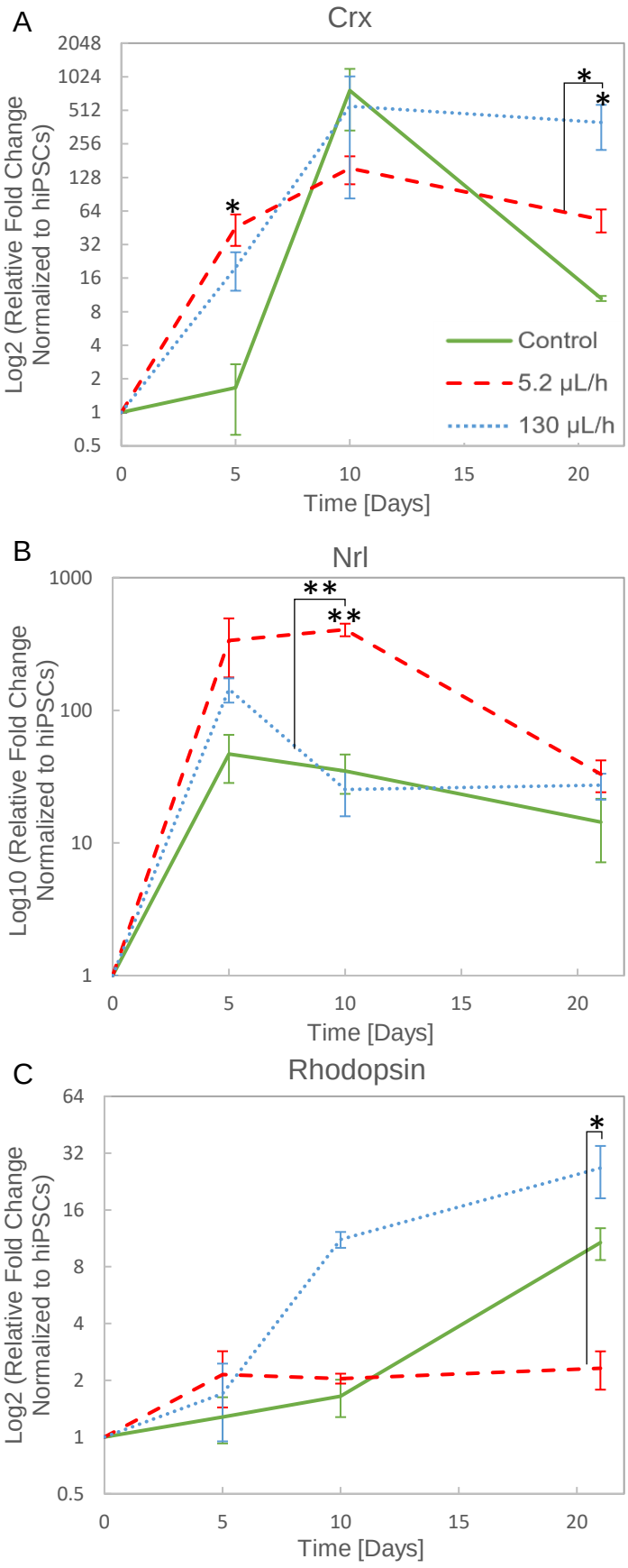

Figure 5.19 Gene Expression of Crx, Nrl and Rhodopsin During Retinal Differentiation of hiPSCs.

*(A) Shows expression of the retinal precursor marker Crx. Both perfused devices showed higher expression of this marker on day 5 and 21. MFCD with lower flow rate showed significantly higher expression of this marker on day 5 compared to the control culture. Whereas, MFCD with higher flow rate showed significantly higher expression of this marker on day 21 compared to the control culture and other MFCD. (B) Shows expression of the rod specific marker Nrl. Expression of this marker was highest in MFCD with lower flow rate on day 10 of the culture, where it was significantly ($p<0.01$) higher than the control and other MFCD. Expression of this marker was downregulated after day 10, where it was at the similar levels across all three culture formats. (C) Shows expression of Rhodopsin during the differentiation culture. The highest expression of this marker was observed on day 21 in MFCD with higher flow rate, where the expression was significantly higher than the other MFCD. Error bars represent one SEM about the mean of 3 independent data points (n=3). A repeated measures ANOVA test was used to indicate a significant difference in the expression of each gene between the perfused cultures and the static control culture, at each time point: *$p<0.05$; **$p<0.01$. To establish exactly which conditions were significantly different from each other, a Tukey's post-test was applied.*

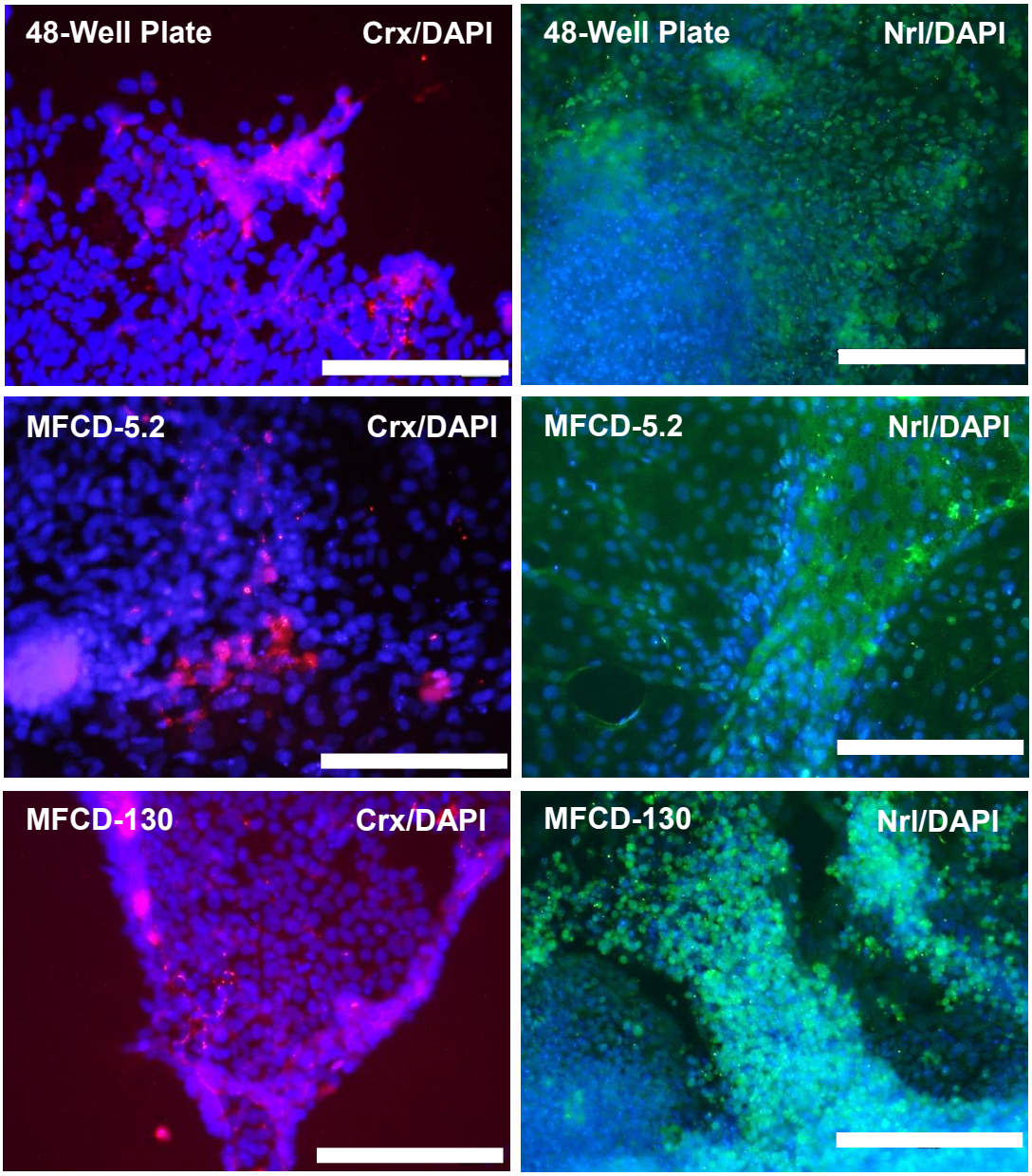

Figure 5.20 Expression of Crx and Nrl in Control and Perfused Cultures on Day 21 of Retinal Differentiation of hiPSCs.

Showing immunocytochemical staining images for positive expression of the retinal precursor markers Crx and Nrl across all culture devices on day 21. Crx is expressed in both rod and cone photoreceptor and Nrl is a rod specific marker. Both genes play a key role in development of the photoreceptors. Clinical studies on rat models has shown that retinal progenitor cells that are expressing both Crx and Nrl have a better chance of integrating into the host retinal after transplantation. Secondary antibodies used Alexa 488 (Nrl) and Alexa 555 (Crx). Scale bar represents 200 µm.

5.5 Summary

Prior to performing perfusion experiments number of normalisation steps were considered for accurate gene expression analysis of the samples. In chapter 3, housekeeping genes that had the lowest M-value (highest stability) in hiPSCs and the differentiated samples were identified. In this chapter, further normalisation steps were carried out in obtaining the same sample size from control and MFCDs. Following this step, number of cells in MFCD and the 48-well plate were compared, and results showed comparable sample sizes in both cultures. Next, total RNA from all samples were extracted. To minimise effect of concentration spread between the samples total RNA concentrations were normalised to one sample of hiPSCs. Next, due to large number of low concentration of the RNA samples (<100ng/mL), the whole genome of the samples was amplified prior to cDNA step and used equal concentration of the cDNA for qPCR analysis.

In morphological studies of the cultures, expansion of the EBs, common and exclusive features appeared at each time point were analysed. Overall, EBs expanded in the same fashion and rate across the culture formats at the initial 5 days of the differentiation cultures. Some of the common features appeared in each culture device were aggregation of the EBs in the 48-well plates that lead to formation of dense, complex 3D structures. Monolayer population of the cells in the MFCD with lower flow rate and multi-layer but uniform expansion of the cells in the MFCD with higher flow rate. Among exclusive features appeared in each culture formats, were delayed formation of the neural rosettes and appearance of the polygonal RPE like cells in MFCD with

lower flow rate. Taking gene expression analysis into account, overexpression of marker Vsx2/Chx10 can provide an answer for lack of pigmentation in the RPE like cells. (Rowan et al., 2004) The MFCD with higher flow rate did not show appearance of neural rosettes or RPE like cells. Showing that formation of the unique structures in MFCD with lower flow rate are dependent on the flow rate.

However, differences in morphology did not necessarily reflected the same features in gene expression in these cultures. For instance, the MFCD with the lower flow rate of 5.2 µL/h showed higher expression of Pax6 (4.5 times, $p<0.05$), Vsx2/Chx10 (426 times, $p<0.01$), Crx (26.5 times, $p<0.05$) and Nrl (7.2 times) on day 5 of the culture compared to the control. Moreover, Nrl showed significantly higher expression (12 times, $p<0.01$) in this culture on day 10 compared to the control and MFCD with higher flow rate of 130µL/h. In MFCD with higher flow rate, steady and continuous increase of Lhx2 (3.7 times), Vsx2/Chx10 (71 times) and Crx (11.9 time) was observed compared to the control culture on day 5. On day 21, significantly higher expression of Crx (40 time, $p<0.05$) and Rhodopsin (11 times, $p<0.05$) was observed compared to the control culture. Table 5-1, provides an overview of the genes expression across different culture devices throughout the culture.

Overall, significantly higher expression of Vsx2/Chx10 on day 5, Nrl on day 10 and Crx on days 5 and 21 was observed in both perfused cultures compared to the control culture. Boucherie *et al.* work on retinal differentiation of hESCs reported successful formation of retinal precursors by day 10 while used Matrigel™ and supplemented the culture with N2 and B27. In their studies

increased population of the Crx and Nrl positive cells were due to incubation with Matrigel™. (Boucherie et al., 2012) Same time-shifts in expression of these key markers were observed in our control cultures. Moreover, significantly higher expression of these markers in perfused MFCDs show impact of steady-state of soluble factors on retinal differentiation of hiPSCs. Finally, the flow rate and time dependent higher expression of the key retinal progenitor marker suggests that, a marker specific production can be achieved by adjusting the perfusion time and the respective flow rate for highest production yield, reducing the associated production and development costs.

Table 5-1 Overview of Expression of Different Markers Throughout Retinal Differentiation of hiPSCs in Control and Perfused Cultures.

Table below provides average expression of genes at different time-points across control and perfused cultures. Boxes highlighted with colour green indicate higher expression, and boxes in yellow, indicate lower expression of the marker compared to the 48-well plate control culture. Boxes with red borders indicate statistically significant expression of the marker compared to control at the given device and time-point.

Time	5 Days			10 Days			21 Days		
Device / Gene	48wp	5.2 µL/h	130 µL/h	48wp	5.2 µL/h	130 µL/h	48wp	5.2 µL/h	130 µL/h
Oct4	0.29	0.60	0.33	0.13	0.04	0.11	0.00	0.01	0.01
Nanog	0.20	0.29	0.24	0.06	0.04	0.17	0.04	0.01	0.03
Sox2	0.51	0.57	0.55	1.50	0.57	0.90	2.28	0.63	2.75
Sox17	1.10	1.24	1.16	0.53	0.52	0.48	0.08	0.33	0.07
Brachyury	2.01	8.47	13.60	0.16	0.40	0.91	0.11	0.33	0.84
Nestin	1.68	1.57	1.71	3.75	2.53	5.03	7.63	3.30	5.86
Otx2	1.16	0.61	0.55	4.11	2.10	3.25	0.80	0.56	1.26
Pax6	1.80	7.35	0.85	59.70	32.60	15.56	68.65	32.52	25.41
Lhx2	142.94	298.80	532.77	257.21	289.30	763.11	$1.73x10^3$	$3.18x10^3$	$2.84x10^3$
Six6	158.01	74.47	29.10	$3.63x10^3$	$1.28x10^3$	110.13	900.08	$3.37x10^3$	122.80
Vsx2/Chx10	10.12	$4.26x10^3$	714.28	$60.10x10^3$	$26.83x10^3$	$178.60x10^3$	$148.60x10^3$	$187.76x10^3$	$6.66x10^3$
Crx	1.67	45.38	19.82	770.78	154.60	557.02	10.52	53.58	399.04
Nrl	46.85	335.35	144.28	34.95	405.92	25.31	14.33	33.03	27.25
Rhodopsin	1.28	2.14	1.70	1.64	2.04	11.15	10.74	2.31	26.68

Chapter 6 Final Conclusions and Future Work

6.1 Conclusions

Advances made in therapeutic applications of hiPSCs and development of protocols for differentiating these cells, has brought regenerative medicine closer to fulfil what it has promised in the first place. Lack of complete understanding of intrinsic cellular processes, precise control of large number of operational parameters and high costs of process development, delay materialisation of readily available stem cell therapies. Microfluidic cell culture devices have shown great promise in controlling operational parameters in an accurately defined range. A microfluidic culture device designed for regenerative medicine process development has been developed by Szita group and was used in this work for retinal differentiation of hiPSCs. (Reichen et al., 2012)

The aim of this thesis was to first, find a flow rate for creating steady-state concentration of key growth factors in retinal differentiation of hiPSCs and second, to investigate upregulation of retinal progenitor (Pax6, Lhx2, Six6 and VSX2/Chx10) and precursor markers (Crx and Nrl) as a result of steady-state conditions.

In addressing the first aim of the thesis, degradation and consumption of key growth factors used in retinal differentiation of hiPSCs were carried out. Degradation study of the growth factors showed that in the first 8 hours only 48% of the initial stock of DKK-1 remained. bFGF and Noggin degradation showed 69% and 46% drop in their initial concentrations within the first 24

hours and IGF-1 showed no degradation at 37°C in the first 96 hours (Fig 3.16 A-D). In regards to consumption of these growth factors in the first 96 h, Noggin, IGF-1 and DKK-1 showed the highest demand by the cells respectively. bFGF on the other hand, showed production of this growth factor by the cells. Based on cellular demands and stability of the growth factors, the ideal flow rate for creating the steady-state concentration of soluble factors, would deliver Noggin and DKK-1 to the cells during differentiation culture.

The second objective of the thesis was to establish critical perfusion rate boundaries for creating steady-state concentration of soluble factors. To establish the perfusion rate boundaries, previous studies on effects of shear stress on adherent cell cultures were used for selecting the upper limits. Shear rate of 1.6×10^{-3} Pa was chosen as the upper boundary since it has shown to be the lowest shear rate for inducing a gene expression response in mESCs. (Toh et al., 2011). Flow rate for the lower boundary was selected based on minimum exchange rate required in the MFCD and calculated at 2.5 µL/h. (Fig. 4.1) To find critical perfusion rate for steady-state condition, the Pe number was used to arrive at a flow rate of 130 µL/h. At such flow rate, all molecules with a molecular weight of 20 kDa and higher are delivered to the cells by fluid flow, which includes molecules such as DKK-1, Noggin, BSA and transferrin. This method has shown to be effective in creating a steady-state concentration as DKK-1 concentration measurements in MFCD showed a steadier concentration of this growth factor in MFCD compared to the 48-well plate control culture.

The third objective of the thesis was to assess suitability of the MFCD for long-term retinal differentiation culture and make the necessary changes accordingly. Series of the preliminary cell culture experiments such as MEF and their co-culture with hiPSCs showed suitability of the MFCD for adherent 2D cultures. However, in 3D EB cultures, there were differences between the control and MFCD in regard to EB expansion rate. Further investigation into the cultures revealed that, the one-hour incubation time with Matrigel™ prior to EB cultures prohibited EBs expansion rate compared with the control culture. Shortening this incubation time to 15 minutes, proved to resolve the issue and provide comparable expansion rate of the EB in MFCD.

The last objective of the thesis was to evaluate effects of the steady-state conditions on expression of key retinal progenitor and precursor markers. Morphological studies of the perfused cultures during 5, 10 and 21 days showed formation of the similar key 3D structures such as neural rosettes and neuroepithelium in MFCD with lower flow rate and the control culture. Delayed appearance of the neural rosettes in this MFCD indicated the fluid flow related nature of these 3D formations. Moreover, appearance of the RPE like structures in MFCD with lower flow rate, showed more heterogeneity present at this flow rate compared to the other devices. Morphological analysis of the cultures in MFCD with higher flow rate, showed more uniform multilayer expansion of the EBs, indicating effects of fluid flow on wash-out of the waste molecules from the culture area. Simple observations such as the medium colour in the outlet of both MFCDs, showed the device with faster flow rate was more efficient in maintaining a uniform pH.

Gene expression analysis revealed that effects of perfusion on expression of key retinal markers does not provide upregulation of all the retinal progenitor and precursor markers at the same time. Overall, the MFCD with higher flow rate showed statistically higher expression of markers such as Crx (40 time compared to control, $p<0.05$) and Rhodopsin (11.3 time compared to lower MFCD, $p<0.05$) on day 21, which indicates its suitability for production of retinal precursors. The MFCD with lower flow rate, showed significantly higher expression of Pax6 (4.5 times, $p<0.05$), Vsx2/Chx10 (426 times, $p<0.01$) and Crx (26.5 times, $p<0.05$) on day 5, Nrl (7.2 times, $p<0.01$) on day 10 and Six6 (3.7 times, $p<0.05$) on day 21. Higher expression of various markers at different time-points in perfused cultures showed that cellular requirements are much more diverse during retinal differentiation. Higher expression of earlier retinal progenitor genes at MFCD with lower flow rate, could suggest that a slower flow rate is more suitable for production of progenitors and as culture proceeds to later stages, the flow rate can be increased to assist maturation steps.

Measurement of DKK-1 concentration during the course of 10-days cultures, showed that there is no need for this growth factor by day 7-8 of the culture. This finding showed that steady-state concentration of the soluble factors must be adapted to the cellular needs during the course of differentiation. Moreover, dynamics of the other growth factors are still unknown and a comprehensive approach is needed to fully understand the cellular requirements of the retinal differentiation culture.

Significantly increased expression of some the markers in perfused cultures, confirmed the stated hypothesis to some extent. However, to fully confirm the thesis hypothesis, a revised protocol of retinal differentiation adapted for perfusion culture must be developed. In which, growth factors can be added separately when they are required by the cells and the flow rate must be adjusted so it delivers them convectively. Therefore, this finding requires longer (21 Days) and expanded (including all growth factors) revision of the first objective of the thesis in mapping out the retinal differentiation dynamics. The boundary conditions obtained for steady-state, can be utilised to adjust the required flow rate. Finally, full repeat of the perfusion cultures using the revised protocol and addition of the flow cytometry as an end-point analysis, can provide a better distinction between static and customised perfusion cultures.

6.2 Future Work

Based on the work carried out in this thesis, the future works can be broken down to two main groups; recommended extensions and improvements in the cell culture experiments and next are the engineering improvements in use of the microfluidic culture device.

Immediate extension of the cell culture experiments includes repeat of the perfusion experiments with a mixed flow rate where lower perfusion is used for the first 10 days and higher flow rate of 130 µL/h for the rest of the differentiation.

On the qualitative data obtained via phase contrast microscopy and immunocytochemical staining, other methods of analysis could have been used to enhance the results. First, is the use of image processing to analyse and quantify spread of the MEFs in the culture flasks. The quantitative results obtained from image analysis could have provided the study with a more accurate measure for comparison between the two MEF densities studied. Moreover, data obtained this way, could have been correlated with the healthy hiPSC colonies for detection of the pluripotency in future cultures. Furthermore, image processing could also have been used in frame-by-frame analysis to map movement of the cells and hence providing a better understanding of how various 3D structures like neural rosettes form at early stages of the retinal differentiation culture.

Immunocytochemical staining in general is a qualitative tool to ensure that expression of the target markers occurred in the right place in cells. However,

immunostaining alone does not provide any quantitative data and use of image processing for detection of a particular marker can indeed assist in making a better use of such data sets. For example, in case of a nuclear marker of interest, the overlay of DAPI with the target marker indicates the correct expression of the marker. Using image analysis could provide a fairly accurate percentage of the marker expressed across a known surface area.

That said, there are some barriers in using image processing that must be overcome to ensure its accuracy. Among such are quality of the phase contrast images compared to the immunofluorescence images. The phase contrast images often have higher level of noise, presence of halo effects around the objects and shade-off effects. Moreover, methods must be developed that could adapt to unique requirement of various differentiation cultures and be able to detect common patterns as well as anomalies in such cultures. (Jaccard et al., 2014) The other challenge is that differentiation cultures often start with cells in aggregate forms such as EBs and then expand to multi-layered population of the cells during experiment. Using 2D images to monitor cellular behaviour ignores any cellular behaviour taking place in 3D and are incapable of obtaining the full picture of what is taking place within the culture. It must be noted that ongoing monitoring of the cultures using a microscope requires addition of other equipment such as image acquisition software, a controllable platform and gas controlled incubators for maintaining a suitable environment for the cultured cells. Differentiation cultures are often long and online monitoring of such cultures place high and exclusive demands on use of the lab equipments.

The second method that could be used to enhance the qPCR data is flow cytometry. Flow cytometry is an antibody-dependent method that utilises the specificity of antibodies for specific cell markers inside or on the surface of the cells and sorts cells based on their interaction with the light stream. Flow cytometry can provide multiparametric analysis of a heterogeneous cell sample to provide specific cell numbers, size and expression of multiple markers. (Robinson et al., 2004)

Using flow cytometry for retinal differentiation could provide us with specific expression of each marker at different stages of differentiation as well as differentiation yield at the end of 21 days. However, it must be noted that use of a single MFCD with culture area of 0.52 cm^2 does not provide sufficient data to draw a meaningful conclusion from each experiment. Therefore, technical replicates as well as biological replicates are required to successfully obtain sufficient material for analysis and provide a comparable dataset to well-plate cultures.

Using flow cytometry, there are also limitations in number of markers that could be analysed at the same time depending on the number of laser channels imbedded in the flow cytometry machine itself. (Basiji et al., 2007) The latter could add to the number of samples required if multiple markers are studied at the same time. Using the current format of the MFCD it could be very time-consuming and labour intensive to gather similar data as obtained in qPCR to studying two flow rates at the same time. However, if MFCD could be designed in a platform with at least six devices in parallel (each three devices are allocated to one flow rate), sufficient number of samples can be obtained in a

reasonable time frame. It must be noted that in flow cytometry, the information about cellular structures and their morphology is not obtained and perhaps use of other forms of cytometry such as image cytometry can assist in solving the problem by allowing collection of cell imagery along with raw fluorescence data. (McFarlin et al., 2016)

Finally, confocal microscopy could be used to provide an in-depth analysis of the immunocytochemical staining and provide a higher resolution expression of the markers in thick, multi-layered formations of the cells. (Zanacchi et al., 2011) This method perhaps is more useful for analysing cell populations at the end of the differentiation culture on day 21. It was estimated that in some areas of the culture, the thickness of the cells could be over 200µm. Moreover, markers such as Crx and Nrl were found to be expressed more in denser layers of the culture, which is the reason for lower quality of the immunostainings images for these markers. Therefore, confocal microscopy can be used to provide better visualisation of these markers and hence improving culture conditions by understanding the surrounding cells population.

In reducing the number of variabilities available during retinal differentiation culture, use of a feeder free cell line is strongly recommended as it can remove cultural variations and unknown effects of the MEFs on differentiation process. Using other cell lines, also add more credibility in obtaining repeatable results. Another source of possible variability introduced into the culture were the use of Matrigel™ as the ECM. Matrigel™ is made of 60% laminin, 30% collagen IV, 8% entactin and the rest is mix of several growth factors and murine

sarcoma derived products. (Giri et al., 2015) Matrigel™ is used in the original retinal differentiation protocol by Lamba (2006). However, it is known that, there is a batch-to-batch variability in Matrigel™, it also includes complex compositions that makes it hard to provide similar experimental controls and it contains proteins from other species which could makes it impossible to be used in cell therapy applications. (Serban et al., 2008) Therefore, use of other ECM products with simpler content and without animal products can improve the repeatability of the experiments and remove the unknown effects of such materials on the differentiation process.

Next, is expansion of the consumption study of the growth factors Noggin, DKK-1, IGF-1 and bFGF to 21 days to obtain a full consumption profile of the growth factors during the course of differentiation. The 10 days investigation of the DKK-1 concentration in the MFCD revealed that the most demand for this growth factor is in the first 4 days of the culture and the need for this growth factors is non-existent from day 7-8 onward. It would be interesting to expand this study for other growth factors as well. Knowing at which stage of the differentiation process these growth factors are needed will assist in optimising the current retinal differentiation protocols and assists in development of a more economic manufacturing process.

Finally, in cell culture experiments, it would be interesting to repeat differentiation studies using the optimised protocol mentioned above and study the changes made to expression of retinal progenitor markers and the subsequent yield of the differentiation protocol.

Regarding engineering aspects of the project, recommendations can be further broken down into parts associated with, use of computer models for mass transfer, optimisation of the MFCD design and development of an automated MFCD system.

Using data from the consumption and degradation studies, a computer model can be devised to better predict spatial distribution of the growth factors inside the MFCD culture area. Moreover, such models can assist in optimisation of the flow rate boundaries set to create steady-state concentration of soluble factors and possible redesign of microfluidic chip adapted for retinal differentiation culture.

Modular design of the MFCD and lid configuration allowed direct access to culture chamber, which was hugely beneficial in adapting the MFCD for retinal differentiation culture. However, the cell culture surface area shape and geometry made it difficult to provide accurate well-plate controls with the same dimensions. In normalisation steps taken for accurate qPCR analysis, providing the same sample size is one of the initial steps. Having a surface area, between 96 well-plates and 48-well plates, made it difficult to choose the right control for the perfusion cultures. Choosing a control culture smaller/larger than the MFCD, can create a bias for the perfused cultures or alternatively hides the advantages of such devices.

The second changes required in the MFCD design, is the height of the culture chamber. It was reported that EBs with diameter of 200-400 µm were more suitable for ectodermal differentiation. (Van Winkle et al., 2012) In MFCD, EBs

with diameter of 200 µm were the largest size that could be used, due to the medium inlet and culture chamber heights. Redesign of the MFCD in a way that could house larger EBs, can potentially result in higher turnover of the retinal progenitors.

Other recommendations to the MFCD design, include fluidic channels for exclusive delivery of the growth factors in a way that releases growth factors directly into the culture area or in its upstream. This way growth factors do not have to travel through the tubing to reach the culture area, are subject to less degradation and their quantity can be adjusted based on the cellular needs.

This feature naturally leads to development of the fully automated culture platforms, where operational parameters can be monitored and controlled accurately. Use of multiple MFCDs in a single platform allows to study more diverse experimental conditions at the same time. Larger number of replicates can be obtained for end-point analysis and reduces the manual labour. Live monitoring of oxygen concentration in the culture area or the pH at the outlet can be achieved by utilising sensors. Controlling such process parameters in a defined range will be beneficial in studying effects of these soluble factors on retinal differentiation.

Finally, in scaled down cultures such as microfluidics, where biological samples are relatively at smaller quantities, live analysis methods such as online monitoring and characterisation of the culture can track changes taking place in the perfused cultures without the need for invasive end-point analysis. Furthermore, use of live staining tools such as peptide conjugated quantum

dots targeted at specific retinal markers could provide real-time data on key events during the course of differentiation study.

The multi-parametric requirements of differentiation cultures such as retinal differentiation makes it very challenging to adapt it to large-scale production systems. Unfortunately, unlike suspension cultures used for large-scale manufacturing of the other mammalian cells, there are few options currently available for adherent cultures such as hESCs and hiPSCs. (Fernandes et al., 2013) Most of the cell culture systems used include multilayer culture areas such as Cell Factory System™ by Thermo Fisher Scientific or stacked flasks like Millicel HY™ Flasks by Millipore, and HYPERFlasks™, CellStacks™, and CellCubes™ by Corning. However, none of the above systems provide controlled culture condition and monitoring of the cells during production.

Other systems that include use of microcarriers could provide a more feasible transition to large-scale production, however, precise control of culture conditions and increased level of variations in terms of cell adhesion, density variations, formation of large aggregates and their interactions in the culture will add more challenges to such processes. In addition, recovery of the cells from microcarriers and their purification at the end of the differentiation have shown to be very difficult. (Serra et al., 2012; Fernandes et al., 2013) Hollow fibre based bioreactors on the other hand provide fine control over microenvironmental conditions and cells are protected against shear stress. However, they lack monitoring capabilities of the cell cultures and recovery of the cells at the end is very difficult. (Roberst et al., 2012)

Spinner-flasks and rotating wall bioreactors are another option for scale-up of differentiation cultures. Previous studies using cellular aggregates in such systems for expansion and differentiation of PSCs are promising. (Steiner et al., 2010; Serra et al., 2010; Ungrin et al., 2011; Olmer et al., 2012) However, such devices have been used for suspension cultures mostly and their adaptation for adherent cultures such as retinal differentiation will require further studies. Similar to previous culture systems monitoring of the cells is still a challenge in these devices and it is even more difficult to adapt other monitoring systems such as image processing to such systems.

Given the nature of patient-specific therapies for retinal degenerating conditions, scale-out strategies may provide a more appropriate approach to production of these cells. Parallelization of the current MFCD in platforms with custom-made designed parts specific to retinal differentiation protocol can be a more feasible solution. This way, small scale studies, such as the one performed in this work can be validated much easier and require less adaptations for larger production of the retinal progenitor cells.

Chapter 7 Appendices

Appendix 7.1

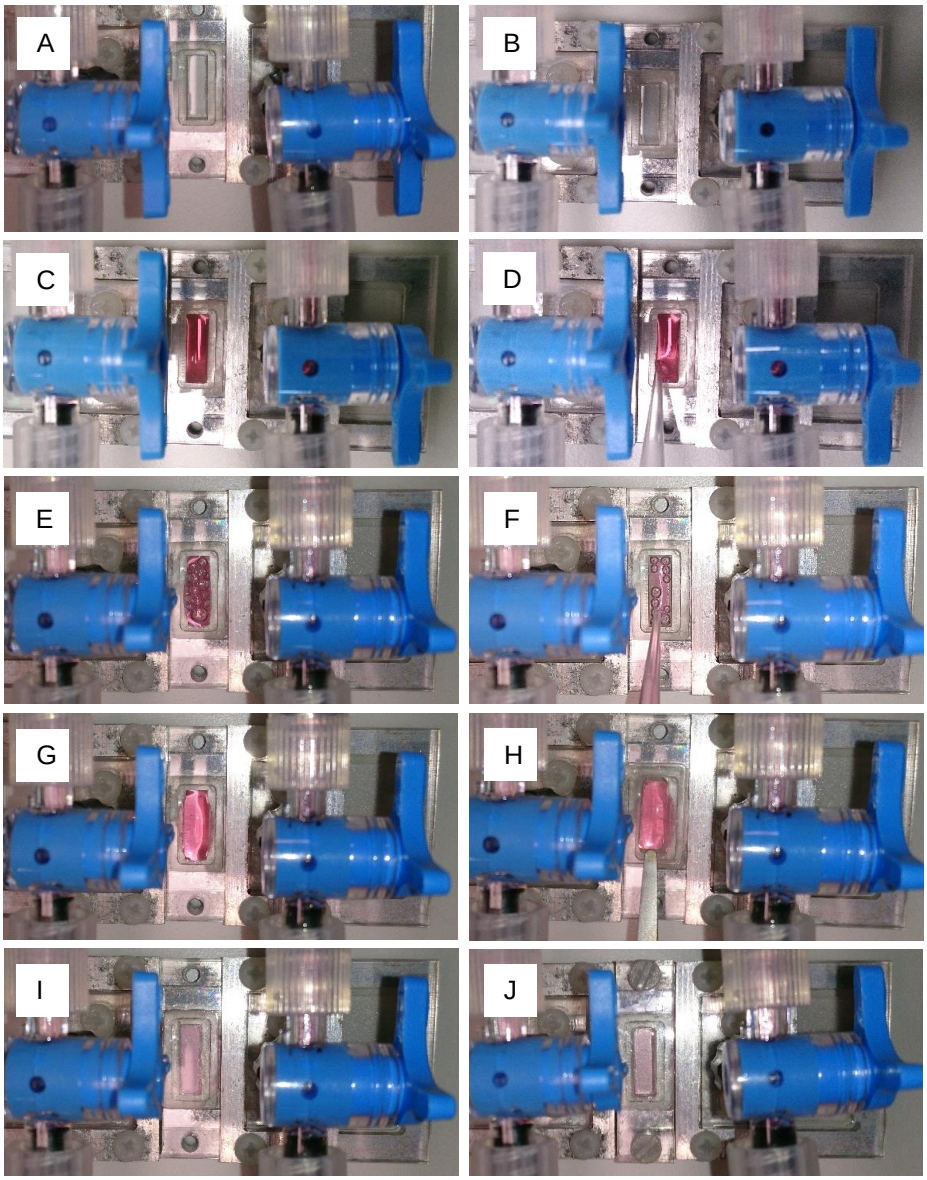

Figure 7.1 Bubble-free Priming of the Microfluidic Culture Device.

(A-B) Priming and bubble removal in the fluidics via the bypass through to the waste bottle. (C-D) Priming of upstream of the MFCD by switching the flow through the inlet. (E-F) Priming of downstream of the MFCD by switching the flow through the outlet. (G-H) Placement of the gas-permeable PDMS lid. (I-J) Placement of the lid cover and full assembly of the lid.

Appendix 7.2

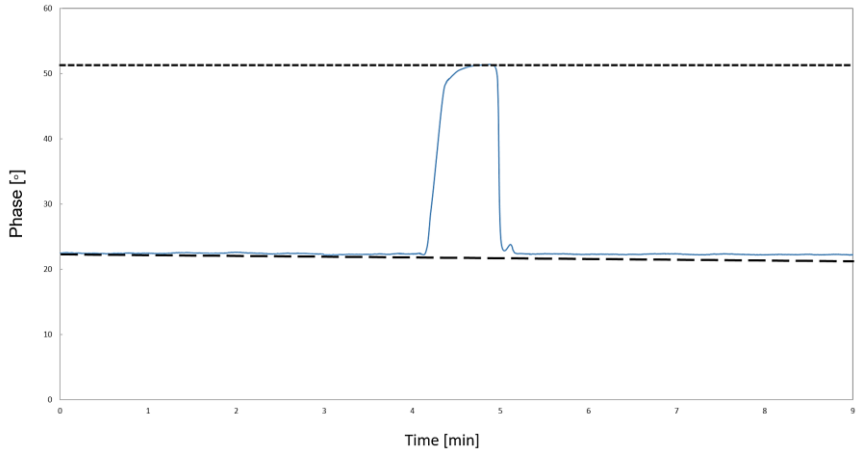

Figure 7.2 Calibration of the Oxygen Sensors.

The long-dashed line, represents the 0% oxygen, and the short-dashed line, represents the 100% oxygen. The Blue line is the phase reading of the oxygen sensor (PreSens, Germany). The 0% was achieved with a sodium sulphite solution and the 100% oxygen with a water that was sparged with compressed air for 20 minutes to saturate the oxygen content. All calibrations were taken at 37°C and adjusted on the Oxy-4 mini programme for all channels.

References

Abu-Absi, S.F., Yang, L., Thompson, P., Jiang, C., Kandula, S., Schilling, B., Shukla, A.A., 2010. Defining process design space for monoclonal antibody cell culture. Biotechnol Bioeng 106, 894–905. doi:10.1002/bit.22764

Adachi, K., Nikaido, I., Ohta, H., Ohtsuka, S., Ura, H., Kadota, M., Wakayama, T., Ueda, H.R., Niwa, H., 2013. Context-dependent wiring of Sox2 regulatory networks for self-renewal of embryonic and trophoblast stem cells. Mol Cell 52, 380–392. doi:10.1016/j.molcel.2013.09.002

Ahsan, T., Nerem, R.M., 2010. Fluid shear stress promotes an endothelial-like phenotype during the early differentiation of embryonic stem cells. Tissue Eng Part A 16, 3547–3553. doi:10.1089/ten.TEA.2010.0014

Akimoto, M., Cheng, H., Zhu, D., Brzezinski, J.A., Khanna, R., Filippova, E., Oh, E.C.T., Jing, Y., Linares, J.-L., Brooks, M., Zareparsi, S., Mears, A.J., Hero, A., Glaser, T., Swaroop, A., 2006. Targeting of GFP to newborn rods by Nrl promoter and temporal expression profiling of flow-sorted photoreceptors. Proc Natl Acad Sci USA 103, 3890–3895. doi:10.1073/pnas.0508214103

Allen, J.W., Bhatia, S.N., 2003. Formation of steady-state oxygen gradients in vitro:Application to liver zonation. Biotechnol Bioeng 82, 253. doi:10.1002/bit.10569

Andreazzoli, M., 2009. Molecular regulation of vertebrate retina cell fate. Birth Defects Res C Embryo Today 87, 284–295. doi:10.1002/bdrc.20161

Andreazzoli, M., Gestri, G., Angeloni, D., Menna, E., 1999. Role of Xrx1 in Xenopus eye and anterior brain development.

Arya, M., Shergill, I.S., Williamson, M., Gommersall, L., Arya, N., Patel, H.R.H., 2005. Basic principles of real-time quantitative PCR. Expert Rev Mol Diagn 5, 209–219. doi:10.1586/14737159.5.2.209

Banin, E., Obolensky, A., Idelson, M., Hemo, I., Reinhardtz, E., Pikarsky, E., Ben-Hur, T., Reubinoff, B., 2005. Retinal incorporation and differentiation of neural precursors derived from human embryonic stem cells. Stem Cells 24, 246–257. doi:10.1634/stemcells.2005-0009

Barakat, A.I., Lieu, D.K., 2003. Differential Responsiveness of Vascular Endothelial Cells to Different Types of Fluid Mechanical Shear Stress. Cell Biochemistry and Biophysics 38, 323. doi:10.1385/cbb:38:3:323

Barber, A.C., Hippert, C., Duran, Y., West, E.L., Bainbridge, J.W.B., Warre-Cornish, K., Luhmann, U.F.O., Lakowski, J., Sowden, J.C., Ali, R.R., Pearson, R.A., 2012. Repair of the degenerate retina by photoreceptor transplantation. Proc Natl Acad Sci USA 110, 354–359. doi:10.1073/pnas.1212677110

Basiji, D.A., Ortyn, W.E., Liang, L., Venkatachalam, V., Morrissey, P., 2007. Cellular image analysis and imaging by flow cytometry. Clin Lab Med 27, 653. doi:10.1016/j.cll.2007.05.008

Bauwens, C.L., Peerani, R., Niebruegge, S., Woodhouse, K.A., Kumacheva, E., Husain, M., Zandstra, P.W., 2008. Control of human embryonic stem cell colony and aggregate size heterogeneity influences differentiation trajectories. Stem Cells 26, 2300–2310. doi:10.1634/stemcells.2008-0183

Becker, C., Hammerle-Fickinger, A., Riedmaier, I., Pfaffl, M.W., 2010. mRNA and microRNA quality control for RT-qPCR analysis. Methods 50, 237–243. doi:10.1016/j.ymeth.2010.01.010

Becker, H., Gärtner, C., 2007. Polymer microfabrication technologies for microfluidic systems. Anal Bioanal Chem 390, 89–111. doi:10.1007/s00216-007-1692-2

Berthier, E., Young, E.W.K., Beebe, D., 2012. Engineers are from PDMS-land, Biologists are from Polystyrenia. Lab Chip 12, 1224–1237. doi:10.1039/c2lc20982a

Bilic, J., Belmonte, J.C.I., 2012. Concise Review: Induced Pluripotent Stem Cells Versus Embryonic Stem Cells: Close Enough or Yet Too Far Apart? STEM CELLS 30, 33–41. doi:10.1002/stem.700

Blauwkamp, T.A., Nigam, S., Ardehali, R., Weissman, I.L., Nusse, R., 2012. Endogenous Wnt signalling in human embryonic stem cells generates an equilibrium of distinct lineage-specified progenitors. Nat Commun 3, 1070. doi:10.1038/ncomms2064

Boucherie, C., Mukherjee, S., Henckaerts, E., Thrasher, A.J., Sowden, J.C., Ali, R.R., 2012. Brief report: self-organizing neuroepithelium from human pluripotent stem cells facilitates derivation of photoreceptors. Stem Cells 31, 408–414. doi:10.1002/stem.1268

Bouwmeester, T., Kim, S.-H., Sasai, Y., De Robertis, E.M., 1996. Cerberus is a head-inducing secreted factor expressed in the anterior endoderm of Spemann's organizer. Nature 382, 595. doi:10.1038/382595a0

Brafman, D.A., Chang, C.W., Fernandez, A., Willert, K., Varghese, S., Chien, S., 2010. Long-term human pluripotent stem cell self-renewal on synthetic polymer surfaces. Biomaterials 31, 9135–9144. doi:10.1016/j.biomaterials.2010.08.007

Braga, J., Desterro, J.M.P., Carmo-Fonseca, M., 2004. Intracellular macromolecular mobility measured by fluorescence recovery after photobleaching with confocal laser scanning microscopes. Mol Biol Cell 15, 4749–4760. doi:10.1091/mbc.E04-06-0496

Brzezinski, J.A., Kim, E.J., Johnson, J.E., Reh, T.A., 2011. Ascl1 expression defines a subpopulation of lineage-restricted progenitors in the mammalian retina. Development 138, 3519–3531. doi:10.1242/dev.064006

Bunce, C., Xing, W., Wormald, R., 2010. Causes of blind and partial sight certifications in England and Wales: April 2007-March 2008. Eye (Lond) 24, 1692–1699. doi:10.1038/eye.2010.122

Butler, P.J., Norwich, G., Weinbaum, S., Chien, S., 2001a. Shear stress induces a time- and position-dependent increase in endothelial cell membrane fluidity. Am J Physiol, Cell Physiol 280, C962–9.

Butler, P.J., Tsou, T.-C., Li, J.Y.-S., Usami, S., Chien, S., 2001b. Rate sensitivity of shear-induced changes in the lateral diffusion of endothelial cell membrane lipids: a role for membrane perturbation in shear-induced MAPK activation. FASEB J 16, 216–218. doi:10.1096/fj.01-0434fje

Cai, J., Cheng, A., Luo, Y., Lu, C., Mattson, M.P., Rao, M.S., Furukawa, K., 2003. Membrane properties of rat embryonic multipotent neural stem cells. Journal of Neurochemistry 88, 212. doi:10.1046/j.1471-4159.2003.02184.x

Carpenedo, R.L., Bratt-Leal, A.M., Marklein, R.A., Seaman, S.A., Bowen, N.J., McDonald, J.F., McDevitt, T.C., 2009. Homogeneous and organized differentiation within embryoid bodies induced by microsphere-mediated delivery of small molecules. Biomaterials 30, 2507–2515. doi:10.1016/j.biomaterials.2009.01.007

Carpenedo, R.L., Sargent, C.Y., McDevitt, T.C., 2007. Rotary suspension culture enhances the efficiency, yield, and homogeneity of embryoid body differentiation. Stem Cells 25, 2224–2234. doi:10.1634/stemcells.2006-0523

Cartwright, J.H.E., Piro, O., Tuval, I., 2004. Fluid-dynamical basis of the embryonic development of left-right asymmetry in vertebrates. Proc Natl Acad Sci USA 101, 7234–7239. doi:10.1073/pnas.0402001101

Chaudhry, M.A., Bowen, B.D., Piret, J.M., 2009. Culture pH and osmolality influence proliferation and embryoid body yields of murine embryonic stem cells. Biochemical Engineering Journal 45, 126. doi:10.1016/j.bej.2009.03.005

Chen, T., Shen, L., Yu, J., Wan, H., Guo, A., Chen, J., Long, Y., Zhao, J., Pei, G., 2011. Rapamycin and other longevity-promoting compounds enhance the generation of mouse induced pluripotent stem cells. Aging Cell 10, 908–911. doi:10.1111/j.1474-9726.2011.00722.x

Chen, K.G., Mallon, B.S., Robey, P.G., 2014. Human pluripotent stem cell culture: considerations for maintenance, expansion, and therapeutics. Cell Stem Cell 14, 13–26. doi:10.1016/j.stem.2013.12.005

Choi, Y.Y., Chung, B.G., Lee, D.H., Khademhosseini, A., Kim, J.-H., Lee, S.-H., 2010. Controlled-size embryoid body formation in concave microwell arrays. Biomaterials 31, 4296–4303. doi:10.1016/j.biomaterials.2010.01.115

Chung, B.G., Flanagan, L.A., Rhee, S.W., Schwartz, P.H., Lee, A.P., Monuki, E.S., Jeon, N.L., 2005. Human neural stem cell growth and differentiation in a gradient-generating microfluidic device. Lab Chip 5, 401–406. doi:10.1039/b417651k

Cigognini, D., Lomas, A., Kumar, P., Satyam, A., English, A., Azeem, A., Pandit, A., Zeugolis, D., 2013. Engineering in vitro microenvironments for cell based therapies and drug discovery. Drug Discov Today 18, 1099–1108. doi:10.1016/j.drudis.2013.06.007

Cimetta, E., Cannizzaro, C., James, R., Biechele, T., Moon, R.T., Elvassore, N., Vunjak-Novakovic, G., 2010. Microfluidic device generating stable concentration gradients for long term cell culture: application to Wnt3a regulation of β-catenin signaling. Lab Chip 10, 3277–3283. doi:10.1039/c0lc00033g

Cimetta, E., Figallo, E., Cannizzaro, C., Elvassore, N., Vunjak-Novakovic, G., 2008. Micro-bioreactor arrays for controlling cellular environments: design principles for human embryonic stem cell applications. Methods 47, 81–89. doi:10.1016/j.ymeth.2008.10.015

Cimetta, E., Sirabella, D., Yeager, K., Davidson, K., Simon, J., Moon, R.T., Vunjak-Novakovic, G., 2012. Microfluidic bioreactor for dynamic regulation of early mesodermal commitment in human pluripotent stem cells. Lab Chip 13, 355–364. doi:10.1039/c2lc40836h

Cimetta, E., Vunjak-Novakovic, G., 2014. Microscale technologies for regulating human stem cell differentiation. Exp Biol Med (Maywood) 239, 1255–1263. doi:10.1177/1535370214530369

Da Cruz, L., Chen, F.K., Ahmado, A., Greenwood, J., Coffey, P., 2007. RPE transplantation and its role in retinal disease. Prog Retin Eye Res 26, 598–635. doi:10.1016/j.preteyeres.2007.07.001

Dalby, M.J., Andar, A., Nag, A., Affrossman, S., Tare, R., McFarlane, S., Oreffo, R.O.C., 2008. Genomic expression of mesenchymal stem cells to altered nanoscale topographies. J R Soc Interface 5, 1055–1065. doi:10.1098/rsif.2008.0016

Damon, D. H., Lobb, R. R., D'Amore, P. A. and Wagner, J. A. (1989), Heparin potentiates the action of acidic fibroblast growth factor by prolonging its biological half-life. J. Cell. Physiol., 138: 221–226. doi:10.1002/jcp.1041380202

Danno, H., Michiue, T., Hitachi, K., Yukita, A., Ishiura, S., Asashima, M., 2008. Molecular links among the causative genes for ocular malformation: Otx2 and Sox2 coregulate Rax expression. Proc Natl Acad Sci USA 105, 5408–5413. doi:10.1073/pnas.0710954105

De Jong, P, T.V.M. 2006. Age-related macular degeneration. N Engl J Med 355, 1474–1485. doi:10.1056/NEJMra062326

Derda, R., Li, L., Orner, B.P., Lewis, R.L., Thomson, J.A., Kiessling, L.L., 2007. Defined substrates for human embryonic stem cell growth identified from surface arrays. ACS Chem Biol 2, 347–355. doi:10.1021/cb700032u

Desbordes, S.C., Placantonakis, D.G., Ciro, A., Socci, N.D., Lee, G., Djaballah, H., Studer, L., 2008. High-throughput screening assay for the identification of compounds regulating self-renewal and differentiation in human embryonic stem cells. Cell Stem Cell 2, 602–612. doi:10.1016/j.stem.2008.05.010

Di Carlo, D., Aghdam, N., Lee, L.P., 2006. Single-Cell Enzyme Concentrations, Kinetics, and Inhibition Analysis Using High-Density Hydrodynamic Cell Isolation Arrays. Analytical Chemistry 78, 4925–4930. doi:10.1021/ac060541s

Discher, D.E., Mooney, D.J., Zandstra, P.W., 2009. Growth factors, matrices, and forces combine and control stem cells. Science 324, 1673–1677. doi:10.1126/science.1171643

Do Rhee, K., Nusinowitz, S., Chao, K., Yu, F., Bok, D., Yang, X.-J., 2013. CNTF-mediated protection of photoreceptors requires initial activation of the cytokine receptor gp130 in Müller glial cells. Proc Natl Acad Sci USA 110, E4520–9. doi:10.1073/pnas.1303604110

Draper, J.S., Moore, H.D., Ruban, L.N., Gokhale, P.J., Andrews, P.W., 2004. Culture and characterization of human embryonic stem cells. Stem Cells Dev 13, 325–336. doi:10.1089/scd.2004.13.325

Eberle, D., Schubert, S., Postel, K., Corbeil, D., Ader, M., 2011. Increased Integration of Transplanted CD73-Positive Photoreceptor Precursors into Adult Mouse Retina. Investigative Opthalmology & Visual Science 52, 6462. doi:10.1167/iovs.11-7399

Eiraku, M., Takata, N., Ishibashi, H., Kawada, M., Sakakura, E., Okuda, S., Sekiguchi, K., Adachi, T., Sasai, Y., 2011. Self-organizing optic-cup morphogenesis in three-dimensional culture. Nature 472, 51–56. doi:10.1038/nature09941

Eiselleova, L., Peterkova, I., Neradil, J., Slaninova, I., Hampl, A., Dvorak, P., 2008. Comparative study of mouse and human feeder cells for human embryonic stem cells. The International Journal of Developmental Biology 52, 353. doi:10.1387/ijdb.082590le

Ema, M., Rossant, J., 2003. Cell Fate Decisions in Early Blood Vessel Formation. Trends in Cardiovascular Medicine 13, 254. doi:10.1016/S1050-1738(03)00105-1

England, S.J., Blanchard, G.B., Mahadevan, L., Adams, R.J., 2006. A dynamic fate map of the forebrain shows how vertebrate eyes form and explains two causes of cyclopia. Development 133, 4613–4617. doi:10.1242/dev.02678

Evans, M.J., Kaufman, M.H., 1981. Establishment in culture of pluripotential cells from mouse embryos. Nature 292, 154. doi:10.1038/292154a0

Fernandes, T.G., Diogo, M.M., 2013. Stem cell bioprocessing for regenerative medicine. Journal of Chemical Technology & Biotechnology 89, 34. doi:10.1002/jctb.4189

Figallo, E., Cannizzaro, C., Gerecht, S., Burdick, J.A., Langer, R., Elvassore, N., Vunjak-Novakovic, G., 2007. Micro-bioreactor array for controlling cellular microenvironments. Lab Chip 7, 710–719. doi:10.1039/b700063d

Flaim, C.J., Chien, S., Bhatia, S.N., 2005. An extracellular matrix microarray for probing cellular differentiation. Nat Methods 2, 119–125. doi:10.1038/nmeth736

Fleige, S., Pfaffl, M.W., 2006. RNA integrity and the effect on the real-time qRT-PCR performance. Mol Aspects Med 27, 126–139. doi:10.1016/j.mam.2005.12.003

Fuhrmann, S., 2010. Eye morphogenesis and patterning of the optic vesicle. Curr Top Dev Biol 93, 61–84. doi:10.1016/B978-0-12-385044-7.00003-5

Furukawa, T., Mukherjee, S., Bao, Z.-Z., Morrow, E.M., Cepko, C.L., 2000. rax, Hes1, and notch1 Promote the Formation of Müller Glia by Postnatal Retinal Progenitor Cells. Neuron 26, 383. doi:10.1016/s0896-6273(00)81171-x

Gallego-Perez, D., Higuita-Castro, N., Sharma, S., Reen, R.K., Palmer, A.F., Gooch, K.J., Lee, L.J., Lannutti, J.J., Hansford, D.J., 2010. High throughput assembly of spatially controlled 3D cell clusters on a micro/nanoplatform. Lab Chip 10, 775–782. doi:10.1039/b919475d

Gatlik-Landwojtowicz, E., Aänismaa, P., Seelig, A., 2004. The rate of P-glycoprotein activation depends on the metabolic state of the cell. Biochemistry 43, 14840–14851. doi:10.1021/bi048761s

Giri, S., Acikgöz, A., Bader, A., 2015. Isolation and Expansion of Hepatic Stem-like Cells from a Healthy Rat Liver and their Efficient Hepatic

Differentiation of under Well-defined Vivo Hepatic like Microenvironment in a Multiwell Bioreactor. J Clin Exp Hepatol 5, 107–122. doi:10.1016/j.jceh.2015.03.003

Gonzalez-Cordero, A., West, E.L., Pearson, R.A., Duran, Y., Carvalho, L.S., Chu, C.J., Naeem, A., Blackford, S.J.I., Georgiadis, A., Lakowski, J., Hubank, M., Smith, A.J., Bainbridge, J.W.B., Sowden, J.C., Ali, R.R., 2013. Photoreceptor precursors derived from three-dimensional embryonic stem cell cultures integrate and mature within adult degenerate retina. Nat Biotechnol 31, 741–747. doi:10.1038/nbt.2643

Gottwald, E., Giselbrecht, S., Augspurger, C., Lahni, B., Dambrowsky, N., Truckenmüller, R., Piotter, V., Gietzelt, T., Wendt, O., Pfleging, W., Welle, A., Rolletschek, A., Wobus, A.M., Weibezahn, K.-F., 2007. A chip-based platform for the in vitro generation of tissues in three-dimensional organization. Lab Chip 7, 777–785. doi:10.1039/b618488j

Guénin, S., Mauriat, M., Pelloux, J., Van Wuytswinkel, O., Bellini, C., Gutierrez, L., 2009. Normalization of qRT-PCR data: the necessity of adopting a systematic, experimental conditions-specific, validation of references. J Exp Bot 60, 487–493. doi:10.1093/jxb/ern305

Gómez-Sjöberg, R., Leyrat, A.A., Pirone, D.M., Chen, C.S., Quake, S.R., 2007. Versatile, fully automated, microfluidic cell culture system. Anal Chem 79, 8557–8563. doi:10.1021/ac071311w

Haidekker, M.A., L'Heureux, N., Frangos, J.A., 2000. Fluid shear stress increases membrane fluidity in endothelial cells: a study with DCVJ fluorescence. Am J Physiol Heart Circ Physiol 278, H1401–6.

Hartong, D.T., Berson, E.L., Dryja, T.P., 2006. Retinitis pigmentosa. The Lancet 368, 1795. doi:10.1016/s0140-6736(06)69740-7

Hashimoto, H., Itoh, M., Yamanaka, Y., Yamashita, S., Shimizu, T., Solnica-Krezel, L., Hibi, M., Hirano, T., 2000. Zebrafish Dkk1 functions in forebrain specification and axial mesendoderm formation. Dev Biol 217, 138–152. doi:10.1006/dbio.1999.9537

Hazeltine, L.B., Selekman, J.A., Palecek, S.P., 2013. Engineering the human pluripotent stem cell microenvironment to direct cell fate. Biotechnol Adv 31, 1002–1019. doi:10.1016/j.biotechadv.2013.03.002

Heavner, W., Pevny, L., 2012. Eye development and retinogenesis. Cold Spring Harb Perspect Biol 4. doi:10.1101/cshperspect.a008391

Heavner, W.E., Andoniadou, C.L., Pevny, L.H., 2014. Establishment of the neurogenic boundary of the mouse retina requires cooperation of SOX2 and WNT signaling. Neural Dev 9, 27. doi:10.1186/1749-8104-9-27

Hemmati-Brivanlou, A., Kelly, O.G., Melton, D.A., 1994. Follistatin, an antagonist of activin, is expressed in the Spemann organizer and displays direct neuralizing activity. Cell 77, 283. doi:10.1016/0092-8674(94)90320-4

HENG, B.C., LIU, H., CAO, T., 2004. FEEDER CELL DENSITY—A KEY PARAMETER IN HUMAN EMBRYONIC STEM CELL CULTURE. In Vitro Cellular & Developmental Biology - Animal 40, 255. doi:10.1290/0407052.1

Hiyama, E., Hiyama, K., 2007. Telomere and telomerase in stem cells. Br J Cancer 96, 1020–1024. doi:10.1038/sj.bjc.6603671

Hoffman, L.M., Carpenter, M.K., 2005. Characterization and culture of human embryonic stem cells. Nat Biotechnol 23, 699–708. doi:10.1038/nbt1102

Hongisto, H., Vuoristo, S., Mikhailova, A., Suuronen, R., Virtanen, I., Otonkoski, T., Skottman, H., 2011. Laminin-511 expression is associated with the functionality of feeder cells in human embryonic stem cell culture. Stem Cell Research 8, 97–108. doi:10.1016/j.scr.2011.08.005

Horsford, D.J., Nguyen, M.-T.T., Sellar, G.C., Kothary, R., Arnheiter, H., McInnes, R.R., 2004. Chx10 repression of Mitf is required for the maintenance of mammalian neuroretinal identity. Development 132, 177–187. doi:10.1242/dev.01571

Hough, S.R., Laslett, A.L., Grimmond, S.B., Kolle, G., Pera, M.F., 2009. A continuum of cell states spans pluripotency and lineage commitment in

human embryonic stem cells. PLoS ONE 4, e7708. doi:10.1371/journal.pone.0007708

Huang, Y., Jia, X., Bai, K., Gong, X., Fan, Y., 2010. Effect of fluid shear stress on cardiomyogenic differentiation of rat bone marrow mesenchymal stem cells. Arch Med Res 41, 497–505. doi:10.1016/j.arcmed.2010.10.002

Huggett, J., Dheda, K., Bustin, S., Zumla, A., 2005. Real-time RT-PCR normalisation; strategies and considerations. Genes Immun 6, 279–284. doi:10.1038/sj.gene.6364190

Hwang, Y.-S., Chung, B.G., Ortmann, D., Hattori, N., Moeller, H.-C., Khademhosseini, A., 2009. Microwell-mediated control of embryoid body size regulates embryonic stem cell fate via differential expression of WNT5a and WNT11. Proc Natl Acad Sci USA 106, 16978–16983. doi:10.1073/pnas.0905550106

Hägglund, A.-C., Dahl, L., Carlsson, L., 2011. Lhx2 is required for patterning and expansion of a distinct progenitor cell population committed to eye development. PLoS ONE 6, e23387. doi:10.1371/journal.pone.0023387

Helmke, B.P., Rosen, A.B., Davies, P.F., 2003. Mapping Mechanical Strain of an Endogenous Cytoskeletal Network in Living Endothelial Cells. Biophysical Journal 84, 2691. doi:10.1016/S0006-3495(03)75074-7

Huang, H., Kamm, R.D., Lee, R.T., 2004. Cell mechanics and mechanotransduction: pathways, probes, and physiology. Am J Physiol, Cell Physiol 287, C1–11. doi:10.1152/ajpcell.00559.2003

Ikeda, H., Osakada, F., Watanabe, K., Mizuseki, K., Haraguchi, T., Miyoshi, H., Kamiya, D., Honda, Y., Sasai, N., Yoshimura, N., Takahashi, M., Sasai, Y., 2005. Generation of Rx+/Pax6+ neural retinal precursors from embryonic stem cells. Proceedings of the National Academy of Sciences 102, 11331. doi:10.1073/pnas.0500010102

Iomini, C., Tejada, K., Mo, W., Vaananen, H., Piperno, G., 2004. Primary cilia of human endothelial cells disassemble under laminar shear stress. J Cell Biol 164, 811–817. doi:10.1083/jcb.200312133

Irwin, E.F., Gupta, R., Dashti, D.C., Healy, K.E., 2011. Engineered polymer-media interfaces for the long-term self-renewal of human embryonic stem cells. Biomaterials 32, 6912–6919. doi:10.1016/j.biomaterials.2011.05.058

Itsykson, P., Ilouz, N., Turetsky, T., Goldstein, R.S., Pera, M.F., Fishbein, I., Segal, M., Reubinoff, B.E., 2005. Derivation of neural precursors from human embryonic stem cells in the presence of noggin. Mol Cell Neurosci 30, 24–36. doi:10.1016/j.mcn.2005.05.004

Jaccard, N., Macown, R.J., Super, A., Griffin, L.D., Veraitch, F.S., Szita, N., 2014. Automated and online characterization of adherent cell culture growth in a microfabricated bioreactor. J Lab Autom 19, 437–443. doi:10.1177/2211068214529288

Jager, R.D., Mieler, W.F., Miller, J.W., 2008. Age-related macular degeneration. N Engl J Med 358, 2606–2617. doi:10.1056/NEJMra0801537

Jalali, S., del Pozo, M.A., Chen, K., Miao, H., Li, Y., Schwartz, M.A., Shyy, J.Y., Chien, S., 2001. Integrin-mediated mechanotransduction requires its dynamic interaction with specific extracellular matrix (ECM) ligands. Proc Natl Acad Sci USA 98, 1042–1046. doi:10.1073/pnas.031562998

Jayakody, S.A., Gonzalez-Cordero, A., Ali, R.R., Pearson, R.A., 2015. Cellular strategies for retinal repair by photoreceptor replacement. Prog Retin Eye Res 46, 31–66. doi:10.1016/j.preteyeres.2015.01.003

Jeon, J.S., Bersini, S., Whisler, J.A., Chen, M.B., Dubini, G., Charest, J.L., Moretti, M., Kamm, R.D., 2014. Generation of 3D functional microvascular networks with human mesenchymal stem cells in microfluidic systems. Integr Biol (Camb) 6, 555–563. doi:10.1039/c3ib40267c

Jones, E.A.V., Baron, M.H., Fraser, S.E., Dickinson, M.E., 2004. Measuring hemodynamic changes during mammalian development. Am J Physiol Heart Circ Physiol 287, H1561–9. doi:10.1152/ajpheart.00081.2004

Jones, E.A.V., le Noble, F., Eichmann, A., 2006. What determines blood vessel structure? Genetic prespecification vs. hemodynamics. Physiology (Bethesda) 21, 388–395. doi:10.1152/physiol.00020.2006

Karp, J.M., Yeh, J., Eng, G., Fukuda, J., Blumling, J., Suh, K.-Y., Cheng, J., Mahdavi, A., Borenstein, J., Langer, R., Khademhosseini, A., 2007. Controlling size, shape and homogeneity of embryoid bodies using poly(ethylene glycol) microwells. Lab Chip 7, 786–794. doi:10.1039/b705085m

Katoh, K., Omori, Y., Onishi, A., Sato, S., Kondo, M., Furukawa, T., 2010. Blimp1 suppresses Chx10 expression in differentiating retinal photoreceptor precursors to ensure proper photoreceptor development. J Neurosci 30, 6515–6526. doi:10.1523/JNEUROSCI.0771-10.2010

Kawada, J., Kimura, H., Akutsu, H., Sakai, Y., Fujii, T., 2012. Spatiotemporally controlled delivery of soluble factors for stem cell differentiation. Lab Chip 12, 4508–4515. doi:10.1039/c2lc40268h

Kazanskaya, O., Glinka, A., Niehrs, C., 2000. The role of Xenopus dickkopf1 in prechordal plate specification and neural patterning. Development. 127, 4981–4992.

Kilian, K.A., Bugarija, B., Lahn, B.T., Mrksich, M., 2010. Geometric cues for directing the differentiation of mesenchymal stem cells. Proc Natl Acad Sci USA 107, 4872–4877. doi:10.1073/pnas.0903269107

Kim, C., Lee, K.S., Bang, J.H., Kim, Y.E., Kim, M.-C., Oh, K.W., Lee, S.H., Kang, J.Y., 2011. 3-Dimensional cell culture for on-chip differentiation of stem cells in embryoid body. Lab on a Chip 11, 874. doi:10.1039/c0lc00516a

Kim, D.-S., Lee, J.S., Leem, J.W., Huh, Y.J., Kim, J.Y., Kim, H.-S., Park, I.-H., Daley, G.Q., Hwang, D.-Y., Kim, D.-W., 2010. Robust enhancement of

neural differentiation from human ES and iPS cells regardless of their innate difference in differentiation propensity. Stem Cell Rev 6, 270–281. doi:10.1007/s12015-010-9138-1

Kim, L., Vahey, M.D., Lee, H.-Y., Voldman, J., 2006. Microfluidic arrays for logarithmically perfused embryonic stem cell culture. Lab Chip 6, 394–406. doi:10.1039/b511718f

Kinney, M.A., McDevitt, T.C., 2012. Emerging strategies for spatiotemporal control of stem cell fate and morphogenesis. Trends Biotechnol 31, 78–84. doi:10.1016/j.tibtech.2012.11.001

Kiprilov, E.N., Awan, A., Desprat, R., Velho, M., Clement, C.A., Byskov, A.G., Andersen, C.Y., Satir, P., Bouhassira, E.E., Christensen, S.T., Hirsch, R.E., 2008. Human embryonic stem cells in culture possess primary cilia with hedgehog signaling machinery. J Cell Biol 180, 897–904. doi:10.1083/jcb.200706028

Kirouac, D.C., Zandstra, P.W., 2008. The systematic production of cells for cell therapies. Cell Stem Cell 3, 369–381. doi:10.1016/j.stem.2008.09.001

Klassen, H., 2015. Stem cells in clinical trials for treatment of retinal degeneration. Expert Opin Biol Ther 16, 7–14. doi:10.1517/14712598.2016.1093110

Koike, M., Sakaki, S., Amano, Y., Kurosawa, H., 2007. Characterization of embryoid bodies of mouse embryonic stem cells formed under various culture conditions and estimation of differentiation status of such bodies. J Biosci Bioeng 104, 294–299. doi:10.1263/jbb.104.294

Kolb, H., Dekorver, L., 1991. Midget ganglion cells of the parafovea of the human retina: a study by electron microscopy and serial section reconstructions. J Comp Neurol 303, 617–636. doi:10.1002/cne.903030408

Korin, N., Bransky, A., Dinnar, U., Levenberg, S., 2009. Periodic “flow-stop” perfusion microchannel bioreactors for mammalian and human embryonic

stem cell long-term culture. Biomedical Microdevices 11, 87–94. doi:10.1007/s10544-008-9212-5

Korin, N., Bransky, A., Khoury, M., Dinnar, U., Levenberg, S., 2008. Design of well and groove microchannel bioreactors for cell culture. Biotechnol Bioeng 102, 1222–1230. doi:10.1002/bit.22153

Korin, N., Levenberg, S., 2007. Engineering human embryonic stem cell differentiation. Biotechnol Genet Eng Rev 24, 243–61.

Kurosawa, H., 2007. Methods for inducing embryoid body formation: in vitro differentiation system of embryonic stem cells. J Biosci Bioeng 103, 389–398. doi:10.1263/jbb.103.389

Lakowski, J., Baron, M., Bainbridge, J., Barber, A.C., Pearson, R.A., Ali, R.R., Sowden, J.C., 2010. Cone and rod photoreceptor transplantation in models of the childhood retinopathy Leber congenital amaurosis using flow-sorted Crx-positive donor cells. Hum Mol Genet 19, 4545–4559. doi:10.1093/hmg/ddq378

Lakowski, J., Han, Y.-T., Pearson, R.A., Gonzalez-Cordero, A., West, E.L., Gualdoni, S., Barber, A.C., Hubank, M., Ali, R.R., Sowden, J.C., 2011. Effective Transplantation of Photoreceptor Precursor Cells Selected via Cell Surface Antigen Expression. Stem Cells N/A. doi:10.1002/stem.694

Lamba, D., Karl, M., Reh, T., 2008a. Neural regeneration and cell replacement: a view from the eye. Cell Stem Cell 2, 538–549. doi:10.1016/j.stem.2008.05.002

Lamba, D.A., Gust, J., Reh, T.A., 2008b. Transplantation of Human Embryonic Stem Cell-Derived Photoreceptors Restores Some Visual Function in Crx-Deficient Mice 1–7. doi:10.1016/j.stem.2008.10.015

Lamba, D.A., Karl, M.O., Ware, C.B., Reh, T.A., 2006. Efficient generation of retinal progenitor cells from human embryonic stem cells. Proc Natl Acad Sci USA 103, 12769–12774. doi:10.1073/pnas.0601990103

Lamba, D.A., McUsic, A., Hirata, R.K., Wang, P.-R., Russell, D., Reh, T.A., 2010. Generation, Purification and Transplantation of Photoreceptors Derived from Human Induced Pluripotent Stem Cells. PLoS ONE 5, e8763. doi:10.1371/journal.pone.0008763

Lanfer, B., Seib, F.P., Freudenberg, U., Stamov, D., Bley, T., Bornhäuser, M., Werner, C., 2009. The growth and differentiation of mesenchymal stem and progenitor cells cultured on aligned collagen matrices. Biomaterials 30, 5950–5958. doi:10.1016/j.biomaterials.2009.07.039

Lawrence, B.J., Devarapalli, M., Madihally, S.V., 2008. Flow dynamics in bioreactors containing tissue engineering scaffolds. Biotechnol Bioeng 102, 935–947. doi:10.1002/bit.22106

Leahy, A., Xiong, J.W., Kuhnert, F., Stuhlmann, H., 1999. Use of developmental marker genes to define temporal and spatial patterns of differentiation during embryoid body formation. J Exp Zool 284, 67–81.

Le Noble, F., Moyon, D., Pardanaud, L., Yuan, L., Djonov, V., Matthijsen, R., Bréant, C., Fleury, V., Eichmann, A., 2003. Flow regulates arterial-venous differentiation in the chick embryo yolk sac. Development 131, 361–375. doi:10.1242/dev.00929

Li, Y., Lu, W., King, T.D., Liu, C.-C., Bijur, G.N., Bu, G., 2010. Dkk1 stabilizes Wnt co-receptor LRP6: implication for Wnt ligand-induced LRP6 down-regulation. PLoS ONE 5, e11014. doi:10.1371/journal.pone.0011014

Lii, J., Hsu, W.-J., Parsa, H., Das, A., Rouse, R., Sia, S.K., 2008. Real-time microfluidic system for studying mammalian cells in 3D microenvironments. Anal Chem 80, 3640–3647. doi:10.1021/ac8000034

Lim, M., Ye, H., Panoskaltsis, N., Drakakis, E.M., Yue, X., Cass, A.E.G., Radomska, A., Mantalaris, A., 2007. Intelligent bioprocessing for haemotopoietic cell cultures using monitoring and design of experiments. Biotechnol Adv 25, 353–368. doi:10.1016/j.biotechadv.2007.02.002

Ling, D., Salvaterra, P.M., 2011. Robust RT-qPCR data normalization: validation and selection of internal reference genes during post-experimental data analysis. PLoS ONE 6, e17762. doi:10.1371/journal.pone.0017762

Linker, C., Stern, C.D., 2004. Neural induction requires BMP inhibition only as a late step, and involves signals other than FGF and Wnt antagonists. Development 131, 5671–5681. doi:10.1242/dev.01445

Liu, L.-L., Zhao, H., Ma, T.-F., Ge, F., Chen, C.-S., Zhang, Y.-P., 2015. Identification of valid reference genes for the normalization of RT-qPCR expression studies in human breast cancer cell lines treated with and without transient transfection. PLoS ONE 10, e0117058. doi:10.1371/journal.pone.0117058

Liu, S.V., 2008. iPS Cells: A More Critical Review. Stem Cells and Development 17, 391–398. doi:10.1089/scd.2008.0062

Lu, H., Koo, L.Y., Wang, W.M., Lauffenburger, D.A., Griffith, L.G., Jensen, K.F., 2004. Microfluidic shear devices for quantitative analysis of cell adhesion. Anal Chem 76, 5257–5264. doi:10.1021/ac049837t

MacLaren, R.E., Pearson, R.A., MacNeil, A., Douglas, R.H., Salt, T.E., Akimoto, M., Swaroop, A., Sowden, J.C., Ali, R.R., 2006. Retinal repair by transplantation of photoreceptor precursors. Nature 444, 203–207. doi:10.1038/nature05161

Macown, R.J., Veraitch, F.S., Szita, N., 2014. Robust, microfabricated culture devices with improved control over the soluble microenvironment for the culture of embryonic stem cells. Biotechnol J 9, 805–813. doi:10.1002/biot.201300245

Madihally, S.V., 2010. Principles of Biomedical Engineering (Engineering in Medicine & Biology) 1–499.

Mallon, B.S., Park, K.-Y., Chen, K.G., Hamilton, R.S., 2006. Toward xeno-free culture of human embryonic stem cells. Int J Biochem Cell Biol 38, 1063–1075. doi:10.1016/j.biocel.2005.12.014

McFarlin, B.K., Gary, M.A., 2016. Flow cytometry what you see matters: Enhanced clinical detection using image-based flow cytometry. Methods 112, 1–8. doi:10.1016/j.ymeth.2016.09.001

Marks, H., Kalkan, T., Menafra, R., Denissov, S., Jones, K., Hofemeister, H., Nichols, J., Kranz, A., Stewart, A.F., Smith, A., Stunnenberg, H.G., 2012. The transcriptional and epigenomic foundations of ground state pluripotency. Cell 149, 590–604. doi:10.1016/j.cell.2012.03.026

Markway, B.D., Tan, G.-K., Brooke, G., Hudson, J.E., Cooper-White, J.J., Doran, M.R., 2009. Enhanced chondrogenic differentiation of human bone marrow-derived mesenchymal stem cells in low oxygen environment micropellet cultures. Cell Transplant 19, 29–42. doi:10.3727/096368909X478560

Masland, R.H., 2001. The fundamental plan of the retina. Nat Neurosci 4, 877–886. doi:10.1038/nn0901-877

Matthews, B., Judy, J.W., 2006. Design and Fabrication of a Micromachined Planar Patch-Clamp Substrate With Integrated Microfluidics for Single-Cell Measurements. Journal of Microelectromechanical Systems 15, 214. doi:10.1109/jmems.2005.863606

Mazzoni, F., Novelli, E., Strettoi, E., 2008. Retinal ganglion cells survive and maintain normal dendritic morphology in a mouse model of inherited photoreceptor degeneration. J Neurosci 28, 14282–14292. doi:10.1523/JNEUROSCI.4968-08.2008

McGrath, K.E., Koniski, A.D., Malik, J., Palis, J., 2002. Circulation is established in a stepwise pattern in the mammalian embryo. Blood 101, 1669–1676. doi:10.1182/blood-2002-08-2531

Mears, A.J., Kondo, M., Swain, P.K., Takada, Y., Bush, R.A., Saunders, T.L., Sieving, P.A., Swaroop, A., 2001. Nrl is required for rod photoreceptor development. Nature Genetics 29, 447–452. doi:10.1038/ng774

Mehta, K., Linderman, J.J., 2006. Model-based analysis and design of a microchannel reactor for tissue engineering. Biotechnol Bioeng 94, 596–609. doi:10.1002/bit.20857

Mellough, C.B., Sernagor, E., Moreno-Gimeno, I., Steel, D.H.W., Lako, M., 2012. Efficient stage-specific differentiation of human pluripotent stem cells toward retinal photoreceptor cells. Stem Cells 30, 673–686. doi:10.1002/stem.1037

Merryman, W.D., Engler, A.J., 2009. Innovations in cell mechanobiology. J Biomech 43, 1. doi:10.1016/j.jbiomech.2009.09.001

Meyer, J.S., Howden, S.E., Wallace, K.A., Verhoeven, A.D., Wright, L.S., Capowski, E.E., Pinilla, I., Martin, J.M., Tian, S., Stewart, R., Pattnaik, B., Thomson, J.A., Gamm, D.M., 2011. Optic vesicle-like structures derived from human pluripotent stem cells facilitate a customized approach to retinal disease treatment. Stem Cells 29, 1206–1218. doi:10.1002/stem.674

Meyer, J.S., Shearer, R.L., Capowski, E.E., Wright, L.S., Wallace, K.A., McMillan, E.L., Zhang, S.-C., Gamm, D.M., 2009. Modeling early retinal development with human embryonic and induced pluripotent stem cells. Proc Natl Acad Sci USA 106, 16698–16703. doi:10.1073/pnas.0905245106

Michalczyk, K., Ziman, M., 2005. Nestin structure and predicted function in cellular cytoskeletal organisation. Histol Histopathol 20, 665–671.

Minassian, D.C., Reidy, A., Lightstone, A., Desai, P., 2011. Modelling the prevalence of age-related macular degeneration (2010-2020) in the UK: expected impact of anti-vascular endothelial growth factor (VEGF) therapy. Br J Ophthalmol 95, 1433–1436. doi:10.1136/bjo.2010.195370

Mohr, J.C., Zhang, J., Azarin, S.M., Soerens, A.G., de Pablo, J.J., Thomson, J.A., Lyons, G.E., Palecek, S.P., Kamp, T.J., 2009. The microwell control of embryoid body size in order to regulate cardiac differentiation of human embryonic stem cells. Biomaterials 31, 1885–1893. doi:10.1016/j.biomaterials.2009.11.033

Moore, K.A., 2006. Stem Cells and Their Niches. Science 311, 1880. doi:10.1126/science.1110542

Mukhopadhyay, M., Shtrom, S., Rodriguez-Esteban, C., Chen, L., Tsukui, T., Gomer, L., Dorward, D.W., Glinka, A., Grinberg, A., Huang, S.P., Niehrs, C., Belmonte, J.C.I., Westphal, H., 2001. Dickkopf1 is required for embryonic head induction and limb morphogenesis in the mouse. Dev Cell 1, 423–434.

Nakano, T., Ando, S., Takata, N., Kawada, M., Muguruma, K., Sekiguchi, K., Saito, K., Yonemura, S., Eiraku, M., Sasai, Y., 2012. Self-formation of optic cups and storable stratified neural retina from human ESCs. Cell Stem Cell 10, 771–785. doi:10.1016/j.stem.2012.05.009

Narsinh, K.H., Sun, N., Sanchez-Freire, V., Lee, A.S., Almeida, P., Hu, S., Jan, T., Wilson, K.D., Leong, D., Rosenberg, J., Yao, M., Robbins, R.C., Wu, J.C., 2011. Single cell transcriptional profiling reveals heterogeneity of human induced pluripotent stem cells. J Clin Invest 121, 1217–1221. doi:10.1172/JCI44635

Nishida, A., Furukawa, A., Koike, C., Tano, Y., Aizawa, S., Matsuo, I., Furukawa, T., 2003. Otx2 homeobox gene controls retinal photoreceptor cell fate and pineal gland development. Nat Neurosci 6, 1255–1263. doi:10.1038/nn1155

Nivison, M.P., Ericson, N.G., Green, V.M., Bielas, J.H., Campbell, J.S., Horner, P.J., 2017. Age-related accumulation of phosphorylated mitofusin 2 protein in retinal ganglion cells correlates with glaucoma progression. Experimental Neurology 296, 49–61. doi:10.1016/j.expneurol.2017.07.001

Nolan, T., Hands, R.E., Bustin, S.A., 2007. Quantification of mRNA using real-time RT-PCR. Nat Protoc 1, 1559–1582. doi:10.1038/nprot.2006.236

Nonaka, S., Shiratori, H., Saijoh, Y., Hamada, H., 2002. Determination of left–right patterning of the mouse embryo by artificial nodal flow. Nature.

Nsiah, B.A., Ahsan, T., Griffiths, S., Cooke, M., Nerem, R.M., McDevitt, T.C., 2014. Fluid shear stress pre-conditioning promotes endothelial

morphogenesis of embryonic stem cells within embryoid bodies. Tissue Eng Part A 20, 954–965. doi:10.1089/ten.TEA.2013.0243

Oehrtman, G.T., Wiley, H.S., Lauffenburger, D.A., 1999. Escape of autocrine ligands into extracellular medium: experimental test of theoretical model predictions. Biotechnol Bioeng 57, 571–582.

Olmer, R., Lange, A., Selzer, S., Kasper, C., Haverich, A., Martin, U., Zweigerdt, R., 2012. Suspension culture of human pluripotent stem cells in controlled, stirred bioreactors. Tissue Eng Part C Methods 18, 772–784. doi:10.1089/ten.TEC.2011.0717

Oh, E.C.T., Khan, N., Novelli, E., Khanna, H., Strettoi, E., Swaroop, A., 2007. Transformation of cone precursors to functional rod photoreceptors by bZIP transcription factor NRL. Proc Natl Acad Sci USA 104, 1679–1684. doi:10.1073/pnas.0605934104

Osakada, F., Ikeda, H., Mandai, M., Wataya, T., Watanabe, K., Yoshimura, N., Akaike, A., Sasai, Y., Takahashi, M., 2008. Toward the generation of rod and cone photoreceptors from mouse, monkey and human embryonic stem cells. Nature Biotechnology 26, 215–224. doi:10.1038/nbt1384

Osakada, F., Ikeda, H., Sasai, Y., Takahashi, M., 2009. Stepwise differentiation of pluripotent stem cells into retinal cells. Nat Protoc 4, 811–824. doi:10.1038/nprot.2009.51

Ouyang, A., Yang, S.-T., 2008. A two-stage perfusion fibrous bed bioreactor system for mass production of embryonic stem cells. Expert Opin Biol Ther 8, 895–909. doi:10.1517/14712598.8.7.895

Owen, C.G., Jarrar, Z., Wormald, R., Cook, D.G., Fletcher, A.E., Rudnicka, A.R., 2012. The estimated prevalence and incidence of late stage age related macular degeneration in the UK. Br J Ophthalmol 96, 752–756. doi:10.1136/bjophthalmol-2011-301109

Paguirigan, A.L., Beebe, D.J., 2008. Microfluidics meet cell biology: bridging the gap by validation and application of microscale techniques for cell biological assays. BioEssays 30, 811–821. doi:10.1002/bies.20804

Park, I.-H., Zhao, R., West, J.A., Yabuuchi, A., Huo, H., Ince, T.A., Lerou, P.H., Lensch, M.W., Daley, G.Q., 2007. Reprogramming of human somatic cells to pluripotency with defined factors. Nature 451, 141–146. doi:10.1038/nature06534

Park, J.Y., Kim, S.-K., Woo, D.-H., Lee, E.-J., Kim, J.-H., Lee, S.-H., 2009. Differentiation of neural progenitor cells in a microfluidic chip-generated cytokine gradient. Stem Cells 27, 2646–2654. doi:10.1002/stem.202

Pearson, R.A., Hippert, C., Graca, A.B., Barber, A.C., 2014. Photoreceptor replacement therapy: challenges presented by the diseased recipient retinal environment. Vis Neurosci 31, 333–344. doi:10.1017/S0952523814000200

Peng, G.-H., Ahmad, O., Ahmad, F., Liu, J., Chen, S., 2005. The photoreceptor-specific nuclear receptor Nr2e3 interacts with Crx and exerts opposing effects on the transcription of rod versus cone genes. Hum Mol Genet 14, 747–764. doi:10.1093/hmg/ddi070

Pera, E.M., Wessely, O., Li, S.Y., De Robertis, E.M., 2001. Neural and head induction by insulin-like growth factor signals. Dev Cell 1, 655–665. doi:10.1016/s1534-5807(01)00069-7

Peterson, E.T.K., Papautsky, I., 2006. Microtextured polydimethylsiloxane substrates for culturing mesenchymal stem cells. Methods Mol Biol 321, 179–197. doi:10.1385/1-59259-997-4:179

Placzek, M.R., Chung, I.-M., Macedo, H.M., Ismail, S., Blanco, T.M., Lim, M., Cha, J.M., Fauzi, I., Kang, Y., Yeo, D.C.L., Ma, C.Y.J., Polak, J.M., Panoskaltsis, N., Mantalaris, A., 2008. Stem cell bioprocessing: fundamentals and principles. J R Soc Interface 6, 209–232. doi:10.1098/rsif.2008.0442

Preti, R.A., 2005. Bringing safe and effective cell therapies to the bedside. Nat Biotechnol 23, 801–804. doi:10.1038/nbt0705-801

Pronko, P.P., Dutta, S.K., Squier, J., Rudd, J.V., Du, D., Mourou, G., 1995. Machining of sub-micron holes using a femtosecond laser at 800 nm. Optics Communications 114, 106. doi:10.1016/0030-4018(94)00585-I

Puri, M.C., Nagy, A., 2012. Concise Review: Embryonic Stem Cells Versus Induced Pluripotent Stem Cells: The Game Is On. STEM CELLS 30, 10–14. doi:10.1002/stem.788

Rayment, E.A., Williams, D.J., 2010. Concise Review: Mind the Gap: Challenges in Characterizing and Quantifying Cell-and Tissue-Based Therapies for Clinical Translation. Stem Cells.

Recknor, J.B., Sakaguchi, D.S., Mallapragada, S.K., 2005. Growth and differentiation of astrocytes and neural progenitor cells on micropatterned polymer films. Ann N Y Acad Sci 1049, 24–27. doi:10.1196/annals.1334.004

Reeves, P.J., Callewaert, N., Contreras, R., Khorana, H.G., 2002. Structure and function in rhodopsin: high-level expression of rhodopsin with restricted and homogeneous N-glycosylation by a tetracycline-inducible N-acetylglucosaminyltransferase I-negative HEK293S stable mammalian cell line. Proc Natl Acad Sci USA 99, 13419–13424. doi:10.1073/pnas.212519299

Regehr, K.J., Domenech, M., Koepsel, J.T., Carver, K.C., Ellison-Zelski, S.J., Murphy, W.L., Schuler, L.A., Alarid, E.T., Beebe, D.J., 2009. Biological implications of polydimethylsiloxane-based microfluidic cell culture. Lab Chip 9, 2132–2139. doi:10.1039/b903043c

Rehemtulla, A., Warwar, R., Kumar, R., Ji, X., Zack, D.J., Swaroop, A., 1996. The basic motif-leucine zipper transcription factor Nrl can positively regulate rhodopsin gene expression. Proc Natl Acad Sci USA 93, 191–195.

Reichen, M., Macown, R.J., Jaccard, N., Super, A., Ruban, L., Griffin, L.D., Veraitch, F.S., Szita, N., 2012. Microfabricated modular scale-down device

for regenerative medicine process development. PLoS ONE 7, e52246. doi:10.1371/journal.pone.0052246

Reichman, S., Terray, A., Slembrouck, A., Nanteau, C., Orieux, G., Habeler, W., Nandrot, E.F., Sahel, J.-A., Monville, C., Goureau, O., 2014. From confluent human iPS cells to self-forming neural retina and retinal pigmented epithelium. Proceedings of the National Academy of Sciences 111, 8518–8523. doi:10.1073/pnas.1324212111

Resnick, N., Yahav, H., Shay-Salit, A., Shushy, M., Schubert, S., Zilberman, L.C.M., Wofovitz, E., 2003. Fluid shear stress and the vascular endothelium: for better and for worse. Progress in Biophysics and Molecular Biology 81, 177. doi:10.1016/S0079-6107(02)00052-4

Reubinoff, B.E., Pera, M.F., Fong, C.Y., Trounson, A., Bongso, A., 2000. Embryonic stem cell lines from human blastocysts: somatic differentiation in vitro. Nat Biotechnol 18, 399–404. doi:10.1038/74447

Roberts, I., Baila, S., Rice, R. B., Janssens, M., Nguyen, K., Moens, N., Ruban, L., Hernandez, D., Coffey, P. & Mason, C. 2012. Scale-up of human embryonic stem cell culture using a hollow fibre bioreactor. Biotechnology Letters, 34**,** 2307-2315

Robinson, J.P., 2004. Flow cytometry. Encyclopedia of biomaterials and biomedical Engineering. doi: 10.1081/E-EBBE 120013923

Rogers, C.D., Moody, S.A., Casey, E.S., 2009. Neural induction and factors that stabilize a neural fate. Birth Defects Res C Embryo Today 87, 249–262. doi:10.1002/bdrc.20157

Rowan, S., Chen, C.-M.A., Young, T.L., Fisher, D.E., Cepko, C.L., 2004. Transdifferentiation of the retina into pigmented cells in ocular retardation mice defines a new function of the homeodomain gene Chx10. Development 131, 5139–5152. doi:10.1242/dev.01300

Rowley, J.A., 2010. Developing cell therapy biomanufacturing processes, Chemical engineering progress. 50–55 (2010).

Ruiz, S.A., Chen, C.S., 2008. Emergence of patterned stem cell differentiation within multicellular structures. Stem Cells 26, 2921–2927. doi:10.1634/stemcells.2008-0432

Rungarunlert, S., Techakumphu, M., Pirity, M.K., Dinnyes, A., 2009. Embryoid body formation from embryonic and induced pluripotent stem cells: Benefits of bioreactors. World J Stem Cells 1, 11–21. doi:10.4252/wjsc.v1.i1.11

Santos, A., 1997. Preservation of the Inner Retina in Retinitis Pigmentosa. Archives of Ophthalmology 115, 511. doi:10.1001/archopht.1997.01100150513011

Sargent, C.Y., Berguig, G.Y., Kinney, M.A., Hiatt, L.A., Carpenedo, R.L., Berson, R.E., McDevitt, T.C., 2009. Hydrodynamic modulation of embryonic stem cell differentiation by rotary orbital suspension culture. Biotechnol Bioeng 105, 611–626. doi:10.1002/bit.22578

Schlichtenbrede, F.C., MacNeil, A., Bainbridge, J.W.B., Tschernutter, M., Thrasher, A.J., Smith, A.J., Ali, R.R., 2003. Intraocular gene delivery of ciliary neurotrophic factor results in significant loss of retinal function in normal mice and in the Prph2Rd2/Rd2 model of retinal degeneration. Gene Ther 10, 523–527. doi:10.1038/sj.gt.3301929

Schriebl, K., Lim, S., Choo, A., Tscheliessnig, A., Jungbauer, A., 2009. Stem cell separation: a bottleneck in stem cell therapy. Biotechnol J 5, 50–61. doi:10.1002/biot.200900115

Schwartz, S.D., Hubschman, J.-P., Heilwell, G., Franco-Cardenas, V., Pan, C.K., Ostrick, R.M., Mickunas, E., Gay, R., Klimanskaya, I., Lanza, R., 2012. Embryonic stem cell trials for macular degeneration: a preliminary report. The Lancet 379, 713. doi:10.1016/s0140-6736(12)60028-2

Schwartz, S.D., Regillo, C.D., Lam, B.L., Eliott, D., Rosenfeld, P.J., Gregori, N.Z., Hubschman, J.-P., Davis, J.L., Heilwell, G., Spirn, M., Maguire, J., Gay, R., Bateman, J., Ostrick, R.M., Morris, D., Vincent, M., Anglade, E., Del Priore, L.V., Lanza, R., 2015. Human embryonic stem cell-derived retinal

pigment epithelium in patients with age-related macular degeneration and Stargardt's macular dystrophy: follow-up of two open-label phase 1/2 studies. The Lancet 385, 509. doi:10.1016/s0140-6736(14)61376-3

Serban, M.A., Prestwich, G.D., 2008. Modular extracellular matrices: Solutions for the puzzle. Methods 45, 93. doi:10.1016/j.ymeth.2008.01.010

Serra, M., Brito, C., Correia, C., Alves, P.M., 2012. Process engineering of human pluripotent stem cells for clinical application. Trends Biotechnol 30, 350–359. doi:10.1016/j.tibtech.2012.03.003

Sharma, V.S., 2016. Size controlled retinal differentiation of human induced pluripotent stem cells in shaking microwells.

Sharma, V.S., Khalife, R., Tostoes, R., Leung, L., Kinsella, R., Ruban, L., Veraitch, F.S., 2016. Early retinal differentiation of human pluripotent stem cells in microwell suspension cultures. Biotechnol Lett 39, 339–350. doi:10.1007/s10529-016-2244-7

Shepherd, A.J., 2005. Colour vision in migraine: selective deficits for S-cone discriminations. Cephalalgia 25, 412–423. doi:10.1111/j.1468-2982.2004.00831.x

Sia, S.K., Whitesides, G.M., 2003. Microfluidic devices fabricated in poly(dimethylsiloxane) for biological studies. Electrophoresis 24, 3563–3576. doi:10.1002/elps.200305584

Singh, A.M., Chappell, J., Trost, R., Lin, L., Wang, T., Tang, J., Matlock, B.K., Weller, K.P., Wu, H., Zhao, S., Jin, P., Dalton, S., 2013. Cell-cycle control of developmentally regulated transcription factors accounts for heterogeneity in human pluripotent cells. Stem Cell Reports 1, 532–544. doi:10.1016/j.stemcr.2013.10.009

Smith, A.J., Bainbridge, J.W.B., Ali, R.R., 2011. Gene supplementation therapy for recessive forms of inherited retinal dystrophies. Gene Ther 19, 154–161. doi:10.1038/gt.2011.161

Soen, Y., Mori, A., Palmer, T.D., Brown, P.O., 2006. Exploring the regulation of human neural precursor cell differentiation using arrays of signaling microenvironments. Mol Syst Biol 2, 37. doi:10.1038/msb4100076

Sridhar, A., 2013. Nonxenogeneic Growth and Retinal Differentiation of Human Induced Pluripotent Stem Cells. Stem Cells Transl Med 2, 255. doi:10.5966/sctm.2012-0101

Stacey, G.N., Cobo, F., Nieto, A., Talavera, P., Healy, L., Concha, A., 2006. The development of “feeder” cells for the preparation of clinical grade hES cell lines: challenges and solutions. J Biotechnol 125, 583–588. doi:10.1016/j.jbiotec.2006.03.011

Steiner, D., Khaner, H., Cohen, M., Even-Ram, S., Gil, Y., Itsykson, P., Turetsky, T., Idelson, M., Aizenman, E., Ram, R., Berman-Zaken, Y., Reubinoff, B., 2010. Derivation, propagation and controlled differentiation of human embryonic stem cells in suspension. Nature Biotechnology 28, 361–364. doi:10.1038/nbt.1616

Stolberg, S., McCloskey, K.E., 2009. Can shear stress direct stem cell fate? Biotechnology Progress 25, 10. doi:10.1002/btpr.124

Streit, A., Berliner, A.J., Papanayotou, C., Sirulnik, A., Stern, C.D., 2000. Initiation of neural induction by FGF signalling before gastrulation. Nature 406, 74–78. doi:10.1038/35017617

Super, A., Jaccard, N., Marques, M.P.C., Macown, R.J., Griffin, L.D., Veraitch, F.S., Szita, N., 2016. Real-time monitoring of specific oxygen uptake rates of embryonic stem cells in a microfluidic cell culture device. Biotechnol J 11, 1179–1189. doi:10.1002/biot.201500479

Suzuki, T., Higgins, P.J., Crawford, D.R., 2000. Control selection for RNA quantitation. BioTechniques 29, 332–337.

Takahashi, K., Tanabe, K., Ohnuki, M., Narita, M., Ichisaka, T., Tomoda, K., Yamanaka, S., 2007. Induction of pluripotent stem cells from adult human

fibroblasts by defined factors. Cell 131, 861–872. doi:10.1016/j.cell.2007.11.019

Takahashi, K., Yamanaka, S., 2006. Induction of pluripotent stem cells from mouse embryonic and adult fibroblast cultures by defined factors. Cell 126, 663–676. doi:10.1016/j.cell.2006.07.024

Tandon, N., Marolt, D., Cimetta, E., Vunjak-Novakovic, G., 2013. Bioreactor engineering of stem cell environments. Biotechnol Adv 31, 1020–1031. doi:10.1016/j.biotechadv.2013.03.007

Taylor, H.R., Keeffe, J.E., Vu, H.T., Wang, J.J., Rochtchina, E., 2005. Vision loss in Australia. Med J Aust.

Thomas, R.J., Hourd, P.C., Williams, D.J., 2008. Application of process quality engineering techniques to improve the understanding of the in vitro processing of stem cells for therapeutic use. J Biotechnol 136, 148–155. doi:10.1016/j.jbiotec.2008.06.009

Thomson, J.A., Itskovitz-Eldor, J., Shapiro, S.S., Waknitz, M.A., Swiergiel, J.J., Marshall, V.S., Jones, J.M., 1998. Embryonic stem cell lines derived from human blastocysts. Science 282, 1145–1147.

Titmarsh, D.M., Hudson, J.E., Hidalgo, A., Elefanty, A.G., Stanley, E.G., Wolvetang, E.J., Cooper-White, J.J., 2012. Microbioreactor arrays for full factorial screening of exogenous and paracrine factors in human embryonic stem cell differentiation. PLoS ONE 7, e52405. doi:10.1371/journal.pone.0052405

Toh, Y.-C., Voldman, J., 2010. Fluid shear stress primes mouse embryonic stem cells for differentiation in a self-renewing environment via heparan sulfate proteoglycans transduction. FASEB J 25, 1208–1217. doi:10.1096/fj.10-168971

Tonge, P.D., Shigeta, M., Schroeder, T., Andrews, P.W., 2011. Functionally defined substates within the human embryonic stem cell compartment. Stem Cell Research 7, 145–153. doi:10.1016/j.scr.2011.04.006

Tucker, B.A., Park, I.-H., Qi, S.D., Klassen, H.J., Jiang, C., Yao, J., Redenti, S., Daley, G.Q., Young, M.J., 2011. Transplantation of adult mouse iPS cell-derived photoreceptor precursors restores retinal structure and function in degenerative mice. PLoS ONE 6, e18992. doi:10.1371/journal.pone.0018992

Tétreault, N., Champagne, M.-P., Bernier, G., 2008. The LIM homeobox transcription factor Lhx2 is required to specify the retina field and synergistically cooperates with Pax6 for Six6 trans-activation. Dev Biol 327, 541–550. doi:10.1016/j.ydbio.2008.12.022

Trounson, A., McDonald, C., 2015. Stem Cell Therapies in Clinical Trials: Progress and Challenges. Cell Stem Cell 17, 11–22. doi:10.1016/j.stem.2015.06.007

Tucker, B.A., Anfinson, K.R., Mullins, R.F., 2013. Use of a synthetic xeno-free culture substrate for induced pluripotent stem cell induction and retinal differentiation. Stem Cells.

Tucker, B.A., Park, I.-H., Qi, S.D., Klassen, H.J., Jiang, C., Yao, J., Redenti, S., Daley, G.Q., Young, M.J., 2011. Transplantation of adult mouse iPS cell-derived photoreceptor precursors restores retinal structure and function in degenerative mice. PLoS ONE 6, e18992. doi:10.1371/journal.pone.0018992

Ungrin, M.D., Clarke, G., Yin, T., Niebrugge, S., Nostro, M.C., Sarangi, F., Wood, G., Keller, G., Zandstra, P.W., 2011. Rational bioprocess design for human pluripotent stem cell expansion and endoderm differentiation based on cellular dynamics. Biotechnol Bioeng 109, 853–866. doi:10.1002/bit.24375

Ungrin, M.D., Joshi, C., Nica, A., Bauwens, C., Zandstra, P.W., 2008. Reproducible, ultra high-throughput formation of multicellular organization from single cell suspension-derived human embryonic stem cell aggregates. PLoS ONE 3, e1565. doi:10.1371/journal.pone.0001565

Van Winkle, A.P., Gates, I.D., Kallos, M.S., 2012. Mass transfer limitations in embryoid bodies during human embryonic stem cell differentiation. Cells Tissues Organs (Print) 196, 34–47. doi:10.1159/000330691

Vandesompele, J., De Preter, K., Pattyn, F., Poppe, B., Van Roy, N., De Paepe, A., Speleman, F., 2002. Accurate normalization of real-time quantitative RT-PCR data by geometric averaging of multiple internal control genes. Genome Biol 3, RESEARCH0034.

Villa-Diaz, L.G., Ross, A.M., Lahann, J., Krebsbach, P.H., 2012. Concise Review: The Evolution of human pluripotent stem cell culture: From feeder cells to synthetic coatings. Stem Cells 31, 1. doi:10.1002/stem.1260

Vishwasrao, H.D., Heikal, A.A., Kasischke, K.A., Webb, W.W., 2005. Conformational Dependence of Intracellular NADH on Metabolic State Revealed by Associated Fluorescence Anisotropy. Journal of Biological Chemistry 280, 25119. doi:10.1074/jbc.m502475200

Walker, G.M., Zeringue, H.C., Beebe, D.J., 2004. Microenvironment design considerations for cellular scale studies. Lab Chip 4, 91–97. doi:10.1039/b311214d

Wall, D.S., Mears, A.J., McNeill, B., Mazerolle, C., Thurig, S., Wang, Y., Kageyama, R., Wallace, V.A., 2009. Progenitor cell proliferation in the retina is dependent on Notch-independent Sonic hedgehog/Hes1 activity. J Cell Biol 184, 101–112. doi:10.1083/jcb.200805155

Wan, C.-R., Chung, S. & Kamm, R.D., 2011. Differentiation of embryonic stem cells into cardiomyocytes in a compliant microfluidic system. *Annals of biomedical engineering*, 39(6), pp.1840–1847.

Wang, H., Keiser, J.A., 1998. Vascular endothelial growth factor upregulates the expression of matrix metalloproteinases in vascular smooth muscle cells: role of flt-1. Circ Res 83, 832–840.

Warrington, J.A., Nair, A., Mahadevappa, M., Tsyganskaya, M., 2000. Comparison of human adult and fetal expression and identification of 535 housekeeping/maintenance genes. Physiol Genomics 2, 143–147.

Wasserman, S.M., Mehraban, F., Komuves, L.G., Yang, R.-B., Tomlinson, J.E., Zhang, Y., Spriggs, F., Topper, J.N., 2002. Gene expression profile of

human endothelial cells exposed to sustained fluid shear stress. Physiol Genomics 12, 13–23. doi:10.1152/physiolgenomics.00102.2002

Wasserman, S.M., Topper, J.N., 2004. Adaptation of the endothelium to fluid flow: in vitro analyses of gene expression and in vivo implications. Vasc Med 9, 35–45.

Watanabe, K., Kamiya, D., Nishiyama, A., Katayama, T., Nozaki, S., Kawasaki, H., Watanabe, Y., Mizuseki, K., Sasai, Y., 2005. Directed differentiation of telencephalic precursors from embryonic stem cells. Nat Neurosci 8, 288–296. doi:10.1038/nn1402

West, E.L., Gonzalez-Cordero, A., Hippert, C., Osakada, F., Martinez-Barbera, J.P., Pearson, R.A., Sowden, J.C., Takahashi, M., Ali, R.R., 2012. Defining the Integration Capacity of Embryonic Stem Cell-Derived Photoreceptor Precursors. STEM CELLS 30, 1424–1435. doi:10.1002/stem.1123

Williams, R.L., Hilton, D.J., Pease, S., Willson, T.A., Stewart, C.L., Gearing, D.P., Wagner, E.F., Metcalf, D., Nicola, N.A., Gough, N.M., 1988. Myeloid leukaemia inhibitory factor maintains the developmental potential of embryonic stem cells. Nature 336, 684–687. doi:10.1038/336684a0

Whitesides, G.M., 2006. The origins and the future of microfluidics. Nature 442, 368–373. doi:10.1038/nature05058

Wilson, P.G., Stice, S.S., 2006. Development and Differentiation of Neural Rosettes Derived From Human Embryonic Stem Cells. Stem Cell Rev 2, 67. doi:10.1385/scr:2:1:67

Wuertz, K., Godburn, K., Iatridis, J.C., 2009. MSC response to pH levels found in degenerating intervertebral discs. Biochem Biophys Res Commun 379, 824–829. doi:10.1016/j.bbrc.2008.12.145

Xia, Y., Whitesides, G.M., 1998. Soft Lithography. Angewandte Chemie International Edition 37, 550. doi:10.1002/(sici)1521-3773(19980316)37:5

Xu, Y., Zhu, X., Hahm, H.S., Wei, W., Hao, E., Hayek, A., Ding, S., 2010. Revealing a core signaling regulatory mechanism for pluripotent stem cell survival and self-renewal by small molecules. Proc Natl Acad Sci USA 107, 8129–8134. doi:10.1073/pnas.1002024107

Yamamoto, K., Sokabe, T., Watabe, T., Miyazono, K., Yamashita, J.K., Obi, S., Ohura, N., Matsushita, A., Kamiya, A., Ando, J., 2004. Fluid shear stress induces differentiation of Flk-1-positive embryonic stem cells into vascular endothelial cells in vitro. Am J Physiol Heart Circ Physiol 288, H1915–24. doi:10.1152/ajpheart.00956.2004

Yang, H., Zhang, Y., Liu, Z., Chen, P., Ma, K., Zhou, C., 2008. Mouse embryonic stem cell-derived cardiomyocytes express functional adrenoceptors. Biochem Biophys Res Commun 368, 887–892. doi:10.1016/j.bbrc.2008.02.014

Yaron, O., Farhy, C., Marquardt, T., Applebury, M., Ashery-Padan, R., 2006. Notch1 functions to suppress cone-photoreceptor fate specification in the developing mouse retina. Development 133, 1367–1378. doi:10.1242/dev.02311

Yim, E.K.F., Pang, S.W., Leong, K.W., 2007. Synthetic nanostructures inducing differentiation of human mesenchymal stem cells into neuronal lineage. Exp Cell Res 313, 1820–1829. doi:10.1016/j.yexcr.2007.02.031

Young, E.W.K., Beebe, D.J., 2010. Fundamentals of microfluidic cell culture in controlled microenvironments. Chem Soc Rev 39, 1036. doi:10.1039/b909900j

Yu, H., Meyvantsson, I., Shkel, I.A., Beebe, D.J., 2005. Diffusion dependent cell behavior in microenvironments. Lab on a Chip 5, 1089. doi:10.1039/b504403k

Yu, J., Vodyanik, M.A., Smuga-Otto, K., Antosiewicz-Bourget, J., Frane, J.L., Tian, S., Nie, J., Jonsdottir, G.A., Ruotti, V., Stewart, R., Slukvin, I.I., Thomson, J.A., 2007. Induced pluripotent stem cell lines derived from human somatic cells. Science 318, 1917–1920. doi:10.1126/science.1151526

Zanacchi, F.C., Lavagnino, Z., Donnorso, M.P., Del Bue, A., Furia, L., Faretta, M., Diaspro, A., 2011. Live-cell 3D super-resolution imaging in thick biological samples. Nat Methods 8, 1047–1049. doi:10.1038/nmeth.1744

Zeinstra, L., Litjens, S., Oostwaard, D.W.-V., van den Brink, S., van Laake, L., Lebrin, F., Kats, P., Hochstenbach, R., Passier, R., Sonnenberg, A., 2008. Recombinant Vitronectin Is a Functionally Defined Substrate That Supports Human Embryonic Stem Cell Self-Renewal via αVβ5 Integrin. Stem Cells 26, 2257. doi:10.1634/stemcells.2008-0291

Zhao, X., Liu, J., Ahmad, I., 2002. Differentiation of embryonic stem cells into retinal neurons. Biochem Biophys Res Commun 297, 177. doi:10.1016/S0006-291X(02)02126-5

Zhong, J.F., Chen, Y., Marcus, J.S., Scherer, A., Quake, S.R., Taylor, C.R., Weiner, L.P., 2008. A microfluidic processor for gene expression profiling of single human embryonic stem cells. Lab Chip 8, 68–74. doi:10.1039/B712116D

Zhong, X., Gutierrez, C., Xue, T., Hampton, C., Vergara, M.N., Cao, L.-H., Peters, A., Park, T.S., Zambidis, E.T., Meyer, J.S., Gamm, D.M., Yau, K.-W., Canto-Soler, M.V., 2014. Generation of three-dimensional retinal tissue with functional photoreceptors from human iPSCs. Nat Commun 5, 4047. doi:10.1038/ncomms5047

Zhou, L., Wang, W., Liu, Y., de Castro, J.F., Ezashi, T., Telugu, B.P.V.L., Roberts, R.M., Kaplan, H.J., Dean, D.C., 2011. Differentiation of induced pluripotent stem cells of swine into rod photoreceptors and their integration into the retina. Stem Cells 29, 972–980. doi:10.1002/stem.637

Zuber, M.E., Gestri, G., Viczian, A.S., Barsacchi, G., Harris, W.A., 2003. Specification of the vertebrate eye by a network of eye field transcription factors. Development 130, 5155–5167. doi:10.1242/dev.00723